

TECHNISCHE UNIVERSITÄT MÜNCHEN

Lehrstuhl für Biotechnologie

Studying Cellular Protein Folding in Nematodes and Baker's Yeast

Christoph J. O. Kaiser

Vollständiger Abdruck der von der Fakultät für Chemie der Technischen Universität München zur Erlangung des akademischen Grades

Doktor der Naturwissenschaften (Dr. rer. nat.)

genehmigten Dissertation.

Vorsitzender : Univ.-Prof. Dr. A. Itzen

Prüfer der Dissertation:

1. Univ.-Prof. Dr. J. Buchner
2. Univ.-Prof. Dr. S. Weinkauf
3. Univ.-Prof. Dr. A. Bausch

Die Dissertation wurde am 21.08.2012 bei der Technischen Universität München eingereicht und durch die Fakultät für Chemie am 06.12.2012 angenommen.

*für meine Eltern
und meinen Großvater*

in memoriam

Christa Kaiser

Ursula Wassenberg

Werner Wagner

Martha Kretschmer

Publications

Parts of this work have been published or are currently in the process of being published. The asterisk denotes authors that have contributed equally to each study.

- **C. J.O. Kaiser**, S. W. Grötzinger, J. Eckl, K. Papsdorf, S. Jordan and K. Richter.
A network of genes connects polyglutamine aggregation to ploidy control.

Nature Communications.
currently under revision

- **C. J.O. Kaiser**, S. W. Grötzinger and K. Richter.
Polyglutamine stretches impair mitochondrial function.

Manuscript in preparation

- A. M. Gaiser*, **C. J.O. Kaiser***, V. Haslbeck* and K. Richter.
Downregulation of the Hsp90 system causes defects in muscle cells of *Caenorhabditis elegans*.

PLoS One.
2011. 6(9):e25485. Epub 2011 Sep 28.
PubMed PMID: 21980476; PubMed Central PMCID: PMC3182237.

- L. Sun*, F. T. Edelmann*, **C. J.O. Kaiser***, K. Papsdorf, A.M. Gaiser, and K. Richter.
The lid domain of *Caenorhabditis elegans* Hsc70 influences ATP turnover, cofactor binding and protein folding activity.

PLoS One.
2012. 7(3):e33980. Epub 2012 Mar 29.
PubMed PMID: 22479492; PubMed Central PMCID: PMC3315512.

- V. Haslbeck, **C. J.O. Kaiser** and K. Richter.
Hsp90 in non-mammalian metazoan model systems.

Biochim Biophys Acta.
2012. 1823(3):712-21. Epub 2011 Sep 22.
PubMed, PMID: 21983200

“Ἐν οἶδα, ὅτι οὐδὲν οἶδα.

Socrates

Content

A	Summary	7
B	Introduction	9
1	Protein folding within the cell	11
2	Models for protein aggregation and chaperone networks	24
3	Aims of this work	28
C	Materials and Methods	29
1	Materials	31
1.1	Reagents	31
1.2	Buffers	33
1.3	Enzymes, kits and standards	35
1.4	Antibodies	35
1.5	Equipment	36
1.6	Strains and organisms	37
1.7	Plasmids	38
1.8	Oligonucleotides	39
1.9	Media	40
1.10	Computer programs and databases	41
2	Methods	43
2.1	<i>Escherichia coli</i>	43
2.2	<i>Saccharomyces cerevisiae</i>	43
2.3	<i>Caenorhabditis elegans</i>	45
2.4	Molecular biology	47
2.5	Protein purification and analytics	50
2.6	Bioinformatics	55
2.7	Imaging	55
D	Results	57
1	Characterization of Hsc70 function in <i>C. elegans</i>	59
1.1	Hsp70 systems are adapted to physiological temperatures	59
1.2	The Hsp70 system is required to prevent folding stress	61
1.3	Hsp70 is the central essential factor of its chaperone network	61
1.4	The NEF-function of nematodal BAG-1 is conserved	63
1.5	DNJ-13 forms complexes with CeHsc70	64
1.6	DNJ-13 and BAG-1 compete for binding to CeHsc70	65
1.7	Substrate refolding requires BAG-1 at an optimum concentration	66

1.8	The lid domain is required for substrate refolding	68
2	Hsp90's function in the muscle of <i>C. elegans</i>	71
2.1	A compromised Hsp90 system leads to motility defects and mortality	71
2.2	<i>Daf-21</i> is ubiquitously expressed	72
2.3	DAF-21 suppresses the muscular heat shock response	73
2.4	DAF-21 and UNC-45 are responsible for proper myosin deposition	74
2.5	DAF-21 and UNC-45 are differentially distributed in muscles	76
2.6	Chaperone association to specific bands can be dynamic or stable	79
3	A network of genes connects polyglutamine toxicity to ploidy control	83
3.1	A relatively short polyQ stretch is cytotoxic	83
3.2	Q ₅₆ -YFP leads to enlarged and polyploid cells	85
3.3	The phenotype is dependent on the ploidy status	86
3.4	A genome-wide screen for genes influencing Q ₅₆ -YFP toxicity	89
3.5	Specific genes establish the toxicity of Q ₅₆ -YFP	90
3.6	The identified genes also mediate the toxicity of Htt103Q	93
3.7	Q ₅₆ -YFP toxicity is independent of prions	94
3.8	Hsp104 and Pho5 affect the oligomerization behavior of Q ₅₆ -YFP	96
3.9	Pho5 and Hsp104 affect the aggregation of polyQ proteins	99
3.10	PolyQ proteins interfere with septin ring formation	99
4	Several systems influence aggregation toxicity	103
4.1	25 genes suppress the toxicity of Q ₅₆ -YFP	103
4.2	A specific transcriptional response to Q ₅₆ -YFP toxicity	104
4.3	Q ₅₆ -YFP affects carbon source utilization	109
4.4	Q ₅₆ -YFP expression affects mitochondria	112
4.5	Aggregates interact differentially with chaperones	113
E	Discussion	117
1	The Hsc70 and Hsp90 machineries in <i>C. elegans</i>	119
1.1	The Hsc70 system	119
1.2	The Hsp90 system	121
2	Aggregation in <i>S. cerevisiae</i>	124
F	Acknowledgements	129
G	Figures	131
H	Tables	135
I	References	137

A Summary

Maintaining the proteome in a biologically active folded state is an everyday challenge for organisms. Chaperone systems have evolved to maintain the folding balance. However, in a group of disease states, mainly affecting neurons, protein homeostasis has been found to be severely compromised. In addition to these clinical states, chaperone systems support a vast amount of cellular processes in their normal function. Consequently, it is essential to understand the biochemistry and cell biology of chaperone networks as well as the impact of protein misfolding on cellular life.

This study on the one hand probes basic functional aspects of the two pivotal chaperone systems Hsc90 and Hsc70 and their cofactors in the anatomically relatively simple metazoan *Caenorhabditis elegans*, in respect to their biochemistry, association with their cofactors, their organismal functionality and expression patterns and their subcellular localization. The data indicate that the chaperone HSP-1 (Hsc70) is the central essential factor of its chaperone network. It interacts with the two potential cofactors BAG-1 and DNJ-13 during its hydrolytic cycle. Both cofactors are essential for efficient refolding of a model substrate. Its paralogue HSP-70 is not essential, but upregulated in response to heat stress and compromised HSP-1 function. For the Hsc90 system, it was found that DAF-21 (Hsc90) is required for the maintenance of the muscular ultrastructure in nematodes together with its cofactor UNC-45. Both proteins are differentially distributed in the myofibrillar lattice. DAF-21 seems to fulfill its function in the maintenance of muscular function as a soluble factor, whereas UNC-45 appears in a soluble form and in a form stably associated to specific parts of the myofibrillar lattice.

To understand which cellular factors govern the behavior of disease-associated polyglutamine (polyQ) proteins and human superoxide dismutase 1 (Sod1) variants, appropriate and highly comparable models in *Saccharomyces cerevisiae* were established. PolyQ proteins are found to be toxic when longer than a threshold known to be responsible for the development of Huntington's disease. Contrarily, Sod1 variants are non-toxic. Both proteins are shown to interact with a specific set of cellular factors which even proves to be mutant-specific for Sod1. To study the cytotoxic effect of polyQ proteins, a genome-wide screen was performed, yielding two sets of genes which are responsible to either suppress or enhance cytotoxicity. It is further found that the presence of toxic polyQ proteins induces a specific expression response in yeast. Additional analyses indicate that at a compromised mitochondrial function is part of the cytotoxicity exerted by polyQ proteins. However, additional experiments indicate that cellular division is compromised through the interference of toxic polyQ proteins with the proper assembly of septin ring, a structure which is a prerequisite for mitosis in yeast. A last aspect of this study is the previously undescribed finding, that diploid cells are resistant to polyQ toxicity and haploid cells may escape cytostasis by spontaneous hyperploidy or polyQ shortening. Mitochondrial pathogenesis and hyperploidy events have both been described before in the context of human neurodegenerative pathogenesis.

Extending the studies initiated in this work may lead to an understanding of the differences and similarities of chaperone systems and the reaction to misfolding proteins at the transition from unicellular to metazoan organisms.

B Introduction

1 Protein folding within the cell

Proteins need to adopt a specific three-dimensional structure in order to fulfill their biological functionality. As such, monomeric enzymes will acquire a structure that exposes little hydrophobicity on the surface and properly forms the active site or substrate binding pocket in order to provide an appropriate chemical surrounding for enzymatic activity and ligand coordination. For multimeric enzymes, or enzymes that are part of multimeric complexes, an additional requirement is to expose appropriately charged, polar, apolar or hydrophobic patterns on their surface to enable specific interactions with their binding partners. This is also valid for proteins that may not possess a specific catalytic activity, but are adaptors in multiprotein complexes or build up larger, higher-order structures such as ribosomes or cytoskeletal components.

The protein folding problem

Upon synthesis, the polypeptide chains undergo conformational changes that finally end in the biologically active structure. In 1969, Cyrus Levinthal illustrated the paradoxon of folding: the linear amino acid chains must use routes other than random sampling of all possible peptide bond angle combinations as folding occurs at a velocity that is acceptable for biological processes and comparable to empirical timescales, which is in the range from microseconds to minutes. According to Levinthal's calculations, the temporal order of magnitude for folding by random sampling of peptide bond angles would be at 10^{24} years for a polypeptide of 150 amino acids.

By now, it is known how proteins reach their final biological functionality by a stochastic search through all possible conformations. The efficiency of this process is also depending on the starting point of folding (Dill & Chan, 1997; Karplus, 1997). Several situations can be discriminated: *de novo* folding of single domain proteins, *de novo* folding of multidomain proteins, refolding of denatured proteins, folding upon binding to ligands or binding partners or under specific environmental conditions. All of these processes must follow specific kinetic tracks.

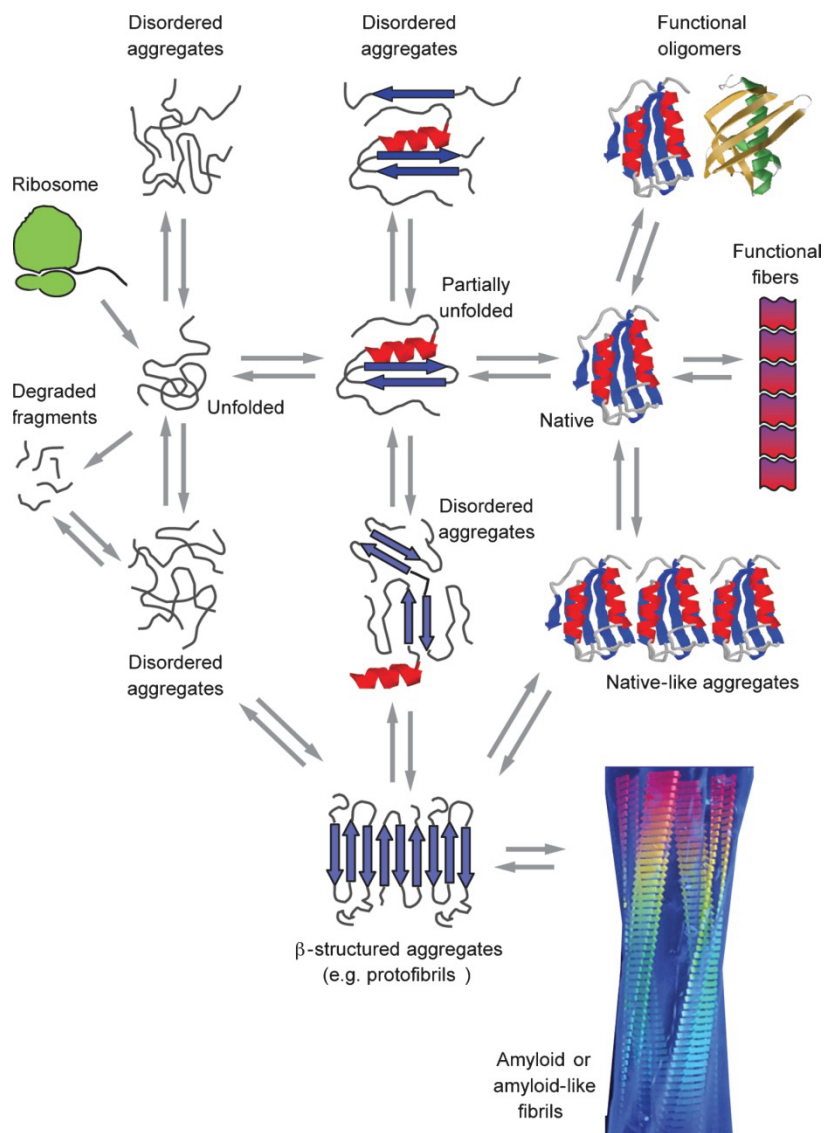
In addition, it has also become evident and has been experimentally confirmed that the 'native' tertiary structure is not a single stably folded state, but rather consists of subpopulations of molecules exhibiting a considerable amount of structural variation at physiological temperatures. Recent developments in structural biology and bioinformatics methods, e.g. in nuclear magnetic resonance spectroscopy, X-ray crystallography, and especially in single particle cryoelectron microscopy allowed to demonstrate the coexistence of conformationally heterogeneous 'native' structures for a large amount of proteins (Schnell *et al.*, 2004; Smith *et al.*, 2005). Moreover, protein folding studies delivered evidence for complex folding energy landscapes with several intermediates corresponding to energetic minima at similar levels (Morozova-Roche *et al.*, 1999).

These findings led to a paradigm shift: biologically active structures exhibit high degrees of flexibility and freedom due to metastability. This metastability in turn allows conformational changes upon ligand or protein binding or a specific environmental change, a prerequisite for

Introduction

many biological processes (Bernado & Blackledge, 2010; Changeux & Edelstein, 2005; Frauenfelder *et al.*, 2009). To understand the implications for protein folding, it is helpful to look at alternative folding landscapes that are specific for a single primary sequence.

A protein whose folding energy landscape exhibits one global minimum will always re-acquire its well defined structure at a given physiological temperature. In contrast, proteins with complex folding energy landscapes and a fairly low release of free folding energy with local minima nearby will tend to populate several minima at physiological temperatures and will possess a higher degree of flexibility. The latter situation, which reflects metastability, has major implications for the protein's tendency to aggregate. The different metastable states as well as




 Chiti F, Dobson CM. 2006.
Annu. Rev. Biochem. 75:333–66

Figure 1: Possible states of a generic polypeptide chain. A schematic overview of possible polypeptide states, independent of their environment and sequence. Unfolded proteins are able to form aggregates and partially folded species. Aggregates may further mature to protofibrils and fibers or be degraded immediately. The partially folded state is on the route to approach the native state, but may as well participate in the formation of higher order structures, which in turn may form aggregates or protofibrils. The native state may be finally reached and itself participate in the assembly of native or alternative ‘non-native’ assemblies. Which of the states will mainly be populated by a specific protein is dependent on the chemical environment, the primary sequence and physical parameters like temperature or pressure. Reprinted with permission from Annual Reviews (Chiti & Dobson. 2006).

the transitions between them correspond to states of either partial or total unfolding. Partially folded or unfolded proteins expose extended hydrophobic patches which may interact unspecifically with other regions of the same protein or with other proteins, which will favor aggregation of these polypeptides (Figure 1) (Chiti & Dobson, 2006).

Heat stress and protein folding

Organisms have to deal with their environments and environmental conditions such as temperature. Microorganisms, plants and lower animals are directly exposed to the thermal conditions of their habitat, usually around these organisms' optimum growth temperature. Nevertheless, there are occasions on which they will be challenged with temperatures well above and below their physiological optima. Although higher animals possess modes of regulating their body temperature, there are deviations from this temperature, either locally or globally, under conditions of strong heat exposure or infection. In an experimental setup, a raise in temperature is usually achieved fast and in a defined way. Here, the spontaneous increase in temperature in the order of magnitude of 5-10 K over the growth temperature of an organism for most species – mesophilic or thermophilic – constitutes a heat shock (Brown & Lupas, 1998; D'Amico *et al.*, 2006; Takai *et al.*, 1998).

An elevated temperature equals external input of thermal energy, increasing the energy of the system, e.g. within a cell. Consequently, the loss of free folding energy is decreased and proteins will populate different conformational states, depending on their folding energy landscape. For extremely stable proteins, a moderate raise in temperature will only lead to a slightly higher flexibility. However, for proteins that are only marginally stable – a large fraction of proteins – this slight rise in temperature will lead to unfolding events, exposing hydrophobic residues that are normally shielded from the surrounding (Chiti & Dobson, 2009).

In dilution, most proteins may refold after unfolding, albeit potentially following a different pathway than for unfolding. In a cellular environment, however, protein concentrations are extremely high; depending on the cell type up to 300-400 mg/ml (Ellis & Minton, 2003). Consequently, the probability for a protein exposing hydrophobic residues to interact with another protein that also provides such hydrophobic interaction sites is high (Gershenson & Gierasch, 2011). This interaction may be energetically favored and counteract the refolding process. If the amount of proteins that unfold is high enough, or the populated intermediates are kinetically trapped, this process may perpetuate and lead to extensive interaction of polypeptide chains, resulting in protein aggregation recruiting more unfolded polypeptides.

As proteins aggregating under heat shock conditions are non-functional and may interfere with cellular structures destroying their integrity, cells counteract this deleterious process by inducing systems that have evolved to suppress aggregation and to support refolding. The induction of these systems has been termed the heat shock response.

Heat shock proteins and chaperones

During the heat shock response, the expression of a specific set of proteins exerting a variety of functions is induced. The seven gene classes that may be discerned include (Richter *et al.*, 2010):

Introduction

the initially discovered heat shock proteins, i.e. molecular chaperones (Ellis *et al.*, 1989), components of the protein degradation machinery, nucleic acid repair enzymes, metabolic enzymes, transcription factors and kinases, proteins maintaining the cellular structure as well as genes, responsible for detoxification and membrane modulation. Among these heat shock proteins, the molecular chaperones constitute a class of major importance. They fulfill different functions directly related to protein folding and are for the largest part highly conserved throughout all kingdoms of life, reflecting their importance in maintaining the proteome in a folded state that is capable to fulfill biological functions.

Chaperones generally bind substrates promiscuously (Bukau *et al.*, 1996; Sharma *et al.*, 2008; Viitanen *et al.*, 1992) and can be subdivided into ‘foldases’ and ‘holdases’. Foldases are ATP consuming enzymes and transform the energy released by ATP hydrolysis into allosteric movements inducing conformational changes or unfolding reactions in substrate proteins (Figure 2).

The ubiquitous Hsc70 machinery and its heat-inducible homologues (Hsp70) participate in refolding processes, disassemble multimeric protein complexes and aggregates and are involved in protein translocation across membranes (Bocking *et al.*, 2011; Craig *et al.*, 1989; Feige *et al.*, 2010; Mayer & Bukau, 2005; Palleros *et al.*, 1991; Su & Li, 2010; Wiech *et al.*, 1993; Young *et al.*, 2004). In eukaryotes such as yeast, cytosolic isoforms may be discerned. Ssb1, Ssb2 and Ssz1 are part of the ribosome associated complex (RAC) (Pfund *et al.*, 1998). Other isoforms are constitutively expressed (Saa1 and Ssa3) or heat-inducible (Ssa2 and Ssa4) (Werner-Washburne *et al.*, 1987). The members of the Hsc70 chaperone family have three domains: an aminoterminal nucleotide binding domain (NBD), a substrate binding middle domain (SBD), and a carboxyterminal helical lid domain, covering the substrate binding groove of the SBD (Morshauer *et al.*, 1995; Popp *et al.*, 2005) tightly grasping unfolded stretches of substrate proteins in an ATP dependent manner (Schlecht *et al.*, 2011). While the helical lid domain diverges strongly between eukaryotic and prokaryotic species, the NBD and SBD are highly conserved. Biochemical studies of the bacterial Hsp70-protein DnaK described many aspects of the ATP-hydrolysis mechanism and established a hydrolytic cycle, which is coupled to the substrate processing activity. An ATP-bound state of Hsp70 binds substrates weakly. After trinucleotide hydrolysis, the substrate is efficiently bound by ADP-Hsp70, a complex which is resolved slowly by the release of ADP and substrate (Mayer & Bukau, 2005; Young *et al.*, 2004). All Hsp70 domains are supposedly participating in and communicating during this process (Rist *et al.*, 2006; Schlecht *et al.*, 2011; Swain *et al.*, 2007). While it was shown that the helical lid domain covers the substrate binding groove of the SBD (Zhu *et al.*, 1996) and is important for efficient protein folding (Freeman *et al.*, 1995) it is still unclear how this domain influences the hydrolytic mechanism of Hsc70 proteins.

In all species studied, Hsc70 proteins possess two specific types of cofactors that influence their catalytic cycle: J-domain containing proteins and nucleotide exchange factors (NEF) (Kampinga & Craig, 2010; Young, 2010). J-domain containing proteins have been shown necessary for substrate recognition and accelerate the hydrolytic reaction of Hsc70s (Russell *et al.*, 1999). On the other hand, NEFs, like bacterial GrpE or human Bag1, specifically facilitate the release of the nucleotide after hydrolysis, also contributing to an elevated hydrolytic activity (Harrison *et al.*, 1997; Liberek *et al.*, 1991; Packschies *et al.*, 1997). The combined action of both cofactors is synergistic in accelerating ATP turnover (Hohfeld & Jentsch, 1997; Packschies *et al.*, 1997).

The Hsp70 family is closely related to the Hsp110 family of heat shock proteins, sharing extended sequence homologies. During the past years, their role in protein folding has been revisited. Originally, they were considered to be cofactors of the Hsp70 system, merely accelerating the ATPase hydrolysis cycle by supporting the release of the tightly bound nucleotide after hydrolysis and thus enhancing Hsp70's activity. Recent studies, however, point to a more specific function of Hsp110 family members as adaptor proteins enhancing the disaggregation capacity of Hsc70/Hsc40 complexes (Duennwald *et al.*, 2012; Shorter, 2011).

Another important representative of the ATP consuming chaperones is Hsp90. This chaperone is essential and highly conserved in all eukaryotic species studied to date (Borkovich *et al.*, 1989). Hsp90s consist of an aminoterminal nucleotide binding domain, a charged linker region followed by a middle domain and a carboxyterminal dimerization domain. A conserved motif at the very

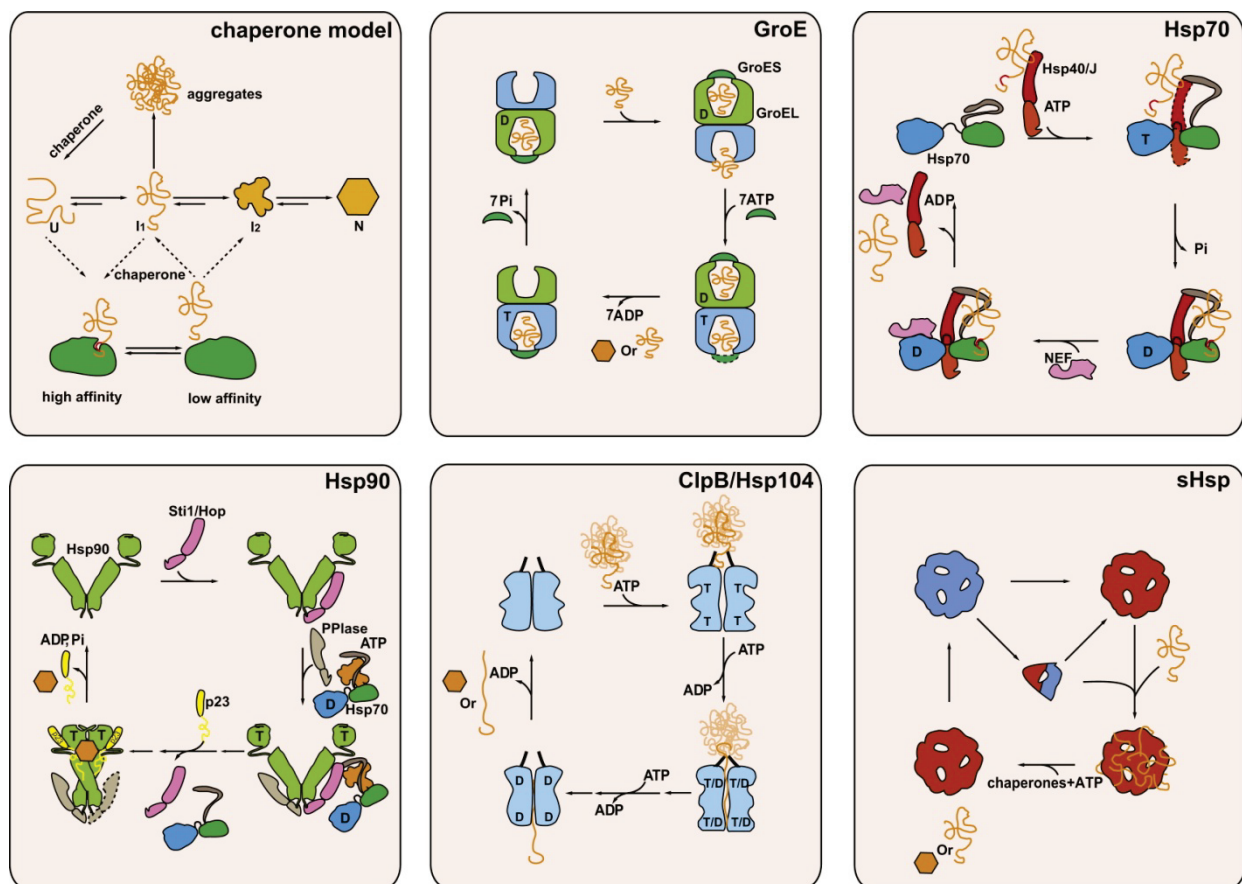


Figure 2: Models of chaperone functionality. In a generic model of chaperone function (chaperone model), chaperones may interact with different folding states of proteins, as indicated by the simplified protein folding pathway depicted here. The GroEL/S system (GroE) binds its substrate at the apical domain of one GroEL ring. ATP and GroES join this complex. The substrate is released into the cavity, enabling folding. Upon hydrolysis of ATP, the substrate is released from the opposite ring. The Hsp70 system (Hsp70) is presented with its two cochaperones, a J-domain protein (red/orange) and a nucleotide exchange factor (purple). The J-protein delivers the substrate to Hsp70 in an ATP bound state. Upon hydrolysis, the substrate is bound tightly. An NEF joining the complex accelerates the hydrolytic cycle by facilitating the release of nucleotide. This exchange of nucleotide also releases the substrate in a state that is capable of refolding. Hsp90 (Hsp90) is shown for completeness but will be described in detail below. The Hsp100 family (ClpB/Hsp104) enables refolding by unfolding. The chaperone is considered to thread its aggregated substrates through the central pore in the hexameric ring, deploying the energy of sequential hydrolysis of ATP. Small heat shock proteins (sHsp) exist in an inactive state at physiological temperature and are considered to be activated by heat. After activation, the sHsps will bind partially or fully denatured proteins, supporting refolding through other chaperone classes. Whether the activation involves dissociation of the oligomeric state is unclear. Reproduced with permission from Cell Press (Richter *et al.*, 2010).

Introduction

carboxyterminus is responsible for the binding of cochaperones that possess a tetratricopeptide repeat (TPR) domain (Louvion *et al.*, 1996; Scheufler *et al.*, 2000; Young *et al.*, 1998). Hsp90 is present in high amounts in cells and more than 200 client proteins have been described, taking part in a diverse set of signaling and regulative pathways (Welch & Feramisco, 1982). A database of all described client proteins is maintained by the Picard lab and may be accessed at www.hsp90.org. The mechanism of this ATPase has been under intense scrutiny during the past years and important aspects of the regulation have been uncovered (Figure 3) (Hessling *et al.*, 2009; Krukenberg *et al.*, 2011; Li *et al.*, 2011; Richter *et al.*, 2008). Hsp90's impact on the structure of client proteins seems to be less general and more subtle or surgical in comparison to the sHsps or Hsp70 (Jakob *et al.*, 1995; Picard, 2002; Pratt & Toft, 2003; Smith, 1998).

According to the current opinion in the field, Hsp90 is rather a structure modulator. It is accompanied by set of roughly 20 cochaperones that are essential for the processing of client

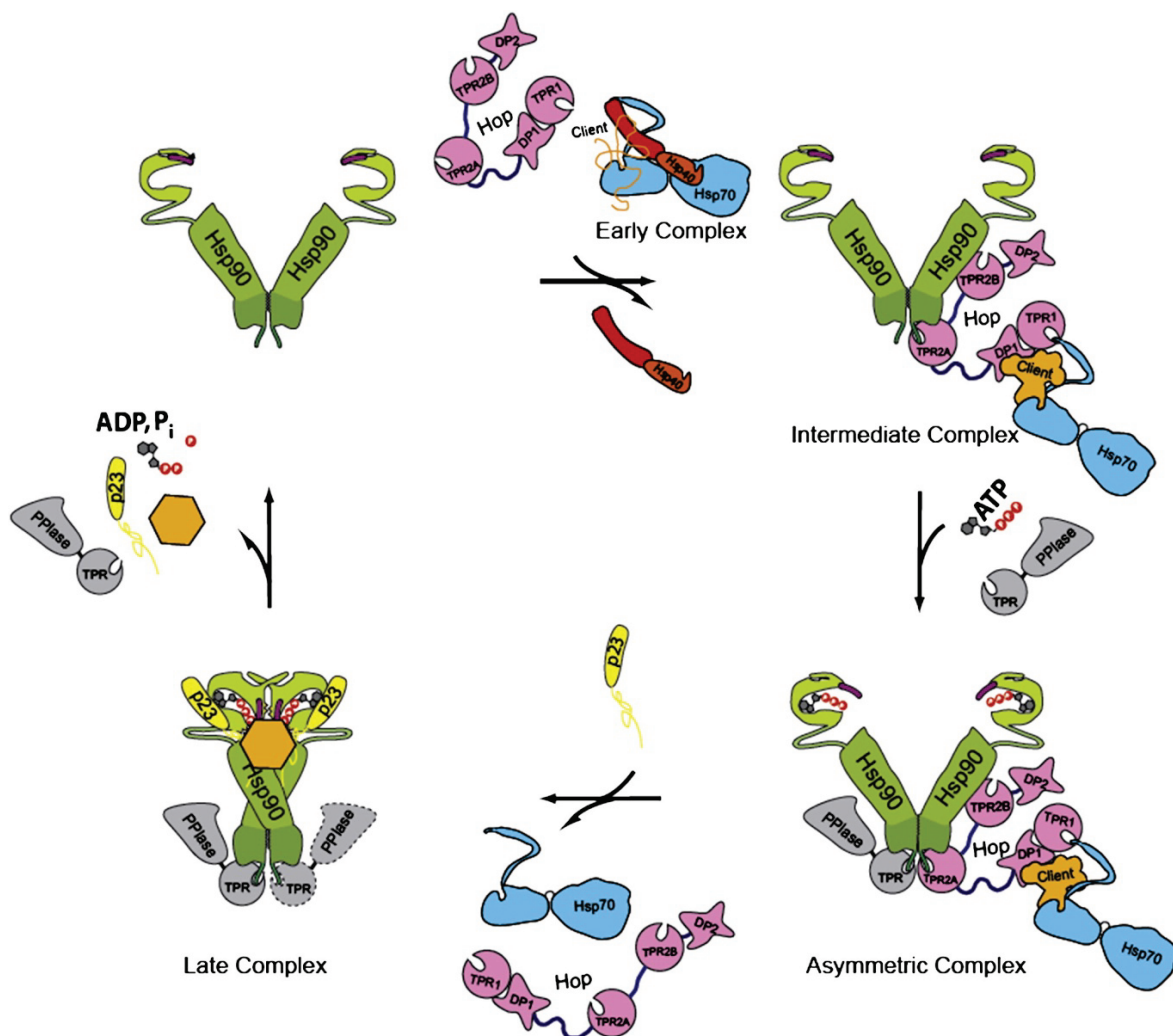


Figure 3: The chaperone cycle of Hsp90. The transitions of the Hsp90 complex as suggested from studies on SHRs are depicted. The substrate is bound to Hsp70 and a J-protein. This is considered the 'early complex' of substrate maturation. The adaptor protein Hop/Stil is able to simultaneously bind Hsp70 and Hsp90 and consequently assembles the 'intermediate complex' in which Hsp90 is stabilized in its open conformation by Hop/Stil. The other MEEVD motif of the Hsp90 dimer is still capable to bind e.g. a PPIase, which supports the folding of the client. The binding of ATP induces the closed conformation, which can be stabilized by p23/Sba1 and concurrently weakens the binding of Hop/Stil. Another PPIase may join at the newly uncovered interaction site (dashed) to form the 'late complex', which is subsequently resolved by the release of the cochaperones, the folded substrate and ADP/P_i after hydrolysis. Reproduced with permission from Elsevier (Li *et al.*, 2012).

proteins. Steroid hormone receptors (SHR) for instance are highly dependent on Hsp90 concerning their ligand binding and nuclear translocation. In a so-called 'early complex' Hsp70 and Hsp40 bind the receptor. The cochaperone Hop/Sti1 mediates the recruitment of Hsp90 to this assembly and the transition to an 'intermediate complex'. To complete maturation, the cochaperone p23/Sba1 and a peptidyl prolyl isomerase (PPI) join in and constitute the 'late complex' (Li *et al.*, 2012). This cycle and the set of cochaperones that is recruited are thought to be dependent on the nature and requirements of specific clients (Figure 3).

The fourth group of chaperones are the Hsp100 ATPases associated with diverse cellular activities (AAA) comprising the two classes I and II. Class I proteins are peculiar to bacteria (ClpA, B, C, E), fungi (Hsp104) and plants (ClpD). They possess two nucleotide binding sites per monomer and form a hexameric ring structure (Martin *et al.*, 2005). Class II Hsp100 proteins are found in bacteria (ClpX, Y) and contain only one nucleotide binding site per monomer (Schirmer *et al.*, 1996). Homologues for this class of Hsp100 proteins are found in mammals as well, contributing to protein quality control and degradation (Schrader *et al.*, 2009). Upon binding of ATP and subsequent hydrolysis, Hsp100s are capable of unfolding and even disaggregating proteins. The mechanism proposed is threading of the substrate through the central pore of the ring, unfolding the substrate and enabling it to undergo a refolding attempt (Doyle *et al.*, 2007; Schaupp *et al.*, 2007; Weber-Ban *et al.*, 1999).

A last group of ATP consuming chaperones are the chaperonins or Hsp60 proteins. Functional homologues of this family can be found throughout all kingdoms of life. In bacteria the GroEL/S system performs chaperonin functionality, being substituted by the TRiC/CCT complex in eukaryotes (Dunn *et al.*, 2001; Horwich *et al.*, 2006). The GroEL/S system is the best-understood class of chaperones. It forms a barrel-shaped heptameric oligomer exposing hydrophobic surfaces inside the chamber. When a client protein is bound at these surfaces, the hydrolysis of ATP induces a conformational change, hiding the hydrophobic surfaces at the interior and exposing more hydrophilic residues. Through this conformational change, the substrate protein can attempt to fold in a 'hydrophilic cage' where it is shielded from the environment and consequently prevented from interacting undesirably with other cellular proteins (Figure 2) (Grallert & Buchner, 2001; Hartl & Hayer-Hartl, 2002; Todd *et al.*, 1994). The activity of GroEL/S is restricted to polypeptides lighter than 60 kD. As it was shown to still assist about 50% of *E. coli* proteins in folding, the substrate spectrum is considered promiscuous, (Viitanen *et al.*, 1992). Additionally, the functionally homologous TRiC/CCT family proved to be restricted in its substrate spectrum and paradoxically downregulated upon heat stress (Eisen *et al.*, 1998; Yam *et al.*, 2008).

The only class of non-ATP-consuming chaperones is the class of holdases, comprising the small heat shock proteins (sHsp). The presence of an α -crystallin domain defines the sHsp class. Although the mechanism of their function and their substrate specificity are still largely enigmatic, it is verified that sHsps inhibit the aggregation of partially folded or unfolded proteins, helping to avoid irreversible aggregation until the clients may be refolded by Hsp70 or Hsp100 proteins (Haslbeck *et al.*, 2005a; Horwitz, 2003; Lee *et al.*, 1997; McHaourab *et al.*, 2009; Mogk *et al.*, 2003). *In vitro*, the holdases are capable to suppress aggregate formation upon thermal or chemical denaturation of model substrate proteins. Recently, sHsps have also been shown to influence the aggregation behavior of amyloids and assist in their disassembly by the Hsp40/70/110 machinery (Duennwald *et al.*, 2012; Shorter, 2011).

Introduction

The levels of all major classes of heat shock proteins were shown to be controlled by the transcription factor Hsf1, which is conserved in all eukaryotes. *Escherichia coli* and archaea possess the functional homolog σ^{32} . Under physiological conditions, Hsf1 is bound in equilibrium to the Hsp90 and Hsp70 systems and potentially continuously degraded in analogy to σ^{32} in *E. coli* (Rodriguez *et al.*, 2008). Upon heat stress, these chaperone systems are engaged in handling unfolding proteins and Hsf1 is released, leading to a trimerization of Hsf1 molecules and their import into the nucleus, where the subunits are hyper phosphorylated and sumoylated (Akerfelt *et al.*, 2010; Hietakangas *et al.*, 2003; Holmberg *et al.*, 2001). This activated Hsf1 trimer then binds to the heat shock responsive elements (HSE) and stimulates the transcription of downstream genes, which are chaperones and other proteins such as metabolic enzymes.

Protein aggregation in disease

Although most of the studies on protein aggregation have been carried out under heat shock conditions, the phenomenon is not restricted to this environmental challenge. For example, modification of proteins by reactive oxygen species as well as drastic changes in pH and osmolarity may render proteins prone to aggregation. During the last two decades, protein misfolding and aggregation of single protein species have been implied to contribute to a large variety of diseases (Chiti & Dobson, 2006; Ross & Poirier, 2004; Taylor *et al.*, 2002).

These so-called proteopathies are typical diseases of age in which protein misfolding leads to a loss of function or a toxic gain of function. They may also be subdivided into diseases mainly exhibiting intracellular protein deposits (e.g. Parkinson's disease, amyotrophic lateral sclerosis, Huntington's disease) and diseases of the extracellular space (e.g. systemic amyloidoses, Alzheimer's disease).

Among the intracellular loss of function aggregation diseases, cystic fibrosis is probably the best-known. In this disease, the cystic fibrosis transmembrane receptor is highly aggregation prone mostly due to mutations. These mutations lead to a compromised assembly and consequently to the retention of the receptor in the endoplasmic reticulum (ER). The misfolded receptors are subsequently degraded and cannot reach the cell's surface to perform their task (Dobson, 2004). A loss of function due to the aggregation of the tumor suppressor p53 has also been described to be causative for certain cancers (Xu *et al.*, 2011).

The group of proteopathies in which not the loss of function of a specific protein leads to disorder, are considered to have undergone a toxic gain of function. These gain of toxicity diseases can arise in hereditary and spontaneous forms. For example, amyotrophic lateral sclerosis (ALS) is largely sporadic. However, roughly 10% of all cases are hereditary. Approximately 20% of these hereditary cases can be attributed to a familial hereditary form (FALS), for which a plethora of single site mutations in the gene encoding superoxide dismutase 1 (SOD1) have been described to be causative (Bosco & Landers, 2010; Rosen *et al.*, 1993). It was previously supposed that the loss of SOD1 function would lead to the observed degeneration of motor neurons due to the accumulation of reactive oxygen species. Experiments in mouse models disproved this hypothesis, as animals retaining the wild type (WT) mouse enzyme and the mutant human FALS variants, suffered extensively from neurodegeneration, whereas knockout mice for WT mouse Sod1 showed no or hardly any pathological changes. The

loss of the mitochondrial isoform (SOD2) proved to be lethal (Borchelt *et al.*, 1994; Gurney *et al.*, 1994).

Another hereditary neurodegenerative disorder is Huntington's disease (HD). In this disease, the huntingtin protein (Htt) with yet unattributed functions exhibits an extensive tendency to aggregate within cells. Previous work has firmly established that the age of onset of this disease and the severity of its progress closely correlate to the length of a stretch of glutamines (polyQ) with a sharp increase of incidence at more than 30 glutamine residues (Bates, 2003). Interestingly, this phenomenon of polyQ based aggregation disease is not limited to HD, but approximately a dozen of diseases are similarly associated to extended glutamine stretches in different proteins (Table 1) (Gatchel & Zoghbi, 2005; Williams & Paulson, 2008; Zoghbi & Orr, 2000).

Other gain of function proteopathies such as Kuru and Creutzfeldt-Jakob's disease are attributed to misfolding of the human prion protein. This protein of unknown function is able to switch between a physiologically non-toxic helical structure and a β -sheet rich structure assembling into amyloid fibrils and leading to the loss of neurons (Aguzzi *et al.*, 2007; Brown & Mastrianni, 2010). This conformational transition leading to the disease can be induced by the intracerebral injection or ingestion of material containing the misfolded species (Prusiner, 1982). It is the only demonstrably infectious amyloid disorder.

Several other neurodegenerative diseases have been weakly linked to genetic variations and are less well-defined in respect to whether intracellular or extracellular protein causes neuronal degeneration. For instance, Alzheimer's (AD) and Parkinson's diseases exhibit a largely sporadic incidence. For both diseases, clinical states of protein misfolding could be attributed as causative. In case of AD, frequently the aggregation of A β peptide is observed. The peptide is generated from the amyloid precursor transmembrane protein APP by proteolytic processing (Thinakaran & Koo, 2008). These peptides subsequently assemble in the extracellular space to form amyloid plaques. Specific oligomeric conformers seem to be most cytotoxic (Knobloch *et al.*, 2007; Lee *et al.*, 2006; Shankar *et al.*, 2008; Walsh *et al.*, 2000). However, a certain fraction of the peptide can also be detected within cells after endocytosis from the extracellular space and may generate toxicity via this pathway.

It is remarkable that the onset of clinical symptoms of all toxic gain of function aggregation diseases is related to age. As such, HD generally will not manifest until the age of 40 and the risk for AD rises steeply at the age of 70 (Mattson & Magnus, 2006; Walker, 2007). This age dependency may be attributed to a generally reduced capacity of cellular quality control systems (Powers *et al.*, 2009). In *C. elegans*, it was shown that the presence of a temperature sensitive mutation accelerates aggregate formation, indicating that the presence of misfolded proteins can disrupt the homeostatic balance of the cell (Gidalevitz *et al.*, 2006). Additionally, in worms, it was recently shown, that the age-related loss of capacity for protein quality control leads to the aggregation of several hundred proteins (David *et al.*, 2010).

HD, FALS and familial Parkinson's disease are the only neurodegenerative proteopathies, for which the development of the disease is not only genetically predisposed, but determined. Consequently, this clear correlation renders them ideal subjects to study the link between aggregation and toxicity. It is important to note, that for all neurodegenerative disorders, fibrillar aggregation – either extracellular or intracellular – has been described. The ability to form these

Introduction

structures seems to be a shared property of a vast majority of proteins (Caughey & Lansbury, 2003; Chiti & Dobson, 2006; Davies *et al.*, 1997; Goldschmidt *et al.*, 2010).

Disease	Protein	Group
Alzheimer's disease (AD)	App, Presenilin 1/2	Non-polyQ aggregation neuropathies
Parkinson's disease	A-synuclein, parkin, Uchl-1, Pink1, Dj1	
Lewy-body dementia	α/β -synuclein, ApoE, CyP2D6	
Familial amyotrophic lateral sclerosis (FALS)	Sod1	
Creutzfeldt-Jakob's disease	Prp	
Huntington's disease (HD)	Htt	
Spinocerebellar ataxia type 1	Ataxin-1	PolyQ related neuropathies
Spinocerebellar ataxia type 2	Ataxin-2	
Spinocerebellar ataxia type 3	Ataxin-3	
Spinocerebellar ataxia type 6	Isoform of α_{1A} Ca ²⁺ channel subunit	
Spinocerebellar ataxia type 7	Ataxin-7	
Spinocerebellar ataxia type 17	TATA box binding protein	
Dentatorubropallidoluysian atrophy	Atrophin1	
Spinal and bulbar muscular atrophy	Androgen receptor	

Table 1: Neurodegenerative aggregation diseases. A list of neurodegenerative diseases that are related to protein aggregation highlights that a large number of proteopathies damaging neurons are associated to elongated glutamine stretches.

Aggregation toxicity

A major issue in the field of cellular protein aggregation is the quest for the toxic species. A short overview on the current hypotheses concerning FALS and HD will highlight that there is no conclusive evidence on a single mechanism of toxicity or a specific toxic species leading to disease.

Originally, the toxicity of polyQ proteins was attributed to their ability to form intracellular aggregates in mouse models (Davies *et al.*, 1997). However, the low correlation between brain areas affected by aggregation and those affected by a loss of neurons as well as the appearance of detectable aggregates after the onset of disease symptoms weakened the hypothesis that inclusion formation is cytotoxic *per se* (Gutekunst *et al.*, 1999; Kuemmerle *et al.*, 1999). *In vitro*, polyQ proteins can form fibers and amorphous aggregates (Chen *et al.*, 2001). Recent studies suggested that globular or protofibrillar oligomeric species are crucial for cytotoxicity (Poirier *et al.*, 2002; Sanchez *et al.*, 2003) and β -sheet rich oligomers and monomers have been shown to be cytotoxic upon microinjection into cells (Nagai *et al.*, 2007). The toxic species may exert their cytotoxic effect by the recruitment or sequestration of cytosolic proteins with short polyQ stretches into the growing fiber or aggregate. Indeed, many proteins contain short polyQ stretches such as the creb binding protein (CBP). This co-transcriptional regulator in neurons can form aberrant interactions with Htt *in vitro* and this interaction with polyQ proteins affects the structure of CBP to prime it for proteasomal degradation (Jiang *et al.*, 2003). This 'sequestration hypothesis' recently was supported by a major study using a mass-spectrometric approach to

analyze aggregate content, that uncovered numerous metastable cellular proteins to be sequestered into aggregates (Olzscha *et al.*, 2011). Other studies showed that polyQ aggregates are highly ubiquitinated and consequently bound for degradation. As proteasomes hardly digest polyQ proteins, the essential degradation machinery may become blocked (Bence *et al.*, 2001; Venkatraman *et al.*, 2004). Additionally, the yet to be defined toxic species may interfere with general protein quality control, as it ties all available chaperone activity to the aggregation process, which is consequently not available to control protein homeostasis. This may lead to a propagation of folding defects to other cellular proteins (Balch *et al.*, 2008; Bence *et al.*, 2001; Gidalevitz *et al.*, 2006). Additional experiments on model membranes suggested soluble oligomers of polyQ to be able to compromise the integrity of cellular membranes (Lashuel & Lansbury, 2006). This may also be the mechanism through which mitochondrial membrane potential and Ca^{2+} levels are altered upon addition of purified extended polyQ proteins (Panov *et al.*, 2002). A purely mechanical constriction of neuronal axonal trafficking by aggregates has also been suggested to be responsible for the loss of neurons (Parker *et al.*, 2001; Piccioni *et al.*, 2002).

In the case of FALS, in *post mortem* samples, motorneurons can be found to react intensely to immunohistochemical staining for Sod1 (Bruijn *et al.*, 1998; Jonsson *et al.*, 2004; Shibata *et al.*, 1996). Aggregates can be found in the cytoplasm, mitochondria and vacuoles as well as axonal processes and dendrites (Deng *et al.*, 2006; Fukada *et al.*, 2001; Jaarsma *et al.*, 2008; Jonsson *et al.*, 2006; Sasaki *et al.*, 2005). There is some evidence that microscopically detectable aggregates are not necessarily formed prior to or in parallel with the occurrence of neurodegeneration symptoms, but detergent soluble species accumulate well before onset and throughout the course of the disease. The aggregates exhibit similar fibrillar morphology as in other neurodegenerative diseases (Basso *et al.*, 2006; Wang *et al.*, 2005). Nevertheless, *in vitro* aggregation studies of mutant Sod1 did not faithfully correlate to FALS pathogenesis (Prudencio *et al.*, 2009; Vassall *et al.*, 2011; Wang *et al.*, 2008). Although several different processes as axonal transport, mitochondrial function, ER-stress, and oxidative stress response have been described to be compromised by the expression of mutant Sod1, precise insight into how these effects are generated is still elusive (Bosco *et al.*, 2011; Chattopadhyay & Valentine, 2009).

The diversity of observations concerning the mechanism of pathogenesis and the pathogenic species highlights the necessity to obtain a more profound knowledge on the exact sequence of events that lead to cellular death mediated by aggregation prone proteins. It is also to be considered that the ultrastructure of aggregates and their interaction behavior with other proteins has been shown to be very divergent, comparing polyQ proteins and SOD1 mutants (Matsumoto *et al.*, 2006).

Despite the very diverse set or simple lack of information concerning the toxic species, several scientists support the hypothesis that large aggregates or even amyloid deposits are not the species to blame for neurodegeneration. Studies argue that aggregation is not necessarily a specific feature of disease, but a rather common phenomenon (David *et al.*, 2010; Dobson, 2003; Gidalevitz *et al.*, 2006). As such, in yeast more than 200 proteins were found in deposits in stationary phase and are resolubilized when returning to normal growth (Narayanaswamy *et al.*, 2009).

Dealing with aggregation

What cellular mechanisms inhibit the accumulation of self-perpetuating aggregation of improperly folded proteins or its toxic precursors? Cells have evolved several lines of defense to avoid deleterious effects. However, the production of a toxic protein may be suppressed by the downregulation of its expression, an effect that has not been observed in context with aggregation disease, potentially due to the fact that overexpression systems are mostly deployed in model systems. Upon translation, newly synthesized proteins in yeast are safeguarded by the nascent chain associated complex (NAC) and a ribosome-specific combination of the Hsp70/J-protein/Hsp110 proteins Ssb/Ssz/Zuo (Gautschi *et al.*, 2002). Some substrate proteins may further require members of the Hsp60 family (TriC/CCT) or other members of the Hsp70/J-protein/Hsp110 system (Kramer *et al.*, 2009).

Once folded, proteins will – depending on their structure and stability – remain in this state for a certain part of their lifetime. Special cases are proteins that require immediate action of chaperones to fulfill their biological function such as the clients of the Hsp90 machinery already described above (Li *et al.*, 2012). As chaperones are ubiquitously present in the cell, the unfolding of a protein should recruit members of the sHsp family. sHsps are able to bind partially or fully denatured proteins to avoid the formation of aggregate oligomers (Haslbeck *et al.*, 2005a; McHaourab *et al.*, 2009).

Once these rescue mechanisms fail, oligomeric species and aggregates may arise. Hsp70 proteins in combination with Hsp110 and J-proteins as well as chaperones of the Hsp100 family have the capacity to disintegrate aggregates or aggregation nuclei that already have been formed (Duennwald *et al.*, 2012; Lee *et al.*, 1997; Mogk *et al.*, 2003). Notably, sHsps may also be incorporated into growing aggregate structures to facilitate aggregate resolubilization and protein refolding (Cashikar *et al.*, 2005; Haslbeck *et al.*, 2005b; Liberek *et al.*, 2008). If refolding attempts fail, proteins can be ubiquitinated and targeted for proteasomal degradation (Ciechanover & Brundin, 2003; Goldberg, 2003). Nevertheless, a failure of the above mechanisms to avoid large scale unfolding of cytoplasmic proteins supports aggregate formation.

Current opinion in the field suggests that aggregate formation is a final line of defense and potentially rather beneficial, than detrimental. As such, the inhibition of the proteasome or proteasomal overload leads to the controlled accumulation of protein in aggresomes (Johnston *et al.*, 1998; Kopito, 2000). These structures are highly dependent on dynein mediated retrograde transport of misfolded protein (Garcia-Mata *et al.*, 1999; Johnston *et al.*, 2002). Controlled aggregation consequently seems to sweep the cytoplasm from misfolded species. For Htt, it was shown that the inhibition of ubiquitination will abolish the formation of ubiquitinated intranuclear inclusions and increase the cytotoxicity (Saudou *et al.*, 1998). Observing neuronal fate in time lapse experiments also confirmed that aggregation is not coincident with neuronal death and the visible accumulation of protein actually increases neuronal survival, potentially by decreasing the amount of soluble toxic Htt species (Arrasate *et al.*, 2004). Both, the solubilization of aggregating proteins and increasing visible aggregation of misfolded proteins by small molecule inhibitors relieved toxicity in HD models (Bodner *et al.*, 2006; Ehrnhoefer *et al.*, 2006). Similar results were obtained for the A β peptide and the human prion protein (Treusch *et al.*, 2009).

A recent landmark study was able to discern different types of aggregation in yeast cells (Kaganovich *et al.*, 2008). These aggregate types were termed IPOD (insoluble perivacuolar deposit) and JUNQ (juxtannuclear quality control). The JUNQ inclusion contains misfolded proteins that accumulate upon compromised maturation of proteins, whereas the IPOD will form from proteins previously located to the JUNQ or disease-causing proteins like polyQs. It is furthermore noteworthy, that proteins directed to the JUNQ are highly ubiquitinated and this is required for the formation of the quality control compartment, whereas IPOD proteins are not ubiquitinated and the formation of the compartment is independent of the ubiquitin proteasome system (UPS). The location of the IPOD next to the vacuole may hint to autophagic pathways as subsequent detoxification or protein removal strategies. The localized deposition enables targeted bulk degradation by autophagy, a system responsible to recycle large parts of bulk cytoplasm or organelles (Taylor *et al.*, 2003; Wigley *et al.*, 1999). Structures resembling multilamellar autophagosomes were found in degenerating neurons (Mayer *et al.*, 1989; Okamoto *et al.*, 1991) and cells exposed to proteasome inhibitors or expressing aggregation prone proteins (Johnston *et al.*, 1998; Wojcik *et al.*, 1996).

Neuronal cells either are incapable to deploy protein folding rescue mechanisms fully, or exhibit a specific sensitivity towards the aggregates' or aggregation prone protein's interference with certain cellular processes and may consequently be more susceptible to cytotoxicity of any species, be it monomer, oligomer or aggregate.

2 Models for protein aggregation and chaperone networks

To study the cell biology of chaperones and aggregation, different eukaryotic model systems have been established before. Here, the results from *in vivo* studies with high relevance to this work will be discussed.

Hsp90 models

Hsp/Hsc90 is essential in eukaryotes. Its function in an organismal context has been under scrutiny in several organisms, but the analysis of this chaperone system in higher organisms is difficult, as in vertebrates the disruption of Hsp90's function leads to lethal damage during early development (Voss *et al.*, 2000; Yeyati *et al.*, 2007). Consequently, most of our knowledge on Hsp90s from these organisms is derived from cell culture and *in vitro* studies.

The sequence of Hsp90 proteins is highly conserved across eukaryotic species. As a matter of fact, homologues from yeast to human can be assigned unambiguously (Pearl & Prodromou, 2006). The same holds true for the canonical cochaperones (Haslbeck *et al.*, 2012). Despite high homologies, the number of paralogues found in one organism varies considerably. Mammals and yeast possess two differentially regulated isoforms of Hsp90 (Borkovich *et al.*, 1989). *Danio rerio* exhibits three paralogues, whereas *C. elegans* and *Drosophila melanogaster* contain only one gene encoding an Hsp90 protein.

Studies in *D. melanogaster* illustrated that a plethora of phenotypes may appear when Hsp90 is inhibited pharmaceutically during embryogenesis (Rutherford & Lindquist, 1998). Despite being essential for proper overall organismal development in vertebrates, studies on the nature of the developmental defects upon Hsp90 depletion have uncovered its requirement for the proper formation of muscle structures. When Hsp90a.1 was knocked down in zebrafish embryos, the formation of the myofibrillar ultrastructure was strongly compromised. This effect was phenocopied by a knockdown of its potential cofactor Unc-45 (Du *et al.*, 2008). Unc-45 is considered to be a cofactor of Hsp90 due to the presence of a TPR-domain. It also contains a myosin II interacting UCS domain, and has consequently previously been suspected to facilitate the folding process of the myosin head domain, potentially by the recruitment of Hsp90. Unc-45 depletion in fruit flies and the overexpression of Unc-45b also lead to irregularities in their myofibrillar organization (Bernick *et al.*, 2010; Lee *et al.*, 2011). In nematodes, solely UNC-45 was shown to be associated with muscle thick filaments and required for muscle development (Ao & Pilgrim, 2000; Epstein & Thomson, 1974; Venolia & Waterston, 1990), more specifically for thick filament assembly (Barral *et al.*, 1998).

The only protein homologous to Hsp90 that may be discerned in worms is DAF-21. This protein to date has been described to be essential for proper gonadal and vulval development as well as oocyte maturation (Gaiser *et al.*, 2009; Gillan *et al.*, 2009; Inoue *et al.*, 2006). It is interesting to note that a protruding vulva phenotype is induced by the downregulation of Hsc90. A similar phenotype is obtained, when specific kinases and kinase associated proteins are depleted. This implies that the effects of Hsp90 downregulation are also related to its capacity to aid kinase maturation (Ceron *et al.*, 2007). However, neither the contribution of DAF-21 to the formation of the muscular ultrastructure nor its mechanistic aspects have been under scrutiny before.

Another aspect of chaperone biology may be considered relevant. In yeast, most of the factors of the Hsp90 system are expressed within a single cell, albeit at different levels (Eisen *et al.*, 1998). Expression or protein levels are not uniform among tissues of the metazoan model systems or humans. In zebrafish and fruit flies, Hsp90 and its cofactors are expressed at varying levels at almost every developmental stage and in various organs. As these organs are usually composed of different cell types, it is hard to discriminate whether specific chaperone or cochaperone requirements are organ or cell-type specific (Haslbeck *et al.*, 2012). For nematodes, an individual expression pattern for most of the Hsp90 cofactors can be discerned (Dupuy *et al.*, 2007).

To be able to understand the Hsp90 system in one single organism from *in vivo* and *in vitro* perspectives, a holistic approach, trying to assemble biochemical data on Hsp90's mechanism, its cofactor interactions, their expression patterns and the phenotypic consequences on the development and maintenance of the organism from interfering with parts of the system is missing. As a consequence, studying the Hsp90 system of *C. elegans* should provide an ideal model to gain a more profound understanding on the specific requirements of cell types in respect to this chaperone machinery and how this relates to the protein's biochemistry.

Hsp70 models

Hsp/Hsc70 has a versatile chaperone function within the cell. The acceleration of the ATPase cycle of Hsc70 through J proteins and NEFs has been described for the bacterial system consisting of DnaK, DnaJ and GrpE, (Jordan & McMacken, 1995; Liberek *et al.*, 1991; Packschies *et al.*, 1997; Pierpaoli *et al.*, 1997; Szabo *et al.*, 1994) as well as the eukaryotic system comprising Hsp70, Hsp40 and Bag1 (Hohfeld & Jentsch, 1997). For bacteria, the whole system consisting of DnaK, DnaJ and GrpE is required to efficiently refold substrate proteins (Brehmer *et al.*, 2001; Schroder *et al.*, 1993; Szabo *et al.*, 1994). It is notable though, that in eukaryotes the influence of Bag1 and other NEFs in the folding process has been reported to be (paradoxically) both unfavorable (Bimston *et al.*, 1998; Takayama *et al.*, 1997) or supportive (Gassler *et al.*, 2001; Tzankov *et al.*, 2008).

Yeast possesses four homologues of Hsc70; two of them, namely SSA1 and SSA2, are expressed at normal growth temperature and correspond to Hsc70, whereas the other two, SSA3 and SSA4, are expressed in response to heat stress and correspond to Hsp70. The knockout of both SSA1 and SSA2 is lethal at elevated temperatures (Craig & Jacobsen, 1984). However, it is complicated to analyze the Hsp70/Hsc70 system in yeast due to the genetic redundancy.

In *C. elegans*, only one Hsc70-like protein is found: HSP-1 (referred to as CeHsc70). The three Hsp70-proteins (HSP-70, F44E5.4, F44E5.5) are known to be exclusively expressed in response to heat-shock (Gaiser *et al.*, 2011; GuhaThakurta *et al.*, 2002). The knockdown of CeHsc70 through RNAi leads to increased protein aggregation (Nollen *et al.*, 2004) and an arrested development at early larval stages (Gaiser *et al.*, 2009; Kamath *et al.*, 2003) confirming that it is essential for development.

In addition to the Hsp70-like proteins mentioned above, a mitochondrial isoform (HSP-6), two ER isoforms (HSP-3 and HSP-4) and one ribosomally associated isoform (F11F1.1) may be discerned in *C. elegans* (Heschl & Baillie, 1990). For the sole and essential CeHsc70 protein, only few studies provide biochemical and structural data (Gaiser *et al.*, 2009; Worrall &

Introduction

Walkinshaw, 2007). The CeHsc70 system is also peculiar in respect to BAG-1, which seems to be shortened and only distantly related to human Bag1 (Symersky *et al.*, 2004; Wormbase). The only Sis1 (or DNAJB) homolog in worms is DNJ-13. It appears to be essential (Wormbase).

The mammalian Hsp70/Hsc70 system is extremely complex due to a large amount of genes that are significantly homologous to Hsp70, J-domain proteins and NEFs (Hageman & Kampinga, 2009).

As *C. elegans* is a well-studied model system in terms of its genetics and development, a detailed *in vitro* and *in vivo* analysis of the function of Hsc70 should provide information on the evolution of this chaperone machinery.

Aggregation models

To date, more than 45 metazoan model systems for neuronal degeneration diseases have been established in *C. elegans*, *D. rerio*, *D. melanogaster*, *Mus musculus*, and *Rattus norvegicus* (Gama Sosa *et al.*, 2012). In this section, only models for HD and FALS will be discussed as they are most clearly related to the aggregation of mutant Htt and Sod1, respectively.

In mouse, currently one single model is available for ALS. It is based on transgenic animals, expressing the human Sod1 mutant G93A. Those mice develop progressive motor neuron disorder associated with limb paralysis and death at an age of 5 to 6 months (Gurney *et al.*, 1994). This system exhibits mitochondrial degeneration and a compromised ER in spinal cord neurons as well as aggregate formation, reiterating hallmarks of human pathology. For HD, four models have been created in *M. musculus* by different transgenesis approaches. All of these models are based on either full length Htt or Htt exon 1 with expanded GAG repeats (Gray *et al.*, 2008; Hodgson *et al.*, 1999; Mangiarini *et al.*, 1996; White *et al.*, 1997). All of these systems reproduce neurodegeneration, albeit to a different extent.

In zebrafish, no Sod1 based model for ALS is available. The photoreceptor-directed expression of Htt exon1 with 71Q fused to EGFP resulted in aggregation of the fusion protein and degeneration of rod shaped photoreceptors (Williams & Paulson, 2008).

Furthermore, the motorneuron and photoreceptor-specific expression of wildtype (WT) and mutant human Sod1 in fruit flies both led to progressive motorneuron dysfunction, but mutant-specific degeneration was also observed (Parkes *et al.*, 1998). For HD, the two models established in *D. melanogaster* confirmed a neurodegenerative effect of extended polyQ stretches in the context of human Htt. Also, intranuclear Htt was detected preceding neurodegeneration (Jackson *et al.*, 1998). It was also shown that a knockout of the drosophila homolog of HTT led to reduced mobility, longevity and altered axonal complexity (Zhang *et al.*, 2009).

In *C. elegans*, an age-dependent dysfunction of sensory neurons was observed for a HTT-150Q construct (Faber *et al.*, 1999). A genome-wide RNAi screen for modifiers of aggregation behavior in worms expressing a 'naked' polyQ (Q40-YFP) revealed genes of the protein folding and degradation machineries to increase aggregation occurrence upon their knockdown (Nollen *et al.*, 2004). A model for the toxicity of human Sod1 was also established. Pan-neuronal expression of the mutant Sod1G85R resulted in aggregation and locomotion defects, presumably

mediated through a reduced number of neuromuscular junctions and synaptic vesicles. A whole-genome RNAi screen revealed a group of chaperones, as well as proteins responsible for protein modification and degradation to suppress neuronal aggregation of Sod1G85R-YFP.

As the systems described above are difficult to manipulate and *in vivo* data acquisition is limited due to the heterogeneity of organs with respect to cell types, specific questions concerning basic cellular biological processes are usually addressed in cell cultures, using human cell lines. In this system, it has been shown that polyQ proteins form perinuclear inclusions that are cytotoxic. These aggregates are dynamic protein assemblies (Kim *et al.*, 2002). Toxicity and aggregation can be inhibited by Hsp40 proteins (DNAJB6 and DNAJB8) (Hageman *et al.*, 2010), as well as CCT (Kitamura *et al.*, 2006; Tam *et al.*, 2006). Aggregation is further inhibited by overexpression of the Hsp70 dependent ubiquitin ligase CHIP (Jana *et al.*, 2005) and Hsp27 (HSPB1) (Wytttenbach *et al.*, 2002) or Hsp22 (HSPB8) (Carra *et al.*, 2008).

The simplest and genetically most easily accessible model organism is *S. cerevisiae*. As a matter of fact, two systems for polyQ aggregation have been established. Using these systems, genome-wide screens were performed. One system, established by the Hartl lab in 1999, consisted of non-toxic constructs of Htt exon 1 with 20 or 53 glutamine residues (HD20Q and HD53Q). HD53Q proved to be aggregation prone. Hsp70 and Hsp40 inhibited the aggregation of HD53Q (Muchowski *et al.*, 2000). Using a genome-wide approach, this system was subsequently exploited to uncover genes that are responsible to suppress the toxicity intrinsic to HD53Q (suppressors of toxicity). Stress response genes, genes associated to protein folding and ubiquitin-dependent protein catabolism were significantly enriched in comparison to the library (Willingham *et al.*, 2003). In a second genome-wide approach, the toxic variant Htt103Q was used to screen for genes that help to establish the toxicity (enhancers of toxicity). The system revealed contributions of proteins involved in vesicular transport and transcription, prion proteins and most notably the kynurenine synthesis pathway. It suggested that the levels of neurotoxic 3-hydroxykynurenine and quinolic acid are increased in brains of HD patients by the expression of mutant Htt (Giorgini *et al.*, 2005). Later studies showed the toxicity of this Htt fragment in yeast to be highly dependent on its flanking sequences and endogenous prions, which need to be present in their insoluble prion conformation to obtain Htt toxicity (Duennwald *et al.*, 2006a; Duennwald *et al.*, 2006b).

Despite the diverse approaches to study neurodegeneration in different systems, in yeast a system that is comparable to the bare polyQ stretch used in some nematode studies is missing. For FALS no yeast model based on Sod1 mutants has been published.

3 Aims of this work

As previously stated, the protein folding machinery and the control of cellular aggregation processes are tightly interwoven. It is yet unclear to what extent both processes exactly influence each other. Consequently, this work should contribute to the understanding of their interfaces on different levels.

The chaperone biology of yeast and mammals has been under intense scrutiny and most of our current knowledge is derived from the study of these organisms. As yeast is a unicellular organism, the regulation of chaperone activity is restricted to the temporal axis. In mammals, due to their organismal complexity most mechanistic knowledge is derived from studies of bulk tissue samples or cell culture, consequently, little is known about the spatio-temporal change of chaperone requirements in more complex organisms. However, there are hints from expression analysis, that on the organ level, the expression of chaperone genes is divergent. It is hard to examine, whether these expression differences are also observed on a protein level. Furthermore, tissues of mammals are highly complex assemblies of different cell types. Thus, the analysis of chaperone levels due to potentially increased requirements for folding capacity in a specific cell type is hard to perform and tissue-specific effects difficult to perceive. A system that has proven valuable to understand developmental processes is *C. elegans*. It is therefore obvious to deploy this organism to study which cell types exhibit a specific requirement for certain classes of chaperones due to a specialized composition of their subproteome. These requirements may also change during the ontogenesis of the organism and this simple metazoan system should shed light on how chaperone systems (number of homologous chaperones, cofactors and their spatial expression pattern) evolved during phylogenesis, once the situation in mammals is dissected more clearly.

The aggregation of neurodegeneration-associated proteins has been largely studied in cells, *post mortem* human tissue samples and a vast amount of animal models. There are a handful of models available in yeast and worms. As aggregation toxicity should be a conserved cellular effect, studying cytotoxicity should be possible in simple organisms. An approach to establish such systems was already taken for Htt in yeast and worms as well as for Sod1 mutants in worms. The current models for Htt aggregation in yeast are – in terms of toxicity – highly dependent on the presence of the endogenous prion phenotype. Consequently, to re-establish a system previously deployed in *C. elegans* will help to understand whether the factors governing aggregation or aggregation toxicity are similar in unicellular organisms and metazoans. The same is valid for an FALS model based on Sod1 mutants in yeast.

Both approaches combined will lead to an understanding of

the phylogenetic development of chaperone systems, safeguarding proteomes

the cellular factors required for the suppression or development of folding disease

the extent of the regulation of aggregation processes by chaperones

C Materials and Methods

1 Materials

1.1 Reagents

If not stated adversely, the chemicals deployed in this study were of the highest purity available. All solutions were prepared using highly purified water (ddH₂O).

Reagent	Distributor
1,4-Dithiothreitol (DTT)	Roth (Karlsruhe, Germany)
2,3,5-triphenyltetrazolium chloride (TTC)	Sigma (St. Louis, USA)
5-(and-6)-carboxyfluorescein succinimidylester	Life Technologies (Darmstadt, Germany)
5-Fluoroorotic acid (5-FOA)	Fermentas (St. Leon-Rot, Germany)
Acetic acid	Roth (Karlsruhe, Germany)
Acrylamide/Bis Solution, 19:1 (40% w/v)	Serva (Heidelberg, Germany)
Adenine	Sigma (St. Louis, USA)
Agar-Agar for microbiology	Merck (Darmstadt, Germany)
Agarose	Serva (Heidelberg, Germany)
Albumin, bovine serum (BSA)	Sigma (St. Louis, USA)
Alexa Fluor 488 C ₅ -maleimide	Life Technologies (Darmstadt, Germany)
Ampicillin sodium salt	Roth (Karlsruhe, Germany)
Arginine	Sigma (St. Louis, USA)
Aspartic acid	BD (Franklin Lakes, USA)
Bacto-tryptone	Difco (Detroit, USA)
Bromphenol blue S	Serva (Heidelberg, Germany)
Calcium chloride dihydrate	Merck (Darmstadt, Germany)
Citric acid	Roth (Karlsruhe, Germany)
Coomassie Protein Assay Reagent	Pierce (Rockford, USA)
Coomassie Brilliant-Blue R250	Serva (Heidelberg, Germany)
Desoxyribonucleotidetriphosphate (dNTP)	Roche (Mannheim, Germany)
Dimethyl sulfoxide (DMSO)	Sigma (St. Louis, USA)
Dipotassium phosphate (K ₂ HPO ₄)	Merck (Darmstadt, Germany)
Disodium phosphate (Na ₂ HPO ₄)	Sigma (St. Louis, USA)
DNA-Stain G	Serva (Heidelberg, Germany)
Ethanol for analysis	Merck (Darmstadt, Germany)
Ethylenediaminetetraacetic acid (EDTA)	Merck (Darmstadt, Germany)
Formaldehyde (37% (w/v))	Sigma (St. Louis, USA)
G418, disulfide salt	Sigma (St. Louis, USA)
Galactose	Sigma (St. Louis, USA)
Glucose	Serva (Heidelberg, Germany)
Glycerol, 99% (v/v)	Roth (Karlsruhe, Germany)
Glycine	Sigma (St. Louis, USA)
Guanidinium chloride (GdnHCl)	Merck (Darmstadt, Germany)

Materials and Methods

Guanidinium chloride (GdnHCl) spectroscopic	Sigma (St. Louis, USA)
Histidine	Sigma (St. Louis, USA)
Hydrochloric acid	Merck (Darmstadt, Germany)
Isopropanol	Roth (Karlsruhe, Germany)
LB-Medium	Serva (Heidelberg, Germany)
Leucine	Sigma (St. Louis, USA)
Lithium acetate (LiOAc)	Roth (Karlsruhe, Germany)
Lysine	Sigma (St. Louis, USA)
Magnesium sulfate	Sigma (St. Louis, USA)
Methanol	Roth (Karlsruhe, Germany)
Methionine	Sigma (St. Louis, USA)
Milk powder	Roth (Karlsruhe, Germany)
Monopotassium phosphate (KH ₂ PO ₄)	Sigma (St. Louis, USA)
Phenylalanine	Sigma (St. Louis, USA)
Polyethyleneglycol 4000 (PEG4000)	Merck (Darmstadt, Germany)
Potassium chloride	Roth (Karlsruhe, Germany)
Propidium iodide	Sigma (St. Louis, USA)
Protease Inhibitor Cocktail FY	Serva (Heidelberg, Germany)
Protease Inhibitor Cocktail HP	Serva (Heidelberg, Germany)
Roti-phenol	Roth (Karlsruhe, Germany)
Silicone grease, high vacuum	Wacker (Burghausen, Germany)
Sodium azide	Merck (Darmstadt, Germany)
Sodium chloride	Merck (Darmstadt, Germany)
Sodium dodecyl sulfate (SDS)	Serva (Heidelberg, Germany)
Sodium hydroxide	Roth (Karlsruhe, Germany)
Sodium thiosulfate (Na ₂ S ₂ O ₃)	Merck (Darmstadt, Germany)
Sodium carbonate	Merck (Darmstadt, Germany)
ssDNA from salmon testes (Carrier DNA)	Sigma (St. Louis, USA)
Sypro Orange	Life Technologies (Darmstadt, Germany)
Threonine	Sigma (St. Louis, USA)
Trichloro acetic acid (TCA)	Roth (Karlsruhe, Germany)
Tris(hydroxymethyl)aminomethane	Roth (Karlsruhe, Germany)
Trisodium citrate	Sigma (St. Louis, USA)
Tryptophan	Sigma (St. Louis, USA)
Tween 20	Merck (Darmstadt, Germany)
Tyrosine	Sigma (St. Louis, USA)
Uracil	Sigma (St. Louis, USA)
Yeast Nitrogen Base	BD (Franklin Lakes, USA)
YPD-Medium	Roth (Karlsruhe, Germany)
α -chymotrypsin	Sigma (St. Louis, USA)
β -mercaptoethanol	Sigma (St. Louis, USA)

Table 2: Reagents.

1.2 Buffers

Name	Substance	Amount/Conc.
DNA loading buffer (10x)	Glycerol	50% (v/v)
	EDTA/NaOH (pH 8.0)	10 mM
	Bromphenol blue S	0.2% (w/v)
	Xylene cyanol	0.2% (w/v)
FACS normalization buffer	Trisodium citrate (pH 7.0)	50 mM
	Sodium azide	0.01% (w/v)
Yeast preparation buffer	Tris/HCl (pH 7.5)	100 mM
	NaCl	50 mM
Fairbanks A	Coomassie Brilliant-Blue R250	0.05% (w/v)
	Isopropanol	25% (v/v)
	Acetic acid	10% (v/v)
Fairbanks D	Acetic acid	10% (v/v)
Laemmli sample buffer (5x)	Tris/HCl (pH 6.8)	312.5 mM
	SDS	10% (w/v)
	β -mercaptoethanol	25% (w/v)
	Glycerol	50% (w/v)
	Bromphenol blue S	0.05% (w/v)
NAGE loading buffer (5x)	Tris/HCl (pH 8.3)	32 mM
	Glycerol	50% (v/v)
	Bromphenol blue S	0.1% (w/v)
NAGE running buffer	Glycine	190 mM
	Tris	25 mM
PBS pH 7.4 (10x)	KH_2PO_4	40 mM
	$\text{Na}_2\text{HPO}_4 \cdot 2 \text{H}_2\text{O}$	160 mM
	NaCl	1.15 M
PBST	1x PBS	
	Tween 20	0.1% (v/v)
PLATE mix	sterile PEG4000	40% (w/v)
	LiOAc	100 mM
	Tris/HCl (pH 7.5)	10 mM
	EDTA	1 mM
SDS running buffer (10x)	Tris/HCl (pH 6.8)	250 mM
	Glycine	2.0 M
	SDS	1% (w/v)
Separating gel buffer (4x)	Tris/HCl (pH 8.8)	1.5 M
	SDS	0.8% (w/v)
Stacking gel buffer (2x)	Tris/HCl (pH 6.8)	250 mM
	SDS	0.4% (w/v)
M9 buffer	KH_2PO_4	3 g/l
	Na_2HPO_4	6 g/l

Materials and Methods

	NaCl	85 mM
	MgSO ₄	1 mM
TAE (50x)	Tris/Acetic acid (pH 8.0)	2.0 M
	EDTA	50 mM
Transfer buffer	Tris/HCl (pH 8.3)	25 mM
	Glycine	192 mM
	Methanol	20% (v/v)
	SDS	0.012% (w/v)
Blocking solution	Milk powder	5% (w/v)
	Tween 20	0.05% (v/v)
	in 1x PBS	
Soft agar freezing solution	NaCl	5.8 g/l
	KH ₂ PO ₄	6.8 g/l
	Glycerol	300 g/l
	1 M NaOH	5.6 ml/l
	Agar	4 g/l
Gel dry	Glycerol	2%
	Ethanol	35%
Yeast lysis buffer	Triton X-100	2%
	SDS	1%
	NaCl	100 mM
	EDTA	1 mM
	Tris/HCl (pH 8)	10 mM
TE buffer	EDTA	1 mM
	Tris/HCl (pH 7.4)	10 mM
Disruption buffer	HEPES/KOH (pH 7.5)	40 mM
	KCl	300 mM
Denaturing buffer	HEPES/NaOH (pH 7.5)	25 mM
	KCl	50 mM
	MgCl ₂	15 mM
	ATP	1 mM
	DTE	10 mM
	BSA	0.05 mg/ml
Luminescence buffer	GdnHCl	5 M
	HEPES/NaOH (pH 7.5)	25 mM
	KCl	50 mM
	MgCl ₂	15 mM
	ATP	1 mM
	DTE	2 mM
	BSA	0.05 mg/ml
	CoA	240 μM
	luciferin	0.1 mM
	PEP	10 mM
pyruvate kinase	50 μg/ml	

Measurement buffer	HEPES/KOH (pH 7.5)	40 mM
	KCl	150 mM

Table 3: Buffers.

1.3 Enzymes, kits and standards

Group	Name	Origin
Enzymes	GoTaq Polymerase	Promega (Fitchburg, USA)
	Phusion DNA-Polymerase	NEB (Frankfurt, Germany)
	Proteinase K	Sigma (St. Louis, USA)
	RNAse A	
Kits	ECL-Western blot Detection Kit	GE Healthcare (Munich, Germany)
	Wizard® Plus SV Minipreps DNA Purification System	Promega (Fitchburg, USA)
	Pure Yield® Midipreps DNA Purification System	
	Wizard® SV Gel and PCR Clean-Up System	
Standards	Precision Plus Protein Dual Color Standard	BioRad (Hercules, USA)
	SDS-PAGE Standard Low Weight	
	peqGOLD 1kb ladder OrangeG	Peqlab (Erlangen, Germany)
	Roti Mark pre-stained	Roth (Karlsruhe, Germany)

Table 4: Enzymes, kits and standards.

1.4 Antibodies

Name	Source	C _{ab}	C _{powder milk}	Origin
primary antibodies				
α-GFP	Goat	1:5k	1% (w/v)	Rockland (Gilbertsville, USA)
α-Hsp104	Rabbit	1:40k	10% (w/v)	Dr. J Pineda (Berlin, Germany)
α-Hsp90	Rabbit	1:80k	10% (w/v)	Dr. J Pineda (Berlin, Germany)
α-PGK [Monoclonal]	Mouse	1:15k	1% (w/v)	Invitrogen (Carlsbad, USA)
secondary antibodies				
α-Goat-Peroxidase	Sheep	1:100k	1% (w/v)	Sigma (St. Louis, USA)
α-Mouse-IgG-Peroxidase	Rabbit	1:15k	1% (w/v)	Sigma (St. Louis, USA)
α-Rabbit-Peroxidase	Goat	1:100k	1% (w/v)	Sigma (St. Louis, USA)

Table 5: Antibodies.

Materials and Methods

1.5 Equipment

Name	Origin
538 MultiCal pH-meter	WTW (Weilheim, Germany)
96-well plates	Sarstedt (Nümbrecht, Germany)
AUC fluorescence detection system	Aviv (Lakewood, USA)
BD FACSCalibur flow cytometer	Becton Dickinson (Franklin Lakes, USA)
Biometra Thermobloc TB1	Biometra (Göttingen, Germany)
Biotech Ultrospec 3000 UV/VIS-spectrophotometer	Amersham Pharmacia (Uppsala, Sweden)
Canon EOS 60D camera	Canon (Tokyo, Japan)
Certomat BS-1 culture shaker	Sartorius (Göttingen, Germany)
Certomat S incubator	Sartorius (Göttingen, Germany)
Cuvettes, half-micro	Sarstedt (Nümbrecht, Germany)
EPS 3500, 35001, 1001 power supply	GE Healthcare (Freiburg, Germany)
GeneChip Yeast Genome 2.0	Affymetrix (Santa Clara, USA)
Glass beads (0.5 ± 0.05 mm)	Roth (Karlsruhe, Germany)
Glass beads (4 ± 0.3 mm)	Roth (Karlsruhe, Germany)
Haake F6-K thermostat	Haake (Karlsruhe, Germany)
Heidolph polymax 2040 shaker	Heidolph (Kelheim, Germany)
Ice machine	Ziegler (Isernhagen, Germany)
Image Quant 300 imaging station	GE Healthcare (Freiburg, Germany)
MM400 bead mill	Retsch (Haan, Germany)
MR2000 magnetic stirrer	Heidolph (Kelheim, Germany)
Mx3000P qPCR system	Agilent (Santa Clara, USA)
Mytron Thermocabinet incubator	Mytron (Heilbad Heiligenstadt, Germany)
Nanodrop NP-1000 spectrophotometer	Peqlab (Erlangen, Germany)
Optimax TR developing unit	MS Laborgeräte (Heidelberg, Germany)
Pre-cast acrylamide gel 43221.00	Serva (Heidelberg, Germany)
Pre-cast acrylamide gel 43243	Serva (Heidelberg, Germany)
Primus 25 thermocycler	MWG (Ebersberg, Germany)
PVDF membranes	Roth (Karlsruhe, Germany)
REAX top vortex unit	Heidolph (Kelheim, Germany)
Reprokid camera stand	Kaiser Fototechnik (Buchen, Germany)
Sonorex RK100H ultrasonic probe	Bandelin electronic (Berlin, Germany)
Tecan GENios microplate reader	Tecan (Crailsheim, Germany)
Tecan Sunrise microplate reader	Tecan (Crailsheim, Germany)
Test tube roller	Heidolph (Kelheim, Germany)
Thermomixer	Eppendorf (Hamburg, Germany)
TS 0.75 cell disruptor	Constant Systems (Northhants, UK)
Typhoon 9200 multimode imager	GE Healthcare (Freiburg, Germany)
Ultra-low temperature freezer C760	New Brunswick (Nürtingen, Germany)
Varioklav EP-Z autoclave	H+P (Oberschleißheim, Germany)
Vortex MS2 vortex unit	IKA (Wilmington, USA)

Whatman 3MM filter paper	Merck (Darmstadt, Germany)
X-OMAT™ AR X-ray film	Kodak (Rochester, USA)
Centrifuges	
5415C tabletop centrifuge	Eppendorf (Hamburg, Germany)
Optima XL-A analytical ultracentrifuge	Beckman (Krefeld, Germany)
ProteomeLab XL-A analytical ultracentrifuge	Beckman Coulter (Brea, USA)
Universal 32R / Rotina 46R	Hettich (Tuttlingen, Germany)
Gel electrophoresis- and blotting	
Fast Blot B44 transfer unit	Biometra (Göttingen, Germany)
Hoefer Mighty Small electrophoresis unit	GE Healthcare (Freiburg, Germany)
Hoefer SE600 Ruby electrophoresis unit	GE Healthcare (Freiburg, Germany)
Microscopes	
Axiovert 200 inverted microscope	Carl Zeiss (Oberkochen, Germany)
MZ16FA stereo microscope	Leica Microsystems (Wetzlar, Germany)
Stemi stereo microscope	Carl Zeiss (Oberkochen, Germany)
TCS SP5 confocal microscope	Leica Microsystems (Wetzlar, Germany)
Scales	
1409MP halfmicroscales	Sartorius (Göttingen, Germany)
BL310 halfmicroscales	Sartorius (Göttingen, Germany)
BP121S analytical scales	Sartorius (Göttingen, Germany)
Chromatography Columns	
Ceramic fluorapatite 20 ml	BioRad (Hercules, USA)
DEAE-sepharose 30 ml	GE Healthcare (Freiburg, Germany)
HisTrap 5 ml	GE Healthcare (Freiburg, Germany)
ResourceQ 6 ml	GE Healthcare (Freiburg, Germany)
ResourceS 6 ml	GE Healthcare (Freiburg, Germany)
Superdex200 HiLoad	GE Healthcare (Freiburg, Germany)
Superdex75 HiLoad	GE Healthcare (Freiburg, Germany)

Table 6: Equipment.

Additional consumables were from VWR (Munich, Germany) or Sarstedt (Nümbrecht, Germany).

1.6 Strains and organisms

Strain	Genotype	Source
<i>E. coli</i>		
DH10B	F ⁻ <i>mcrA</i> Δ(<i>mrr-hsdRMS-mcrBC</i>) Φ80d <i>lacZ</i> ΔM15 Δ <i>lacX74 endA1 recA1 deoR</i> Δ(<i>ara,leu</i>)7697 <i>araD139 galU galK nupG rpsL</i> λ ⁻	Invitrogen (Carlsbad, CA, USA)
OP50	unknown	CGC (Minnesota, USA)
HT115(DE3)	F ⁻ <i>mcrA mcrB</i> IN(<i>rrnD-rrnE</i>)1 λ ⁻ <i>mrc14::Tn10</i>	CGC (Minnesota, USA)
BL21-CodonPlus-RIL	F ⁻ <i>ompT hsdS</i> (rB ⁻ mB ⁻) <i>dcm</i> ⁺ Tet ^r <i>gal</i> λ(DE3)	Merck (Darmstadt, Germany)

Materials and Methods

<i>endA</i> Hte [<i>argU ileY leuW Cam</i> ']		
<i>S. cerevisiae</i>		
BY4741	MAT a; <i>his3Δ1; leu2Δ0; met15Δ0; ura3Δ0</i>	
BY4742	MAT α; <i>his3Δ1; leu2Δ0; lys2Δ0; ura3Δ0</i>	(Brachmann <i>et al.</i> , 1998)
BY4743	MATα/α; <i>his3Δ0/0; leu2Δ0/0; met15Δ0/MET15; LYS2/lys2Δ0; ura3Δ0/0</i>	
Single ORF deletion strains	MATα; <i>his3Δ1; leu2Δ0; met15Δ0; ura3Δ0; ORF::kanMX4</i>	(Winzeler <i>et al.</i> , 1999)
PY4993	MATα/α; <i>his3Δ1/1; leu2Δ0/0; met15Δ0/MET15; LYS2/lys2Δ0; ura3Δ0/0</i>	(Storchova <i>et al.</i> , 2006)
PY4994	MATα/α; <i>his3Δ1/1; leu2Δ0/0; met15Δ0/MET15; LYS2/lys2Δ0; ura3Δ0/0</i>	
PY4995	MATα/a; <i>his3Δ1/1; leu2Δ0/0; met15Δ0/MET15; LYS2/lys2Δ0; ura3Δ0/0</i>	
PY5006	MATα/a/a/a; <i>his3Δ1/1/1/1; leu2Δ0/0/0/0; met15Δ0/0/MET15/MET15; LYS2/LYS2/lys2Δ0/0; ura3Δ0/0/0/0</i>	(Storchova <i>et al.</i> , 2006)
PY5007	MATα/a/a/a; <i>his3Δ1/1/1/1; leu2Δ0/0/0/0; met15Δ0/0/MET15/MET15; LYS2/LYS2/lys2Δ0/0; ura3Δ0/0/0/0</i>	
<i>C. elegans</i>		
N2	<i>WT</i>	CGC (Minneapolis, USA)
JT6130	<i>daf-21(p673)</i>	CGC (Minneapolis, USA)
AM134	<i>rmls126</i>	Richard I. Morimoto
RW1596	<i>myo-3(st386)</i>	CGC (Minneapolis, USA)
BC10293	<i>sEx10293</i>	CGC (Minneapolis, USA)
Hsp70-GFP	<i>C12C8.1::GFP</i>	Richard I. Morimoto
EY0986 CDC10-GFP	MATα <i>his3Δ1 leu2Δ0 met15Δ0 ura3Δ0 CDC10::GFP-HIS3MX6 (S288C)</i>	(Huh <i>et al.</i> , 2003)
EY0986 NUD1-GFP	MATα <i>his3Δ1 leu2Δ0 met15Δ0 ura3Δ0 NUD1::GFP-HIS3MX6 (S288C)</i>	(Huh <i>et al.</i> , 2003)
EY0986 TUB1-GFP	MATα <i>his3Δ1 leu2Δ0 met15Δ0 ura3Δ0 TUB1::GFP-HIS3MX6 (S288C)</i>	(Huh <i>et al.</i> , 2003)

Table 7: Strains and Organisms.

1.7 Plasmids

Name	Selection marker	Origin
p425 GPD	Amp, Leu2	(Mumberg <i>et al.</i> , 1995)
p425 GPD SODA4V-YFP	Amp, Leu2	Christoph Kaiser
p425 GPD SODG85R-YFP	Amp, Leu2	Christoph Kaiser
p425 GPD SODG93A-YFP	Amp, Leu2	Christoph Kaiser
p425 GPD SODL126X-YFP	Amp, Leu2	Christoph Kaiser
p425 GPD SODWT-YFP	Amp, Leu2	Christoph Kaiser
p426 GPD	Amp, Ura3	(Mumberg <i>et al.</i> , 1995)
p426 GPD Atg16-CFP	Amp, Ura3	Christoph Kaiser

p426 GPD CFP	Amp, Ura3	Christoph Kaiser
p426 GPD Cox4-CFP	Amp, Ura3	Christoph Kaiser
p426 GPD OM45-CFP	Amp, Ura3	Christoph Kaiser
p426 GPD Sis1-CFP	Amp, Ura3	Christoph Kaiser
p426 GPD Ssa3-CFP	Amp, Ura3	Christoph Kaiser
p426 GPD Vps4-CFP	Amp, Ura3	Christoph Kaiser
p426 GPD Ydj1-CFP	Amp, Ura3	Christoph Kaiser
pQ0	Amp, Leu2	Christoph Kaiser
pQ0cherry	Amp, Leu2	Christoph Kaiser, Julia Eckl
pQ30	Amp, Leu2	Christoph Kaiser
pQ30cherry	Amp, Leu2	Christoph Kaiser, Julia Eckl
pQ56	Amp, Leu2	Christoph Kaiser
pQ56Cherry	Amp, Leu2	Christoph Kaiser, Julia Eckl
pYES2 103Q	Amp, Ura3	Michael Sherman
pYES2 25Q	Amp, Ura3	Michael Sherman

Table 8: Plasmids.

1.8 Oligonucleotides

All used oligonucleotides were ordered from MWG Eurofins (Ebersberg, Germany).

Nucleotide Name	Sequence	Application
<i>act-1</i> FWD	AAT CCA AGA GAG GTA TCC TTA	RT-QPCR
<i>act-1</i> REV	GAT GGC GAC ATA CAT GGC	RT-QPCR
<i>daf-21</i> FWD	AAG ATG AGG AGG CTG TCG A	RT-QPCR
<i>daf-21</i> REV	CAT TGG ACA AGC TCT TGT AGA	RT-QPCR
DNtag D1	CGG TGT CGG TCT CGT AG	KO verification
GATC-GPD_FW-228935	AAA GAC GGT AGG TAT TG	Sequencing
<i>hsp-1</i> FWD	CAC TGT TTT CGA TGC CAA AC	RT-QPCR
<i>hsp-1</i> REV	TCT CCT TCA TCT TCA GCA AAA	RT-QPCR
<i>hsp-16.11</i> FWD	TCT GAA TCT TCT GAG ATT GTT AA	RT-QPCR
<i>hsp-16.11</i> REV	CTT CTG AAA GAT TTG AAG CAA CT	RT-QPCR
<i>hsp-70</i> FWD	TTT CAA TGG GAA GGA CCT CAA	RT-QPCR
<i>hsp-70</i> REV	TTG GAA GCT TTG GCA GGA ATT	RT-QPCR
KanB	CTG CAG CGA GGA GCC GTA AT	Sequencing
MAT a	ACT CCA CTT CAA GTA AGA GTT TG	MAT verification
MAT locus	AGT CAC ATC AAG ATC GTT TAT GG	MAT verification
MAT α	GCA CGG AAT ATG GGA CTA CTT CG	MAT verification
pEGFP-N	CCG TCC AGC TCG ACC AG	Sequencing
<i>pgk-1</i> FWD	TTT GAT CCG TGT TGA CTT CAA T	RT-QPCR
<i>pgk-1</i> REV	GAA GAG AAC ATC TTT TTT CAA GA	RT-QPCR
UPtag U1	GAT GTC CAC GAG GTC TCT	KO verification

Table 9: Oligonucleotides.

Materials and Methods

1.9 Media

Name	Substance	Amount / Conc.
SMM	YNB	6.7 g
	selective amino acid mixture*	1000 mg
	glucose / galactose	20 g
	ddH ₂ O	ad 1 l
	for plates	20 g agar
NGM	NaCl	3 g
	peptone	2.5 g
	agar	17 g
	ddH ₂ O	ad 1 l
	add after autoclaving	
	1 M CaCl ₂	1 ml
	5 mg/ml cholesterol	1 ml
	1M MgSO ₄	1 ml
1 M KPO ₄ (pH 6.0)	25 ml	
LB	LB medium	20 g/l
	for plates	20 g/l agar
YPD	YPD medium	50 g/l
	for plates	20 g/l agar

Table 10: Media.

The amino acid mixtures mentioned in Table 10 (indicated by the asterisk) have been prepared according to Table 11.

Name	CSM	SM
Adenine	0.5 g	0.5 g
Alanine	2.0 g	
Arginine	2.0 g	2.0 g
Asparagine	2.0 g	
Aspartic acid	2.0 g	2.0 g
,Cysteine	2.0 g	
Glutamine	2.0 g	
Glutamic acid	2.0 g	
Glycine	2.0 g	
Histidine	2.0 g	2.0 g
Inositol	2.0 g	
Isoleucine	2.0 g	
Leucine	10.0 g	10.0 g
Lysine	2.0 g	2.0 g
Methionine	2.0 g	2.0 g

<i>para</i> -Aminobenzoic acid	0.2 g	
Phenylalanine	2.0 g	2.0 g
Proline	2.0 g	
Serine	2.0 g	2.0 g
Threonine	2.0 g	2.0 g
Thryptophan	2.0 g	2.0 g
Tyrosine	2.0 g	
Uracil	2.0 g	2.0 g
Valine	2.0 g	

Table 11: Composition of amino acid mixtures.

The amino acids were triturated in a MM400 bead mill for 10 min at 30 Hz.

1.10 Computer programs and databases

Name	Origin
Programs	
ApE (a plasmid editor) [V2.0.37]	Freeware, http://biologylabs.utah.edu/jorgensen/wayned/ape/
BD FACSCalibur Application software	Becton Dickinson (Heidelberg, Germany)
Cytoscape [V2.8.2]	Freeware, http://www.cytoscape.org
ImageQuant 300	GE Healthcare (Munich, Germany)
Leica Application Suite [LAS]	Leica Microsystems (Wetzlar, Germany)
MacBiophotonics ImageJ [V1.43m]	Freeware, http://www.macbiophotonics.ca/downloads.htm
Microsoft Office 2007	Microsoft (Unterschleißheim, Germany)
Oligo Analyzer [V1.5]	Freeware, http://www.genelink.com/tools/gl-downloads.asp
OriginPro8	OriginLab (Northampton, USA)
FlowJo	Tree Star (Ashland, USA)
Adobe Illustrator CS3	Adobe (San Jose, USA)
Databases	
BLAST	http://blast.ncbi.nlm.nih.gov/Blast.cgi
Euroscarf	http://web.uni-frankfurt.de/fb15/mikro/euroscarf/yeast.html
ExpASy	http://expasy.org/
GeneDB [V2.1]	http://old.genedb.org/
Protein data base (PDB)	http://www.rcsb.org/pdb/home/home.do
Saccharomyces genome database	http://www.yeastgenome.org/
Spell [V2.0.3]	http://spell.yeastgenome.org/
String [V9.0]	http://string-db.org/
Wormbase	http://www.wormbase.org/

Table 12: Computer programs and databases.

2 Methods

2.1 *Escherichia coli*

2.1.1 Cultivation and storage

E. coli strains were cultivated at 37 °C on LB₀-Plates in 5 - 50 ml LB₀ solution. Selection was achieved by the addition of the appropriate antibiotic. Plates and liquid cultures were stored at 4 °C for short terms. For long term storage, 500 µl of an exponentially growing culture were mixed with 1000 µl of 45% (v/v) glycerol. This solution was frozen in liquid N₂ and stored at -80 °C.

2.1.2 Transformation

Plasmids were transformed into chemically competent DH10B cells. Frozen aliquots were thawed on ice and 100-500 ng of plasmid DNA were added. After incubation for 15 min on ice, cells were heat shocked for 1 min at 42 °C and incubated on ice for 1 min. Fresh LB₀ medium was added and cells were plated on LB agar containing the appropriate antibiotic after 30 min of regeneration at 37 °C. Cultures were incubated at 37 °C over night.

2.2 *Saccharomyces cerevisiae*

2.2.1 Cultivation and storage

S. cerevisiae WT or knockout strains were cultivated at 30 °C in YPD medium. The antibiotic G418 (Geneticin) (Davies & Jimenez, 1980) was added when required.

Strains transformed with plasmids were grown on appropriate SM media plates or in SMM 5 ml liquid culture supplemented with all essential amino acids except for the selection marker encoded on the plasmid. All carbon sources were added at a concentration of 2% (w/v). If not otherwise stated, the carbon source was glucose.

Yeast cultures were stored for short terms at 4 °C. For long term storage, 500 µl of fresh stationary culture were mixed with 1 ml of 45% (w/v) glycerol. Alternatively, cultures were scraped from fresh plates and directly resuspended in 15% (w/v) glycerol solution. Cryo-vials containing yeast stocks were frozen in liquid N₂ and stored at -80 °C.

Glycerol stocks in a 96-well format were prepared analogously. 50 µl of fresh stationary culture were added to round-bottom plates containing 100 µl of 45% (w/v) glycerol solution. Plates were covered with aluminum seals and frozen on dry ice or at -80 °C.

2.2.2 Transformation

Yeast transformations were performed using an adapted version of the simplified lithium acetate yeast transformation method (Elble, 1992). The same transformation protocol was deployed for single tube transformations as well as transformations in a 96-well format. For single tube transformations the plasmid was added before PLATE/DNA/DTT, for 96-well transformations, the plasmid was added directly to the PLATE/DNA/DTT mixture. Transformations were carried out according to the subsequent protocol:

Materials and Methods

1. Grow cells for 2 d at 30 °C
2. Transfer 200 μ l o to reaction tube or well
3. Centrifuge for 10 min (96-well) or 1 min (single tube) at maximum speed
4. Discard supernatant
5. Add plasmid (for single well/tube transformations)
6. Add 150 μ l of PLATE/DNA/DTT or PLATE/DNA/DTT/Plasmid (cf. Table 13)
7. Resuspend pellet thoroughly
8. Incubate at room temperature for ~16 hours
9. Heat shock for 1 h at 42 °C
10. Plate transformation mixture onto appropriate medium
11. Incubate at 30 °C

Transformation mixture

<i>150μl PLATE per transformation (cf. Table 3) supplemented with (final concentration)</i>	
Salmon testes DNA	5.1 μ g/ml
DTT	0.4mM
Plasmid DNA	100ng

Table 13: Transformation mixture.

For plating, 9 to 11 glass beads (0.5 ± 0.05 mm) were placed on agar plates. After adding the transformation mixture, plates were shaken to evenly distribute the suspension.

2.2.3 Fluorescence activated cell sorting (FACS)

FACS was applied to determine the ploidy status of yeast cells. Cells were harvested from agar plates by washing colonies off with yeast preparation buffer (cf. Table 3). When WT strains exhibiting a toxicity phenotype were analyzed, large colonies were removed before harvesting cells. Survivor colonies were analyzed from a 5 ml culture incubated for 2 d, harvested by centrifugation and resuspended in yeast preparation buffer. All preparations for FACS analysis were performed in a 96-well format. Cells were fixed over night by the addition of ethanol to a final concentration of 70% (v/v). Samples were stored in 70% (v/v) ethanol for a maximum of one week 4°C. To normalize cell numbers, cells were sedimented by centrifugation and resuspended in FACS normalization buffer (cf. Table 3). After sonication for 30 s, cell densities were determined by their absorption at 600 nm. To achieve equal densities, wells were adjusted to yield a final OD_{600nm} of 0.2. The samples were treated over night with 0.25 mg/ml boiled RNase A, at 37 °C, and subsequent digestion with proteinase K at 1 mg/ml for 2 h at 50 °C removed proteins. After two washing steps, the cell suspension was stained with 20 μ g/ml propidium iodide and stored at 4 °C. Shortly before FACS measurements, the samples were sonicated for 30 s to ensure dissociation of cell clumps.

Fluorescence intensity distributions were recorded on a FACS Calibur instrument simultaneously recording forward scatter (FSC) and side scatter (SSC) as well as the peak width (FL-2W) and area of fluorescence channel 2 (FL2-A). The peak area provides information concerning absolute fluorescence intensity, whereas the peak width is applied to gate out cell doublets. FSC and SSC were gated generously to only remove small particles with low scatter signal and negligible fluorescence. FL2-A was adjusted to set the 1N peak to a fluorescence intensity of ~150 AU. The same setting was applied to channel FL2-W. Cells that exhibited a strongly increased peak FL2-W signal were gated out.

For most strains, histograms were acquired in linear mode and measurements were repeated in log mode, if cells exhibited states of ploidy >4N. All histograms between FACS batches were normalized to the fluorescence intensity of the 1N peak of strain BY4741. This procedure yielded histograms, directly reflecting genome copy numbers and directly comparable, independent of measurement in linear or log modes. Normalization also allowed comparison between separate experiments as BY4741 and BY4743 were present for ploidy reference.

2.2.4 Prion curing

To achieve a loss of the prion state of all endogenous yeast prions, BY4741 cells were passaged on YPD plates containing 3 mM GdnHCl (Manogaran *et al.*, 2011). After 3 d of incubation, a mixture of colonies was re-streaked on the same plates. This was repeated twice to obtain a glycerol stock of prion-free BY4741.

2.2.5 Viability assays

To determine viability of yeast cells, their capacity to found new colonies was probed. Single colonies were resuspended in 100 μ l of PBS and cell density was determined using a Neubauer chamber. 1×10^4 cells were plated on the appropriate medium and plates were incubated for 3 d. Colonies were counted to determine the number of colony forming units (CFU) present in the original sample.

2.3 *Caenorhabditis elegans*

2.3.1 Nematode cultivation and storage

All *C. elegans* strains used in this study were grown on nematode growth medium (NGM) agar plates seeded with *E. coli* OP50 strain at 20 °C. Strain stocks were generated by washing worms off five freshly starved plates, concentrating them by centrifugation to 1 ml and putting them on ice for 15 min. An equal volume of soft agar freezing solution (cf. Table 3) was added and the solution was transferred to cryovials. The vials were frozen at a controlled cooling rate of 1 °C/min at -80 °C.

2.3.2 RNA interference experiments

RNAi experiments were performed by feeding dsRNA-expressing *E. coli* to the nematodes according to standard procedures (Kamath *et al.*, 2003). Individual colonies of dsRNA expressing *E. coli* HT115(DE3) were grown in LB_{Amp,Tet} medium (100 μ g/ml ampicillin, 12 μ g/ml tetracycline). IPTG was added to a final concentration of 1 mM to induce dsRNA expression. NGM agar plates containing 50 μ g/ml ampicillin, 6 μ g/ml tetracycline, 1 mM IPTG

Materials and Methods

and 5 µg/ml cholesterol were seeded with these bacteria after 4 h of induction. Staged L1 larvae were added and incubated on these plates at 20 °C until the indicated age for scoring was reached.

2.3.3 Synchronization of cultures

For synchronization, worms were bleached in 0.5 M NaOH / 50% (v/v) bleach solution. The eggs obtained were washed thoroughly with M9 medium. After incubation for 14 h, staged L1 larvae were transferred to fresh NGM plates or RNAi plates.

2.3.4 Analysis of the heat shock response

To analyze the heat shock response, seeded NGM plates containing ~100 synchronized nematodes were sealed in plastic bags and heat shocked at the indicated temperature in a water bath for two hours. Plates were removed from the plastic bags and recovered for 12 h at 20 °C. After this recovery period, GFP expression was scored by visual inspection assigning percentage values to the induction intensity. '100% induction' required bright expression in all nematodes on the plate in the following cells: pharyngeal muscle cells, intestinal rings 1, 8 and 9, both spermathecae, body wall muscle cells and a visible induction in hypodermal cells. Incomplete induction patterns or heterogeneity among individuals was expressed by assigning intermediate percentage values. Survival was scored 24 h after heat shock.

2.3.5 Lifespan assays

In order to determine the adult lifespan, synchronized L1 larvae were grown on NGM plates at 20 °C. On day 4, young adult (YA) stage nematodes were picked and transferred to new NGM plates, thereby excluding nematodes that had entered the *dauer* state before. Nematodes were transferred to new NGM plates every other day to separate them from their progeny. The number of live animals was scored upon transfer. The response to prodding with an eyelash and the absence of pharyngeal pumping were the criteria applied to distinguish live from dead animals. Additionally, nematodes which contained larvae within their body (bagged worms) were considered dead.

2.3.6 Motility assays

To estimate the motility of worms, thrashing assays were performed. The nematodes were placed into a drop of M9 buffer and the number of thrashes performed per minute was counted. The assays were performed on day 4, day 7 and day 10 after hatching, scoring 15 adult hermaphrodites.

2.3.7 Generation of transgenic nematodes

Microinjections were performed by mounting YA worms on dried 2% agarose pads in a drop of halocarbon oil. 100 µg/ml plasmid DNA was injected and the animals were recovered by adding 0.5 µl of M9 medium and placing them on fresh NGM plates. The injections were performed on a Zeiss Axiovert 200 microscope (Zeiss Microimaging, Jena, Germany) equipped with an injection device (Eppendorf, Hamburg, Germany). Plates containing injected adult worms were scored starting at day 3 after injection for fluorescent F1 progeny using a Leica MZ-16FA (Leica Microsystems, Wetzlar, Germany) fluorescence stereomicroscope. To obtain stable lines, fluorescent offspring were transferred to new NGM plates.

2.4 Molecular biology

2.4.1 Plasmid isolations from *E. coli*

Plasmid isolations on a small scale were performed using the Pure Yield miniprep kit (Promega), disrupting 5 ml of an overnight culture. For larger scale preps, plasmid was isolated from 50 ml overnight cultures using the Pure Yield midiprep kit. All extractions were performed following the manufacturer's instructions. Plasmid stocks were stored at -20 °C.

2.4.2 DNA isolation from *S. cerevisiae*

To isolate either plasmid or genomic DNA a 5 ml freshly stationary culture was harvested by centrifugation (Amberg *et al.*, 2006). The pellet was resuspended in 0.5 ml of ddH₂O and sedimented in a reaction tube at maximum speed for 30 s. The supernatant was discarded and the pellet resuspended in the residual liquid. 0.2 ml of yeast preparation buffer were added (cf. Table 3) as well as 600 mg of acid-washed glass beads. Cells were disrupted by vigorous shaking for 10 min in an MM400 bead mill. After disruption, 0.2 ml of yeast lysis buffer and 0.2 ml of Roti-phenol were added and the mixture was vortexed. After a centrifugation step at maximum speed for 5 min, the aqueous layer was transferred to a new reaction tube. This solution was directly used for transformation of competent *E. coli* cells to recover plasmids. For the preparation of genomic DNA, 1 ml of 100% ethanol was added and the sample was mixed by inversion. Centrifugation for 2 min at maximum speed recovered the DNA in the pellet. To remove RNA, the pellet was resuspended in 0.4 ml of TE buffer and 3 µl of a 10 mg/ml RNase A solution were added. The reaction was incubated for 5 min at 37 °C. To precipitate genomic DNA, 10 µl of 4 M NH₄Ac and 1 ml of 100% ethanol were added. After a last centrifugation step for 2 min at maximum speed, the supernatant was removed and the pellet allowed to air dry. DNA was resuspended in sterile ddH₂O and stored at -20 °C.

2.4.3 Spectroscopic determination of DNA concentration

Concentration and purity of DNA preparations were determined by UV/Vis spectroscopy using a Nanodrop ND-1000 spectrophotometer. The absorption was determined at a wavelength of 260 nm ($A_{260\text{nm}}$) and 280 nm ($A_{280\text{nm}}$). $A_{260\text{nm}}$ reflects DNA content and $A_{280\text{nm}}$ protein content. All DNA preparations in this study typically yielded high purity DNA with an absorption ratio $A_{260\text{nm}}/A_{280\text{nm}}$ of 1.8 ± 0.2 .

2.4.4 Generation of yeast plasmids

Expression constructs were designed to contain 0, 30 or 56 glutamine codons at the 5' end of a polylinker upstream of the eYFP gene (Figure 4). The coding sequences were synthesized by GeneArt AG (Regensburg, Germany) and subcloned via the BamHI and SalI unique restriction sites into the plasmid p425GPD (Mumberg *et al.*, 1995), resulting in pQ0, pQ30 and pQ56.

2.4.6 DNA agarose gel electrophoresis

DNA was analyzed on agarose gels. 1% (w/v) agarose was dissolved in 100 ml TAE buffer (cf. Table 3). After cooling of the solution to 60 °C it was supplemented with Serva DNA Stain G at a dilution of 1:20,000. Samples were prepared by adding 10 x BJ sample buffer (cf. Table 3) and loaded onto gels. For sizing of DNA fragments, 1 µl of peQ Gold 1kb DNA-ladder per mm of lane width was loaded. Electrophoretic separation was performed in TAE buffer at a constant potential of 120 V for 20 min. Fluorescence was detected on an Image Quant 300 imaging station with UV transillumination.

2.4.7 DNA Sequencing

Sanger sequencing was performed on purified DNA by GATC Biotech (Konstanz, Germany) or Eurofins MWG Biotech (Ebersberg, Germany).

2.4.8 Microarray based gene expression analysis

To analyze gene expression changes in response to the presence of polyQ proteins of different lengths, global microarray-based analysis of mRNA levels was performed. Samples were obtained as for yeast protein lysates (cf. C2.5.1). As the amount of biomass generated on plates is dependent on the sample type, several plates had to be harvested for some samples (Table 14).

Sample	Incubation time	Sample set	Number of plates
Q0	2	2	1
Q0	3	1	1
Q30	3	1	1
Q56	3	1	19
Q56	4	2	19
Without vector ("Empty")	3	2	43

Table 14: Samples for microarray analysis.

Cells were pelleted for 10 min at 2500 x g and shock frozen in liquid N₂. The isolation and enrichment of mRNA as well as further preparation for microarray analysis were carried out by the Kompetenzzentrum für Fluoreszente Bioanalytik (Regensburg, Germany). Datasets were provided normalized to one another within one sample set.

2.4.9 Gene expression analysis by Real-Time Quantitative PCR

To analyze gene activation in *C. elegans* in response to heat shock on a transcriptional level, Real Time quantitative PCR (RT-qPCR) experiments were performed. Heat-shocked worms were washed off their plates with M9 medium. The bacteria were removed by sedimenting the worms by centrifugation for 1 min at 2000 x g and repeating this step, until the supernatant remained clear. The RNeasy Mini Kit (Qiagen, Hilden, Germany) was used to isolate total RNA. Worms were disrupted in buffer RLT, supplemented with β-mercaptoethanol using glass beads in a MM400 swing mill (Retsch, Haan, Germany) at 30 Hz three times for 2 min. The lysate was applied to spin columns and the manufacturer's protocol was followed. A total amount of 10 µg of RNA was subjected to reverse transcription with random hexamer primers using ALV reverse transcriptase (Promega, Madison). RT-qPCR was carried out according to the manufacturer's instructions, using the GoTaq qPCR MasterMix (Promega, Madison, USA) in an MX3000P

Materials and Methods

qPCR System (Agilent Technologies, La Jolla, USA) using the settings described by the manufacturer. Primer annealing temperature was set to 50 °C and elongation time to 20 s. Primer pairs (cf. Table 9) were designed to amplify a 200 to 250 bp segment of spliced target gene mRNA by using at least one primer per pair that binds on exon-exon junctions. Specificity of the RT-qPCR reaction also was confirmed on 1% agarose gels. The log₂-fold change of the amount of transcript of genes of interest upon heat shock was calculated versus *act-1* and *pgk-1* as normalizers and averaged for both normalizers using the MX3000P software package. The average of four separate biological experiments yielded the final information on regulation.

2.5 Protein purification and analytics

2.5.1 Protein purification

C. elegans proteins were expressed in BL21-CodonPlus (DE3)-RIL. Bacteria were grown in LB_{Kan} at 37 °C to an OD₆₀₀ of 0.8. Expression was induced after cooling the culture to 20 °C by the addition of IPTG to a final concentration of 1 mM. After four hours, bacterial cells were harvested and resuspended in disruption buffer supplied with protease inhibitor HP at a dilution of 1:100. The cells were lysed mechanically using the cell disruption instrument TS 0.75. The lysate was centrifuged for 15 min at 15,000 x g and the soluble fraction was applied to a HisTrap 5 ml column. The protein was eluted with disruption buffer containing 300 mM imidazole. CeHsc70 and BAG-1 were further purified by ion exchange chromatography on a ResourceQ column and subsequent size exclusion chromatography on a Superdex 75 HiLoad column. After affinity capture, DNJ-13 was further purified on a ResourceS ion exchange column and size exclusion chromatography using a Superdex 75 HiLoad column. HsHsc70 was expressed as described previously (Bendz *et al.*, 2007). Briefly, purification was achieved deploying DEAE-Sephacrose, Resource Q, ceramic fluoroapatite and a Superdex 200 HiLoad column for polishing. The purity of all proteins was assessed by SDS-PAGE and determined to be more than 95%. Protein concentrations of stock solutions were determined to be 220 μM for BAG-1, 160 μM for DNJ-13 and 60 μM for CeHsc70 and its fragments.

2.5.1 Yeast protein extracts

To obtain native protein extracts from yeast cultures, cells were harvested from agarose plates by washing them off using yeast preparation buffer (cf. Table 3). In case of pQ56 transformed WT yeast, large colonies were removed before harvesting. The cell suspension was centrifuged at 2500 x g for 10 min. The supernatant was removed and the pellet resuspended in 250 μl of yeast preparation buffer, supplemented with protease inhibitor cocktail FY at a 1:25 dilution and 10 mM β-mercaptoethanol. 900 mg of acid-washed 0.25-0.50 mm glass beads were added and the liquid meniscus adjusted to be ~ 4 mm above the meniscus of the glass beads. Shaking the bead mixture four times for 2 min each at 30 Hz in the MM400 bead mill at 4 °C was usually sufficient to disrupt roughly 90% of the cells. This was verified by phase contrast microscopy. Lysates were kept at 4 °C until further processing.

2.5.2 Lysate normalization

To determine the protein concentration of cell lysates, protein concentrations were determined by Bradford assays. Coomassie Protein Assay Reagent was diluted according to the manufacturer's

instructions. For large content determinations, 200 μ l of this mixture were added to 96-well flat bottom plates and 2 μ l of lysate were added. For single determinations, 1 ml of diluted reagent was added to cuvettes and supplemented with 5 μ l of lysate solution. All samples were thoroughly mixed and incubated for 5 min at room temperature before the $A_{595\text{nm}}$ was determined. In case the absorption was above or below the linear range, a new dilution of the protein solution was prepared. All samples were normalized to correspond to the extract concentration achieved for BY4741 yeast transformed with pQ56.

2.5.3 Native agarose gel electrophoresis (NAGE)

To be able to separate potentially very large sub-microscopic oligomeric protein species from monomeric or dimeric species, native agarose gel electrophoresis (NAGE) was employed, using a protocol adapted from a previously published protocol (van Ham *et al.*, 2010).

Yeast lysates (cf. 2.5.1) were normalized (cf. 2.5.2) and supplied with 5 x NAGE loading buffer (cf. Table 3). 30 μ l of the normalized lysates were loaded onto a gel containing 1% agarose (w/v) in NAGE buffer (cf. Table 3). Gel solutions were boiled thoroughly before pouring, to avoid air bubble formation. Electrophoretic separation was achieved at a potential of 3 V/cm of gel length for 17 h at 4 °C. PolyQ proteins were detected via their YFP moiety using a Typhoon 9200 multimode imager.

2.5.4 Denaturing polyacrylamide electrophoresis (SDS-PAGE)

To resolve cellular proteins under denaturing conditions, sodium dodecyl sulfate polyacrylamide gel electrophoresis (SDS-PAGE) was used. Gels were either poured manually or ServaGel neutral pH 7.4 gradient gels were deployed. Stacking gels contained 5% (w/v) and separating gels 12.5% (w/v) acrylamide according to Table 15

Component	12.5% Separating gel	5% Stacking gel
Separating gel buffer (4x) (cf. Table 3)	1.3 ml	-
Stacking gel buffer (2x) (cf. Table 3)	-	1.3 ml
Acrylamide/Bisacrylamide solution, 19:1 40%(w/v)	1.6 ml	0.3 ml
ddH ₂ O	2.2 ml	0.9 ml
TEMED	5 μ l	2.5 μ l
APS (10%(w/v))	50 μ l	25 μ l

Table 15: Composition of SDS-PAGE gels.

Samples were prepared by adding the appropriate amount of 5 x Laemmli loading buffer (cf. Table 3). To achieve full denaturation, the samples were incubated for at least 15 min at 95 °C. A maximum of 25 μ l of sample were applied per lane. As standards (cf. Table 4) 5 μ l of low range SDS-PAGE molecular weight standard for standard electrophoresis or Precision Plus Protein Dual Color Standard for western blots were loaded. Electrophoretic separation was achieved at a constant current of 35 mA for 50 min for self-made gels or 20 mA for 1:50 h for ready-to-use gels. Gels were either used for western transfer or proteins were detected by Coomassie brilliant blue staining (cf. 2.5.5).

Materials and Methods

2.5.5 Coomassie brilliant blue staining

Proteins separated by discontinuous SDS-PAGE were detected by applying a simplified protocol of the Fairbanks staining protocol (Fairbanks *et al.*, 1971). After electrophoresis, gels were transferred into Fairbanks A solution (cf. Table 3), boiled and incubated for 10 min. Fairbanks A solution substituted for Fairbanks D (cf. Table 3) for de-staining. Tissue paper was added to increase de-staining efficiency and the gels were repeatedly heated until protein bands became visible. After de-staining, gels were scanned and dried between cellophane sheets after exchanging water to Gel dry solution.

2.5.6 Western blotting

Specific proteins may be detected in cell lysates by western blotting. After separation by SDS-PAGE (cf. 2.5.4) the gels were incubated for 15 min in WB transfer buffer (cf. Table 3). PVDF membranes were activated by a short rinse with methanol and added to the gel together with 6 pieces of 3MM chromatography paper. After 5 min of incubation the transfer stack was assembled (anode to cathode order): three sheets of paper, the PVDF membrane, the gel, three sheets of filter paper. Excess buffer was blotted away using tissues. The proteins were transferred, applying a constant current of 1.5 mA/cm² of gel for 1:30 h. To analyze blotting efficiency and provide an additional loading control, the gel was usually stained with Coomassie blue (cf. 2.5.5). Unsaturated protein binding capacity on PVDF membranes was blocked for 1 h or over night with WB blocking solution (cf. Table 3) at 4 °C. Primary antibodies were applied in PBST containing 1% (w/v) milk powder (cf. Table 3) at the dilutions listed in Table 5 and incubated for 1 h at 4 °C. Unbound primary antibody was removed by washing the membrane three times with a large volume of PBST for 10 min. All secondary antibodies (cf. Table 5) were added at the dilutions indicated in Table 5 in PBST, containing 1% (w/v) milk powder and incubated at 4 °C for 1 h. Unbound secondary antibody was removed by washing the membrane three times with a large volume of PBST for 10 min.

The ECL-Western blot Detection Kit was used as described by the manufacturer to detect the horseradish-peroxidase-conjugated secondary antibodies by chemiluminescence. The wet membrane was placed below a transparent plastic sheet and the emitted photons were detected exposing an X-o-Mat x-ray film. For longer incubation times, the detection assembly was placed into lightproof cassettes. Films were developed in the Optimax TR.

2.5.7 Fluorescent labeling

BAG-1 and DNJ-13 were labeled fluorescently, yielding *BAG-1 and *DNJ-13, respectively. BAG-1 was labeled at its single cysteine, Cys7, using Alexa Fluor 488 C₅-maleimide. DNJ-13 was labeled with 5-(and-6)-carboxy-fluorescein succinimidylester at neutral pH to primarily label the aminoterminal amine group. Both labels were added to the protein (1 mg/ml) under continuous mixing at a threefold molar excess. After an incubation period of 2 h at room temperature, unreacted label was quenched by adding DTT to a final concentration of 20 mM in the case of *BAG-1 or TRIS to a final concentration of 100 mM in the case of *DNJ-13. To separate free label from the labeled protein, size-exclusion chromatography was performed. The labeling efficiency for BAG-1 and DNJ-13 was determined according to the manufacturer's guidelines to be 0.95 and 1.2, respectively.

2.5.8 Analytical ultracentrifugation (AUC)

AUC allows probing molecular complex formation between different proteins. The sample is exposed to a centrifugal force field, and the sedimentation of proteins or protein complexes is followed over time. Different methods of detection may be applied such as interference optics, UV/Vis spectrometry or epifluorescence. Epifluorescent detection allows the determination of the sedimentation properties of a single fluorescently labeled protein species in highly complex matrices. In principle, the exact molecular mass can be determined using Equation 1:

$$s = \frac{v}{\omega^2 r} = \frac{MD(1 - \bar{V}\rho)}{RT}$$

Equation 1: The Svedberg equation. s = sedimentation coefficient (S), v = radial velocity (m/s), ω = angular velocity (m/s^2), r = radial distance of the sedimentation boundary, M = molecular weight (g/mol), \bar{V} = partial specific volume (cm^3/g), ρ = solvent density (g/cm^3), D = diffusion coefficient (m^2/s), R = gas constant ($\text{J mol}^{-1} \text{K}^{-1}$), T = temperature (K).

AUC was performed with a ProteomeLab XL-A ultracentrifuge equipped with a fluorescence detection system. Centrifugation was performed at 20 °C at 42,000 rpm. Labeled protein was generally sedimented at a concentration of 300 nM in the absence and presence of binding partners and different nucleotides. Sedimentation velocity experiments were evaluated using dc/dt analysis as described before (Stafford, 1992). Species distributions in dc/dt plots were fit to Gaussian or bi-Gaussian functions in order to obtain the $s_{20,w}$ values of the observed sedimentation boundaries. It is important to note, that in particular when binding affinities are low and the interaction is dynamic, sedimentation boundary analysis by the dc/dt -approach can result in an apparently reduced $s_{20,w}$ value, in comparison to a stable protein complex of the same molecular mass. To obtain information on the complex for this specific situation, runs were evaluated using the Finite Element Whole Boundary Fitting method and C(s) methods of the UltraScan software package (Demeler *et al.*, 2010). The data sets are fitted by the program assuming a single species of particles and the sedimentation coefficient $s_{20,w}$ as well as the diffusion coefficient $D_{20,w}$ are accordingly determined. These values were then used to calculate the molecular weight of the sedimenting particle. The molecular weight, $s_{20,w}$ and $D_{20,w}$ of labeled DNJ-13 and labeled BAG-1 corresponded well to the values obtained for the unlabeled proteins.

2.5.9 Differential scanning fluorimetry (DSF)

DSF was deployed to determine the unfolding temperature of CeHsc70, its fragments and HsHsc70. This method exploits an increase in the fluorescence of SYPRO orange upon binding to exposed hydrophobic parts of proteins (Niesen *et al.*, 2007). The dye is diluted 1:100 in measurement buffer. This pre-mix is diluted again 1:10 in a buffer solution containing 0.5 mg/ml protein to be investigated. Temperature dependent unfolding of the analyte proteins was followed by recording the fluorescence intensity in an Mx3000P qPCR System. Fluorescence reads were performed at a heating rate of 0.5 °C/min every minute. All measurements were performed in triplicates. Melting curves were normalized and averaged. To determine the transition point, the derivative of the denaturation curves was calculated using Origin. ADP was added to 2 mM as indicated.

Materials and Methods

2.5.10 Circular dichroism (CD) thermal transitions

CD temperature transitions were recorded in measurement buffer to determine the loss of secondary structure in Hsc70 proteins and truncations. The structural changes were tracked at a wavelength of 217 nm with a heating rate of 0.5 °C/min, starting at 12 °C. To reduce noise, curves were smoothed by applying a moving average at a window size of 5 data points. The curves were normalized to allow comparison. Fitting to obtain thermodynamic unfolding parameters was not performed, as irreversibility was observed, precluding thermodynamic evaluation. Melting temperatures were again determined by derivatization of the melting curve using Origin.

2.5.11 Steady-state ATPase activity measurements

Steady-state ATPase activities were determined as described earlier (Ali *et al.*, 1993). In short, an ATP-regenerating system was used, employing lactate dehydrogenase, NADH, phosphoenol pyruvate and pyruvate kinase in measurement buffer supplied with 5 mM MgCl₂. Assays were started by the addition of 2 mM ATP. The assay temperature was 25 °C for all experiments, if not indicated otherwise. The temperature of the experiments was varied by an attached thermostat to the spectrophotometer

The influence of cofactors on CeHsc70 activity was analyzed by titration. ATPase activities at different cofactor concentrations were fit to obtain apparent K_D-values according to Equation 2:

$$v = v_0 + (v_{max} - v_0) * \frac{L_{tot}}{L_{tot} + K_D}$$

Equation 2: Simple substoichiometric binding model. v = turnover rate, v_0 = initial turnover rate, v_{Max} = maximum turnover rate, L_{tot} = absolute concentration of the binding partner, K_D = apparent dissociation constant.

In cases where the apparent affinity of the interaction was so high that stoichiometric or substoichiometric binding was observed, the kinetics were fitted to Equation 3:

$$v = v_{max} + \frac{1}{2 * M_{tot}} * (v_{max} - v_0) * \left(L_{tot} + K_D - M_{tot} - \sqrt{(L_{tot} + K_D - M_{tot})^2 + 4 * M_{tot} * K_D} \right)$$

Equation 3: Complex binding model. v = turnover rate, v_0 = initial turnover rate, v_{Max} = maximum turnover rate, L_{tot} = absolute concentration of the binding partner, M_{tot} = absolute concentration of the investigated protein, K_D = apparent dissociation constant.

2.5.12 Luciferase refolding

Recombinant luciferase (10 µM) was denatured for 45 min at room temperature in denaturing buffer. For refolding, denatured luciferase was diluted 1:125 in luminescence buffer. The concentrations of chaperones and cofactors were 3.2 µM for CeHsc70, 0.8 µM for DNJ-13 and 0.4 µM for BAG-1. Reactions were carried out in white 96-well plates. The recovery of luciferase activity was detected continuously over a time period of 2 h at 25 °C by using a GENios™ microplate reader.

2.5.13 Limited proteolysis

The CeHsc70 fragments Δ512, Δ545 and the full-length protein were digested by chymotrypsin at 25 °C. The reaction was carried out in 40 mM HEPES/KOH, pH 7.5, 20 mM KCl, 10 mM CaCl₂ with a final concentration of 20 µg/ml α-chymotrypsin and 600 µg/ml of the

corresponding proteins. By adding PMSF, dissolved in DMSO to a final concentration of 33 mM at the indicated time points, the digestion was stopped by immediate boiling in 1x loading buffer and resolved electrophoretically on 12% polyacrylamide gels.

2.6 Bioinformatics

2.6.1 Sequence alignments and determination of homologies

Domain boundaries of proteins were defined according to the Conserved Domain Database after a conserved domain query on the protein sequence. In order to determine the degree of conservation within one domain, identical and homologous residues, as identified by the BLAST algorithm, were determined and percentage values for each domain were calculated (cf. Table 12 for programs).

2.6.2 Interaction networks

To generate interaction networks, gene identifiers were uploaded to the String database. The obtained interaction network was further layouted using Cytoscape. Grouping according to biological function was performed according to the literature cited and gene annotation in the Saccharomyces Genome Database (cf. Table 12 for programs).

2.7 Imaging

2.7.1 Agarose plate imaging

Phenotypes of yeast strains upon transformation with polyQ proteins were documented by taking photographs of whole petri dishes. A Canon EOS 60D digital camera mounted on a Repro stand was used for this purpose.

2.7.2 Low magnification fluorescence microscopy

A Leica MZ16-FA stereo microscope was used for low magnification fluorescence microscopy of yeast colonies and screening for transgenic *C. elegans*. RNAi motility phenotypes were scored using a Stemi stereo microscope.

2.7.3 High magnification fluorescence microscopy

For high resolution imaging, samples were mounted. For yeast, an appropriate SM medium based 2% (w/v) agarose pad was prepared. Cells were transferred to this pad and a coverslip was placed on the cells before imaging. For *C. elegans* samples, similar pads were prepared, using 2% (w/v) agarose in M9 medium. Worms to be imaged were selected and placed in a drop of M9 medium containing 2.5 mM tetramisole. After a 5 min incubation period, the animals were transferred into a drop of M9 tetramisole on the pad. A coverslip was placed on top. Mounted samples were sealed with silicone grease to avoid drying.

2.7.4 Confocal microscopy

Confocal microscopy renders the visualization of very small fluorescent structures possible. This is most relevant for structures that exhibit a complex three dimensional architecture or are hardly

Materials and Methods

discernible due to a strongly fluorescent background outside the focal plane. A Leica SP5 laser scanning microscope was deployed for this purpose. Scan speed, resolution and laser intensity were adapted to avoid photobleaching of the chromophores. Gain and offset were adjusted to fully exploit the dynamic range of the photomultipliers. The scanning resolution of the images was adjusted to be slightly below the theoretical resolution limit, as calculated according to Abbé's equation.

$$d = \frac{\lambda}{2n * \sin\alpha} = \frac{\lambda}{2 * NA}$$

Equation 4: Resolution limit according to Abbé. d = the minimum resolution, λ = the wavelength, n = the refractive index of the medium, α = the half angle of the incident light beam, NA = the numerical aperture.

YFP and CFP were excited, using the 514 nm and 458 nm lines of an Argon laser, respectively. The distance of single imaging planes in Z-stacks was determined by the microscope software. For intensity profile plots, the appropriate plugin of ImageJ was used. Image manipulations, if necessary, were linear adaptation of contrast and brightness and were performed using ImageJ.

2.7.5 Fluorescence recovery after photobleaching (FRAP)

FRAP in live worms or yeast cells was performed to determine the kinetic association state of proteins to cellular structures, using the Leica SP5. A defined area was scanned at imaging speed in zoom-in mode at 70% of the full laser power. Recovery was tracked until a stable plateau was reached. Quantitation of recovery was achieved by determining the integrated intensities of the bleached area normalizing this intensity to an equally sized control field in the same frame using the LAS AF software suite.

2.7.6 Analysis of cell size by microscopy

Cell size analysis was performed by picking single colonies from agar plates and resuspending them in 70% (v/v) ethanol for fixation. The solution was immediately supplied with an equal volume of 0.1% methylene blue solution in ddH₂O to obtain high image contrast in bright field illumination. Images were recorded on an Axiovert 200 microscope. Using Image J, the images were thresholded to obtain black and white representations. Deploying the particle analysis plugin, cells were picked and the cross-sectional area was determined. Cells out of focus or touching the image border were excluded from analysis.

D Results

Results

1 Characterization of Hsc70 function in *C. elegans*¹

Hsc70 has proven to be a highly versatile chaperone in many studies (cf. section B2). Consequently, it is highly relevant to understand its function in the development and maintenance of a multicellular organism of reduced complexity. Hsc70 also allows addressing the relation of structural changes to its hydrolytic and protein folding activities. The overall amino acid sequence of nematodal Hsc70 (CeHsc70) is strongly conserved among species, although the helical lid domain is highly diverse (Aponte *et al.*, 2010). This stretch of 130 amino acids is only distantly related among bacterial and metazoan Hsc70 proteins. Consequently, it is essential to elucidate in which respect and to what extent the biochemistry of this major chaperone class has changed at specific transitional steps in evolution.

1.1 Hsp70 systems are adapted to physiological temperatures

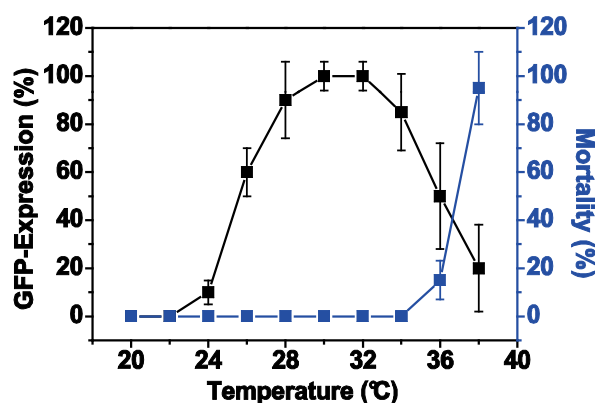


Figure 5: Heat shock response and lethality in *C. elegans*. The induction of the heat shock response as measured by the expression of *hsp-70::GFP* (black squares, left ordinate) in comparison to lethality at the corresponding temperatures (blue squares, right ordinate). YA stage worms were exposed to the indicated temperatures for 2 h and scored for fluorescence induction after a recovery period of 12 h. The worms were grown at 20 °C before shifting them to the respective heat-shock temperature. The percentage of mortality was determined from these samples as well. The values presented are an average of three independent experiments and the error bars represent the standard deviation (SD).

As differences in the primary sequence preclude an *a priori* judgment of the consequences on a protein's biochemistry and functionality, a first step to understand *C. elegans* chaperone biology is the initial characterization of one of the key chaperones of the Hsp70 machinery, the constitutively expressed Hsc70 protein HSP-1. To obtain an initial picture of the inducibility of the nematodal Hsp70 system in response to the canonical stressor heat and until which point heat stress is sub-lethal, worms expressing a *hsp-70::gfp* transcriptional reporter were heat-stressed and their reaction concerning induction and lethality was scored (Figure 5). The data indicate that maximal induction of the heat shock response is reached at 29-32 °C and declines above this

¹ This section is adapted from the corresponding publication as indicated under 'Publications'.

Results

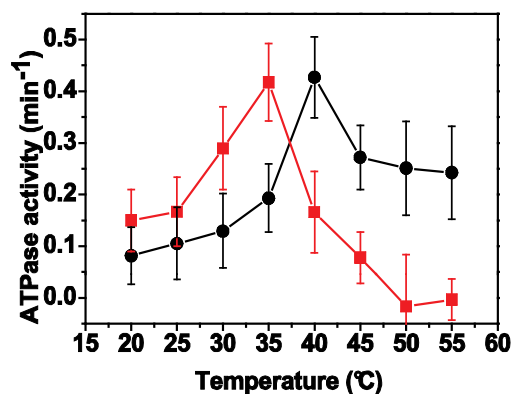


Figure 6: Temperature dependence of the Hsc70 ATPase. The hydrolytic activity of CeHsc70 (red squares) and HsHsc70 (black circles) was determined at the indicated temperatures under steady-state conditions. The given values are averages of three replicates. The error bars represent the SD.

temperature. Furthermore, above this temperature, lethality rises drastically until it reaches full extent at ~ 37 °C. These results indicate that the heat shock system of nematodes is most active ~ 10 °C above their native growth temperature.

To further elucidate how this adaptation to growth temperature is reflected on the level of CeHsc70's biochemical function, the temperature-dependence of the ATP hydrolysis rate was determined (Figure 6). The results indicate that hydrolysis reaches its maximum at roughly 35 °C, which is slightly above the temperature of maximal induction of CeHsp70. The drop in CeHsc70 activity above this temperature therefore corresponds to the increase in lethality above 34 °C (cf. Figure 5).

The direct comparison to the human Hsc70 system (HsHsc70) may support the notion that the hydrolytic activity of Hsc70s is tightly related to an organism's ideal growth temperature and lethal heat stress. As such, this protein reaches its maximal activity at the slightly sub-lethal temperature of 40 °C. Studying the structural stability of Hsp70s by DSF confirms the adaptation to native growth temperature (Figure 7). The thermal unfolding transition midpoint is at 37 °C and 44 °C for the apo-forms of CeHsc70 and HsHsc70, respectively. Upon binding of ADP, this transition midpoint is shifted to 45 °C for CeHsp70 and 52 °C for HsHsp70, also indicating similar affinities for the nucleotide as the extent of stabilization (8 K for both proteins) directly reflects the ΔG of binding.

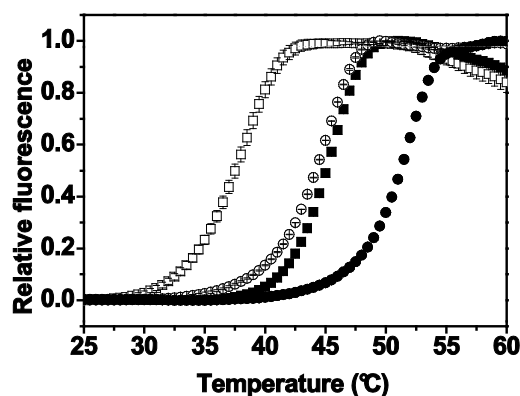


Figure 7: Structural stability of CeHsp70 and HsHsp70. DSF melting curves indicate that Hsc70 from *C. elegans* (\square) is about 10° C less stable than the human ortholog (\circ). Adding ADP stabilized CeHsc70 (\blacksquare) as well as human Hsc70 (\bullet) to a similar extent. Error bars reflect the standard deviation of three experiments.

1.2 The Hsp70 system is required to prevent folding stress

The exposure of nematodes to heat strongly induces the expression of *hsp-70*. It would be intuitive to assume that the induction of heat shock proteins would be homogeneous throughout the organism, at least among cells of the same type, reflecting an equal requirement for chaperoning capacity due to similar proteomes. Surprisingly, the induction of *hsp-70* proved to be highly diverse throughout the organism and even within the same tissue type (Figure 8). The body wall as well as pharyngeal muscle cells exhibit increased fluorescence after exposure. The spermathecae, as well as specifically the intestinal rings 1 and 9 also induce *hsp-70*. This intestinal pattern may reflect additional sub-typic cellular specialization. Whether this expression pattern reflects a specific requirement for Hsp70s foldase activity or is rather part of a more generalized sensitivity to heat in these cells, potentially involving other chaperones, may be answered by depleting Hsc70. Here, the response of the upregulation of *hsp-70* is restricted to the intestinal tissue. Specifically the first ring as well as the segments 7, 8 and 9 induce HSP-70. This result points to a proteome composition in these cells that specifically requires the presence of an Hsp/Hsc70 chaperoning function and highlights certain heterogeneity even among cells of the same type.

1.3 Hsp70 is the central essential factor of its chaperone network

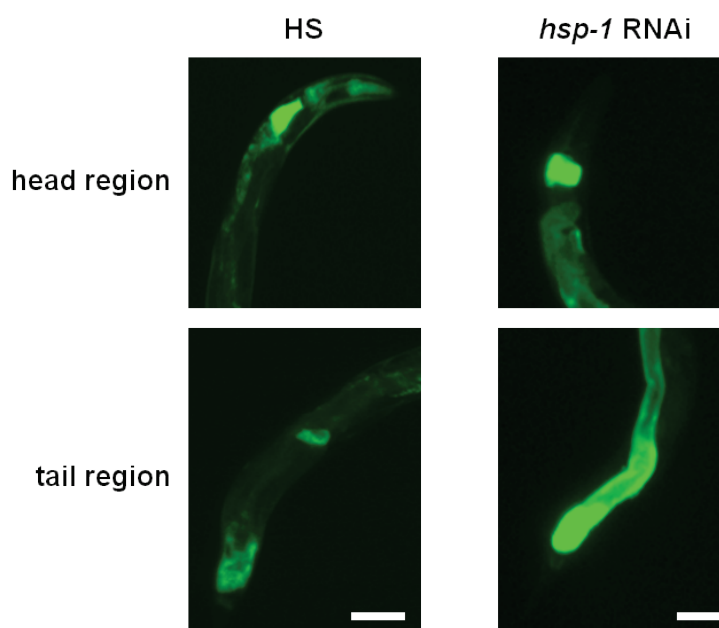


Figure 8: Hsp70 can be induced by heat stress and Hsc70 depletion. The head and tail regions of HSP-70::GFP reporter strains. The animals were either subjected to heat stress (HS) or were treated with RNAi against the Hsc70 *hsp-1*. Upon heat shock the synthesis of HSP-70 is detected in in the body wall muscle cells, pharyngeal muscle cells, and the intestinal ring 1 (head region). The tail region exhibits fluorescence in the spermatheca as well as the intestinal rings 8 and 9. The loss of Hsc70 (HSP-1) functionality by RNAi leads to a compensatory upregulation of HSP-70 primarily in intestinal cells with the intestinal rings 1, 7, 8 and 9 being most intensely fluorescent. The scale bar represents 50 μ m for both columns.

Results

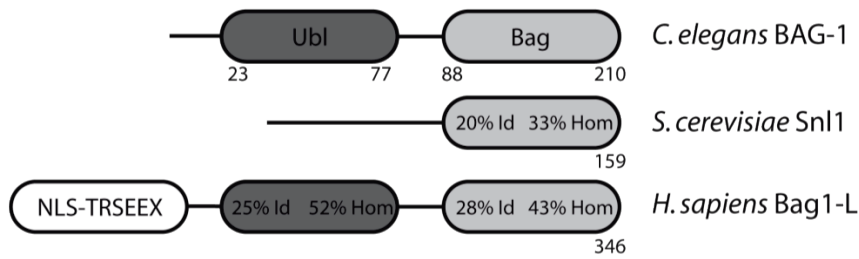


Figure 9: BAG-1 from *C. elegans* is the sole close relative of human Bag1-L. A schematic representation of human Bag1-L, yeast Snl1 and nematodal BAG-1. All three proteins share the well-conserved Bag domain at their carboxyterminus. The ubiquitin-like (Ubl) domain seems to be phylogenetically novel in this protein context and may not be discerned in the yeast protein. In contrast to the human ortholog, nematodal BAG-1 lacks a specific nuclear localization sequence (NLS) and the aminoterminal repetition of the acidic TRSEEX motif. The numbers indicate the domain borders in the primary sequence.

In addition to Hsp70, cochaperones have been considered essential to direct and modulate its chaperone activity. In *C. elegans*, BAG-1 seems to be the only protein that could act as a nucleotide exchange factor homologous to human Bag1-L and yeast Snl1. Yet, this cofactor's sequence is only weakly conserved (Figure 9), sharing only the Bag-domain across all three species with this domain exhibiting only 20% identity and 33% homology. The ubiquitin-like Ubl domain may only be found in higher eukaryotes and exhibits 25% identity and 52% homology comparing nematodes to humans.

Another relevant class of cofactors are the J-proteins (cf. section B1). Several J-domain containing homologues that may potentially be functionally redundant can be discerned in the nematode's genome. However, DNJ-13 seems to be the most likely candidate to be the closest homologue to yeast Sis1 and human DNAJB5 (Figure 10). To further understand which parts of the Hsp70 system of *C. elegans* are necessary for the normal post-hatching development, the levels of Hsc70 and a set of cofactors were knocked-down by RNAi. The data obtained in this experiment are shown in Table 16 and indicate that the sole GEF BAG-1, all potential functional homologs of DNAJB5 and Sis-1 as well as the heat-inducible HSP-70 are dispensable for general larval development. Also, lifespan and motility are uncompromised when these genes are depleted. This stands in stark contrast to the lethal effect of the downregulation of HSP-1 which consequently is the essential constitutively expressed paralogue of Hsc70. It is surprising, however, that its absence may not be compensated for by the presence of HSP-70.

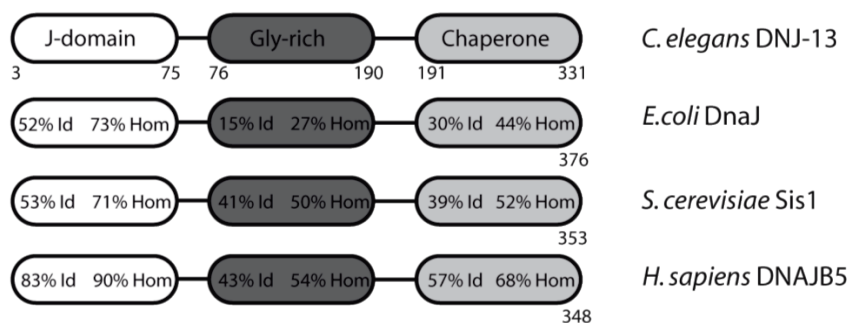


Figure 10: DNJ-13 is closely related to human DNAJB5 and yeast Sis1. The sequence comparison of J-domain proteins from bacteria to man reveals that the class-defining J-domain is highly conserved across kingdoms of life and remarkably homologous between *C. elegans* and humans. The glycine-rich (Gly-rich) and chaperone domains are highly conserved among eukaryotes.

Cofactor	Phenotype
BAG-1	No phenotype detected
DNJ-12	No phenotype detected
DNJ-13	No phenotype detected
DNJ-19	No phenotype detected
HSP-1	Lethal
HSP-70	No phenotype detected

Table 16: Global assessment of RNAi phenotypes of the Hsc70 system. RNAi experiments were performed with WT animals to investigate the effect of the loss of specific factors of the Hsc70 chaperone machinery. Animals were synchronized, placed on RNAi plates and scored at 3 days after hatching.

1.4 The NEF-function of nematodal BAG-1 is conserved

The potential NEF for CeHsc70, BAG-1, is weakly conserved in *C. elegans* (cf. section 1.3). The BAG-domain is known to bind to the NBD of Hsc70, inducing a conformation incapable of nucleotide binding (Sondermann *et al.*, 2001). The protein has been shown to be dimeric and exhibits a structurally distinct binding site for CeHsc70 than human Bag-1 in a study, using the isolated BAG-domain to address this issue (Symersky *et al.*, 2004).

To assess the binding behavior of full-length BAG-1, the protein was recombinantly produced and purified to test its interaction behavior with CeHsc70. To be able to follow the sedimentation of BAG-1 in AUC experiments, it was fluorescently labeled (cf. section C2.5.7, *BAG-1). In the absence of CeHsc70, the apparent sedimentation coefficient of *BAG-1 was 2.1 S (Figure 11). Finite element analysis yielded biophysical parameters, indicative of a monomeric protein ($s_{20,w} = 2.1 \pm 0.4$ S, a ; $D_{20,w} = 7.36 \cdot 10^{-7} \pm 1.5 \cdot 10^{-7}$ m²s⁻¹; MW ~ 23.5 kDa). This result does not conform to the behavior of the isolated BAG-domain, described above. It rather matches earlier observations in the mammalian system (Stuart *et al.*, 1998). Upon the addition of CeHsc70, a protein complex of 4.8 S formed quantitatively, pointing to a strong binding of BAG-1 (Figure 11). This value is slightly larger than the $s_{20,w}$ -value for CeHsc70 without cochaperones, which is 4.3S and comparable to HsHsc70 (Welch & Feramisco, 1982). Nucleotides should influence the

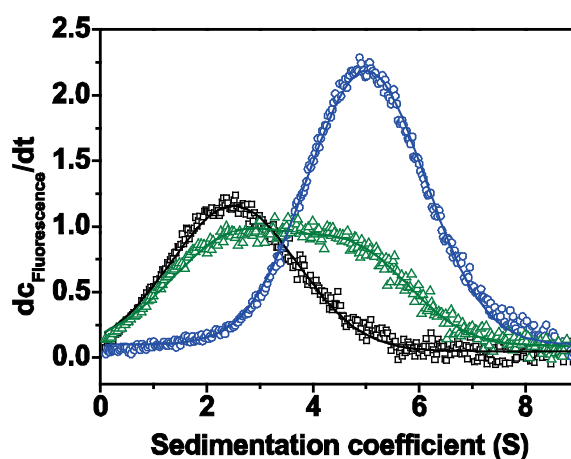


Figure 11: BAG-1 binding to CeHsc70. dc/dt plots of sedimentation velocity experiments of 300 nM *BAG-1 (black), indicate tight binding to 3 μ M CeHsc70 (blue). This interaction is destabilized by the presence of 4 mM ATP (green).

Results

binding behavior of a NEF to Hsc70. Consequently, ATP was added to the binding assay mixtures to a concentration of 4 mM. The presence of the nucleotide appeared to interfere with the binding of *BAG-1 to CeHsc70. Comparing the amount of *BAG-1 bound to CeHsc70 to the nucleotide-free sample, only ~ 22% of the cofactor were associated to Hsc70. ADP as well as the ATP-analogues AMP-PNP and ATP γ S were equally effective to destabilize the complex. The disruption of BAG1•Hsc70 complexes upon nucleotide addition confirms the notion that the function of BAG-1 as a NEF for CeHsc70 is conserved. This fact has also been described before for other eukaryotic systems (Heschl & Baillie, 1990; Hohfeld & Jentsch, 1997).

1.5 DNJ-13 forms complexes with CeHsc70

To assess the degree of conservation of the mode of interaction and effects of nematodal DNAJ-proteins on CeHsc70, DNJ-13 as the closest relative to yeast Sis1 and human DNAJB5 was chosen. The presence of J-proteins should stimulate the rate of ATP hydrolysis. In ATPase assays, the presence of DNJ-13 doubled the rate of turnover of CeHsc70 (Figure 12).

To address the mode of J-domain cofactor binding more directly, DNJ-13 was purified, labeled and subjected to AUC experiments. The sedimentation coefficient for *DNJ-13 was 4.0 S. The calculated parameters ($s_{20,w} = 4.0 \text{ S} \pm 0.6 \text{ S}$; $D_{20,w} = 5.67 \cdot 10^{-7} \pm 1.13 \cdot 10^{-7} \text{ m}^2\text{s}^{-1}$; MW ~ 62 kDa) support a dimeric solution structure which is in agreement with the properties reported for yeast Sis1 and bacterial DnaJ (Sha *et al.*, 2000; Shi *et al.*, 2005). Surprisingly, despite doubling the ATPase activity of CeHsc70, the addition of CeHsc70 did not change the sedimentation behavior of *DNJ-13 (Figure 13). This finding suggests that DNJ-13 binds not or only extremely weakly to CeHsc70 under the assay conditions chosen.

As the binding behavior of DNJ-13 seemed strong in ATPase assays, ADP as well as AMP-PNP and ATP γ S were added to our AUC samples. The association behavior did not change when any of the nucleotide analogs were added. However, upon the addition of ATP, a large protein complex of 12 S formed. The molecular weight of a complex of this size must in theory be equal to or larger than 210 kDa, assuming a spherical shape of the complex and a frictional ratio of 1.

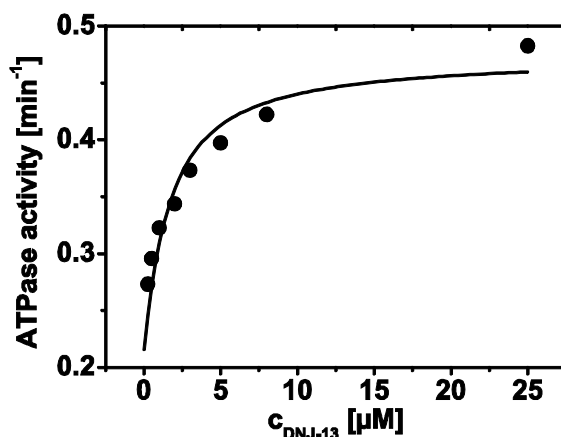


Figure 12: DNJ-13 stimulates CeHsc70. Titrating increasing amounts of DNJ-13 to 1 μM of CeHsc70 reveals that DNJ-13 activates the hydrolytic activity about twofold in comparison to the basal level. It also indicates that the binding to CeHsc70 is tight.

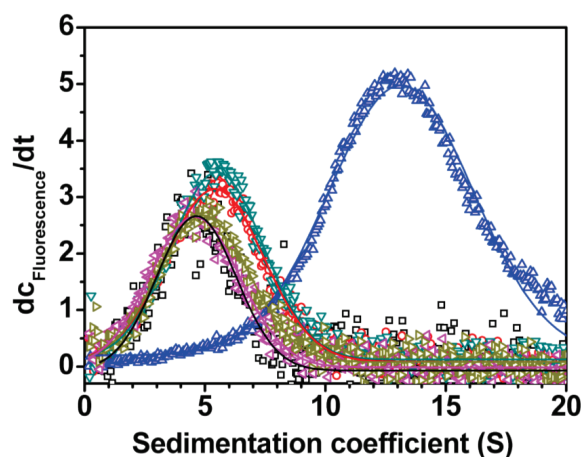


Figure 13: DNJ-13 binding to CeHsc70 is dependent on ATP. The dc/dt plots of sedimentation velocity experiments indicate that *DNJ-13 (black) is dimeric in solution at a concentration of 300 nM. When the sample is supplied with CeHsc70 at 3 μ M (pink), the sedimentation behavior is unchanged. Additional supplementation with either 4 mM ADP (gold) or AMP-PNP (red) or ATP γ S (turquoise) did not change this behavior. Solely ATP (blue) contributed to detectable binding.

The high molecular mass may reflect the assembly of a heterotetrameric complex, consisting of a *DNJ-13 dimer (~62 kDa) that binds one CeHsc70 monomer (~70 kDa) per subunit, yielding a complex of a theoretical mass of 222 kDa. The formation of the *DNJ-13•CeHsc70 complex seems to be strictly dependent on the presence of the hydrolysable trinucleotide ATP. This suggests that DNJ-13 interacts with conformations that are not accessible by the binding of ADP or the non-hydrolysable analogs AMP-PNP and ATP γ S.

1.6 DNJ-13 and BAG-1 compete for binding to CeHsc70

As shown for most Hsp70 systems, the interaction of J-domain proteins and NEFs is competitive, but still synergistic in stimulating the hydrolytic activity of the chaperone (Hohfeld & Jentsch, 1997; Sondermann *et al.*, 2001; Szabo *et al.*, 1994; Terada & Mori, 2000). To probe, whether this aspect of the regulation of the hydrolytic cycle of Hsc70 is conserved for

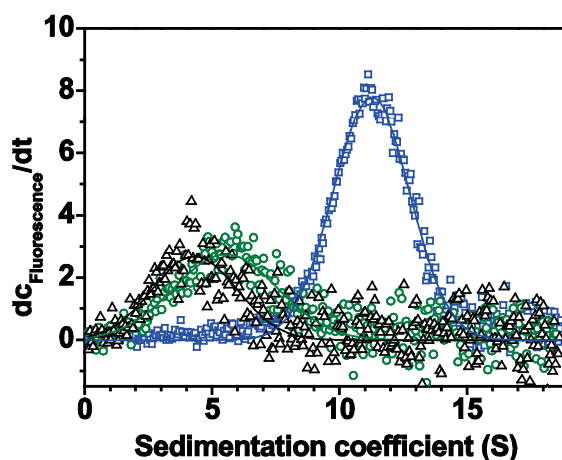


Figure 14: BAG-1 disrupts *DNJ-13•CeHsc70•ATP. dc/dt plots of sedimentation velocity experiments show *DNJ-13 at a concentration of 300 nM (black) to form complexes with CeHsc70 (3 μ M) in the presence of ATP (4 mM, blue). The addition of 15 μ M BAG-1, however, disrupts the *DNJ-13•CeHsc70•ATP complex, releasing *DNJ-13 (green).

Results

nematodes, AUC runs were performed. Surprisingly, when BAG-1 is added, the CeHsc70•*DNJ-13•ATP complex of 12S is disrupted (Figure 14). The stimulatory effect in the presence of both cochaperones has been described to be synergistic.

To confirm this for the nematodal system, the change of the ATPase activity of CeHsc70 was examined upon the addition DNJ-13 in the presence of 2 μ M BAG-1 (Figure 15). At the excess of 25 μ M DNJ-13, the stimulation of CeHsc70 through DNJ-13 is 6-fold higher than in the absence of BAG-1, although the apparent affinity for DNJ-13 ($K_{D,app}=6.8 \mu\text{M} \pm 3.2 \mu\text{M}$) is drastically decreased. This finding highlights that both chaperones act synergistically to activate CeHsc70 despite their competitive binding behavior.

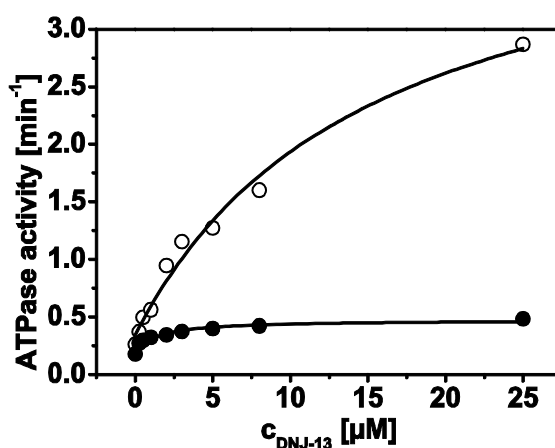


Figure 15: DNJ-13 and BAG-1 accelerate hydrolysis synergistically. Concentration-dependent analysis of the activation of CeHsc70 by DNJ-13 in the absence (●) and presence (○) 2 μ M BAG-1. The titration curves highlight that the twofold stimulation of the ATPase by DNJ-13 increases to ~12-fold in the presence of BAG-1. It also points to a concomitantly lowered apparent affinity of DNJ-13 towards CeHsc70 when the NEF is present.

1.7 Substrate refolding requires BAG-1 at an optimum concentration

How NEFs and J-proteins modulate the chaperoning activity of Hsc70 in the eukaryotic system is largely enigmatic. The case is particularly confusing for NEFs. They have been reported to be both, supportive and inhibitory in different studies (Bimston *et al.*, 1998; Gassler *et al.*, 2001; Takayama *et al.*, 1997; Tzankov *et al.*, 2008). Denatured firefly luciferase is one of the most widely used substrates for refolding experiments with Hsc70. Its advantage as a substrate is its monomeric nature and the straightforward and highly sensitive detection of its activity due to the luminogenic reaction, catalyzed by this enzyme. Refolding heat-denatured luciferase, CeHsc70 exhibited only negligible activity. Supplementing the assay with DNJ-13 rendered CeHsc70 capable of restoring the enzymatic activity of luciferase. Further addition of BAG-1 additionally increased the refolding efficiency already at substoichiometric concentrations (Figure 16).

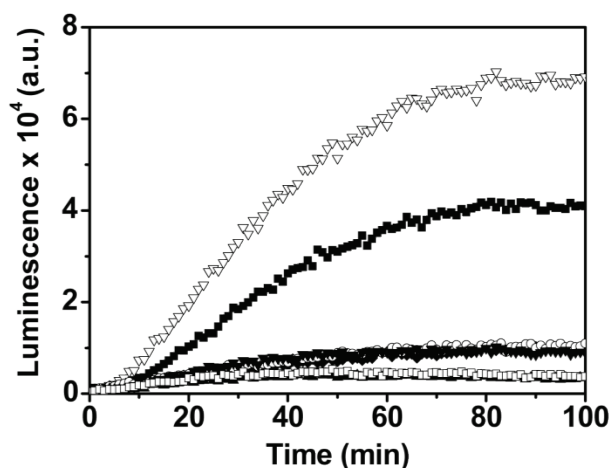


Figure 16: Cochaperones are required for substrate refolding. Monitoring the development of the activity of firefly luciferase over time uncovers a low refolding efficiency in the presence of either CeHsc70 (○), BAG-1 (□), DNJ-13 (▼) or CeHsc70/BAG-1 (◆). CeHsc70 and DNJ-13 (■) in combination, however, clearly enhance refolding yields and accelerate the kinetics. In an assay additionally containing substoichiometric amounts of BAG-1, the refolding reaction is even more efficient and effective (∇).

It is notable, however, that higher amounts of BAG-1 seem to act suppressingly on the refolding reaction down to baseline levels at 6 μM BAG-1 (Figure 17). This result may support a concept previously derived from studies in the prokaryotic system, suggesting that optimum concentrations of NEF are required for maximum refolding efficiency and effectiveness (Popp *et al.*, 2005).

As refolding should be energetically linked to ATP hydrolysis, it is interesting to examine the hydrolytic activity under the very same conditions as refolding. Although for maximum ATPase activity, there seems to be an optimum concentration of NEF at $\sim 2 \mu\text{M}$ this is not coincident with the maximum of refolding activity at $\sim 0.75 \mu\text{M}$ BAG-1. This implies that both processes do not share the same requirements in respect to cochaperone concentrations to be maximally accelerated (Figure 17). The suppression of hydrolysis at BAG-1 concentrations higher than 4 μM suggests competitive inhibition of the hydrolysis cycle through the presence of the NEF.

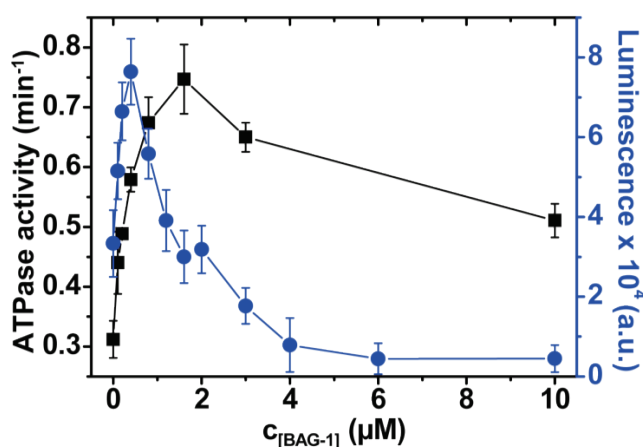


Figure 17: Maximum refolding is not related to maximum hydrolysis. Luciferase refolding activity (blue circles, right ordinate) and hydrolytic turnover rates measured under regenerative conditions at 3.2 μM CeHsc70, 0.8 μM DNJ-13 and increasing amounts of BAG-1.

Results

1.8 The lid domain is required for substrate refolding

Previous studies pointed out that the ATPase of Hsp70 proteins is not only determined by the ATPase domain, but rather regulated through allosteric communication all of the protein's domains. To examine how the lid domain influences the catalytic rate and the refolding activity of CeHsc70, carboxyterminal deletion fragments were planned. The sequence of CeHsc70 can be mapped to the crystal structure of the bacterial homolog DnaK. As the carboxyterminal helix-bundle of the lid domain seems to be stabilized by hydrophobic interactions, specific care was taken to avoid the generation of artificial hydrophobic interaction surfaces. CeHsc70- Δ 384 lacks the complete substrate binding domain, CeHsc70- Δ 512 the full SBD. CeHsc70- Δ 545 retains helix A and half of helix B of the lid-domain, missing the terminal helix bundle Figure 18.

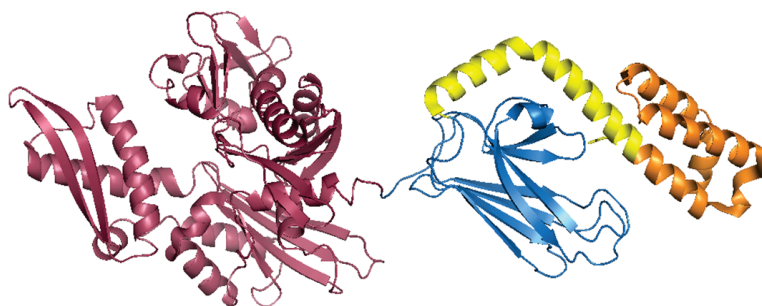


Figure 18: Lid truncations of CeHsc70. Mapping of the sequence of CeHsc70 on the structure of DnaK makes it possible to clearly define domain boundaries. Truncations can be designed containing the NBD only (CeHsc70- Δ 384) colored in red. The NBD and the SBD (red and blue) are part of CeHsc70- Δ 512. The mutant CeHsc70- Δ 545 lacks only the carboxyterminal helix bundle (orange). The mapping was based on the PDB file 2KHO (Bertelsen *et al.*, 2009).

To analyze, whether the hydrolytic activity of these fragments is uncompromised, ATPase assays were measured. All fragments bind ATP tightly and exhibit a slight reduction of their hydrolytic activity with increasing lengths of the lid domain. This effect is most pronounced for CeHsc70- Δ 545, which has approximately half of the activity of the full length protein (Table 17).

Protein	T_M DSF	T_M CD	ΔT_M ADP	K_M	k_{cat}
CeHsc70	38 °C	38 °C	7 °C	tight	$0.18 \pm 0.04 \text{ min}^{-1}$
CeHsc70- Δ 384	38 °C	38 °C	7 °C	tight	$0.21 \pm 0.04 \text{ min}^{-1}$
CeHsc70- Δ 512	38 °C	41 °C	7 °C	tight	$0.14 \pm 0.02 \text{ min}^{-1}$
CeHsc70- Δ 545	37 °C	37 °C	8 °C	tight	$0.09 \pm 0.02 \text{ min}^{-1}$

Table 17: Biophysical properties of CeHsc70 variants. The table lists the truncations of CeHsc70 that were used in this study and their biophysical properties. T_M DSF denotes the melting temperature according to DSF assays, T_M CD denotes the melting temperature according to CD thermal transitions. ΔT_M ADP indicates the stabilization upon the addition of ATP to DSF assays. K_M reflects the apparent K_D value and is given as a semi-quantitative value, as the evaluation of titration curves is not permitted due to substoichiometric saturation. The k_{cat} was determined by titration in regenerative ATPase assays.

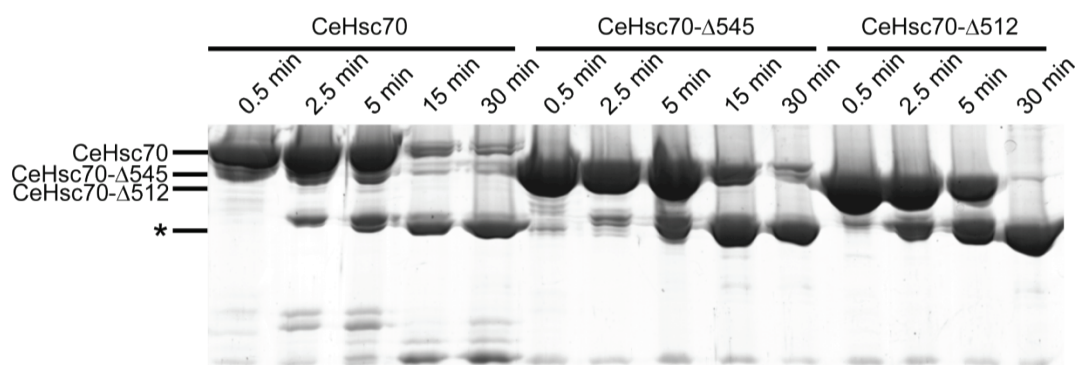


Figure 19: The stability of truncations of CeHsc70 is largely uncompromised. A similar stability of all fragments is indicated by limited proteolysis assays. CeHsc70, CeHsc70- Δ 545, and CeHsc70- Δ 512 were subjected to α -chymotrypsin digestion and subsequent denaturing gel electrophoresis after quenching the reaction at the indicated timepoints. The kinetics are similar for all proteins, which all degrade to the same species. The molecular weight at which the isolated NBD migrates is indicated by the asterisk.

The observed effect could however be related to a compromised stability of the NBD. To assess this option, limited proteolytic digestions were performed on the truncation fragments. All fragments are degraded at a similar rate and yield a similar product which corresponds well to the isolated NBD, suggesting that the stability of the core protein is uncompromised by lid truncations (Figure 19).

The stability of the proteins can also be assessed by CD thermal transitions. In this experimental setup, primarily the loss of secondary structure is detected. The data indicate that upon heating, all variants melt in a very similar temperature range and with a similar cooperativity. The stability of the full length protein is equal to CeHsc70- Δ 384, indicating that the isolated ATPase domain is not destabilized. CeHsc70- Δ 512 may be judged to be slightly more stable than the full length protein and CeHsc70- Δ 545 slightly less stable (Figure 20, Table 17). Both observations may be due to the presence of different parts of the carboxyterminal domains and reflect a signal contribution of these structures. For comparison, HsHsc70 was examined in these experiments to further confirm the data discussed in section 1.1. The experiment confirmed that the CD data correspond well to DSF data for Hsc70 proteins and highlights that the changes in stability observed in CD for CeHsc70 truncations are rather subtle. However, HsHsc70 seems to denature less cooperatively.

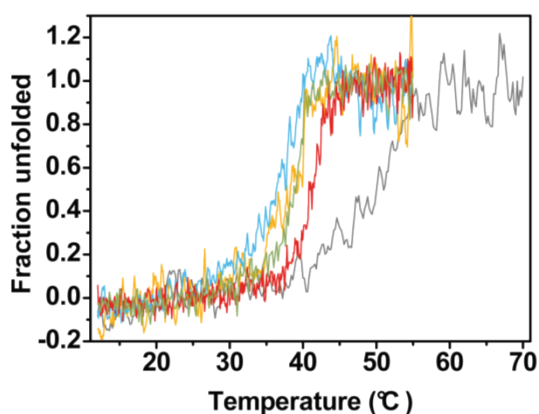


Figure 20: CD thermal transitions of CeHsc70. CD thermal transitions indicate that all variants of CeHsc70 - although generally less stable than the human protein (grey) are comparably stable (CeHsc70, yellow; CeHsc70- Δ 545, light blue; CeHsc70- Δ 512, red; CeHsc70- Δ 384, green).

Results

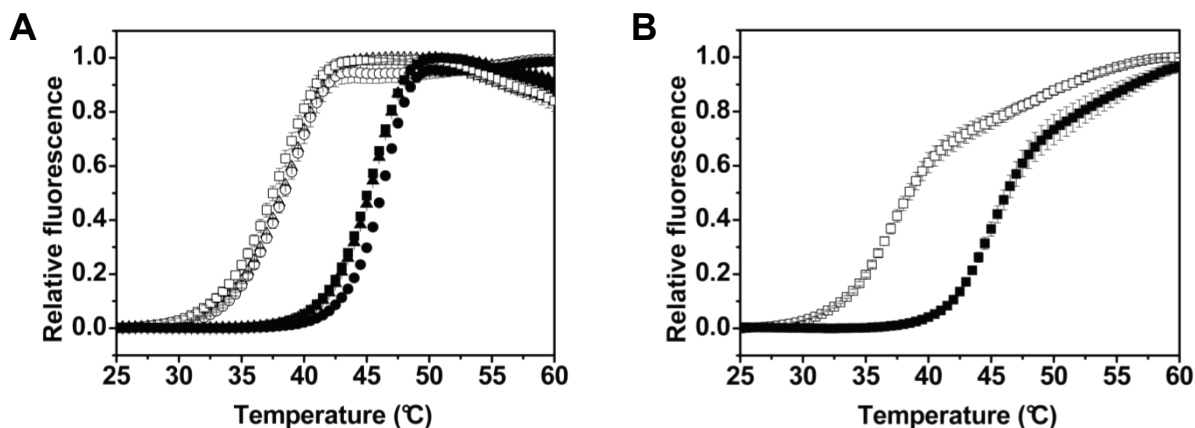


Figure 21: DSF thermal transitions of CeHsc70 truncations. (A) DSF data support a comparable overall stability for CeHsc70 (□), CeHsc70-Δ545 (Δ), and CeHsc70-Δ512 (○). The fragments and the full-length variant are stabilized to the same extent by ADP (■, ▲, ●, respectively). (B) CeHsc70-Δ545 (□) exhibits a slightly different transition curve. The transition midpoint at ~37 °C and the stabilization by ADP (■) by ~8 K is in agreement with the other fragments' properties.

As described in section 1.1, DSF assays are able to assess the general stability of a molecule, but also provide information about ligand binding by thermal stabilization of the structure through the bound molecule. Consequently, the truncation variants were subjected to these assays. Transitions recorded in the absence of ADP indicate that all truncations are identically stable without bound nucleotide (Figure 21 and Table 17). However, upon the addition of ADP the melting temperature is equally shifted for all variants by 7-8 K, which roughly equals the data observed for the human version (cf. Figure 7). These results demonstrate that neither the stability nor the nucleotide binding capability is impaired by carboxyterminal truncation.

As the truncations had no major effect such as abolishing the hydrolytic activity or destabilizing the enzyme's structure or compromising its ATP binding capacity, it was interesting to see, whether the refolding activity would be at least slightly impaired. The fragments of CeHsc70 were unable to refold luciferase to gain activity above baseline (Figure 22). This indicates that the whole lid domain is required for the biological activity of the Hsc70 chaperone machinery from *C. elegans*. The domain is however dispensable for hydrolytic activity and nucleotide binding. Similar observations have been made for the human system (Freeman *et al.*, 1995; Strub *et al.*, 2008).

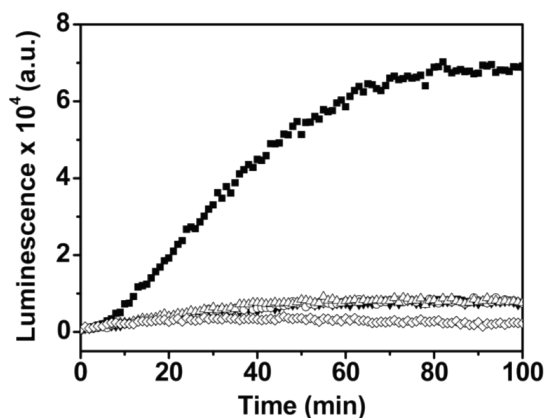


Figure 22: Substrate refolding requires the substrate binding and lid domains. The truncations CeHsc70-Δ545 (▼), CeHsc70-Δ512 (○) and CeHsc70-Δ384 (Δ) are incapable to refold firefly luciferase above control (◇) levels at ideal cochaperone concentrations. Solely the full length protein CeHsc70 (■) is capable to recover luciferase activity.

2 Hsp90's function in the muscle of *C. elegans*²

2.1 A compromised Hsp90 system leads to motility defects and mortality

The nematode strain JT6130 (*daf-21*{*p673*}) is characterized by the single point mutation E292K in the open reading frame of *daf-21* (Birnby *et al.*, 2000). To investigate the influence of this mutation on the lifespan of the nematode, synchronized WT worms and JT6130 nematodes were subjected to lifespan assays. For JT6130 it is known that a fraction of animals enter the dauer state constitutively (Birnby *et al.*, 2000). Consequently, only animals that developed normally and reached adulthood within the same number of days as the control worms were evaluated. About 50% of the JT6130 nematodes died between days 8 and 10, while the remaining 50% did not show a reduced lifespan compared to N2 nematodes (Figure 23). Throughout their life, *daf-21*(*p673*) nematodes were less motile. The amount of thrashes in a defined time period was reduced by about 30% at the beginning of adulthood and remained lower throughout the aging process (Table 18). In order to confirm the involvement of specifically DAF-21 in the observed phenotypes, transcript levels in WT worms were reduced by feeding RNAi using a construct described before (Gaiser *et al.*, 2009). The worms remained sterile as previously described (Inoue *et al.*, 2006). Also upon knockdown of *daf-21*, the worms' capacity to move was markedly reduced. A similar effect could be observed when the cochaperone UNC-45 was depleted. Both proteins are consequently important to maintain normal motility of nematodes upon aging.

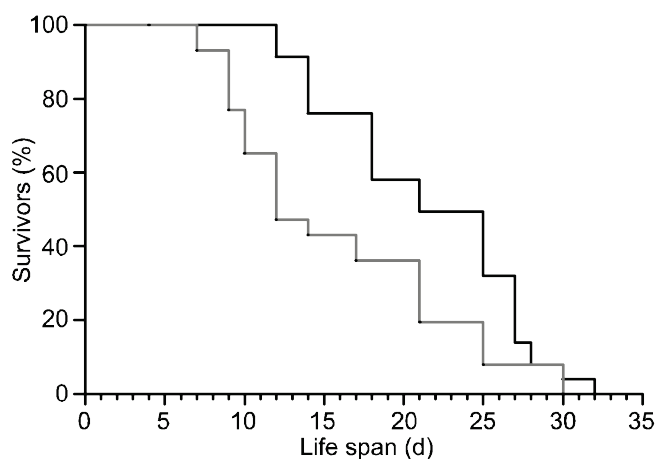


Figure 23: Impaired Hsp90 function reduces the lifespan. A Kaplan-Meier plot comparing N2 (black line) and JT6130 (grey line). 80 individuals of each strain were subjected to lifespan analysis at 20 °C after hatching. The mean lifespan was determined to be 18.7 d \pm 1.7 d for N2 and 12.8 d \pm 1.8 d for JT6130 (mean \pm SD) from five experiments.

² This section is adapted from the corresponding previous publication as indicated under 'Publications'.

Results

Time after hatching	N2	<i>daf-21(p673)</i>	control RNAi	<i>daf-21</i> RNAi	<i>unc-45</i> RNAi
(d)	(Thrashes per min \pm SD)				
4	95 \pm 6	73 \pm 10	85 \pm 8	61 \pm 12	10 \pm 3
7	91 \pm 8	55 \pm 5	87 \pm 9	38 \pm 6	4 \pm 3
10	94 \pm 15	63 \pm 6	n.d.	n.d.	n.d.

Table 18: The dependence of motility on Hsp90 function. The thrashing behavior of N2 animals, JT6130 (*daf-21{p673}*) and N2 depleted for DAF-21 or UNC-45 was determined during aging.

2.2 *Daf-21* is ubiquitously expressed

As the effects of Hsp90 depletion or dysfunction are not restricted to muscular phenotypes, but also have been described to lead to protruding vulvae and an increased fraction of worms entering the *dauer* state constitutively, the tissues expressing *daf-21* should be defined in more detail. These experiments are of high relevance, as in worms no effect of Hsp90 depletion on motility behavior has been observed before. Consequently, the motility defect phenotype was surprising. To detect, which tissues synthesize DAF-21, the stable reporter strain BC10293, which contains a transcriptional fusion of GFP to the *daf-21* promoter (McKay *et al.*, 2003) was subjected to closer inspection. Individuals of this strain exhibited varying expression patterns. The *daf-21* promoter led to GFP expression in the excretory system, pharyngeal muscle cells and

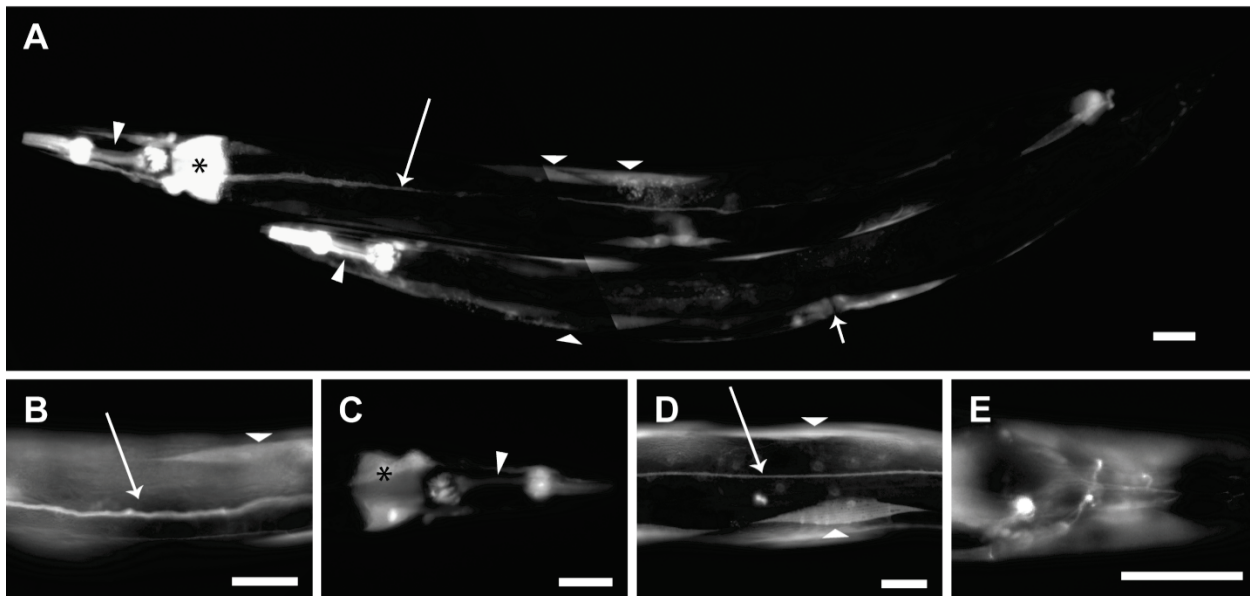


Figure 24: Expression of *daf-21* in stable and transient lines. (A) Nematodes of the strain BC10293 strain, which contains a transcriptional fusion of GFP to the *daf-21* promoter exhibit fluorescence in the excretory canal cell (long arrow), in the pharyngeal muscle cells (sharp triangle) and the cells of the first intestinal ring (asterisk) and the pharyngeal muscle (sharp triangle). Furthermore, individual muscle cells (blunt triangle) and the vulval muscles (short arrow) show fluorescence. (B) Detailed views of the same strain highlight the excretory canal cell (long arrow), an individual muscle cell (blunt triangle), (C) the pharyngeal muscle cells (sharp triangle) and the cells of the first intestinal ring (asterisk). (D) Newly generated transgenic nematodes, carrying a *daf-21* promoter sequence fused to YFP. Fluorescence is detected in the excretory canal cell (long arrow) and body wall muscle cells (wide triangles) and (E) some head neurons. The scale bar represents 40 μ m in all subpanels.

intestinal cells (Figure 24 A-C). Furthermore, sporadic expression could be observed in body wall muscle cells (Figure 24 A and B).

To confirm these expression patterns, a reporter plasmid containing a longer (2.5 kb) genomic sequence upstream of the DAF-21 start codon including the protein's first 4 amino acids fused to YFP was microinjected into WT nematodes. It was possible to obtain about 100 F1 offspring, some of them brightly fluorescent, but not stably transgenic (Figure 24 D and E). Still, these F1 animals exhibited fluorescence patterns similar to the stable reporter BC10293, consequently, the expression in body wall muscle cells was reiterated using a different promoter region, highlighting that the observed patterns of *daf-21* – especially in respect to muscular expression – may be assumed to be robust (Figure 24 D). Additionally, fluorescence in single head neurons could be detected (Figure 24 E). Therefore, according to these data, Hsp90 is constitutively expressed in many tissues of nematodes, including body wall muscle cells, however not to an overall equal extent.

2.3 DAF-21 suppresses the muscular heat shock response

As the Hsp90 class of chaperones has been frequently described as heat shock proteins (Richter *et al.*, 2010), the inducibility of expression in the reporter strains was probed. Although procedures for which the heat shock response can be induced for other heat shock proteins (HSP-16.11 and HSP-70) were applied, no change in tissue patterns or fluorescence intensity in comparison to those stated above (cf. Figure 24) could be detected. To understand, whether this is caused by the way the reporters were constructed, the transcription level of *daf-21* was directly analyzed in WT animals by RT-qPCR on heat shocked and non heat shocked nematodes (Figure 25). The transcription of *daf-21* was not affected by heat stress, although the genes *hsp-70/C12C8.1* and *hsp-16.11/T27E4.2* were about 40-fold overexpressed under this condition. The constitutively expressed Hsc70-homologue *hsp-1/F26D10.3* was slightly reduced in response to heat shock. Thus, *daf-21* is constitutively expressed in various tissues and its expression is not strongly affected by heat shock and therefore cannot be considered a typical heat shock protein in *C. elegans*.

Beyond being a heat shock protein, Hsp90 is known to participate in the regulation of the heat shock response via binding to Hsf1 as described by Voellmy (2004). Inhibition of Hsp90 by

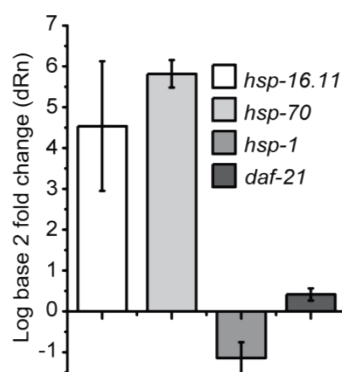


Figure 25: Inducibility of selected heat shock proteins. RT-qPCR data on the relative abundance of the transcripts of *hsp-16.11*, *hsp-70*, *hsp-1* and *daf-21* after heat shock. Relative abundance was determined in relation to the levels of both, *act-1* and *pgk-1* mRNA. The mean and SD comparing four separate biological replicates are given.

Results

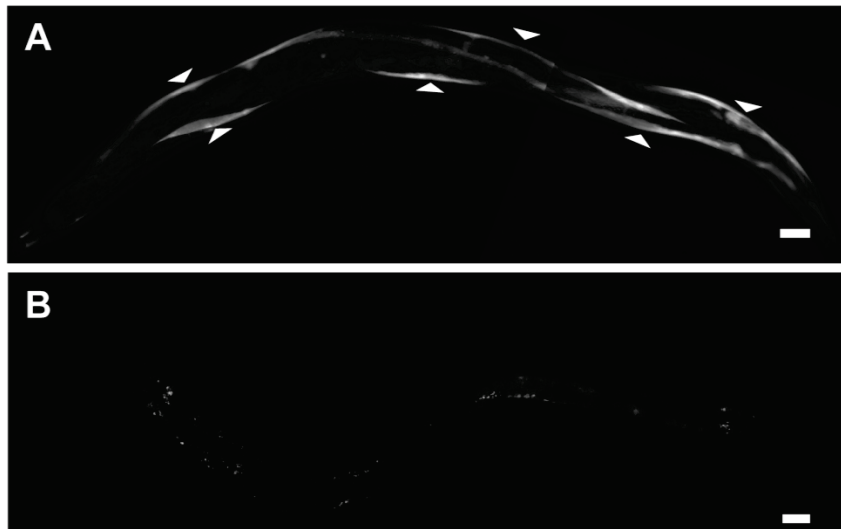


Figure 26: *daf-21* RNAi induces heat shock in muscle cells. (A) Upon feeding RNAi against *daf-21* for three days, nematodes bearing an integrated *hsp-70::GFP* reporter exhibited GFP fluorescence in the body wall muscle cells (blunt triangles). (B) Mock-treated age-matched individuals did not exhibit specific fluorescence, despite longer exposure times. At these longer exposure times unspecific fluorescence in the intestinal cells is detected. The scale bar represents 20 μm in both micrographs.

small molecules strongly induces Hsp70 and other heat shock proteins in mammalian cell culture (Kim *et al.*, 1999). To test whether this function is conserved for DAF-21, a heat shock reporter strain was used, in which the *hsp-70* promoter controls GFP expression (*hsp-70::GFP*). This strain shows the induction of fluorescence in many tissues after heat shock (Morley & Morimoto, 2004). Feeding these nematodes with RNAi directed against *daf-21* resulted in the specific appearance of GFP in body wall muscle cells (Figure 26), while nematodes treated with control RNAi did not show induction. Thus, the reduction of Hsp90 levels particularly initiates the stress response in muscle, leading to the compensatory induction of chaperones.

2.4 DAF-21 and UNC-45 are responsible for proper myosin deposition

A compromised DAF-21 functionality results in a phenotype that may be attributed to the muscle system, the knockdown of *daf-21* reproduces this effect as well as the knockdown of *unc-45* (cf. 2.1). In consequence, the hypothesis was established that the organization of the myofibrillar lattice might be compromised. To test this, the strain RW1596 was chosen. It provides clear

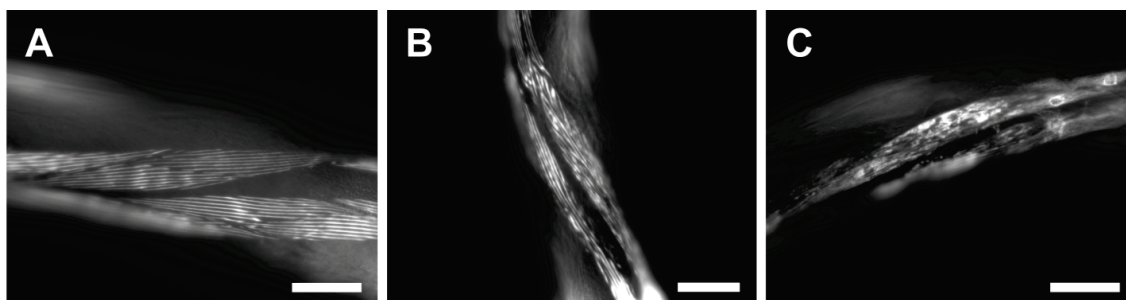


Figure 27: Reduced *daf-21* and *unc-45* levels disrupt the muscular ultrastructure. The strain RW1596 reveals details of muscular organization due to the expression of a MYO-3-GFP fusion protein. The worms were treated either with mock RNAi (A) or RNAi against *daf-21* (B) or *unc-45* (C). The scale bar represents 40 μm for all micrographs.

visualization of the myosin rich M-line due to the fusion of GFP to the myosin heavy chain protein MYO-3 (Campagnola *et al.*, 2002). Muscle striation appeared homogenous and parallel in nematodes of RW1596 exposed to control RNAi (Figure 27 A). In accordance to the hypothesis, worms exposed to *daf-21* RNAi, exhibited an inhomogeneous and disrupted striation pattern (Figure 27 B). This effect was even stronger upon knockdown of the Hsp70/Hsp90-cofactor *unc-45*, exhibiting a more severe disorganization of the muscular actomyosin lattice (Figure 27). This observation may explain the loss of motility upon aging (cf. section 2.1). Scoring 40 animals for each experiment, all animals were affected upon knockdown of *unc-45* at day 5 after synchronization, whereas about 60% of the nematodes were affected from muscular disorganization upon *daf-21* RNAi.

In order to obtain a more profound picture of how the muscular ultrastructure is affected, the nature of the structural disruption was examined more closely by confocal microscopy. As above, animals were treated with RNAi against *daf-21* and *unc-45*. Upon knockdown of both transcripts, the striation of the muscle cells seemed to be surprisingly intact in focal planes close

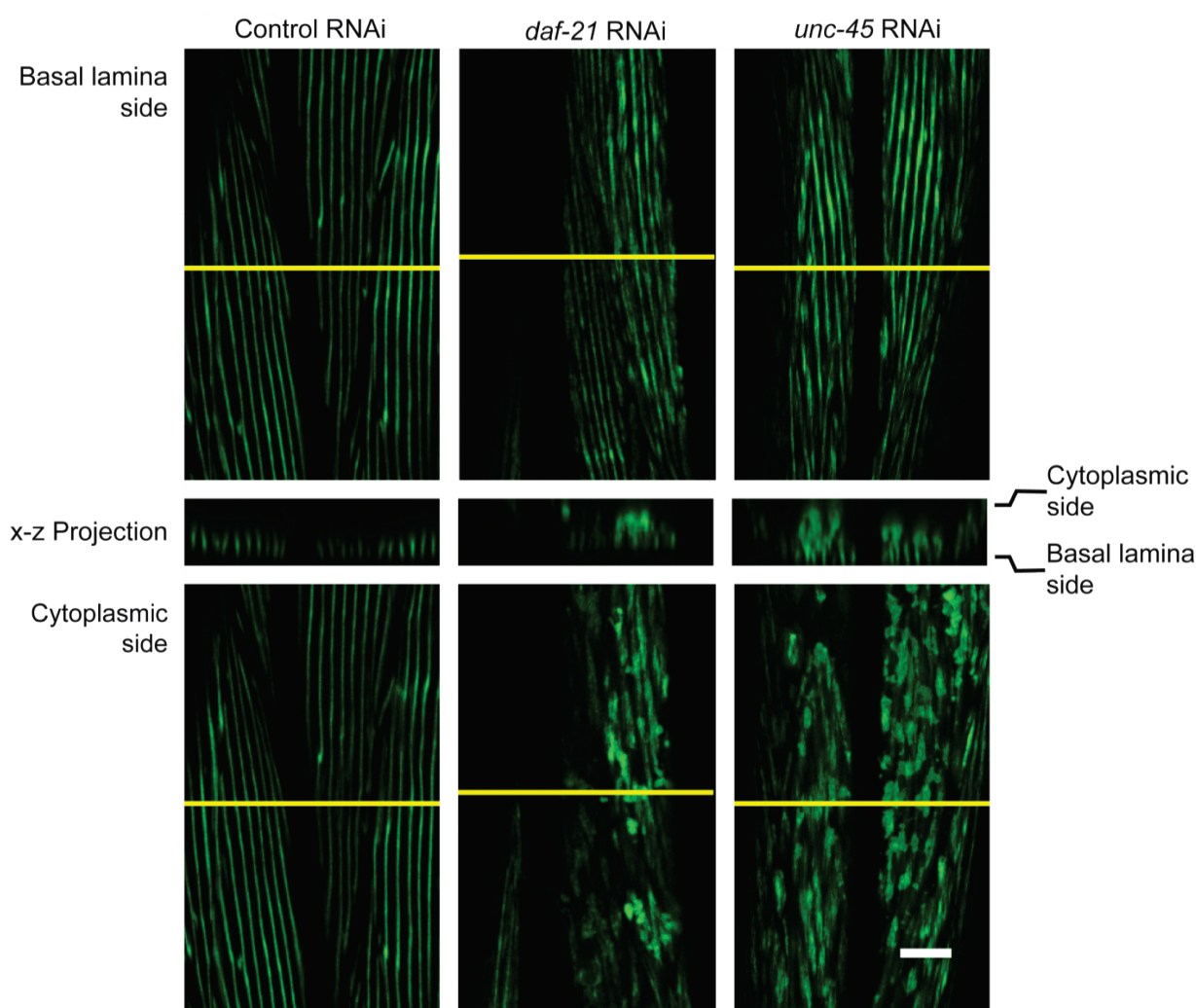


Figure 28: Reduction of *daf-21* or *unc-45* leads to myosin aggregation. Animals, treated as in Figure 27 were analyzed by confocal microscopy. Although the striated pattern seems intact by either knockdown in an optical sectioning plane close to the basal lamina (upper row), in sections closer to the muscle cell body (lower row), aggregates become apparent when UNC-45 or DAF-21 are depleted. A projection of the x-z plane along the yellow line in both x-y planes further highlights the accumulation of misplaced MYO-3 at the cytoplasmic side of the sarcomeric lattice. The scale bar represents 10 μ m in all micrographs of the figure.

Results

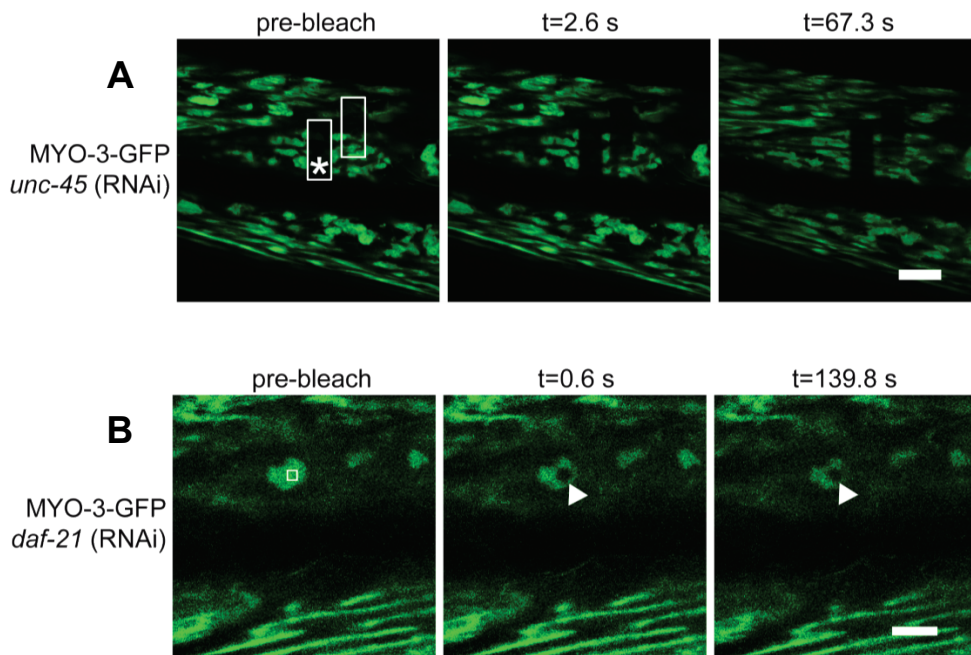


Figure 29: Focal depositions of MYO-3-GFP are non-diffusible. The structures found in animals treated with RNAi against *unc-45* (A) and *daf-21* (B) were subjected to FRAP analysis and recovery was recorded for the indicated times. No recovery is observable for both RNAi experiments. The bleaching sites are boxed in the pre-bleach micrographs. For *unc-45* RNAi the area of a previous bleach is marked with an asterisk and still is visible after several minutes. The scale bars represent 10 μm and apply to all micrographs of one bleaching experiment.

to the basal lamina (Figure 28). Upon the examination of focal planes closer to the cell body slightly outside the myofibrillar lattice, fluorescent patches of GFP-MYO-3 became apparent. FRAP experiments on mislocalized GFP-MYO-3 in both strains revealed that the myosin in these structures is non-diffusible (Figure 29), pointing to protein aggregation. As extensive disruption of the sarcomeric lattice was neither observed upon *daf-21* RNAi nor upon *unc-45* RNAi treatment, it can be speculated that the fluorescent myosin patches are connected to the phenotypic loss of motility and a phenomenon of a compromised myofibrillar building block turnover or assembly during lattice expansion in body growth, which both could both be processes dependent on DAF-21 and UNC-45.

2.5 DAF-21 and UNC-45 are differentially distributed in muscles

The organization of the nematodal muscular ultrastructure is related but not identical to that of higher metazoan systems. The center of the sarcomere is formed by myosin filaments (M-line) and consists of myosin heavy chains, which may be visualized by MYO-3-GFP. The M-line is part of the A-band which additionally contains actin filaments and the myosin head domains responsible for contraction. The myosin-free area of the sarcomere is the I-band, which is subdivided into two half-I-bands by the dense bodies. The dense bodies serve as actin attachment sites and are consequently functionally analogous to the Z-line in mammalian muscles. In contrast to the mammalian striated musculature, the sarcomeres run not perpendicularly to the striation, but obliquely at an angle of 5-7 $^{\circ}$ (Waterston, 1988). The staggered order of sarcomeres still yields the impression of regular striation on a microscopic level (Figure 30).

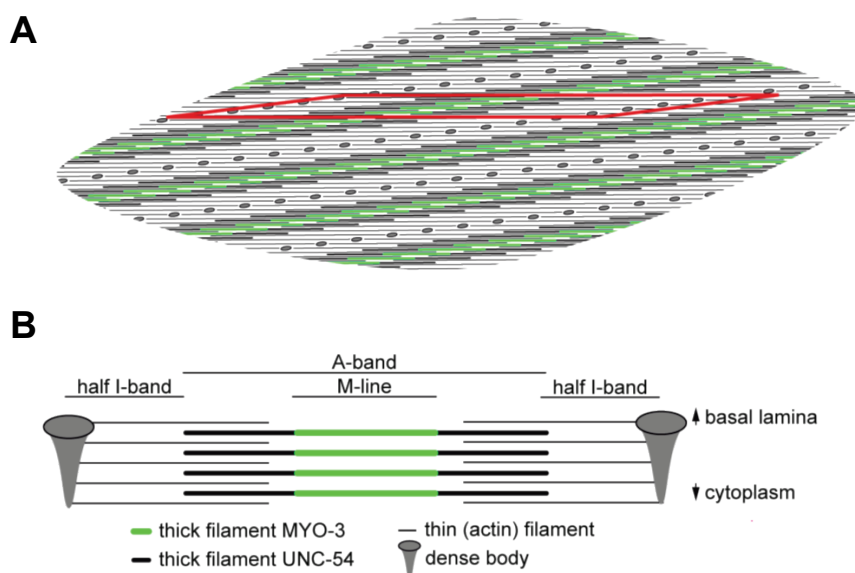


Figure 30: The organization of nematodal body wall muscle cells. (A) A top-view schema of a body wall muscle cell of *C. elegans*. The illustration clearly highlights the oblique character of the striation, as sarcomeres run in an angle of 6° in relation to the macroscopic striation. The MYO3-rich M-line of thick filaments is highlighted in green. The red rhomboid is one sarcomere wide. (B) A section along the long edge of the rhomboid in (A) reveals the sarcomere structure more clearly. Between two rows of dense bodies the actin filaments span into the I- and A-band. Within the A-band the thick filaments are found which consist of UNC-54 (black) and MYO-3 (green) in their center, which is the M-line. The myosin attachment sites in the M-line have been omitted for clarity.

As DAF-21 and UNC-45 are required for the correct localization of myosin into the sarcomeric lattice, the subcellular localization of both proteins was analyzed in live nematodes. Both, the aminotermminus and the carboxyterminus of Hsp90 are known to be important for its enzymatic activity and cofactor interaction. However, the linker region of 60 amino acids has previously been shown to be inessential for proper function (Louvion *et al.*, 1996). Consequently, YFP was inserted into this flexible region of DAF-21 to interfere the least possible with the chaperone's functionality.

To probe the conservation of proper functionality of YFP-DAF-21, the protein was recombinantly expressed and purified. The chaperone activity was uncompromised, the ATPase activity slightly reduced, but retaining its ability to be stimulated by CeAha1. The binding of TPR-containing cofactors such as PPH-5 and an aminoterminal fragment of UNC-45 proved to additionally be preserved. The fusion was able to form heterodimers with WT DAF-21, suggesting that in the cytosol, heterodimer formation with endogenously expressed protein should be possible (Gaiser *et al.*, 2011).

Using the well-established *unc-54* promoter, YFP-DAF-21 was targeted to body wall muscle cells. As no stable transgenic line could be obtained by injection of this construct, transiently transformed animals were analyzed. Interestingly, YFP-DAF-21 was not homogeneously localized within body wall muscle cells. Instead, it exhibited a striated pattern, closely matching the striation of muscle cells. To determine at what band YFP-DAF-21 is enriched, z-stacks of whole cells were recorded in fluorescence and simultaneously in DIC channels on a confocal microscope. The clearly discernible dense bodies were used as landmarks for the localization of the I-band and the relative position of the other bands of the myofibrillar lattice was determined. Overlaying the DIC image and the fluorescence optical section through the lattice in a plane very close to the basal lamina revealed the fluorescence being localized to the space between the

Results

dense bodies, clearly excluded from these structures and the remainder of the I-band (Figure 31). The continuous line of DAF-21-localization between two rows of dense bodies correlates well to the broad A-band, probably even more specifically to the M-line, as localization is sharply restricted to the very middle of the A-band. Comparing several cells with different expression levels, it appeared that the localization to the M-line can only be observed if expression levels are high, while in cells expressing lower levels of YFP-DAF-21, the fusion protein only localized to the I-band. To understand, whether this pattern of localization is characteristic for DAF-21, it was compared to the pattern obtained from strain AM134, which expresses YFP in body wall muscle cells as a reference (Figure 31). YFP was excluded from the dense bodies as well. However, the protein is more uniformly distributed throughout the myofibrillar lattice in this focal plane.

The comparison of the YFP-DAF-21 patterns to that of YFP in an optical sectioning plane closer

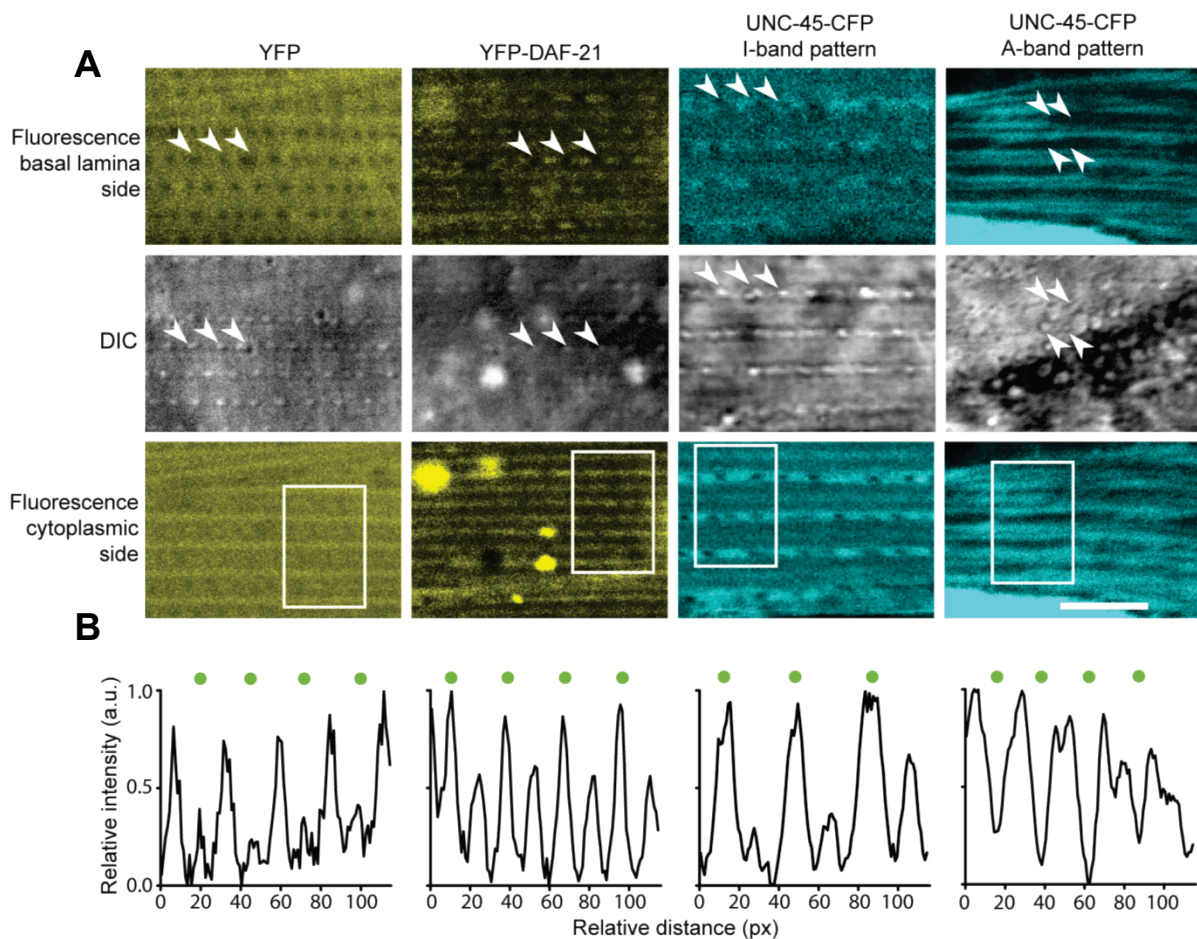


Figure 31: DAF-21 and UNC-45 localize to specific parts of the sarcomeric lattice. Confocal image stacks of muscle cells of YFP (strain AM134), YFP-DAF-21 and UNC-45-CFP expressing nematodes were recorded. (A) Fluorescence micrographs of optical sections through the sarcomeric lattice close to the basal lamina (basal lamina side) are presented together with simultaneously recorded DIC images. The dense bodies are indicated by arrowheads in the DIC images. The corresponding positions are marked in the fluorescence image. Below, fluorescence micrographs of optical sections closer to the muscle cell body (cytoplasmic side) taken from the same image stacks are presented. The scale bar represents 5 μm for all micrographs. (B) The striation patterns within the white frames in the micrographs in (A) at the cytoplasmic side were analyzed in respect to fluorescence intensity distribution. The plots present the normalized and line-averaged pixel intensity along the long edge of the box. The intensities were plotted starting at the bottom of the box. The peaks corresponding to the central I-band (dense body position in DIC images) are marked (green dots) in order to allow the comparison of relative fluorescence distributions.

to the muscle cell body revealed that YFP-DAF-21 was still mainly localized to the I-band, the M-line localization being detectable. Quantification of the bands clearly illustrates that within the repetitive structure of the muscle fiber, the two bands show enrichment of fluorescent protein. In the strain AM134 expressing YFP, the M-line was slightly enriched in fluorescence but still exhibited a high background of homogeneous distribution in a similar sectioning plane. Therefore, a specific enrichment of YFP-DAF-21 in the I-band can be inferred, while both, YFP and YFP-DAF-21 can apparently access the M-line of the muscular structure. YFP-DAF-21 is more restrictively excluded from the actin and myosin containing parts of the A-band.

To compare the localization of DAF-21 to UNC-45, nematodes expressing UNC-45-CFP in body-wall muscles were generated. The protein's localization was determined as described above. Interestingly, the bands containing DAF-21 also contained UNC-45-CFP in most cells (denoted I-band pattern). But in contrast to DAF-21, another distinct pattern of localization could be discerned. About 20% of the cells observed contained UNC-45 specifically in those areas, where DAF-21 had been excluded from. In these cells, a clear localization of UNC-45-CFP to the A-bands is visible, but the thin M-line is excluded (A-band pattern). Thus, the accessibility to the muscular ultrastructure overlaps for both proteins in the I-bands and M-line, while other parts of the myofibrillar lattice are only accessible to UNC-45.

2.6 Chaperone association to specific bands can be dynamic or stable

Association to myofibrillar structures may be dynamic or stable. To determine, whether the

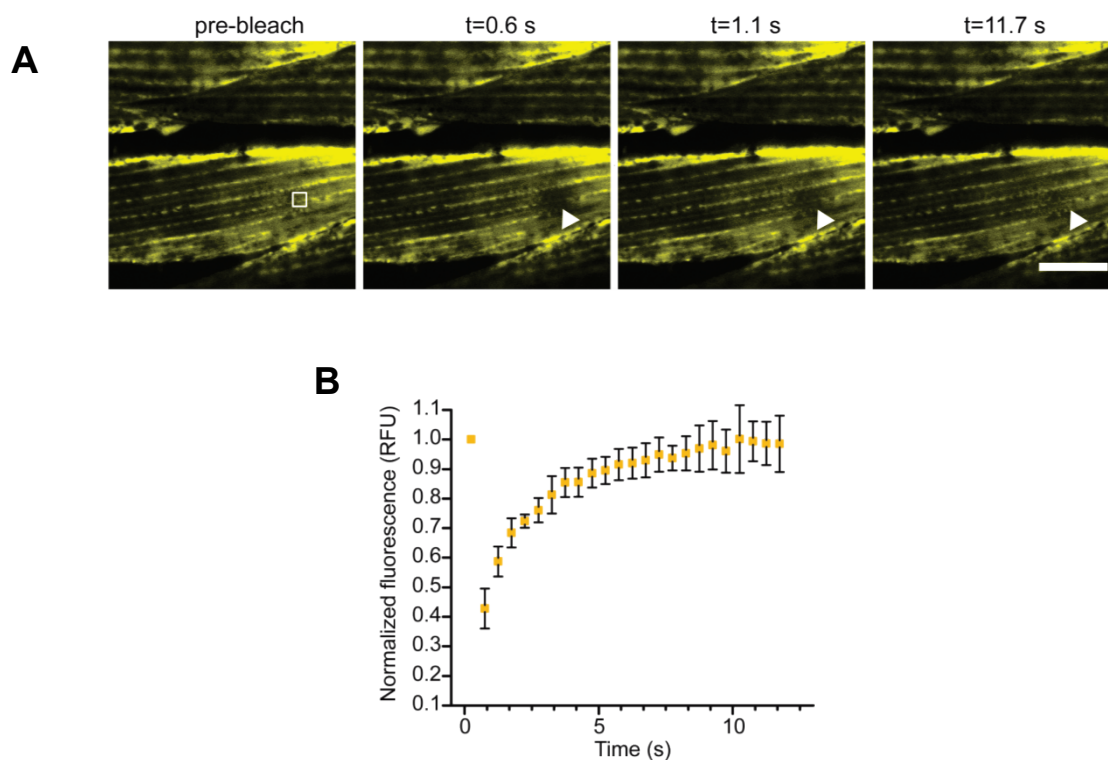


Figure 32: I-band associated Hsp90 is freely diffusible. Nematodes expressing YFP-DAF-21 were subjected to FRAP experiments. (A) Images before bleaching and during recovery at the indicated time points are shown. The bleached area is highlighted by a white frame. The scale bar represents 10 μm for all micrographs in the panel. (B) The kinetic evaluation of YFP-DAF-21 bleaching experiments exhibits a fast recovery with a time constant of ~ 1 s and is derived from triplicate experiments. The error bars reflect the SD.

Results

localization patterns described above (cf. section 2.5) reflect stable association or whether they are dynamic, the respective patterns were analyzed by FRAP.

In the case of YFP-DAF-21, the initial loss of fluorescence was $\sim 60\%$ of the original intensity, indicating a very rapid recovery of fluorescence by freely diffusing YFP-DAF-21 within the first 600 ms after photobleaching. Fluorescence recovered at a time constant of ~ 1 s (Figure 32). From these data, it may be concluded, that the majority of DAF-21-YFP molecules is not stably attached to the muscular structure, despite being able to refold substrates and bind to TPR-

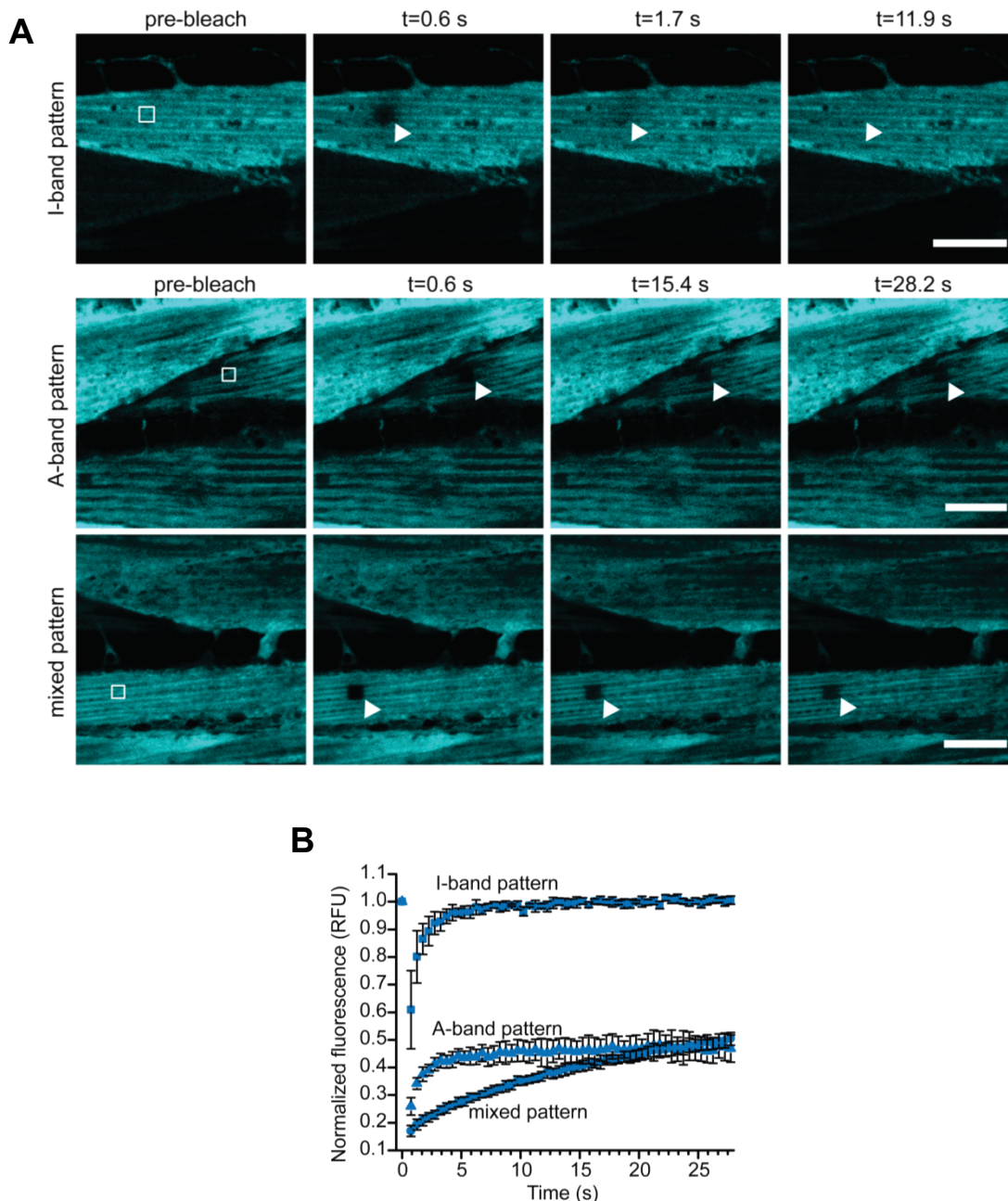


Figure 33: UNC-45 is diffusible in or stably associated to the sarcomeric lattice. Worms expressing UNC-45-CFP were subjected to FRAP experiments. (A) Representative single experiments are shown for each discernible banding pattern. The I-band pattern recovered immediately after photobleaching, while protein localizing to the A-band did not recover within observation time. When a mixed pattern was observed, recovery was generally slow. The scale bar represents $10 \mu\text{m}$ for all micrographs in each experiment. (B) For the kinetic evaluation of the bleaching experiments, cells of the indicated type were evaluated by averaging triplicate FRAP experiments. The error bars represent the SD.

domain containing proteins (Gaiser *et al.*, 2011).

It appears to contribute to muscular stability as a transiently associated factor. A similar analysis for UNC-45-CFP was performed. In cells, which showed the I-band pattern described before (cf. section 2.5), the protein proved to be as freely diffusible as YFP-DAF-21. In cells showing UNC-45-CFP localization to the A-bands (A-band pattern), recovery was slow and even after five minutes, the bleached area had not recovered its fluorescence fully. Through the analysis of a greater pool of cells, intermediate or mixed expression patterns were observed (mixed pattern) (Figure 33). In these mixed pattern cells, the extremely slow recovery may be interpreted as contributions of different populations of protein strongly bound to sarcomeric structures and a subpopulation that is freely diffusible. Thus, UNC-45 appears stably associated to the A-band, while the protein, when localized to the I-band is – like DAF-21 – freely diffusible.

These observations hint to at least two distinct populations of UNC-45 in muscle cells and might be explained by a variable number of accessible UNC-45 binding sites at the A-band, which upon saturation allow the accumulation of a freely diffusible UNC-45 population. Also, under conditions still to be elucidated, UNC-45 may change its localization and consequently its binding state to specific muscular proteins found in these bands.

3 A network of genes connects polyglutamine toxicity to ploidy control³

Although the aggregation of polyglutamine proteins has been under scrutiny before in other organisms as well as in yeast, it seemed justified to establish a different model in this organism that still provides unique means to study the effect of genetic manipulation on a genome-wide scale. Three major issues concerning previously published systems are evident: (I) very long polyQ stretches which are far above the threshold of toxicity observed in humans had been deployed before to obtain toxicity in yeast, (II) the yeast system previously described (Giorgini *et al.*, 2005) is strongly dependent on the endogenous state of the prion RNQ1, rendering the discrimination of effects of prion biology and aggregation biology difficult, and (III) differences in respect to the flanking or capping sequences render generalization to other polyQ proteins than Htt difficult.

3.1 A relatively short polyQ stretch is cytotoxic

To study polyQ aggregation in yeast, a system of three vectors was designed containing a repetitive sequence of CAG and CAA codons, resulting in stretches of zero, 30 or 56 glutamine residues. This polyQ stretch is fused to a short polylinker sequence followed by the enhanced yellow fluorescent protein (Q₀-YFP, Q₃₀-YFP and Q₅₆-YFP). The yeast multi copy plasmid p425GPD (Mumberg *et al.*, 1995) was chosen as it provides high constitutive expression. The plasmids were termed pQ0, pQ30 and pQ56 corresponding to the length of the polyQ stretch. When transformed into WT haploid *MATa* yeast cells (BY4741) and plated on selective agar, a homogeneous population of colonies developed from cells transformed with pQ0 and pQ30. Contrarily, cells transformed with pQ56 yielded an inhomogeneous colony pattern, consisting of roughly 95% of small colonies, 4% intermediately sized colonies and 1% large colonies per plate (Figure 34).

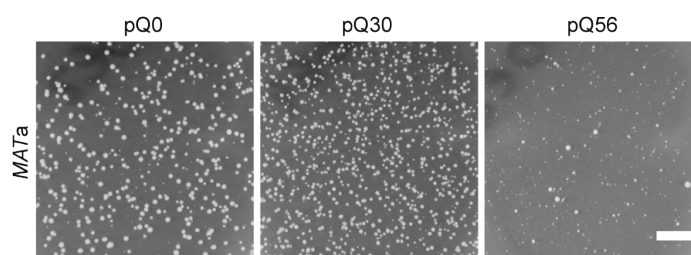


Figure 34: A population-based toxicity phenotype in yeast. WT haploid *MATa* yeast exhibit a toxicity phenotype, which is only apparent after transformation with pQ56 but not in control transformations with equal amounts of pQ0 and pQ30. The scale bar represents 10 mm.

³ A manuscript based on this section has been submitted and is currently being revised as indicated under 'Publications'.

Results

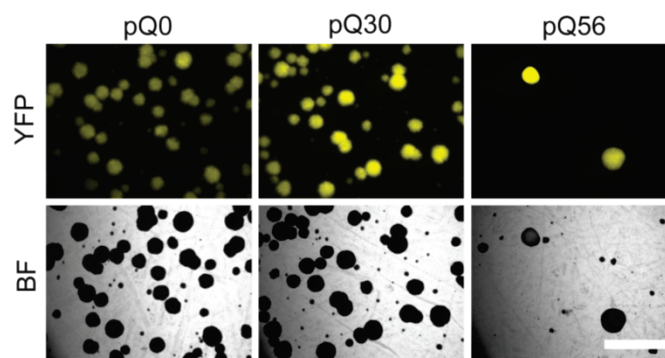


Figure 35: Colony fluorescence of polyQ transformants. Fluorescence (YFP) and bright field (BF) micrographs of WT *MATa* cells reveal that pQ0 and pQ30 transgenic cells yield colony patterns with bright and homogeneous colony fluorescence. When transformed with pQ56, transformant number generally decreased and colonies became inhomogeneous in respect to size and fluorescence intensity. The scale bar represents 5 mm and applies to all micrographs.

To estimate the growth potential of cells making up the average colony on transformant plates, individual colonies were picked and replated on selective agar. The colonies previously transformed with pQ0 and pQ30 contained about 1200 colony forming units (CFU) per 1×10^4 cells plated. A similar number of CFU was observed for the few large colonies on pQ56 transformant plates. The predominant small colony type present upon transformation with pQ56, however, contained only between 1 and 15 CFUs, indicating that the cytostatic effect persists for about 99% of the cells originally forming a colony, rendering them unable to generate vital offspring.

Fluorescence microscopy of the transformant plates also revealed that the expression of Q₅₆-YFP in the predominant small colonies is generally much lower than in control colonies producing Q₃₀-YFP or Q₀-YFP. Only a subset of the few large colonies transformed with pQ56 exhibit high fluorescence levels (Figure 35).

On the cellular level, the fluorescence distribution in all three polyQ variants was analyzed. While no fluorescent foci were present in cells transformed with pQ0, Q₃₀-YFP had a tendency to form clusters of strong fluorescence varying in size and shape, ranging from globular foci to

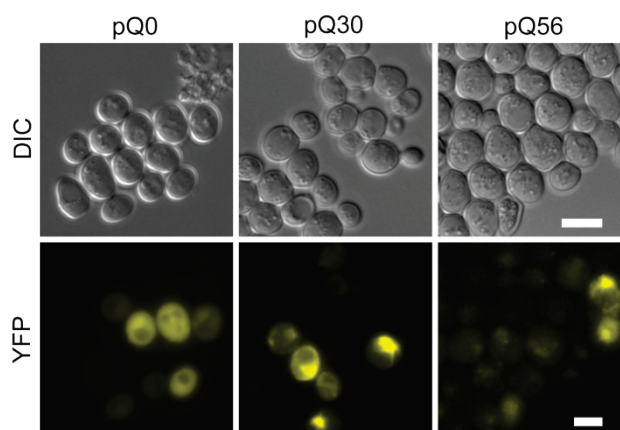


Figure 36: Q₃₀-YFP and Q₅₆-YFP form aggregates of distinct morphology. WT haploid *MATa* yeast transformed with pQ0 exhibited a homogeneous distribution of fluorescence (YFP). This changed for pQ30, where the polyQ protein also could be detected in focal and fibrillar inclusions of high intensity. Cells intoxicated with Q₅₆-YFP generally exhibited reduced fluorescence intensity. Still, many cells possessed inclusions that seemed less dense. Also, very small, bright and highly diffusible foci were detected, but hardly imaged. A small fraction of cells exhibited focal deposits comparable to Q₃₀-YFP. The scale bar represents 5 μ m and applies to all micrographs.

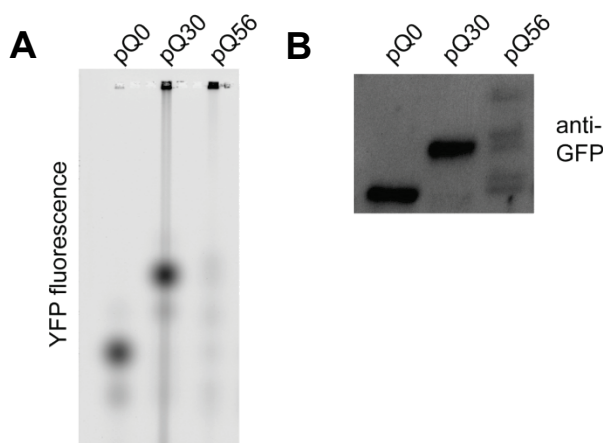


Figure 37: Analysis of polyQ proteins in WT yeast. (A) NAGE was performed on lysates of WT *MATa*, transformed with polyQ plasmids as indicated. Large aggregate species were retained in the gel pockets and the fluorescent YFP-fusions could be detected via their YFP moiety. (B) Western blotting against YFP using an anti-GFP antibody exhibited distinct protein bands of the correct molecular weight for all three constructs, as well as degradation products for Q₅₆-YFP. Lysates for pQ0 and pQ30 were diluted 15-fold in comparison to pQ56 to enable simultaneous detection on one gel.

fibrillar or banded patterns within the cytosol. The incidence of such cells is ~10%. In Q₅₆-YFP producing cells, usually several small bright foci could be detected in the cytoplasm. Additionally, nuclear inclusions of low fluorescence intensity were observed (Figure 36).

Oligomeric species have been described before to be responsible for cytotoxicity in polyQ systems (Poirier *et al.*, 2002; Sanchez *et al.*, 2003). In order to identify such oligomers, lysates of transformants were subjected to NAGE. This method has been applied before to a very similar aggregation system in *C. elegans* (van Ham *et al.*, 2010). None of the polyQ-fusions showed detectable amounts of slowly migrating oligomeric species, but only mobile species (Figure 37). In comparison to Q₀-YFP and Q₃₀-YFP the level of Q₅₆-YFP is greatly reduced, a fact confirmed also by immunodetection of the YFP moiety after SDS-PAGE. The migration behavior proved to be similar to NAGE, indicating that the mobile species observed in Figure 37 is indeed soluble protein. The fact that several species arise for pQ56 in both electrophoretic assays points to the release of a polyQ-free YFP species, potentially generated by proteolytic degradation. Thus, despite much lower expression levels and potential proteolytic degradation of the aminoterminal polyQ stretch, there is detectable aggregation and a pronounced toxicity of Q₅₆-YFP in this yeast model.

3.2 Q₅₆-YFP leads to enlarged and polyploid cells

Cytotoxicity may lead to morphological phenotypes. During initial microscopy, cells from small colonies of pQ56 plates appeared enlarged compared to controls. The determination of individual sizes for roughly 1000 cells per sample confirmed this perception. Cells derived from small pQ56 colonies are overall slightly enlarged and contain a higher amount of large cells than the populations from pQ0- and pQ30-transformed colonies (Figure 38).

Results

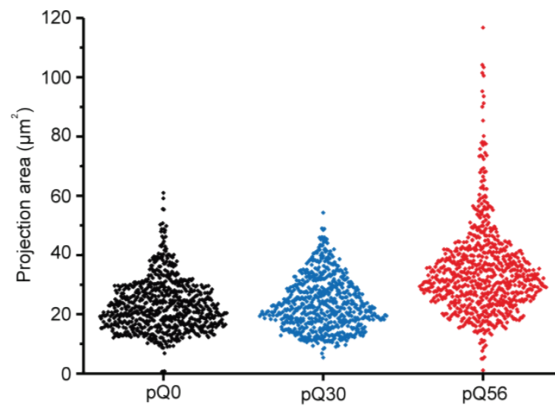


Figure 38: Q₅₆-YFP leads to enlarged cells. Analyzing the cellular cross section area for the predominant colony type reveals that pQ56 transformant colonies are generally slightly enlarged and exhibit a subpopulation with a cross-sectional area up to 6-fold higher than the average uncompromised cell.

As an increase in cell size is typically observed upon an increase in ploidy, alterations to the cell cycle could be responsible for the enlarged cells observed. Cellular DNA content can be determined by staining fixed cells with propidium iodide (PI) and subsequent analysis of fluorescence intensity by FACS. Cells, transgenic for pQ0 and pQ30 exhibit almost superimposable FACS histograms: They mainly comprise haploid cells, cycling between states of one genome copy (1N) and two genome copies (2N). Intoxicated yeast cells derived from small colonies of pQ56 transgenic plates, however, exhibit more 2N cells and a small fraction of cells in a 4N state (Figure 39), implying that the presence of Q₅₆-YFP leads to a duplication of diploid genomes and consequently to a proportionally higher DNA content in a subpopulation of cells. Due to the very proportional increase in fluorescence intensity, the endoreduplication events seem to be euploid.

3.3 The phenotype is dependent on the ploidy status

The presence of large colonies on plates transformed with pQ56 hints to intrinsic mechanisms allowing cells to escape the toxic effects caused by Q₅₆-YFP. These colonies are able to overcome growth inhibition despite partly exhibiting bright fluorescence, i.e. highly expressing the transgene (cf. Figure 35). To understand the reason underlying this effect, large colonies

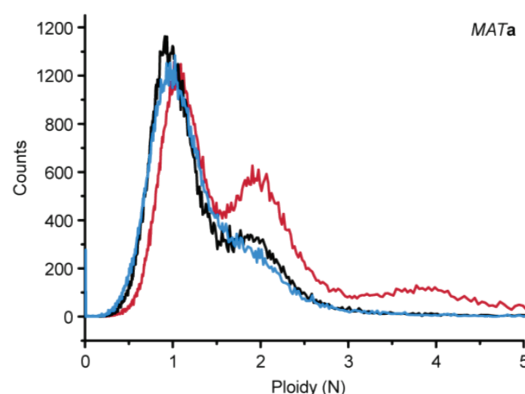


Figure 39: Yeast transformed with pQ56 exhibit increased DNA content. FACS analysis of WT *MATa* transformants reveals a higher incidence of 2N and 4N cells in response to pQ56 transformation (red) compared to pQ0 (black) and pQ30 (blue).

were clonally selected and their plasmids isolated. After amplification in *E. coli* they were sequenced to determine the actual length of the polyQ stretch. Many large colonies – in particular those with high fluorescence levels – had a dramatically shortened polyQ stretch. Some of the large colonies intriguingly grew despite stretches close to the original length of 56 glutamines (Table 19). Particularly colonies with long polyQ stretches exhibited a $\geq 2N$ signature in FACS assays, hinting to genome duplication and subsequent improvement of growth (Figure 40). Diploidization may happen in parallel to mutations in the background that could also influence the sensitivity towards polyQ toxicity. The LiAc transformation method has previously been shown to be mutagenic. Is a mutagenesis effect responsible for survival or is di/hyperploidy sufficient to obtain a loss of the phenotype?

Fluorescence Intensity	Polyglutamine Length	Ploidy
Very strong	Q8	haploid
strong	Q20	haploid
strong	Q16	haploid
strong	Q12	haploid
strong	Q20	haploid
medium	Q30	diploid and higher
medium	Q52	diploid and higher
weak	Q52	diploid and higher
weak	Q12	diploid and higher
weak	Q28	diploid

Table 19: Genetic analysis of spontaneously occurring large colonies. Ten large colonies of different fluorescence properties were picked from WT *MATa* plates transformed with pQ56. The length of the polyQ stretch and the state of ploidy was determined for each clone.

To answer this question, the natively diploid WT strain BY4743 (*MATa/α*) was transformed with pQ56. In this strain, the toxicity phenotype of pQ56 was abolished. FACS histograms confirmed the diploid status of the strain and were superimposable for all three constructs (Figure 41 A and

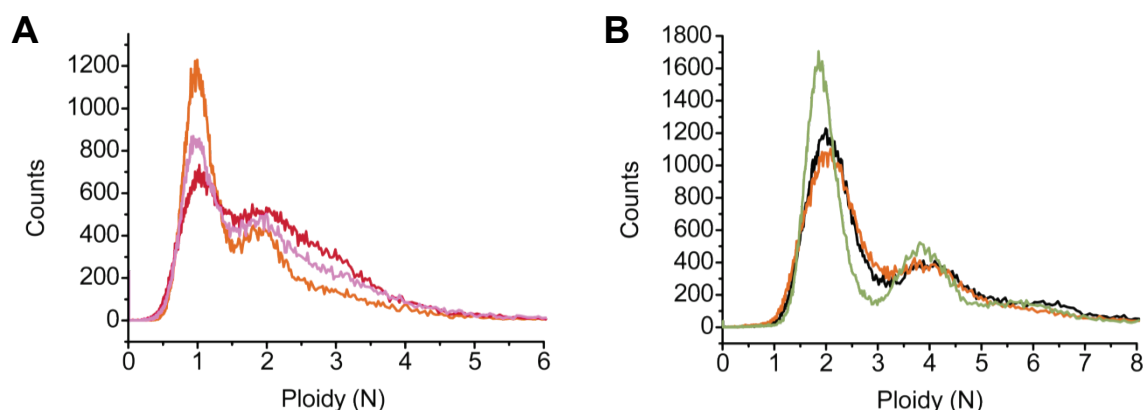


Figure 40: FACS analysis of large survivor colonies. (A) Strongly fluorescent large colonies were picked from plates of WT *MATa* yeast transformed with pQ56 and subjected to FACS analysis. Histograms of three representative samples are shown. All samples exhibit a mainly haploid growth pattern. (B) Weakly fluorescent large colonies were subjected to the same analysis. Three representative histograms are shown, exhibiting a $\geq 2N/4N$ cycling behavior.

Results

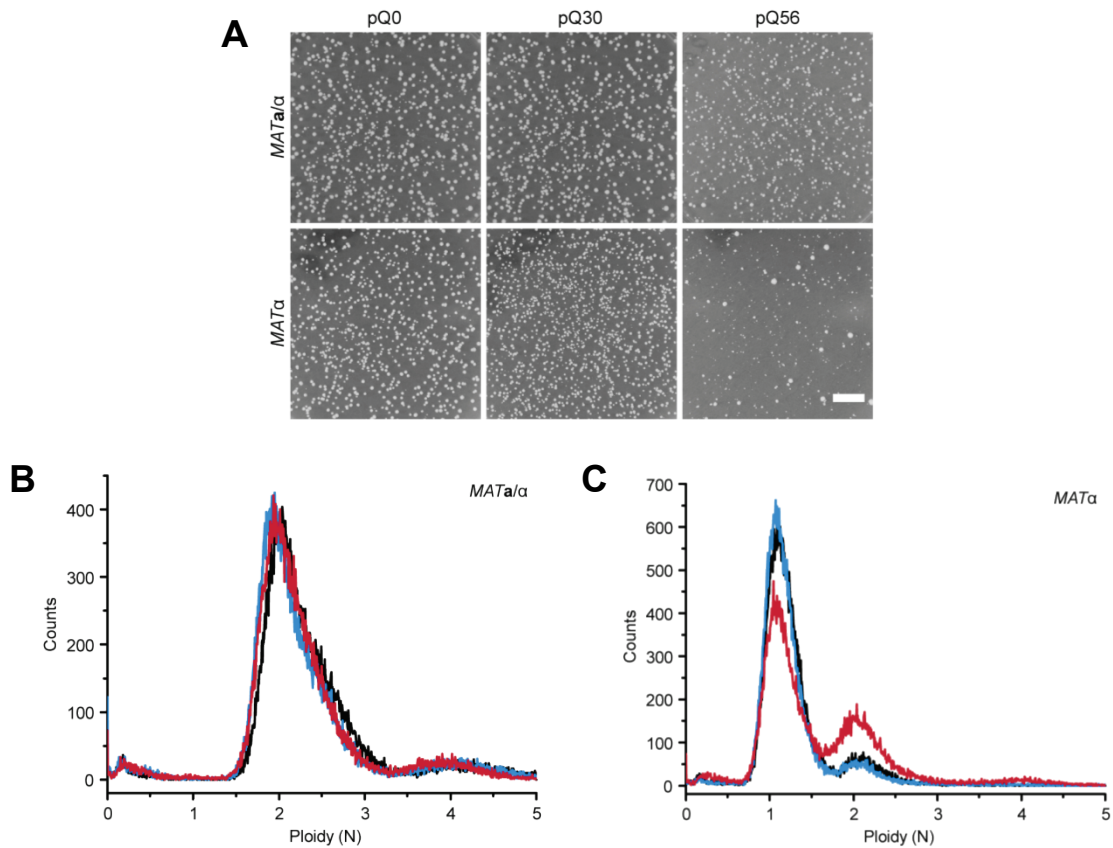


Figure 41: Increased ploidy abolishes polyQ toxicity. (A) Transforming diploid WT *MATa/α* and WT *MATα* shows that the phenotype is conserved in the *MATα* genetic background but absent in the diploid strain. (B) In FACS, WT *MATα* exhibits a haploid state for pQ0 (black) and pQ30 (blue) and an enrichment of 2N and 4N states after pQ56 transformation (red). (C) The diploid WT *MATa/α* strain transformed with pQ56 (red), pQ0 (black) and pQ30 (blue), however, shows an equal shift to the 2N and 4N positions for the whole population.

C). To rule out that the *MATα* cassette being active in the *MAT* locus is responsible for the observed effect, the corresponding haploid *MATα* strain BY4742 was examined. It exhibited the same toxicity phenotype as BY4741 (Figure 41 A and B).

Still, a synergistic effect of the presence of both mating type cassettes in an active form in the normal diploid strain BY4743 may lead to the resistance towards polyQ toxicity by mechanisms unknown. To rule this out, engineered WT diploid strains of *MATa/a* (PY4995) and

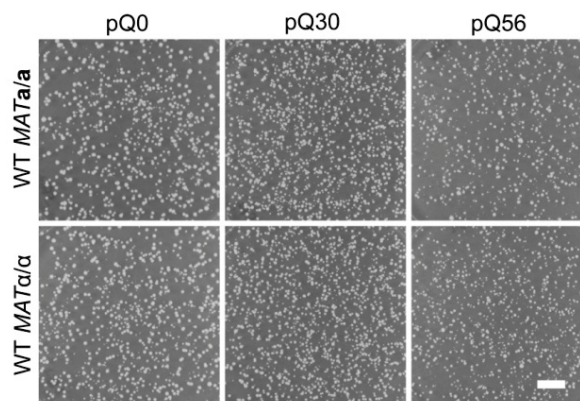


Figure 42: Heterozygosity at the *MAT* locus is not required for rescue. Colony patterns are homogeneous after transformation with pQ56 for the yeast strains PY4995 (*MATa/a*, upper row) and PY4994 (*MATα/a*, lower row) indicating that no toxicity is observable for either strain. The scale bar represents 10 mm.

MATa/a(PY4994) genotypes were chosen for analysis. Both strains should be homozygous throughout the genome (Storchova *et al.*, 2006). The results indicate that both strains are insensitive to pQ56 toxicity, developing normal and homogeneous colony patterns (Figure 42).

The results illustrate that only haploid cells are sensitive to the cytotoxicity exerted by Q₅₆-YFP, while the protein's presence is well tolerated in yeast containing two chromosome sets. This effect seems to be due to genome duplication only, as strains with identical genome copies are also insensitive to Q₅₆-YFP.

3.4 A genome-wide screen for genes influencing Q₅₆-YFP toxicity

As the toxicity phenotype can be rescued spontaneously either by shortening of the polyQ stretch or hyperploidization, it was of interest, whether specific genes do contribute to the toxicity of Q₅₆-YFP. A loss of function could cause a loss of the phenotype or an enhanced phenotype. Consequently, a screening protocol was developed to probe the 5130 non-essential knockout strains generated by the *Saccharomyces* Genome Deletion Project (Winzeler *et al.*, 1999). The *MATa* genetic background haploid library version was chosen to perform this screen. Due to the intense requirement of material, a transformation protocol was developed that allows straightforward transformation of yeast cultures in a 96-well format with a single pipetting step (cf. section C2.2.2). It was also decided to perform the initial search for candidate genes using only the pQ56 construct, presenting a clear phenotype. Strains that exhibited less or more colonies as well as increased or decreased colony heterogeneity were considered hits. This first round of screening yielded 1440 candidate strains either enhancing or suppressing the phenotype. The results were judged on a qualitative scale. As colony number was part of the readout, the pQ30 control was added in the confirmation round. Indeed ~90% of the stains exhibited a generally reduced or decreased number of transformants and were consequently removed from the gene list, yielding 209 strains, specifically influencing the phenotype, leaving the pQ30 control unchanged. The results were confirmed three additional times, also deploying pQ0 as an additional control to be able to judge variance in transformant numbers more profoundly. A representative set of genes considered hits is depicted in Figure 43.

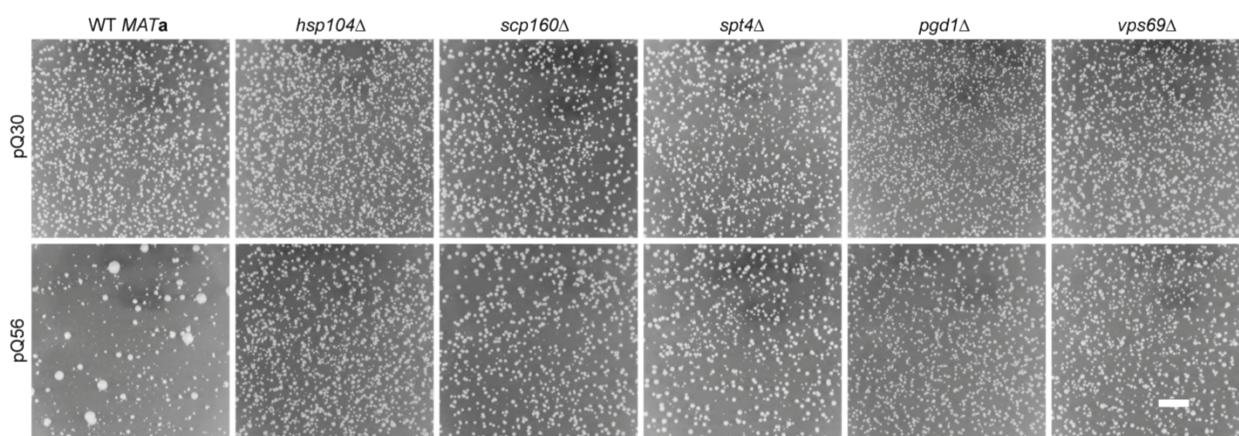


Figure 43: Representative results of the genome-wide screen. Representative images of selected deletion strains resistant Q₅₆-YFP are shown. In many cases the pQ56 induced phenotype (lower row, leftmost column) disappears and normal growth in comparison to pQ30 (upper row) is restored as shown for the strains *hsp104Δ*, *scp160Δ*, *spt4Δ*, *pgd1Δ* and *vps69Δ*. The scale bar represents 10 mm.

Results

3.5 Specific genes establish the toxicity of Q₅₆-YFP

The confirmatory experiments yielded 68 knockout strains, which reliably rescued the toxicity induced by Q₅₆-YFP (Figure 44). Certain strains in the library are annotated to be *MATa/a* diploids and other strains are unclear concerning their mating type status. Notably, the screening recovered all strains previously annotated to be *MATa/a* diploids.

Strain Number	Systematic Name	Standard Name
589***	YMR014W	<i>bud22Δ</i>
1401***	YIL009W	<i>faa3Δ</i>
1440***	YIL047C	<i>syg1Δ</i>
1442**	YIL049W	<i>dfg10Δ</i>
1484**	YIL093C	<i>rsm25Δ</i>
1666**	YOR369C	<i>rps12Δ</i>
2072	YPL180W	<i>tco89Δ</i>
2280**	YIL121W	<i>qdr2Δ</i>
2293	YIL134W	<i>flx1Δ</i>
2316	YIL157C	<i>coa1Δ</i>
2345**	YIR009W	<i>msl1Δ</i>
3223	YBR085W	<i>aac3Δ</i>
3765	YDL068W	<i>YDL068WΔ</i>
3770	YDL073W	<i>YDL073WΔ</i>
3923	YDL225W	<i>shs1Δ</i>
4278	YDR442W	<i>YDR442WΔ</i>
4296	YDR462W	<i>mrp128Δ</i>
4401	YGL033W	<i>hop2Δ</i>
5727	YBR279W	<i>paf1Δ</i>
6421*	YHR191C	<i>ctf8Δ</i>
6422*	YHR193C	<i>egd2Δ</i>
6423*	YLL030C	<i>rrt7Δ</i>
6424*	YLL044W	<i>YLL044WΔ</i>
6426*	YLL049W	<i>ldb18Δ</i>
6797**	YJL029C	<i>vps53Δ</i>
6861**	YJR063W	<i>rpa12Δ</i>
6867	YAL047C	<i>spc72Δ</i>
7316***	YNL138W	<i>srv2Δ</i>
7395***	YPL183W-A	<i>rtc6Δ</i>
7533	YKL096c-B	<i>YKL096c-BΔ</i>

Table 20: Growth restoring *MATa/a* strains uncovered in the library. 68 strains of the *MATa* library were identified to restore growth of Q₅₆-YFP expressing yeast. For all strains genomic DNA was purified and determined whether they are in fact *MATa* or *MATa/a* by PCR. 30 strains were found to be true diploids heterozygous at the *MAT* locus. Many of these strains were already known to be *MATa/a* (*) or assigned with *MET15* (**) or *MET+* (***) in the library directory. For strain 7533 no conclusive result could be obtained.

As a consequence, the status of the *MAT* locus of each strain was assessed by PCR to rule out *MATa/α* false positives. 30 knockout strains turned out to be *MATa/α* (Table 20), while the remaining strains were only positive for *MATa* as expected.

To probe whether the 38 strains finally retained are *de facto* haploid, they were subjected to FACS analysis. The fluorescence intensity distributions obtained for populations transformed with pQ0, pQ30 and pQ56 for each knockout strain were diverse, but could be categorized into three groups (I-III) upon closer inspection. For group I members, the population mainly stayed haploid for all three plasmids and gained a minor population with a $\geq 2N$ signature upon transformation with pQ56 (Figure 44). This equals the observations in the WT background, but toxicity being abolished. This category comprises 9 strains (Table 21). The 4 strains sorted into group II exhibit a haploid 1N/2N cycling behavior, if transformed with pQ0 and pQ30. However, upon transformation with pQ56, the 1N peak is lost and the population is shifted to a mainly 2N state and states of higher ploidy (Figure 44, Table 21). These knockouts seem to facilitate the

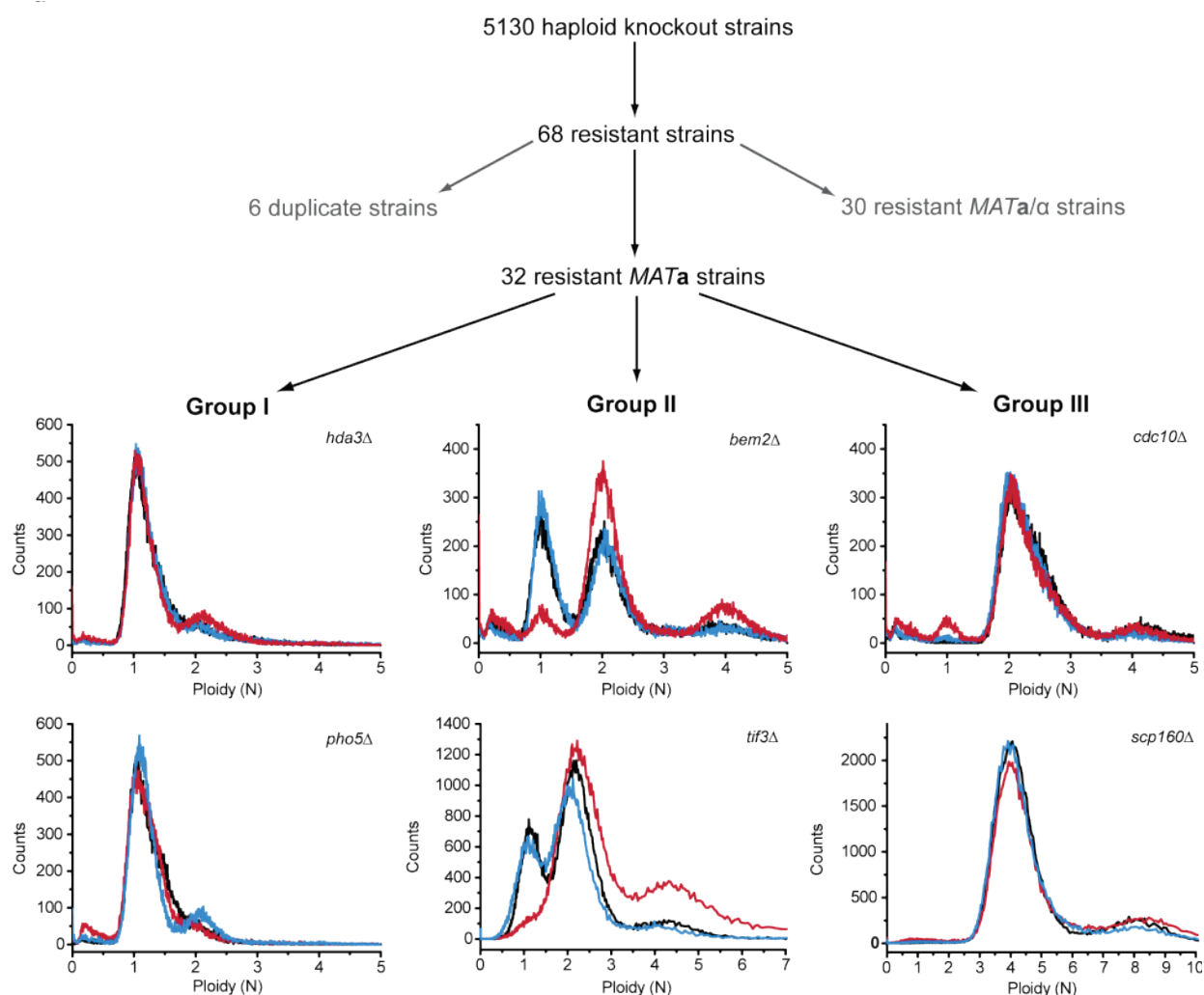


Figure 44: A summary of the screen for genes enhancing the toxicity phenotype of Q₅₆-YFP. All available haploid non-essential knockouts in the *MATa* background were transformed with pQ56 plasmid and their colony growth pattern was evaluated individually. 68 strains were found to reduce the toxicity of pQ56. Six genes were targeted by two strains in the library. 30 diploid *MATa/α* strains were excluded, leaving 32 strains after the screen. By FACS analysis, the enhancers of toxicity were classified into three groups, based on their behavior in response to pQ0 (black), pQ30 (blue) or pQ56 (red). The normalized data for two representative strains are shown for each group.

Results

Gene	Strain No.	Gene function	Q ₅₆ -YFP	Htt103Q	Group
<i>hsp104Δ</i>	1514	Protein folding	+++	+++	I
<i>pho5Δ</i>	3232	Phosphate regulation	+++	+++	
<i>pf1Δ</i>	1246	Protein folding	+++	++	
<i>hda3Δ</i>	5594	Chromatin organization, Transcription	+++	o	
<i>cyk3Δ</i>	3814	Budding	+	+++	
<i>gal11Δ</i> *	1742	RNA-Polymerase II regulation, subunit of Mediator Complex	+++	++	
<i>sin3Δ</i>	1695	Chromatin organization	++	o	
<i>pgd1Δ</i> *	4393	RNA-Polymerase II regulation, subunit of Mediator Complex	+++	++	
<i>rad6Δ</i>	4425	Protein degradation, Cell cycle control	++	+++	
<i>bem2Δ</i> *	7548	Budding	+++	+	
<i>tif3Δ</i>	5578	Translation	+++	o	
<i>asc1Δ</i>	6556	Translation	++	+	
<i>hof1Δ</i> *	7817	Budding	++	o	
<i>med2Δ</i>	3701	RNA-Polymerase II regulation, subunit of Mediator Complex	+++	+++	
<i>sin4Δ</i>	1976	RNA-Polymerase II regulation, subunit of Mediator Complex	+++	++	
<i>eap1Δ</i>	7036	Translation	+++	o	
<i>ymr185wΔ</i>	770	Unknown	+++	o	
<i>1Δ</i> *	3272	Budding	+++	+++	
<i>cdc10Δ</i>	3482	Budding	+++	o	
<i>swa2Δ</i>	3679	Budding / Vesicle transport COP	+++	++	III
<i>kre6Δ</i>	5574	Cell wall biogenesis	+++	o	
<i>hnt3Δ</i>	2514	DNA repair	+++	++	
<i>gpm2Δ</i>	3717	Metabolism	+++	++	
<i>ldb16Δ</i>	3413	Mitochondrion	+++	++	
<i>ybl094cΔ</i>	3120	Unknown	+++	++	
<i>rox3Δ</i>	3119	RNA-Polymerase II regulation, subunit of Mediator Complex	++	++	
<i>spt4Δ</i> *	6986	RNA-Polymerase I/II regulation, pre-mRNA processing	+++	+++	
<i>scp160Δ</i>	1343	Translation	+++	++	
<i>bfr1Δ</i>	2454	Translation, Nuclear segregation	+++	++	
<i>vps69Δ</i>	5504	Vacuolar protein sorting	+++	+	
<i>tho2Δ</i>	2937	Transcription	+++	o	
<i>whi3Δ</i>	2015	Cell cycle control	++	++	

Table 21: Enhancers of Q₅₆-YFP toxicity. A summary of the strains identified in the genome wide screen. Most of the genes rescued toxicity to an extent that no growth difference was evident between cells producing Q₀-YFP, Q₃₀-YFP or Q₅₆-YFP, as indicated by +++ in the fourth column. Few strains rescued to a lesser extent (+ or ++). The same scale was applied for the rescue of HttQ103-GFP induced toxicity. If no rescue was detectable, this is indicated by (o). Genes were classified according to the FACS analyses, assigning them to the groups I, II or III. At least in six separate replicates were performed for the transformation assays for each strain. FACS measurements were four separate experiments for each strain (separate inoculum for every replicate). * *hsl7Δ*: two strains in the library (7539, 3272), of which both rescue, but differ in the group assignment; *gal11Δ*: two strains (1741, 1742) with

similar results; *pgd1Δ*: two strains (4392, 4393) with similar results; *bem2Δ*: two strains (6152, 7548) with similar results; *hof1Δ*: two strains (7817, 608) with similar results; *spt4Δ*: two strains (4694, 6986) with similar results. Gene function was assigned based on literature reviews and annotation in the yeast genome database. For representative images, cf. Figure 43 and Figure 45.

accumulation of further copies of the genome to overcome the selection pressure, exerted by Q₅₆-YFP. Group III holds 19 knockout strains that bear more than one set of chromosomes, even if transformed with the non-toxic pQ0 and pQ30 plasmids (Figure 44, Table 21).

It is notable that for some strains also duplicate knockouts and strains that affect the very same ORF region by an adjacent knockout were recovered. Most interestingly, *YMR185W* knockout affects the upstream region of *HSC82*, which is the constitutive version of Hsp90 of yeast, potentially connecting Hsp90 function to ploidy stability and aggregation cell biology. For the members of group I and group II, the effect on the phenotype must be due to a direct effect of the knockout on the formation of the toxic species or the cell's sensitivity towards this agent. This is less clear for group III genes. For these strains the loss of the phenotype due to hyperploidy or due to the knockout is hardly discernible.

3.6 The identified genes also mediate the toxicity of Htt103Q

Would the genes identified also be required for the toxicity of a previously described aggregation model based on Htt (Giorgini *et al.*, 2005)? Applying the experimental setup for our assays to this system, HttQ103 transformants showed no growth – despite sporadic large colonies – while a homogeneous colony pattern developed for the HttQ25 control (Figure 45). Consequently, the 38 knockout strains that were obtained in the genome-wide screen were re-examined with this system. Indeed, 28 strains also reduce the toxicity of HttQ103 (Table 21). Most of the genes found in our screen are consequently contributing to the generation of the cytostatic effect exerted by polyQ proteins, independent of the system used and its protein context.

In order to understand whether a rescue through higher ploidy may also be common to both systems, we transformed the diploid strains *MATa/a* and *MATα/a*. Diploids exhibit incomplete

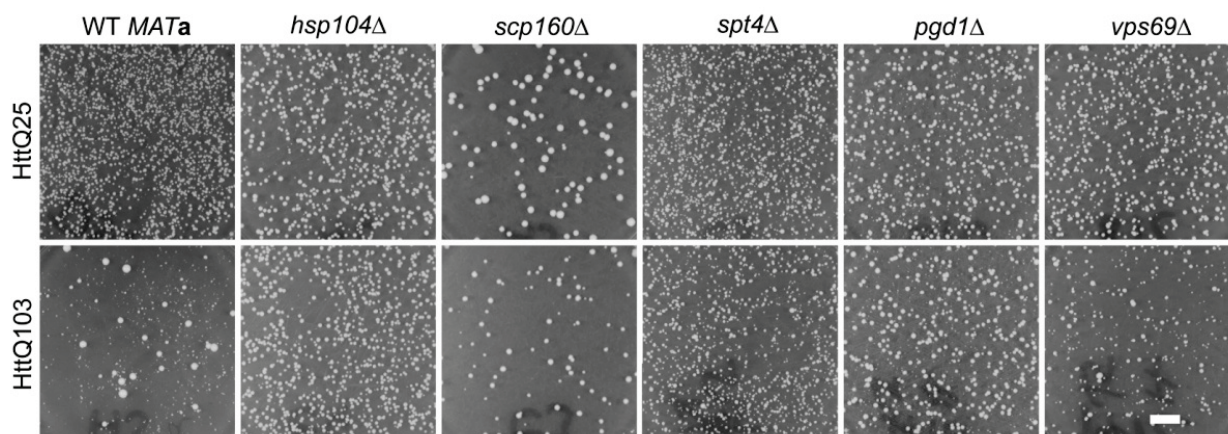


Figure 45: Strains also rescue the toxicity phenotype of HttQ103. The strains identified in the genome wide screen were also examined regarding the toxicity induced by HttQ103 expression (lower panel). Some of the strains fully restore normal growth, while others rescue at least to some extent. In this panel, strong rescue is seen *hsp104Δ*, *spt4Δ*, intermediate rescue for *scp160Δ*, and *pgd1Δ* while weak rescue is seen for *vps69Δ*. The images shown are representative results for these selected strains. *scp160Δ* exhibited generally less colonies in this experiment. The scale bar represents 10 mm.

Results

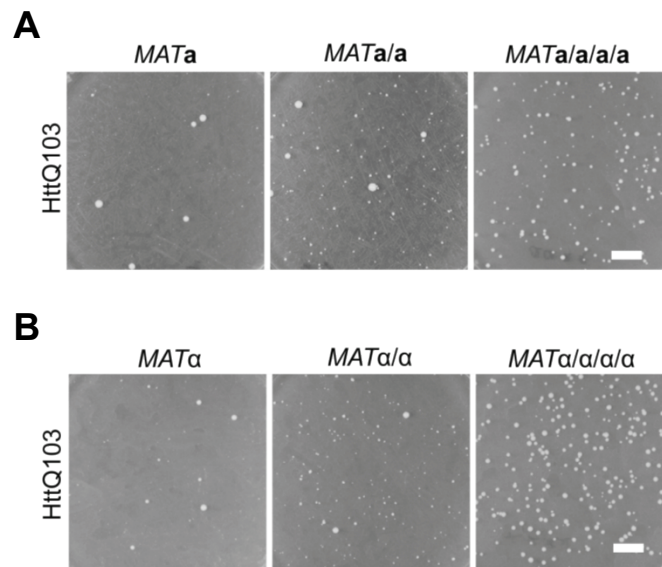


Figure 46: The toxicity of HttQ103 is fully abolished in tetraploid yeast strains. The toxicity of HttQ103 is evident in normal WT cells of both mating types. **(A)** An increase in genome copies from 2N in PY4995 (*MATa/a*) to 4N in PY5006 (*MATa/a/a/a*) successively abolishes the toxicity phenotype. **(B)** The same effect is observable for *MATα*-based strains, where *MATα/a* (PY4996) rescues partially and *MATα/a/a/a* (PY5007) rescues fully. The scale bars represent 10 μm in both panels.

rescue, whereas the analogously constructed tetraploid strains PY5006 (*MATa/a/a/a*) and PY5007 (*MATα/a/a/a*) (Storchova *et al.*, 2006) were fully resistant to Htt103Q toxicity (Figure 46). Thus, not only the identified hits provide resistance to both model systems, but also polyploidy is a shared mechanism of resistance against polyQ toxicity independent of the system used. The fact that diploid strains and specific knockouts are less effective in rescuing the toxicity of the Htt103Q system may be attributed to a generally higher level of toxicity due to the increased length of the polyQ stretch.

3.7 Q₅₆-YFP toxicity is independent of prions

Previous research reported that the toxicity of polyQ constructs is dependent on the state of endogenous prion proteins in yeast (Duennwald *et al.*, 2006a; Duennwald *et al.*, 2006b). Specifically, the protein Rnq1 was described to be required in its [*PIN*⁺] prion state to obtain HttQ103 toxicity. Several strains found in the screen described above (*hsp104Δ*, *spt4Δ*, *scp160Δ*, *bfr1Δ*, *swa2Δ* and *asc1Δ*) (cf. Table 21) also proved positive in a screen for genes that reduce the inducibility of the [*PSI*⁺] phenotype (Manogaran *et al.*, 2011). Particularly Hsp104 has long been known to be a major player in aggregation and prion-related processes in yeast and was also uncovered in our screen (Chernoff *et al.*, 1995). It consequently became essential to rule out that the genetic effects presented here are dependent on or mediated through the state of endogenous prions. Guanidine hydrochloride (GdnHCl) is a known inhibitor of the disaggregase Hsp104 and a prion curing agent (Grimminger *et al.*, 2004). To previously check, whether the toxicity of the pQ56 system may also be abolished by GdnHCl the influence of this small molecule was tested. Plates containing 4 mM GdnHCl strongly reduce the toxicity of Q₅₆-YFP as much as Hsp104 (Figure 47 A) and in FACS analysis the deletion of *HSP104* is accordingly mimicked (Figure 47 B and C).

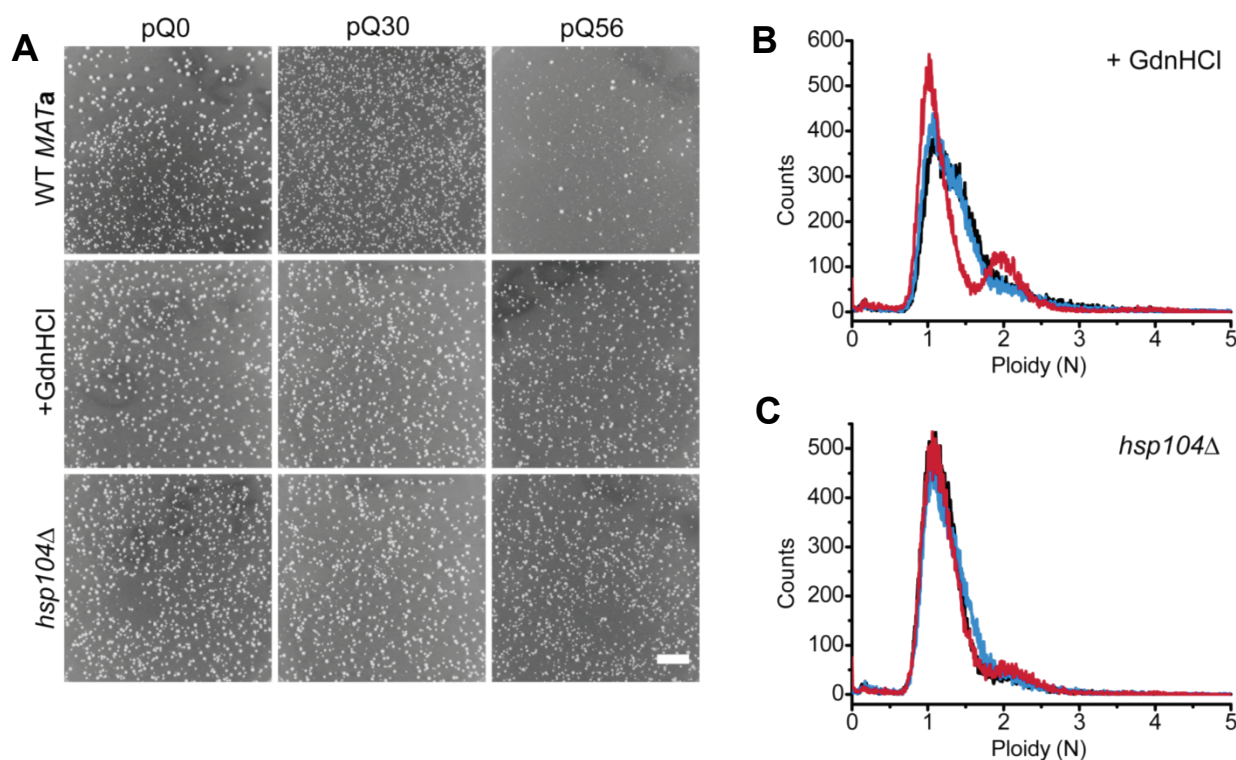


Figure 47: GdnHCl mimicks the deletion of *HSP104*. (A) Addition of 4 mM GdnHCl to plates reduces the pQ56 induced toxicity to undetectable levels (middle row versus upper row). The effect is similarly strong as the rescue effect of *HSP104* deletion (lower row). The scale bar represents 10 mm. (B) FACS histograms of GdnHCl resued pQ56 cultures (red) compared to pQ0 (black) and pQ30 (blue) exhibit only minor differences. (C) Even smaller differences between the three corresponding histograms are seen in the *hsp104Δ* genetic background.

This loss of toxicity, however, could be attributable to the loss of endogenous prion proteins in their prion conformation induced by the presence of GdnHCl. If this assumption was valid, two different approaches should also lead to the loss of the phenotype. The major prion factor, establishing HttQ103 toxicity has been described to be [*PIN*⁺] (Duennwald *et al.*, 2006a; Duennwald *et al.*, 2006b). Consequently, the deletion of *RNQ1* has to equally abolish the toxicity of the pQ56 system. In case the maintenance of the toxicity was due to another protein being in its prion state, a complete loss of endogenous proteins in their prion conformation should abolish the phenotype. This ‘prion curing’ may be achieved by the sequential passage of a strain on a medium containing 4 mM GdnHCl and has been previously applied as a control for prion effects (Manogaran *et al.*, 2011). Both experiments were performed comparing the HttQ103 system to the pQ56 system. The cured *MATa* WT [*prion*⁻] strain clearly abolished the phenotype of HttQ103 and had no effect on the toxicity of pQ56 (Figure 48). When *RNQ1* is absent, the phenotype of the HttQ103 system is abolished as well. However, for pQ56, a slight rescue may be observable. To understand, whether this is due to the presence of different subpopulations present in the bulk cultures derived from glycerol stocks, the correctness of knockout of clonally selected cultures of *rmq1Δ* was confirmed by sequencing. Surprisingly, of 15 separate clones transformed, 2 abolished the phenotype in both systems. 13 clones however exhibited a WT-like phenotype for pQ56 and abolished the toxicity of HttQ103, indicating that the majority of *RNQ1* deletions are incapable to rescue pQ56 toxicity. These results confirm that the impact of gene knockouts, di- or hyperploidy and GdnHCl is not mediated through their impact on endogenous prions resulting in a change of toxicity of Q₅₆-YFP, but rather through a direct mechanism affecting either the toxicity of or the cell’s sensitivity this toxic protein.

Results

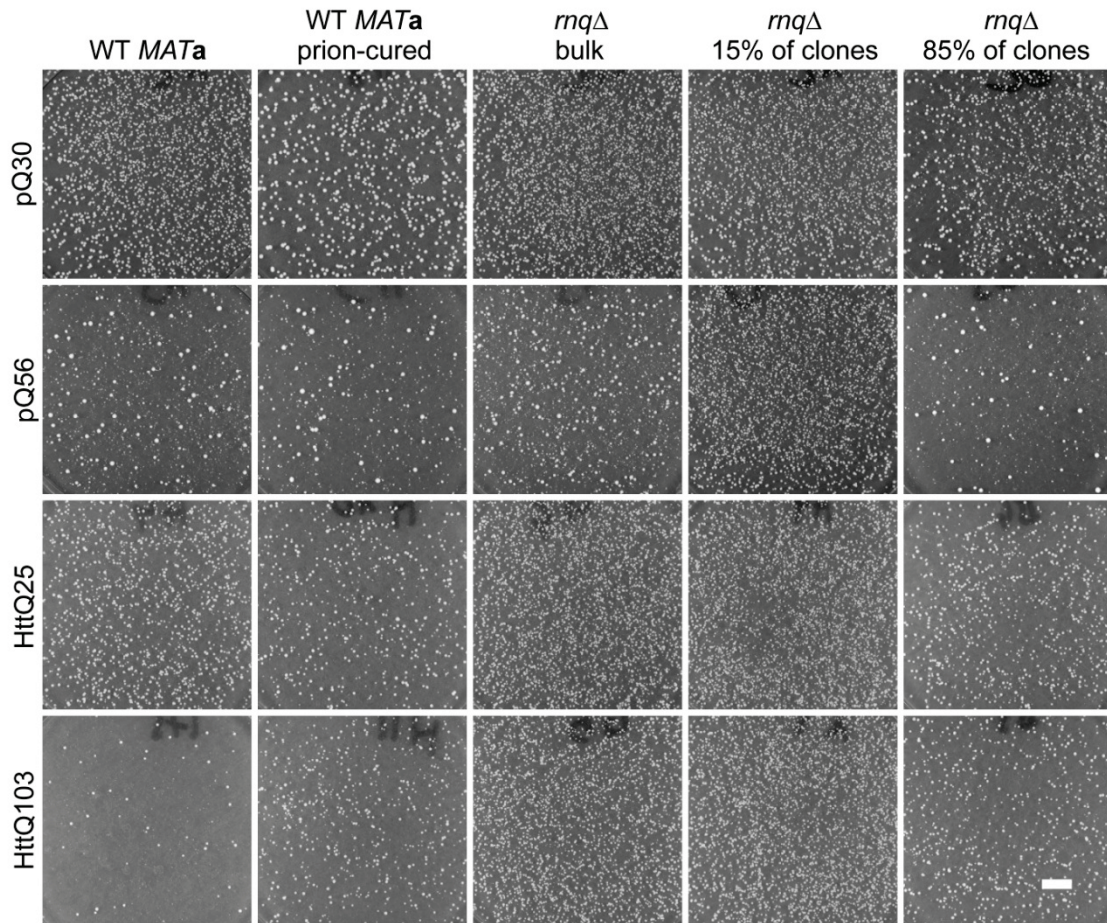


Figure 48: Q₅₆-YFP toxicity is independent of the prion state. Results of transformation assays are shown comparing the reaction of the pQ30/pQ56 and HttQ25/HttQ103 systems in respect to endogenous prion phenotypes. WT BY4741 exhibits a toxicity for both systems. Curing the strain from prions by sequential passage on GdnHCl (indicated by [*prion*']) abolishes HttQ103 toxicity, while it is maintained for pQ56. Similarly, the transformation of bulk stock of an *RNQ1* deletion exhibits no phenotype for HttQ103 and a slight rescue effect for pQ56. This subtle rescue is due to heterogeneity within the knockout strain, as clonally selected deletions for *RNQ1* abolish both phenotypes in 15% of transformed clones. In 85% however, pQ56 toxicity is maintained, while it is lost for HttQ103. The scale bar applies to all photographs and represents 10 mm.

3.8 Hsp104 and Pho5 affect the oligomerization behavior of Q₅₆-YFP

The loss of toxicity by the deletion of enhancing genes may be caused by several mechanisms. The levels of Q₅₆-YFP may be reduced due to decreased transgene expression or increased degradation of the toxic protein. Another option to influence the toxicity of Q₅₆-YFP would be to abolish the toxic species or to modulate the sensitivity of the cellular structures affected by the toxic species. As Hsp104 is known to be a central player in aggregation processes in yeast, it may be hypothesized that the effects observed are mediated through this protein and not direct results of the specific knockout of the genes discovered. The subsequent experiments probe for members of group I, whether either a reduction of Q₅₆-YFP or a loss of functionality of Hsp104 may be responsible for the loss of the phenotype.

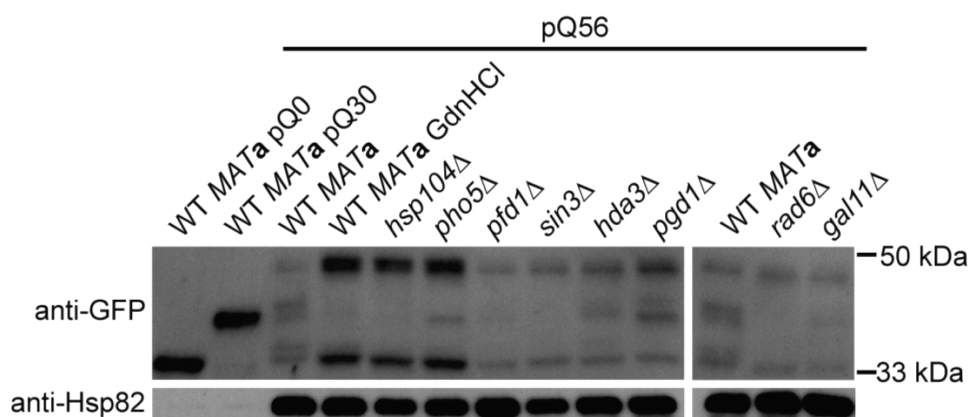


Figure 49: Toxic protein levels are largely unaltered in group I strains. Western blots against GFP reveal that the expression of the Q₅₆-YFP protein is not diminished in group I knockout strains. Instead, the expression is increased in GdnHCl-treated WT cells and strains with deletions of *HSP104* and *PHO5*. Hsp90 was used as a loading control. The lysates of pQ0 and pQ30 transformed cells were diluted 15-fold in comparison to pQ56 transgenic cells to be in the range of detection.

Lysates of the group I strains were subjected to SDS-PAGE and the levels polyQ proteins determined by western blot. While all knockouts contain a similar quantity of polyQ protein at least equaling WT levels, the expression of the toxic transgene is even increased in the strains *hsp104Δ*, *pho5Δ*, and in the presence of GdnHCl (Figure 49), implying that a decrease in Q₅₆-YFP levels is not the mechanism responsible for the loss of toxicity.

The effect of the gene knockouts on toxicity might be mediated through Hsp104 either by decreasing its expression levels or its activity. The levels of Hsp104 were probed by immunoblots to answer this question. As expected, no Hsp104 could be detected in the *hsp104Δ* strain. The levels of Hsp104 were decreased in *sin3Δ* and potentially *hda3Δ*. However, all other strains exhibit normal levels of Hsp104. This suggests that only *sin3Δ* and *hda3Δ* may act on polyQ toxicity through the regulation of Hsp104 (Figure 50). Nevertheless, a change in the chaperone activity of Hsp104 through the remaining knockouts cannot be excluded.

To clarify, whether changes to the molecular oligomerization pattern of Q₅₆-YFP are causative for the loss of toxicity, NAGE-analysis was applied as described above. Indeed, in the lysates of *pho5Δ*, *hsp104Δ*, and GdnHCl-treated WT cells, a gel-permeable but apparently very large species was present (Figure 51). Based on this, it can be concluded that Hsp104 and Pho5 both

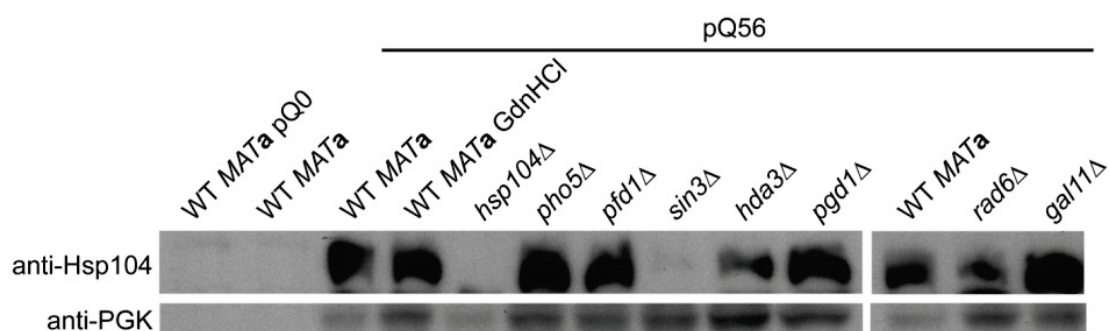


Figure 50: Hsp104 levels are unaltered in most group I strains. Western blotting against Hsp104 reveals that its expression may be reduced in some group I strains. While the level of Hsp104 is unchanged for most strains, the protein is properly absent in *hsp104Δ*. *hda3Δ* and *rad6Δ* exhibit slightly compromised Hsp104 levels. The protein is barely detectable in *sin3Δ*. The lysates of pQ0 and pQ30 transformed cells were diluted 15-fold to be in the dynamic range of immunogenic detection in for polyQ proteins in comparison to pQ56 transgenic cells.

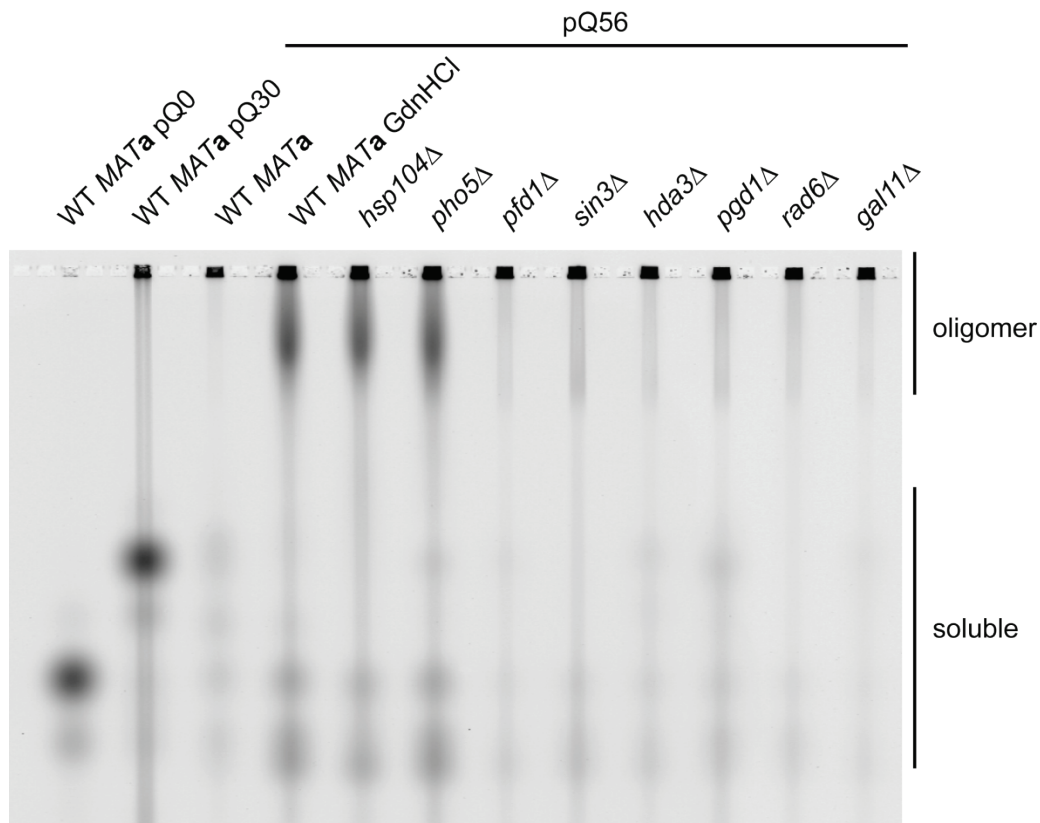


Figure 51: Genes enhance toxicity by different mechanisms. Native agarose gel electrophoresis (NAGE) reveals that oligomeric forms of Q₅₆-YFP can be identified after the addition of GdnHCl and by the deletion of *HSP104* or *PHO5*. This mechanism seems to be exclusive for these genes among group I members. The lysates of WT cells transformed with pQ0 and pQ30 were diluted 15-fold to enable simultaneous detection of all strains on a single gel.

influence the oligomerization status of Q₅₆-YFP in a similar manner, phenocopying each other down to the level of molecular effects.

Notably, the phenotypic similarity among both strains can neither be attributed to a loss of function mutation in the *HSP104* gene in the *pho5Δ* strain. In this strain, the *HSP104* locus has been sequenced and is WT. The expression level of Hsp104 is unchanged. However, it cannot be ruled out that Pho5 influences the activity of Hsp104 by unknown means. Other group I hits do not appear to interfere directly with the oligomerization status of Q₅₆-YFP, further confirming that they influence polyQ toxicity through pathways parallel to Hsp104. It is specifically noteworthy that neither for *sin3Δ* nor *hda3Δ* a marked increase in oligomer formation is detected, which should be the case if their effect was due to a reduction in Hsp104 activity by its downregulation. Consequently, it may be speculated that Hsp104 levels are reduced in parallel to the effect of *sin3Δ* or *hda3Δ* on polyQ toxicity.

3.9 Pho5 and Hsp104 affect the aggregation of polyQ proteins

The deletion of *HSP104* and *PHO5* equally lead to a modulation of the molecular oligomerization state of Q₅₆-YFP (cf. section 3.8). As already shown in Figure 36, cells expressing Q₀-YFP exhibit a homogeneous distribution of fluorescence throughout the cytoplasm. This is not the case for Q₃₀-YFP and Q₅₆-YFP. Both proteins form aggregates, but with a different morphology. To uncover whether a change in oligomerization as observed in protein extracts may also be reflected by morphological changes in aggregates, WT as well as *hsp104Δ* and *pho5Δ* cells were subjected to confocal microscopy. The data (Figure 52) indicate that the loss of functionality of Hsp104 and Pho5 equally renders the aggregate morphology of Q₅₆-YFP in these knockout strains more similar to Q₃₀-YFP in the WT background. Whether this is a result of the change in oligomerization behavior in these strains or rather the cause remains to be elucidated.

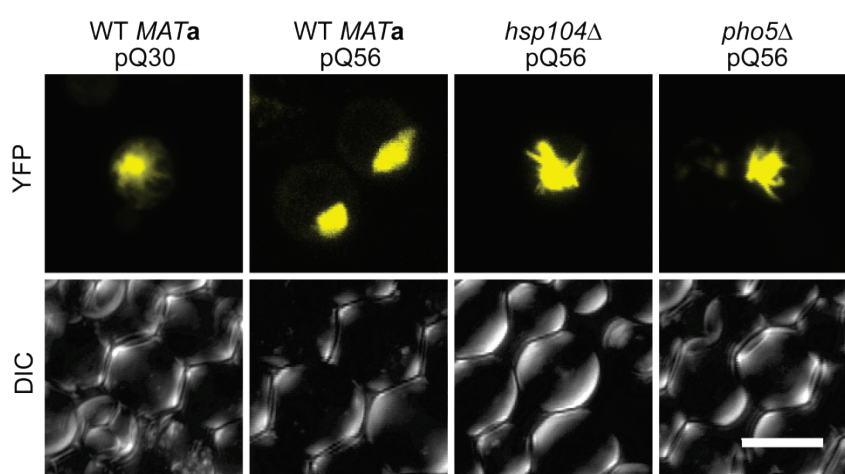


Figure 52: Hsp104 and Pho5 are required to obtain WT-like aggregation. Confocal microscopy of WT cells transformed with pQ30 exhibit compact focal aggregation as well as fibrous protein deposits. This is in marked contrast to WT cells transformed with pQ56 exhibiting extremely small highly diffusible focal protein deposits as well as nuclear or perinuclear aggregation. The deletion of *HSP104* as well as *PHO5* leads to a change in this aggregation pattern, rendering the aggregation patterns in pQ56 transformants morphologically more similar to WT cells transformed with the non-toxic pQ30 construct. All micrographs in the panel are maximum projections of image stacks recorded simultaneously for both channels in fluorescence and transmitted light modes. The scale bar represents 5 μm for all micrographs.

3.10 PolyQ proteins interfere with septin ring formation

The toxic aggregation of the pQ56 system is prion-independent and a set of genes is required to obtain toxicity. *PHO5* and *HSP104* may do so by supporting the generation of the toxic species. As the genome-wide screen points to an involvement of the budding process in the generation of cytotoxicity, and hyperploidy is very potently abolishing the phenotype, the answer to how toxicity is established may be found in the context of the cell division machinery. Several events in the cell division cycle are related to the appearance or reorganization of cellular structures; the septin ring assembles in late G1 phase, followed by spindle pole body (SPB) duplication and their migration to opposite poles of the nuclear membrane until early G2 phase. Metaphase is marked by an extension of tubulin filaments and the spindle into the daughter cell (Howell &

Results

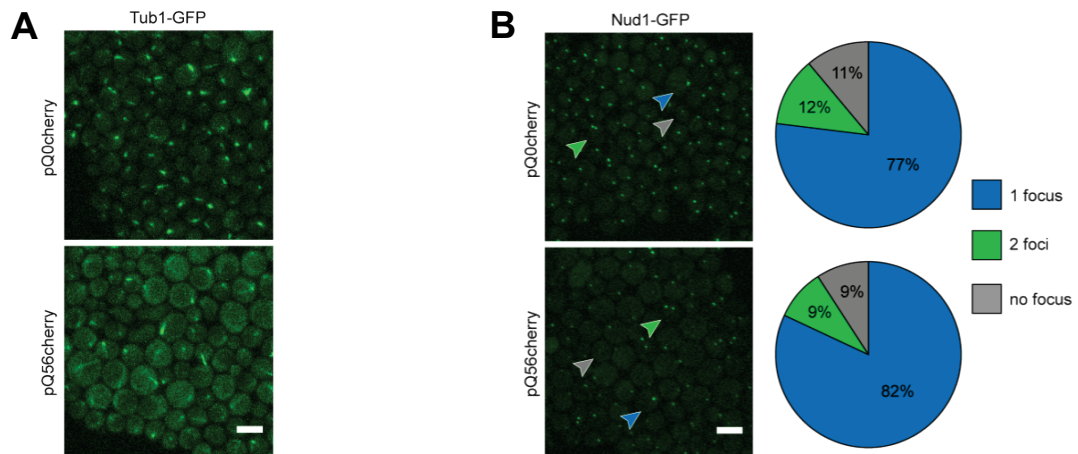


Figure 53: PolyQ toxicity does not severely affect the appearance of spindle markers. Confocal microscopy of cells producing Tub1-GFP as a marker for spindle geometry or Nud1-GFP as a marker for the SPB. Cells were transformed with control plasmid and pQ56cherry. (A) The geometry of assembled microtubules seems to be slightly affected when growth is arrested by the presence of polyQ. Still, more unassembled Tub1 is detected and the relative fluorescence intensity of polymerized tubulin is lower. (B) Nud1-GFP foci seem similar in controls and cells producing Q₅₆-mCherry. Upon quantitation of cells (n=392 for control and n=268 for pQ56 cells) a slight increase of cells without visible SPB becomes evident and the amount of cells with a single SPB decreases proportionally. The scale bar represents 5 μ m in each subpanel and applies to both micrographs. The arrowheads indicate cells representative for each class. The micrographs are maximum projections of image stacks recorded at the same settings for each reporter strain.

Lew, 2012). The yeast model provides a set of fluorescence reporter strains, which each carry a GFP fused to the coding sequence of an endogenous protein. This set covers roughly 75% of the yeast proteome (Huh *et al.*, 2003). Transforming selected strains of this set with pQ56 should yield information, whether one of the hallmark processes of mitosis is compromised. As a starting point, Tub1 was selected to visualize the tubulin cytoskeleton, Nud1 was chosen as a marker for the SPB and Cdc10 as a probe for septin ring assembly. To be able to visualize the polyQ protein simultaneously, the chromophore in pQ0, and pQ56 was exchanged from eYFP to mCherry, yielding pQ0cherry and pQ56cherry. All three marker strains were transformed with these plasmids. They retained the toxicity phenotype.

If cellular division was compromised by polyQ proteins during mitosis, division should be halted at a specific step. As the spindle is an essential structure during this step of the cell cycle, undergoing defined changes in its morphology, specific states of spindle geometry should be enriched. Surprisingly, at this level no drastic changes between control cells and intoxicated cells could be observed (Figure 53 A). The incidence of extended tubulin fibers seemed similar in both samples. However, some cells exhibited bended tubulin structures rarely found in control cells. In addition to this difference, more soluble Tub1-GFP is apparent and assemblies exhibit a decreased intensity of fluorescence, potentially pointing to subtle defects of microtubule assembly.

Nud1 is a component of the SPB outer plaque and in consequence an indicator of this structure's status. If cells were halted in late G2 phase or early mitosis before metaphase an increased number of individual cells exhibiting two SPBs should become apparent. Microscopy of Nud1-GFP cells, however, did not point to a marked enrichment of cells bearing duplicate SPBs or potential severe mislocalization of SPB components. This observation would argue for a post-

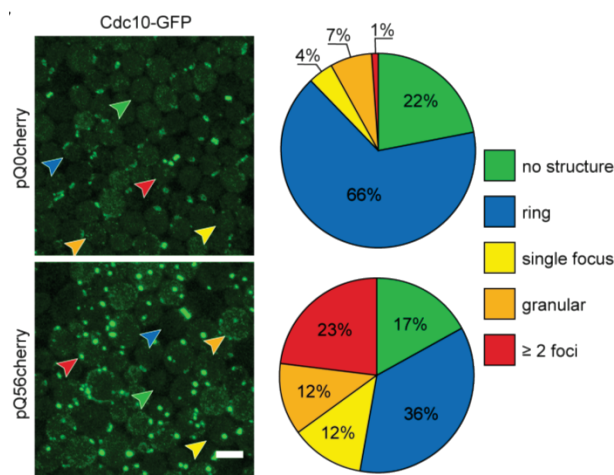


Figure 54: Toxic PolyQ proteins interfere with septin ring assembly. Confocal microscopy of cells synthesizing Cdc10-GFP as a marker for the septin ring, transformed with control plasmids and pQ56cherry. In samples of cells transformed with the control plasmid clear ring structures can be discerned in most cells. The picture changes drastically, when pQ56 is present. Cells with rings and homogeneous distribution (88% in controls) are depleted (53% in pQ56) in favor of cells with granular or focal fluorescence distribution or other morphologies (ring and focal, granular and focal; n=435 for control and n=244 for pQ56 cells). The scale bar represents 5 μ m and applies to both micrographs. The arrowheads indicate cells representative for each class. The micrographs are maximum projections of image stacks recorded at the same settings for both samples.

metaphase arrest or growth inhibition before S phase. However, subtle effects on the SPB machinery may not be ruled out.

Septin ring formation is one of the initial events in the preparation of a mitotic event. The ring is only disassembled after cytokinesis has been completed. Cdc10-GFP localizes to this structure and consequently allows the detection of the proper assembly of the ring (Figure 54). Cells transformed with control plasmids exhibited ring structures in 66%, homogeneous distribution of fluorescence in 22% and a granular distribution, single foci or other morphologies in 12% of cells. This situation changed markedly, when Q56-mCherry was present: only 53% of cells exhibited proper ring formation or homogeneous fluorescence. The cumulated amount of cells with foci or other morphologies rose from 12% to 47%, whereas those exhibiting granular appearance of Cdc10-GFP changed only minimally. This observation points to a mislocalization of septins as a consequence of polyQ aggregation, which could be the primary cause for growth inhibition by Q₅₆ species.

The data presented indicate that toxic polyQ proteins may not interfere directly with the mitotic process itself, but rather by disturbing a process that is a prerequisite for entry into mitosis: the formation of a functional septin ring structure.

Results

4 Several systems influence aggregation toxicity⁴

After having established a model for polyQ toxicity, further analyses of the system were performed. The major aim of these experiments was a more detailed characterization of the model system in order to understand the mechanistic aspects of the development or mediation of cytotoxicity more profoundly.

4.1 25 genes suppress the toxicity of Q₅₆-YFP

Besides genes responsible to establish the toxicity phenotype (cf. section 3.4), 37 candidate knockout strains were retrieved during the genome wide screen that seemed to have lost the residual capacity to form small colonies. The presence of these genes thus seems to be responsible for residual growth. Therefore such genes can be termed suppressors of toxicity. To further define, whether the respective gene knockouts robustly influence the phenotype in a negative manner, transformation assays were performed and the quality of toxicity was assessed after 4, 11 and 21 days of incubation. Table 22 lists 25 strains that exhibited reproducible results and a stable suppression of small colony growth over time.

The genes required for residual growth upon transformation of pQ56 contribute to different extents. While some strains such as *his7Δ*, *ncl1Δ* and *rrn10Δ* are barely capable of residual growth upon transformation with pQ56, 11 of 25 affect the phenotype only slightly, but reproducibly. The genes found participate in a similarly wide variety of cellular processes as the genes responsible for establishing the phenotype (cf. Table 21). Still, it is surprising that 7 of 25 genes of this group are involved in processes mediated by mitochondria or taking part in mitochondrial maintenance.

Gene Knockout	Number	Gene function	Rescue Q ₅₆ -YFP
<i>ada2Δ</i>	4282	Transcription coactivator	-
<i>arg82Δ</i>	3531	Inositol polyphosphate multikinase (IPMK)	--
<i>atp15Δ*</i>	1021	Epsilon subunit of mitochondrial ATP synthase	--
<i>cbf1Δ</i>	6858	Dual function helix-loop-helix protein	-
<i>cem1Δ*</i>	198	Mitochondrial beta-keto-acyl synthase	--
<i>erg2Δ</i>	7700	C-8 sterol isomerase	-
<i>fmp37Δ*</i>	4447	Putative protein of unknown function, detected in mitochondria	-
<i>gcv3Δ*</i>	361	Subunit of the mitochondrial glycine decarboxylase complex	-
<i>gnd1Δ</i>	2877	6-phosphogluconate dehydrogenase	-
<i>his7Δ</i>	3388	Imidazole glycerol phosphate synthase	---

⁴ A manuscript based on this section is currently being prepared. Parts of this section have been adapted from the Master's thesis of Stefan Grötzinger, which has been prepared under my supervision.

Results

<i>hom6Δ</i>	6933	Homoserine dehydrogenase	--
<i>htz1Δ</i>	1703	Histone variant H2AZ	-
<i>ies2Δ</i>	1997	Essential for growth under anaerobic conditions	--
<i>kre28Δ</i>	4366	Subunit of a kinetochore-microtubule binding complex	--
<i>map1Δ</i>	5153	Methionine aminopeptidase	--
<i>mrt4Δ</i>	4858	Protein involved in mRNA turnover and ribosome assembly	-
<i>ncl1Δ</i>	3050	S-adenosyl-L-methionine-dependent tRNA	---
<i>nfu1Δ*</i>	4889	Protein involved in iron metabolism in mitochondria	--
<i>pet8Δ*</i>	5331	SAM transporter of the mitochondrial inner membrane	-
<i>rai1Δ</i>	4613	Nuclear protein with decapping endonuclease activity	-
<i>rpb9Δ</i>	4437	RNA polymerase II subunit	--
<i>rrn10Δ</i>	3051	Subunit of UAF (upstream activation factor) for RNA polymerase I	---
<i>ugo1Δ*</i>	4304	Outer membrane component mitochondrial fusion machinery	--
<i>ybr196c-aΔ</i>	7457	Putative protein of unknown function	--
<i>yvh1Δ</i>	5961	Protein phosphatase	-

Table 22: Suppressors of Q₅₆-YFP toxicity. Genes uncovered during the genome wide screen to suppress toxicity were subjected to experiments confirming the stability of the enhanced phenotype upon their deletion. The intensity of the phenotype is indicated on a qualitative scale: --- almost no residual growth, --: residual growth detectable, -: slight enhancement of the toxicity phenotype. Gene functions are annotated according to the yeast genome database. Genes marked with an asterisk are directly involved in mitochondrial processes.

4.2 A specific transcriptional response to Q₅₆-YFP toxicity

It is common sense that cells react to changes in their physiology with changes in gene transcription. When polyQ proteins are present, the cellular reaction to toxicity should yield insight into endogenous pathways interfering with aggregation independent of their contribution to an enhancement or a suppression of toxicity.

To obtain meaningful data from the analysis of gene expression changes, the choice of appropriate samples needs to be considered. Part of this decisive process is to consider carbon source processing of *S. cerevisiae*. In any glucose-based medium, yeast will deploy this sugar as a carbon source fermentatively, generating ethanol. As soon as glucose levels drop below ~0.5% (w/v), cells will undergo a process termed the ‘diauxic shift’ and adjust their metabolism to the respiratory consumption of ethanol (Werner-Washburne *et al.*, 1993). This effect is of major importance to the polyQ toxicity system presented here. As the phenotype comprises small and large colonies on plates transformed with pQ56, the samples provide an intrinsic control for growth restriction by the availability of carbon sources. After 3 days of incubation, the colony size of large survivor colonies is slightly larger than the colonies on pQ0 and pQ30 plates. Increasing the incubation period, large colonies outgrow colonies on control plates, indicating that pQ56 plates provide more glucose than the non-toxic controls. This is also intuitive, as at equal colony densities, polyQ inhibited small colonies will consume less carbon source than pQ0 and pQ30 colonies due to their reduced growth rate, leaving more glucose to the survivor colonies.

Assay	Sample	Incubation time (days)	Growth phase
A1	Q0	3	Glucose limited
	Q30	3	Glucose limited
	Q56	3	Non-limited
A2	Q0	2	Non-limited
	Q56	4	Non-limited
	Empty	3	Stationary/dormant

Table 23: Overview of samples for gene expression analysis. The table summarizes the assay set, the sample, its incubation time and the presumed growth phase. ‘empty’ denotes untransformed yeast cells.

To control for this situation, samples were chosen accordingly in two separate assay sets. One set contained samples at 3 days after plating. This was the standard incubation time used throughout the study. At this time point, the survivor colonies on pQ56 plates start to outgrow the non-toxic controls. Consequently, colonies on pQ0 and pQ30 transgenic plates should have undergone or undergo the transition through diauxic shift, whereas the colonies on pQ56 are not glucose-deprived and in a growth phase rather corresponding to logarithmic growth in liquid culture. The expression changes potentially observed comparing intoxicated colonies with healthy colonies may consequently be a result of this difference in nutrient supply. To be able to control for this effect, pQ0 transformed cells after 2 days of incubation and pQ56 transformed cells 4 days were sampled. As the biomass generated on pQ56 transgenic plates is low, a non-transformed control was added. This control was meant to uncover expression changes caused by the presence of untransformed cells in the pQ56 samples (Table 23). For data analysis, a signal contribution of a maximum of 10% from untransformed cells was assumed. As the large colonies found on pQ56 transformant plates are either non-haploid or have shortened polyQ stretches (cf. 3.2) and do not

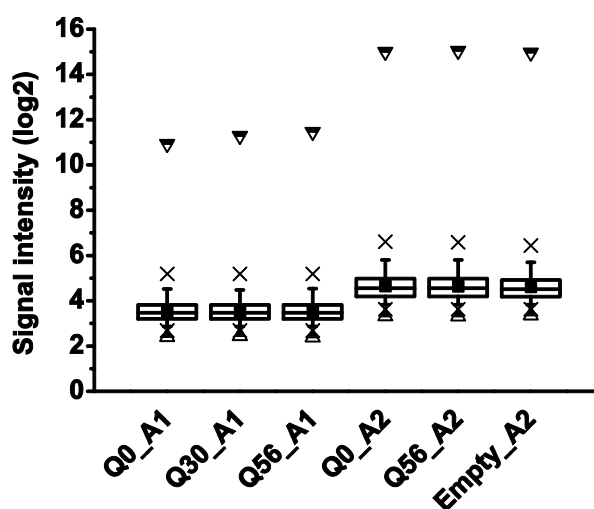


Figure 55: Signal range of *S. pombe* probe sets. The signals obtained for *S. pombe* probe sets were plotted for each experiment performed. The mean for each dataset is represented by a black square. The box represents the second and third quartile of all data with the data median denoted by the horizontal line inside the box. The whiskers represent 3 SD, the crosshair the 99 percentile range and the triangles minimum and maximum values.

Results

represent the majority of transformants, these colonies were removed for sample preparation.

RNA extraction as well as microarray analysis was performed by an external laboratory. The data provided had already been normalized within assay sets, using the robust multi-chip analysis (RMA) algorithm (Bolstad *et al.*, 2003), minimizing the effect of probe specific affinity differences and consequently increasing the sensitivity to changes between different experiments and assay sets, minimizing variance across the dynamic range (Irizarry *et al.*, 2003). To be able to compare both separate assay sets, both sets had to be normalized to allow comparison and the detection of relevant changes.

Extremely low signals can be considered noise, if they are below a certain threshold across all experiments. To define the noise threshold, a control intrinsic to the array system was exploited. The gene chip contains 5744 probe sets for 5841 of the 5845 genes of *S. cerevisiae* as well as 5021 probe sets for 5031 genes of *Schizosaccharomyces pombe*. As both fungi are only distantly related, the *S. pombe* probes will generally not detect transcripts from baker's yeast and consequently define noise. The data obtained for *S. pombe* genes were plotted for both assay sets (Figure 55). The 100th percentile was chosen as the noise threshold. Interestingly the genes with signal intensities above threshold are highly conserved among both species, such as ribosomal subunit genes, phosphoglycerate kinase or pyruvate decarboxylase.

To normalize both assay sets against each other, genes with signals above noise not varying more than a factor of 0.2 within one assay set on a linear data scale were selected. This yielded 1637 'housekeeper' genes per assay set, corresponding to ~28 % of all genes. The mean signal of each housekeeper was calculated within both assay sets and plotted against the other. Linear regression yielded the factors to normalize A2 to A1 (Figure 56): all signals of A2 were adjusted using these parameters. After normalization of the signal values all experiments could be compared among each other.

To obtain a measure for the relevance of expression changes, the non-toxic controls transformed with pQ0 and pQ30 after 3 days of incubation were compared using a scatter plot. Linear regression and subsequent residual analysis is depicted in Figure 58. As both proteins are equally

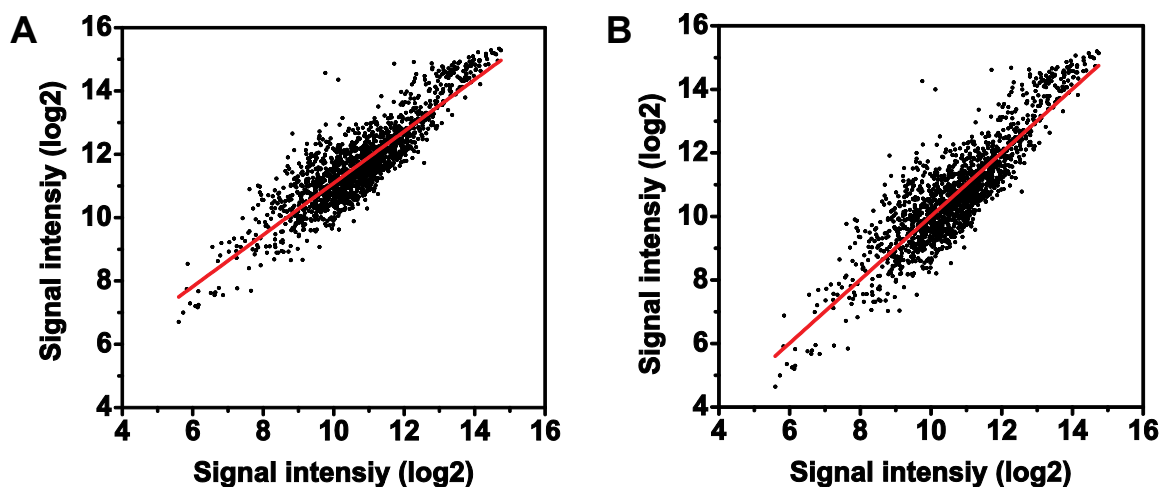


Figure 56: Determination of normalization parameters. To obtain the parameters for normalization of both assay sets, the signal for genes determined to be housekeepers in assay set 2 were plotted against the corresponding values in assay set 1 (A). The normalization parameters for signals in assay set 2 were determined by linear regression and applied to the data, resulting in the normalized dataset, depicted in (B).

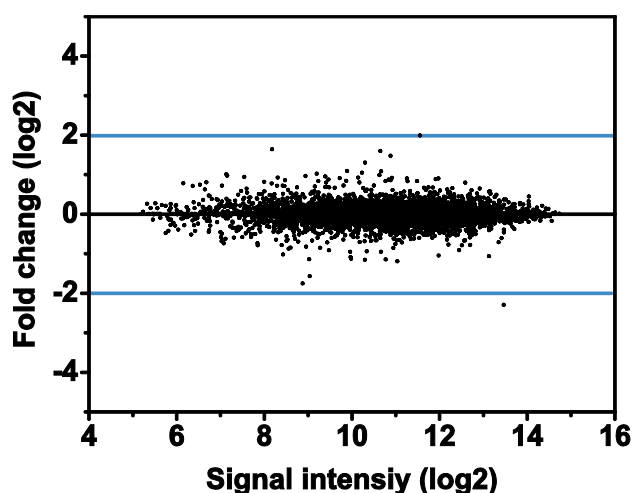


Figure 58: Definition of relevance level. The residual plot of gene expression changes between cells transgenic for pQ0 (abscissa) and pQ30 (fold-change on ordinate) indicates that the majority of genes did not change their expression level in a range of $\pm 2^2$ fold. Consequently, changes outside this range (blue lines) were considered

non-toxic and the nutrient supply should be most similar for these two samples, all changes in expression observed in this experiment should be below a threshold of relevance for cytotoxicity. A 2^2 fold change was consequently considered appropriate, as only one transcript is out of this range comparing both non-toxic samples.

The sample combination that should most appropriately yield information on expression changes upon cytotoxicity are pQ0 transformed cells on day 2 after transformation and pQ56 transformed cells on day 4 after transformation. Both experiments should contain cells in a very similar state of nutrient supply. The comparison of both samples applying the thresholds defined initially yielded 43 genes that change expression in the presence of the toxic Q₅₆-YFP species (Figure 57). However, these signal changes may be influenced by untransformed cells in the background or differences in incubation time or random variation in large sample sizes.

To rule out either source of artifact, two criteria were established for hit validation. Expression changes observed comparing pQ0 transformed cells to the untransformed control were

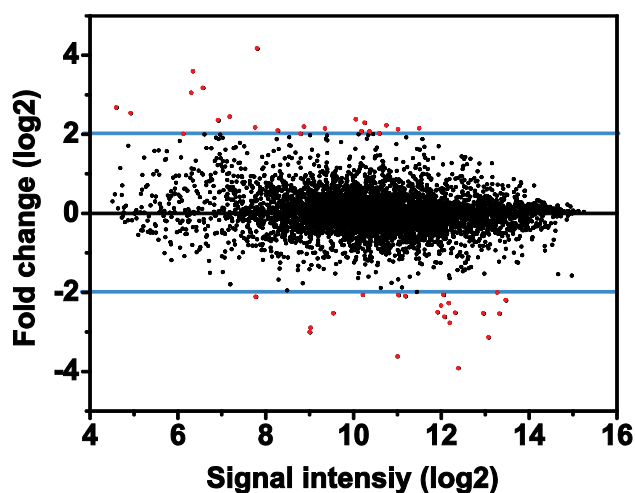


Figure 57: Gene regulation in response to cytotoxicity. A residual plot of gene expression changes comparing cells transformed with pQ0 after 2 days of incubation (abscissa) versus the change of the same gene in pQ56 after 4 days of incubation (ordinate). The previously defined relevance threshold is indicated by the blue lines. Genes outside this range have been marked red.

Results

considered. YFL061W is upregulated 6-fold comparing pQ0 on day 2 to pQ56 on day 4. However, when pQ0 transformed cells are compared to the untransformed sample an upregulation of 124 fold is detected. Consequently, it cannot be ruled out that the measured change in mRNA levels is due to an increased amount of untransformed cells in pQ56 samples. Signal changes due to random variation and incubation time were controlled for by comparing all non-intoxicated samples (pQ0 and pQ30) to both pQ56 transgenic samples. As such, a 6-fold upregulation of YOR028C could only be detected comparing pQ0 after 2 days to pQ56 transformants after 4 days of incubation but not in other non-toxic to toxic comparisons.

Applying these criteria, 29 genes remained that may be considered part of the cellular response to toxic polyQ proteins. They are summarized in Table 24. It is notable, that two transmembrane phosphate transporters (*PHO89* and *PHO84*) as well as two ammonium transmembrane transporters (*ADY2* and *ATO2*) are downregulated. This finding points to an involvement of salt homeostasis and metabolic processes in the response to polyQ toxicity. Furthermore, three genes contribute to mitochondrial maintenance and metabolism.

Fold expression	Systematic name	Gene name	Description
-15,2	YGL158W	<i>RCK1</i>	Protein kinase involved in the response to oxidative stress
-12,4	YPR192W	<i>AQY1</i>	Spore-specific water channel
-8,1	YCR010C	<i>ADY2*</i>	Acetate transporter required for sporulation
-7,5	YDR281C	<i>PHM6</i>	Protein of unknown function regulated by phosphate levels
-6,9	YNR056C	<i>BIO5</i>	Putative transmembrane protein
-5,8	YGR052W	<i>FMP48*</i>	Putative protein of unknown function
-5,8	YHR136C	<i>SPL2</i>	Downregulates low-affinity phosphate transport
-5,7	YBR296C	<i>PHO89</i>	Na ⁺ /Pi cotransporter of early growth phase
-5,7	YBR066C	<i>NRG2</i>	Transcriptional repressor mediating glucose repression
-4,6	YML123C	<i>PHO84</i>	High-affinity Pi transporter
-4,3	YIL057C	<i>RGI2</i>	Protein of unknown function repressed under high glucose
-4,2	YOR032C	<i>HMS1</i>	HLH transcription factor, enhances pseudohyphal growth
-4,2	YBR157C	<i>ICS2</i>	Protein of unknown function
-4,0	YKL043W	<i>PHD1</i>	Transcriptional activator, enhances pseudohyphal growth
-3,9	YHR022C	<i>YHR022C</i>	Putative protein of unknown function
-3,4	YNR002C	<i>ATO2*</i>	Putative transmembrane protein, promotes death in aging
3,8	YHR029C	<i>YHI9</i>	Protein of unknown function
4,0	YOL017W	<i>ESC8</i>	Protein involved in gene silencing, interacts with Gal11
4,2	YNR065C	<i>YNR065C</i>	Protein of unknown function
4,2	YML116W	<i>ATR1</i>	Multidrug efflux pump
4,3	YER175C	<i>TMT1</i>	Trans-aconitate methyltransferase
4,4	YPL058C	<i>PDR12</i>	Multidrug transporter
4,7	YOR383C	<i>FIT3</i>	Mannoprotein of the cell wall, iron metabolism

4,9	YMR095C	<i>SNO1</i>	Potential glutamine aminotransferase induced during stationary phase
5,1	YHR157W	<i>REC104</i>	Protein involved in meiotic recombination
5,8	YKL183C-A	<i>YKL183C-A</i>	Protein of unknown function
8,2	YAR050W	<i>FLO1</i>	Lectin-like protein involved in flocculation
9,0	YPL033C	<i>YPL033C</i>	Protein of unknown function involved in regulation of dNTPs
12,0	YDR042C	<i>YDR042C</i>	Putative protein of unknown function

Table 24: 29 genes are part of the polyQ toxicity response. The table summarizes the genes found to change their expression upon transformation with toxic polyQ construct faithfully, comparing the samples most similar in terms of their growth state – pQ0 on day 2 and pQ56 on day 4. The change of expression is given, as well as the systematic name, trivial name and annotated gene function. Genes marked with an asterisk are contributing to mitochondrial processes.

4.3 Q₅₆-YFP affects carbon source utilization

The genes found to suppress polyQ toxicity as well as the genes up- and downregulated upon the expression of Q₅₆-YFP are members of several different pathways and cellular processes. Despite this, it is noticeable that in all large-scale experiments, genes that are involved in mitochondrial processes and biogenesis are retrieved. *S. cerevisiae* is a Crabtree-positive yeast, growing mainly fermentatively under aerobic conditions at high levels of fermentable carbon source (e.g. glucose). Consequently, growth in liquid full medium at high glucose exhibits a lag-phase, a phase of fermentative exponential growth followed by the diauxic shift where cells adapt their metabolism to the subsequent respirative consumption of residual glucose and ethanol. This linear phase of growth is finally restricted by the exhaustion of carbon sources, resulting in a stationary culture (Werner-Washburne *et al.*, 1993). However, proper mitochondrial function is a prerequisite for fast growth also on glucose as the capacity for respiration is required despite the largest fraction of the carbon source being primarily fermented

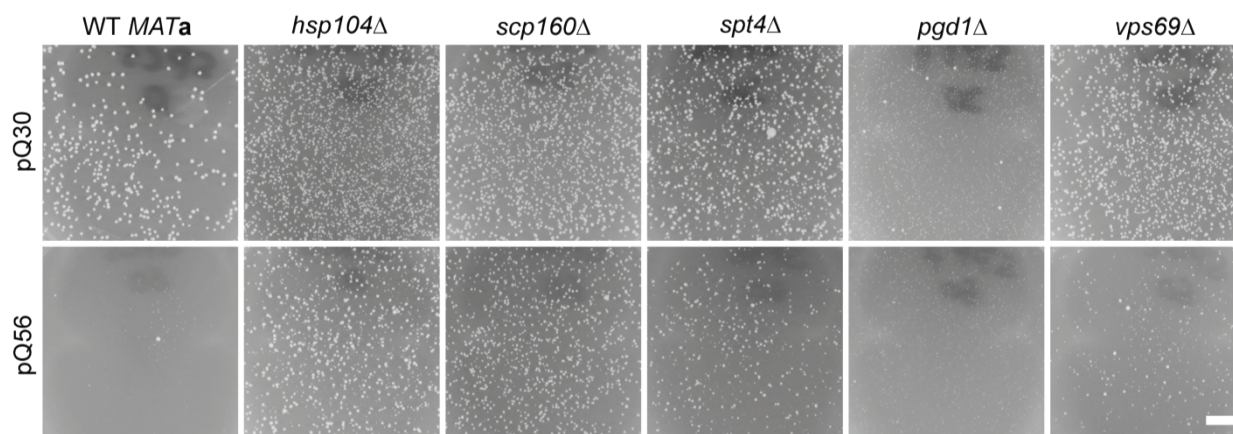


Figure 59: Some hits cure an enhanced phenotype on sorbitol. The phenotype of pQ56 is enhanced when WT *MATa* cells are grown on media containing 2% sorbitol as a carbon source instead of glucose. The deletion of toxicity enhancing genes is in some cases capable of restoring the residual growth of small colonies or even fully abolishing toxicity. Representative images are shown for selected strains (cf. Table 25 for full information). The scale bar represents 10 mm.

Results

(Kappeli, 1986). Mitochondria also contribute to the synthesis of pyrimidines, amino acids, phospholipids, nucleotides, folate coenzymes, heme, urea, and many other metabolites (Attardi & Schatz, 1988). In this context it is also important to mention, that mitochondrial phenotypes have long been known in *S. cerevisiae*. As such, the *[rho]* or *petite* phenotypes are defined as slow-growing colonies on plates containing a fermentable carbon source. On carbon sources requiring aerobic growth, these colonies will not be able to grow. The *[rho]* phenotypes are either caused by the loss of mitochondrial DNA or mutations in nuclear genes encoding proteins essential for mitochondrial biogenesis or maintenance (Contamine & Picard, 2000). Considering the *petite*-like appearance of pQ56 intoxicated yeast cells, and the function of the genes discovered, it may be envisioned that the phenotype of the presented polyQ system is also a result of mitochondrial dysfunction. To support or disprove this hypothesis, WT yeast was transformed with pQ0, pQ30 and pQ56 and plated on selective media containing 2% sorbitol or 3% glycerol instead of glucose. Glycerol must be consumed aerobically. Consequently, a phenotype affecting mitochondria should be most clear under this condition. Sorbitol, however, is a polyol sugar and generally used as an osmolyte in yeast cell biology. Its metabolism is not very well-studied, but *S. cerevisiae* should be generally able to use D-sorbitol as a carbon source after being oxidized to D-fructose upon reduction of a nicotinamide cofactor (Sarthy *et al.*, 1994). This reaction may however require the presence and proper function of mitochondria to regenerate the reduced cofactor.

When transformants were plated on media containing 2% glycerol, growth was extremely slow. Consequently, 2% sorbitol was selected as a carbon source for further investigations, as for this polyol the phenotype was already drastically enhanced, indicating that even the metabolic processing of sorbitol is more difficult for cells producing Q₅₆-YFP (Figure 59). This effect is surprising, as providing one oxidation equivalent for the generation of the fermentable fructose should only be impossible, if the respiratory chain or other pathways regenerating oxidation equivalents are severely compromised. As sorbitol may obviously not be properly exploited as a carbon source by cells expressing Q₅₆-YFP to support residual growth, it was interesting to examine whether the increase of toxicity on sorbitol would be epistatic to the functionality of toxicity enhancing genes. Interestingly, only a fraction of these genes were capable to suppress the enhanced toxicity on sorbitol (Table 24).

The effect seems not to be restricted to one specific group of knockout strains, nor is there any obvious correlation to the initial quality of rescue on glucose as a carbon source.

Gene	Strain No.	Gene function	Q ₅₆ -YFP	Sorbitol	Group
<i>hsp104Δ</i>	1514	Protein folding	+++	++	I
<i>pho5Δ</i>	3232	Phosphate regulation	+++	++	
<i>pdf1Δ</i>	1246	Protein folding	+++	o	
<i>hda3Δ</i>	5594	Chromatin organization, Transcription	+++	++	
<i>cyk3Δ</i>	3814	Budding	+	o	
<i>gal11Δ</i>	1742	RNA-Polymerase II regulation, subunit of Mediator Complex	+++	++	
<i>sin3Δ</i>	1695	Chromatin organization	++	o	
<i>pgd1Δ</i>	4393	RNA-Polymerase II regulation, subunit of Mediator Complex	+++	++	
<i>rad6Δ</i>	4425	Protein degradation, Cell cycle control	++	o	
<i>bem2Δ</i>	7548	Budding	+++	o	
<i>tif3Δ</i>	5578	Translation	+++	o	
<i>asc1Δ</i>	6556	Translation	++	o	
<i>hof1Δ</i>	7817	Budding	++	o	
<i>med2Δ</i>	3701	RNA-Polymerase II regulation, subunit of Mediator Complex	+++	o	
<i>sin4Δ</i>	1976	RNA-Polymerase II regulation, subunit of Mediator Complex	+++	o	
<i>eap1Δ</i>	7036	Translation	+++	o	
<i>ymr185wΔ</i>	770	Unknown	+++	o	
<i>hsl7Δ</i>	3272	Budding	+++	o	
<i>cdc10Δ</i>	3482	Budding	+++	++	III
<i>swa2Δ</i>	3679	Budding / Vesicle transport COP	+++	o	
<i>kre6Δ</i>	5574	Cell wall biogenesis	+++	o	
<i>hnt3Δ</i>	2514	DNA repair	+++	o	
<i>gpm2Δ</i>	3717	Metabolism	+++	++	
<i>ldb16Δ</i>	3413	Mitochondrion	+++	++	
<i>ybl094cΔ</i>	3120	Unknown	+++	o	
<i>rox3Δ</i>	3119	RNA-Polymerase II regulation, subunit of Mediator Complex	++	o	
<i>spt4Δ</i>	6986	RNA-Polymerase I/II regulation, pre-mRNA processing	+++	+++	
<i>scp160Δ</i>	1343	Translation	+++	+++	
<i>bfr1Δ</i>	2454	Translation, Nuclear segregation	+++	++	
<i>vps69Δ</i>	5504	Vacuolar protein sorting	+++	o	
<i>tho2Δ</i>	2937	Transcription	+++	o	
<i>whi3Δ</i>	2015	Cell cycle control	++	o	

Table 25: The deletion of toxicity enhancing genes can suppress stronger toxicity on sorbitol. The table lists deletion strains abolishing the phenotype of pQ56. The hit quality is denoted as in Table 21. Also, the behavior of the respective strain on sorbitol as a carbon source is given (o : no change in comparison to WT on sorbitol; + : slight amelioration; ++ : strong amelioration of toxicity; +++ : no difference between pQ30 and pQ56 transformed cells).

Results

4.4 Q₅₆-YFP expression affects mitochondria

Several indications lead to mitochondrial affects potentially being involved in the generation of the toxicity phenotype described in this study. Seven genes that suppress polyQ toxicity are part of mitochondrial processes or regulating mitochondrial biogenesis. Three genes found to change their expression upon Q₅₆-YFP synthesis are part of mitochondrial processes. Most importantly however, the utilization of sorbitol as a carbon source strongly enhances the toxicity phenotype.

Consequently, the common denominator of these observations may be a compromised mitochondrial function, conferred by the presence of toxic polyQ stretches. To probe this possible explanation, yeast reporter strains synthesizing fusions of the mitochondrial proteins Atp15 and Cox4 to GFP were transformed with pQ56mCherry and pQ0mCherry. Atp15 is the

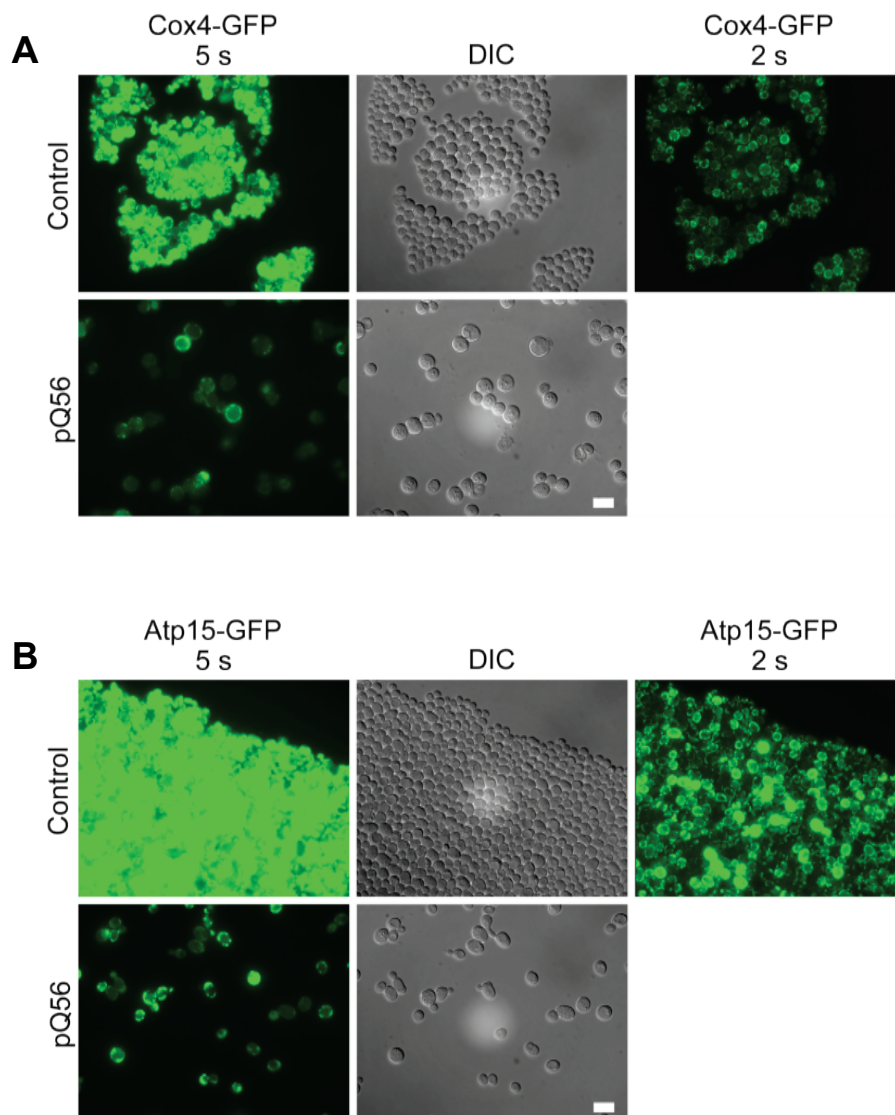


Figure 60: The effects of toxic polyQ stretches on mitochondria. (A) Cells expressing Cox4-GFP were imaged at an exposure time of 5 s in the fluorescence channel for both, control and pQ56 transformants. Whereas this exposure time was appropriate for pQ56 cells, the micrograph of controls is oversaturated. Similar fluorescence intensity could only be achieved, when the exposure time was reduced from 5 s to 2 s as indicated. (B) A similar effect was observed for another mitochondrial marker protein Atp15-GFP. A 5 s exposure was appropriate to document the fluorescence of pQ56 transformants, but oversaturation was strong when the same settings were applied to record micrographs of control cells. A reduction of exposure times (2 s) also yielded similar fluorescence intensities for control transformants here. The scale bar represents 10 μ m.

epsilon subunit of the F_1 sector of the F_1F_0 ATPase. It is non-essential and was recovered during the genome-wide screen for suppressors of toxicity. Cox4 is the subunit IV of cytochrome c oxidase and an integral membrane protein. Both proteins are nuclear-encoded and imported into mitochondria. When fluorescently labeled, both should provide independent markers for overall mitochondrial number and morphology.

Interestingly, when Q₅₆-mCherry was expressed, the overall intensity of fluorescence in comparison to control samples was drastically decreased in both reporter strains, which may be attributed to a reduction of mitochondrial density within the cytoplasm (Figure 60). However, this effect was not evident. Mitochondrial number or shape rather seemed normal, pointing to an overall reduction of mitochondrial membrane protein levels by the presence of polyQ proteins.

4.5 Aggregates interact differentially with chaperones

Aggregation is not necessarily correlated to toxicity. Still, experiments in cell culture revealed intriguing details on differential localization and kinetic parameters of interaction between chaperones and aggregates of polyQ proteins and variants of human Sod1 (Matsumoto *et al.*, 2006). Most importantly, the divergence in behavior between different aggregation prone proteins may be a useful probe for the molecular structure of aggregates.

To investigate which proteins interact with aggregates in the pQ56 system, Ssa3, Atg16, Ydj1 and Sis1 were fused to CFP in high copy overexpression plasmids. Ssa3 is one of four highly homologous isoforms of Hsp70 in yeast (Werner-Washburne *et al.*, 1987). Atg16 is part of the pre-autophagosomal complex and required for autophagy (Mizushima *et al.*, 1999). Ydj1 and Sis1 are the best-studied representatives of the class of J-proteins in yeast and share functional

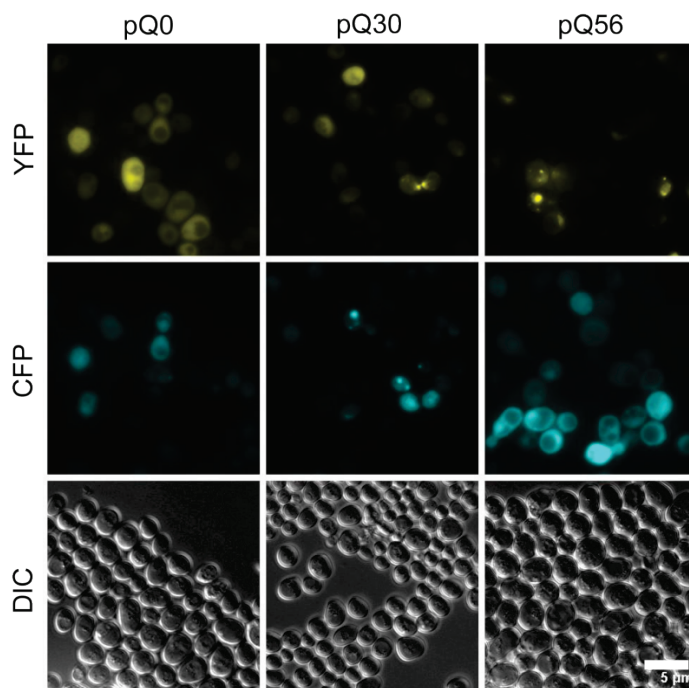


Figure 61: Colocalization pattern of Sis1 and polyQ proteins. Representative images of cells transformed with a plasmid bearing Sis1-CFP (CFP) and the indicated polyQ construct (YFP). The scale bar represents 10 μ m in all micrographs.

Results

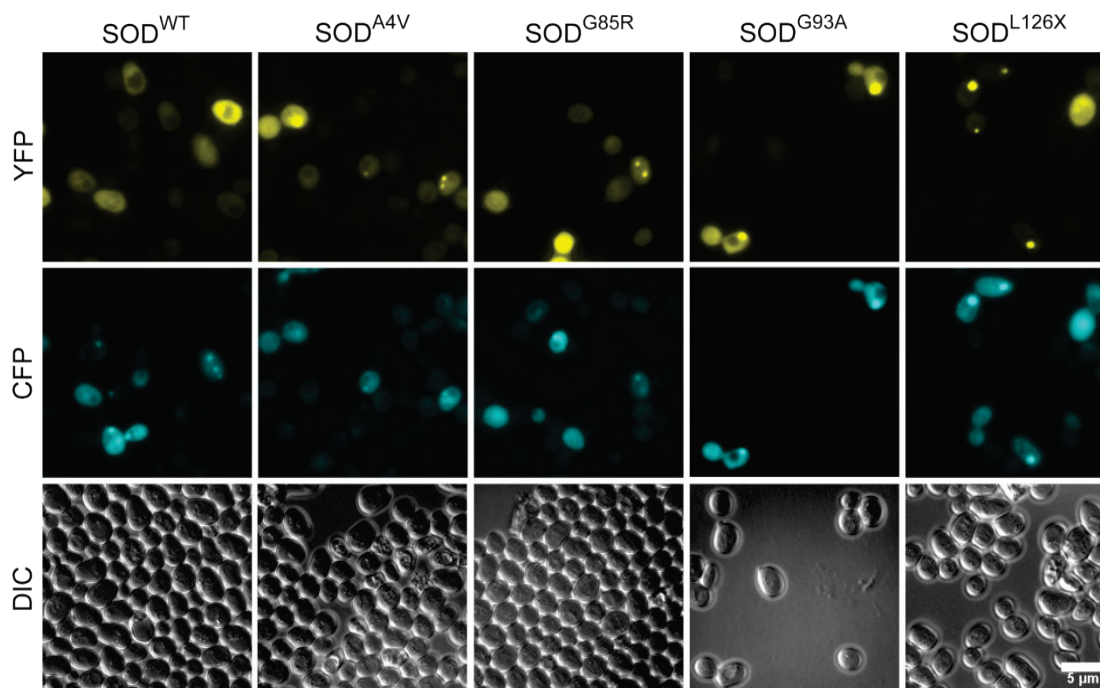


Figure 62: Colocalization pattern of Sis1 and pathogenic SOD1 variants. Representative micrographs of cells transformed with a plasmid bearing Sis1-CFP (CFP) and the indicated variants of human Sod1 variants (YFP). The scale bar represents 10 μm in all micrographs.

similarity. Sis1 in contrast to Ydj1 is essential (Walsh *et al.*, 2004). WT *MATa* cells were transformed with these constructs, subsequently with pQ0, pQ30 and pQ56 and subjected to microscopic studies. Surprisingly, Ssa3-CFP and Atg16-CFP localized to specific cellular structures also in the presence of diffusely distributed Q₀-YFP. This effect was weaker but noticeable for the Hsp40 proteins Sis1-CFP and Ydj1-CFP. When Q₃₀-YFP was present, the CFP-fusions as well as Q₃₀-YFP exhibited focus formation but colocalization was only detectable for Ydj1-CFP. Q₅₆-YFP colocalized to Sis1-CFP foci, but not to Ssa3-CFP and Atg16-CFP. The interaction of Ydj1-CFP with Q₅₆-YFP could not be determined, as transformation of cells overexpressing Ydj1-CFP with pQ56 did not yield any transformants in two separate experiments (Table 26, cf. Figure 61 for representative results).

To probe whether the results obtained for the polyQ system may be generalized to other aggregation-prone proteins, an analogous experiment was performed using pathogenic variants of human Sod1. The coding plasmids of this system were designed to fully equal the polyQ system, substituting the polyQ stretches for SOD^{WT} or mutants previously linked to familial ALS in humans: SOD^{A4V}, SOD^{G85R}, SOD^{G93A} and SOD^{L126X}. The transformation of these constructs into WT yeast does not point to toxicity. Aggregation cannot be observed for SOD^{WT}-YFP, but is apparent at an incidence of 5-10% of individual cells for pathogenic variants. Colocalization experiments uncover that all marker proteins are able to localize to areas of enriched fluorescence. Ssa3-CFP and Sis1-CFP robustly associate with aggregates formed by all pathogenic variants of SOD. Atg16-CFP however seems to only interact with aggregates formed by SOD^{G85R}-YFP and SOD^{L126X}-YFP. Ydj1-CFP seems to exclusively bind to SOD^{G85R}-YFP aggregates *in vivo*. It is furthermore notable, that SOD^{A4V}-YFP and SOD^{L126X}-YFP seem to have lost their propensity to aggregate when Ssa3-CFP and Ydj1-CFP, respectively, are overexpressed (Table 26).

	Atg16-CFP	Sis1-CFP	Ssa3-CFP	Ydj1-CFP
SOD ^{WT} -YFP	C	C	n. d.	no foci
SOD ^{A4V} -YFP	C	CY	no foci	CY
SOD ^{G85R} -YFP	CY	CY	CY	CY
SOD ^{G93A} -YFP	CY	CY	CY	Y
SOD ^{L126X} -YFP	CY	CY	CY	no foci
Q ₀ -YFP	C	C	C	C
Q ₃₀ -YFP	CY	CY	CY	CY
Q ₅₆ -YFP	CY	CY	Y	n. d.

Table 26: A summary of colocalization experiments on polyQ and SOD1 aggregates. The table lists the results obtained from colocalization experiments co-expressing fluorescently labeled marker proteins and polyQ proteins as well as pathogenic variants of human SOD1. The summary indicates whether focal enrichment of cyan (C, cellular factor) or yellow (Y, aggregating protein) fluorescence was detected. Shaded fields indicate colocalization was detected.

The results obtained from these colocalization experiments highlight that the interaction pattern of cellular cofactors with aggregates may not necessarily be generalized although derived from a single aggregation system. For human Sod1, it even becomes evident, that single site mutations leading to protein aggregation can result in interaction patterns peculiar to this mutant. Some cellular proteins such as Sis1 seem to localize to aggregated proteins more promiscuously, whereas others such as Ydj1 and Ssa3 exhibit a preference for certain aggregation prone proteins.

E Discussion

Discussion

1 The Hsc70 and Hsp90 machineries in *C. elegans*⁵

Both, the Hsc70 and Hsc90 systems together with their cochaperones have been attributed to perform essential functions safeguarding the proteome and contributing to the regulation of diverse cellular processes and pathways. Most of the knowledge on these systems and their cell biology is derived from studies in mammalian cell culture or single-celled organisms. It is also known that certain clients require specific subsets of cochaperones to mature or become activated. Peptidyl prolyl isomerases for instance are required for steroid hormone receptor maturation, whereas the cochaperone Cdc37 is typically associated with kinase activation (Li *et al.*, 2012). Consequently, e.g. cells that are highly involved in or responsive to hormone signaling may regulate the expression levels and activity of specific cochaperones according to their needs. Little is known, however, to what extent cell types express chaperone systems or specific sets of cochaperones differentially. *C. elegans* is a model organism that is ideally suited to answer this question, as this transparent metazoan provides well-defined tissues uniformly consisting of single cell types.

1.1 The Hsc70 system

A large number of studies exist on the hydrolysis reaction of Hsc70 proteins from other model organisms and the regulation of their activity by substrate proteins and cofactors. In particular, the DnaK-system of *E. coli* has been characterized in considerable detail. Several mutations in DnaJ and DnaK have been described, which disrupt the binding of cofactors. A mechanism of the interaction had been postulated that explains the stimulation of the ATPase rate of DnaK in the presence of DnaJ, reviewed in Genevaux *et al.* (2007). SBD truncations in DnaK have been characterized and revealed effects on substrate binding and refolding activities, but only weak effects on ATP-hydrolysis (Aponte *et al.*, 2010; Buczynski *et al.*, 2001; Slepnev *et al.*, 2003). It is important to note that strong differences exist between DnaK and the eukaryotic proteins, specifically within the helical lid domain, which is almost unrelated in terms of primary sequence. The function of the lid domain as an inhibitor of the intrinsic hydrolysis rate and thus the potential coupling of its motions to the hydrolysis reaction might therefore be different in the bacterial system (Aponte *et al.*, 2010; Chesnokova *et al.*, 2003). Fewer data are available for eukaryotic systems. In yeast, the very low hydrolysis rates of Ssa1 and Ssa2 makes its comparison to the nematode system difficult (Lopez-Buesa *et al.*, 1998). The best eukaryotic match might be the mammalian system, but no systematic analysis of lid truncations has hitherto been performed. Consequently, it remains to be determined whether the effects observed in this study are of general importance to all Hsp70 systems or whether they represent a specialty of *C. elegans*. The data presented comparing the activity and stability of the human and nematodal versions of Hsc70 point to the fact that the slightly higher basal activity of CeHsc70 at equal temperatures may be due to a shifted activity and stability optimum that coincides surprisingly well to the optimum growth or body temperature of each organism.

⁵ Parts of this section are adapted from papers published before as indicated under ‘Publications’.

Discussion

The finding that heat shock and the depletion of the Hsc70 HSP-1 induce HSP-70 in specific cells, even in specific subgroups of the same cellular type may indicate specific requirements for chaperones in some cells. The data indicate as well that heat shock and chaperone depletion are not necessarily equal in their effects and cells are differentially sensitive to each challenge. It would be interesting to see, which tissues or cell types have specific requirements for chaperones in higher organisms.

In other organisms, a wealth of data exists on the interaction of Hsc70 with its ATPase-stimulating J-domain containing cofactors. The strict dependence of the Hsc70/J-protein interaction on the presence of ATP has been observed in studies using Hsp70-systems from bacteria, eukaryotes and organelles (Buchberger *et al.*, 1995; Greene *et al.*, 1998; Jiang *et al.*, 2007; Swain *et al.*, 2007; Wawrzynow *et al.*, 1995). However, recent data on the ER-resident Hsp70-system highlighted that for some systems complex formation is also possible in the presence of ADP and consequently the regulation may be more complicated (Marcinowski *et al.*, 2011). Moreover, DnaK•DnaJ complexes have been observed in the presence of ADP in NMR experiments (McCarty *et al.*, 1995). For the *C. elegans* system, complexes of Hsc70 and the J-domain protein only form in the presence of ATP. However, based on the fast ATP hydrolysis rates, it has to be assumed that in the detected assemblies represent a post-hydrolysis DNJ-13•CeHsc70•Mg-ADP-P_i complex. As AUC only provides very limited kinetic information, the dissociation rate of this complex could not be determined.

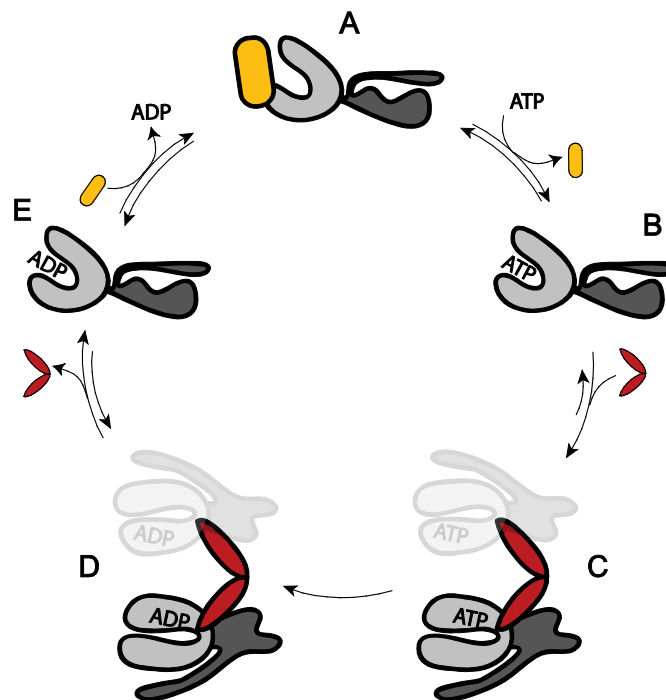


Figure 63: A model for the regulation of CeHsc70's ATPase by DNJ-13 and BAG-1. Based on additional data (Sun *et al.*, 2012), a model for cofactor interaction during the hydrolytic cycle may be established. After the initial binding of ATP to the NBD of CeHsc70 (Step A→B), conformational changes result in a hydrolysis competent conformation (Step B→C). This reaction is favored in CeHsc70, as hydrolysis is not rate-limiting. DNJ-13 (red) seems to bind as a dimeric protein forming a heterotetrameric complex with two Hsc70 monomers (transparent) and accelerates the formation of the hydrolysis-competent conformation, thus promoting ATP hydrolysis, which likely is irreversible (Step C→D). After hydrolysis, DNJ-13 leaves the complex and Hsc70 returns to its open conformation (Step D→E). BAG-1 (yellow) acts to displace the nucleotide (Step E→A). Based on this model, simultaneous BAG-1 and DNJ-13 binding to CeHsc70 would be mutually exclusive, although several intermediate steps may exist during this cycle.

The competitive binding of the NEF BAG-1 and the J-protein DNJ-13 suggests that competition is generated by favoring a specific conformation during the hydrolysis cycle, which excludes or reduces the apparent affinity of the other cofactor, therefore, the presence of BAG-1 weakens the apparent binding constant of DNJ-13. It is generally interesting to note that the strongest effects on ATP turnover occur during the weak cofactor interactions. This may be intuitive, as for a productive acceleration of the hydrolysis reaction an unfavorable conformational transition has to be overcome by cofactor binding.

It is surprising that large heterotetrameric DNJ-13•CeHsc70•Mg-ADP-P_i complexes are formed during AUC experiments. As Hsp40-like proteins contain dimerization sequences at the carboxyterminus, the formation of these assemblies as heterotetrameric complexes appears possible. Certainly, it cannot be ruled out that a combination of specific and unspecific interactions leads to the formation of these assemblies (Wittung-Stafshede *et al.*, 2003). Moreover, given the high concentration of CeHsc70 and the presence of substoichiometric amounts of DNJ-13 in the luciferase-refolding assays, however, it is also possible that this multimeric protein complex reflects a functional species in the refolding of substrate proteins.

1.2 The Hsp90 system

Hsp90 is essential in most organisms, including *S. cerevisiae*, *C. elegans*, *D. melanogaster* and vertebrates (Birnby *et al.*, 2000; Borkovich *et al.*, 1989; Cutforth & Rubin, 1994; Rutherford & Lindquist, 1998; Yeyati *et al.*, 2007). In this study, the functions of the Hsp90-homolog DAF-21 in *C. elegans* was addressed. In this model organism, recently an involvement of Hsp90 in the development of the gonad has been documented (Gaiser *et al.*, 2009; Green *et al.*, 2011; Inoue *et al.*, 2006). A DAF-21 mutation results in motility defects and other phenotypic traits related to dauer development, chemotaxis and thermotaxis (Birnby *et al.*, 2000; Thomas *et al.*, 1993; Vowels & Thomas, 1992). Beyond this, DAF-21 seems to play a crucial role in maintaining the nematode's muscular structure and function.

In this study, the knockdown of *daf-21* led to motility defects, the muscular induction of the heat shock response and the improper deposition of MYO-3 into aggregate-like structures at the myofibrillar lattice (cf. Figure 64). The origin of the aggregated MYO-3 protein is yet unknown, however the muscular patterning is already accomplished before hatching (Waterston, 1988). At this point in development, RNAi has not come into action, as worms were exposed to bacteria as synchronized L1 larvae. As the nematodes pass through the larval stages to become adult, the muscular ultrastructure has to expand by the incorporation of new myosin subunits. Consequently, the effects observed in this study should mainly be due to a compromised muscular growth and not due to initial problems in patterning of the muscular ultrastructure. Nevertheless, from the data it cannot be derived, whether the aggregate-like structures are composed of newly synthesized myosin about to be assembled into the lattice or whether aggregated MYO-3-GFP originates from the existing ultrastructure, potentially bound to be degraded by the proteasome machinery. It is however obvious, that the aggregate-containing parts of the cytosol should not contain detectable amounts of MYO-3 protein in normal muscle cells. Previous *in vitro* studies had indicated that a direct interaction of DAF-21 with its cofactor UNC-45 is required for the folding of the UNC-54 myosin head domain and its correct assembly into the myofibrillar lattice. However, an interaction was never observed with the myosin

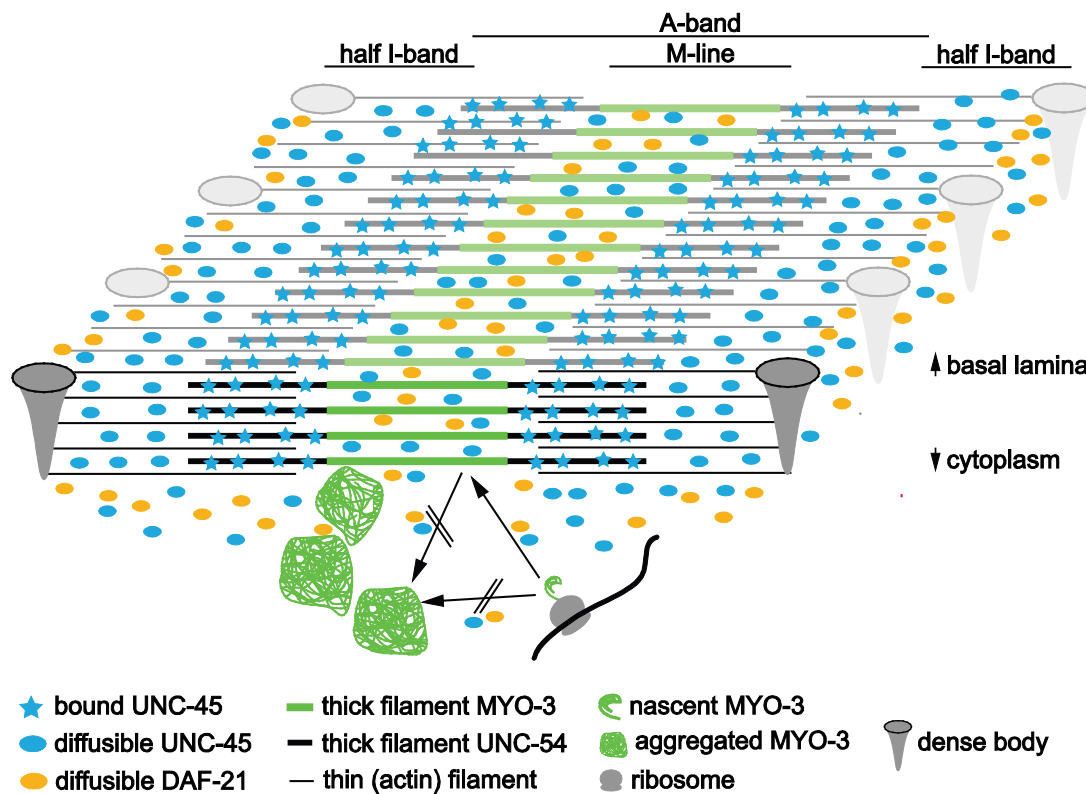


Figure 64: A model for the muscular function and localization of DAF-21 and UNC-45. The model summarizes the data obtained in this study for the localization of UNC-45 and DAF-21 and suggests a mode of action for both proteins in muscle cells. The obliqueness of the striation is omitted for reasons of clarity. The sarcomere spans between two dense bodies. It consists of actin thin filaments on both sides and myosin thick filaments in the central region. The green area of the thick filaments corresponds to the MYO-3 rich M-line. UNC-45 stably associated to the A-band is depicted as light blue stars. DAF-21 (yellow ellipsoids) is mainly found in the space between dense bodies, whereas soluble UNC-45 (light blue ellipsoids) reaches further into the central area of the sarcomere. Cytoplasmic aggregates of MYO-3 are depicted as green tangles, which may result from newly synthesized MYO-3 or MYO-3 derived from the sarcomeric lattice. The inhibition of aggregation of MYO-3 by the presence of UNC-45 and DAF-21 is not necessarily a result of direct interaction, but may result from misincorporation of UNC-54.

MYO-3 before (Barral *et al.*, 2002; Srikakulam *et al.*, 2008). Consequently, the observation that MYO-3 is mislocalized upon depletion of DAF-21 or UNC-45 might be an indicator for a previously unobserved chaperone dependence of MYO-3 or a result of a more complex series of misguided events. It could be postulated that cytoplasmic aggregation of UNC-54 due to depleted chaperones bound to be assembled into the growing myofibrillar lattice leads to the co-aggregation of the physiological interaction partner MYO-3.

The involvement of Hsp90 in the muscular organization has been observed in vertebrates before. Studies in zebrafish showed that Hsp90 is involved in myofibrillogenesis and that specific knockdown of Hsp90a.1 resulted in the distortion of muscle fibres (Du *et al.*, 2008). The morphological homology between muscle cells of vertebrates and nematodes is limited – the striation in nematodes is not arranged perpendicular to the sarcomeric organization, but oblique (Waterston, 1988). Identifying Hsp90 as an important contributor to muscular maintenance in nematodes however recapitulates this finding also in lower metazoan species and may expand the possibilities to address Hsp90 functions mechanistically in another *in vivo* system. As the homolog of UNC-45 in yeast lacks the TPR-domain interacting with Hsp90, the function of Hsp90 in the maintenance of muscle structure may represent an evolutionarily novel utilization

of Hsp90's ability to support client proteins in multicellular eukaryotes adding on to the chaperoning activity for transcription factors and protein kinases.

The exact mechanism of the contribution of DAF-21 and UNC-45 to muscle maintenance is still not clear. In *C. elegans*, solely the involvement of the myosin binding protein UNC-45 in muscle formation has been addressed before. In fixated nematodes it was found to be localized to the myosin containing A-band, the region of the muscle containing the myosin homolog UNC-54 (Ao & Pilgrim, 2000; Barral *et al.*, 1998; Landsverk *et al.*, 2007). Complementary studies in zebrafish observed that a corresponding localization in these animals is a specific result of fixation methods and *in vivo*, the localization of Unc-45 and Hsp90a.1 is dynamic. Specifically both proteins are shuttled between the Z-line and the A-band in response to damage (Etard *et al.*, 2007; Etard *et al.*, 2008). The Z-line in this context is suspected to serve as a 'chaperone reservoir'.

In this study, using live nematodes expressing fluorescently tagged proteins, differences in the subcellular localization of DAF-21 and UNC-45 were observed, potentially hinting to a sophisticated tempo-spatial regulation of their interaction. UNC-45, if present in abundance, is localized mainly to the I-band (Figure 64). All parts of the muscular ultrastructure appear accessible. The bulk of UNC-45 is not stably associated with any structure, as it recovers at a fast rate after photobleaching. Some cells, however, reveal that not all UNC-45 molecules are freely diffusible. Here, UNC-45 can be seen to be stably associated with the A-bands hinting to two populations of UNC-45, one freely diffusible in the cytosol and the other stably attached to myosin filaments. Interestingly, the center of the A-band appears to contain less UNC-45-CFP protein. This space corresponds to the MYO-3 containing M-line and could confirm that stably attached UNC-45 localizes preferentially to the UNC-54 containing part of the A-band (Figure 64). It is interesting to note that these two patterns in all observed cases affect the whole cell and not subcellular regions of the sarcomeric lattice. This concerted reaction inside the cell could hint to a tightly regulated event.

For DAF-21 instead, no stably associated protein was detected (Figure 64). In cells expressing little DAF-21 its localization was restricted to the central I-band between the dense bodies. This localization may correlate to the Z-line localization described for vertebrate skeletal muscle cells (Etard *et al.*, 2008). Additionally, DAF-21 may be detected parts of the A-band. The localization within this band appears specific for the thin M-line that also contains MYO-3. DAF-21 potentially is excluded from the UNC-54 containing part of the thick filament. Thus, the localization of DAF-21 seems spatially more constrained than the localization of UNC-45. This may be due to different affinities or protein-specific exclusion from parts of the ultrastructure. It cannot be ruled out though, that YFP-DAF-21 behaves differently from endogenous DAF-21. Some properties of the chaperone may be altered by the fusion to YFP. Hsp90 seems to contribute to the maintenance of muscular integrity as a soluble, transiently associated factor, while UNC-45 can stably associate with the UNC-54 containing part of the myofibrillar lattice under yet to be defined circumstances.

2 Aggregation in *S. cerevisiae*

This study identified a set of genes that is required to obtain a population-based toxicity phenotype of Q₅₆-YFP (cf. D3.5). Six of the strains uncovered affected the same open reading frame in two separate hits recovered. Both were retrieved independently by the screening procedure in an unbiased fashion, highlighting that strains affecting the phenotype were recovered with high fidelity. Interestingly, a complementary genome wide screen had been performed before, but only three (*HSP104*, *CYK3*, *BFR1*) of the genes uncovered in the screen presented here, overlap (Manogaran *et al.*, 2011). It is a taunting fact that the polyQ aggregation system presented is independent of the endogenous prion state, as removing prions or the deletion of *RNQ1* do not modulate the phenotype observed (cf. D3.7). Obviously, the protein context of Htt103Q renders this model sensitive to the prion state of the cell. It will be interesting to see, whether the toxicity mechanisms described for the ‘naked’ polyQ stretch are also valid for Htt aggregation in humans and generalizable to other polyQ aggregation disorders.

The cellular functions the genes in the present study are annotated with cover a wide spectrum

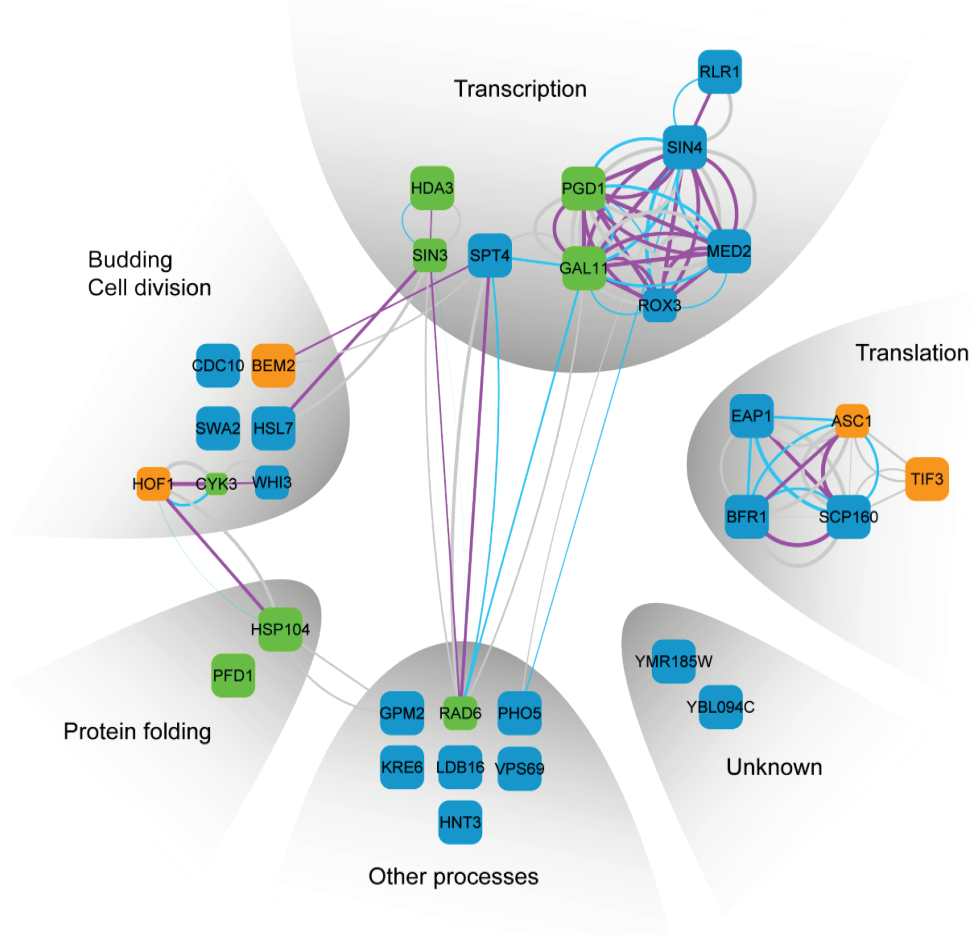


Figure 65: A network of genes enhances polyQ toxicity. The genes uncovered in the genome wide screen may be assembled into a network. Each gene is represented by a square. The size corresponds to the quality of the hit in respect to the pQ56 system. Color represents group association (green: group I, orange: group II, blue: group III). Known interactions of the genes are represented by edges. The width of the edges correlates to the confidence level, the color the type of evidence (purple: physical interaction, cyan: text mining, grey: other method). The genes were clustered according to their annotated biological process contribution.

such as transcription, translation and budding or cellular division (cf. Table 21). They could be classified into haploid strains (group I), strains that became hyperploid when pQ56 was present (group II) and generally hyperploid strains (group III). However, the processes they are involved in interact with each other (Figure 65). Some genes are part of the mediator complex and the regulatory network centered on RNA-Polymerase II. As such, the proteins Gal11, Med2, Rox3 and Pgd1 and Sin4 are subunits of the mediator complex (Casamassimi & Napoli, 2007). Spt4 is a general regulator of the RNA polymerase and pre-mRNA processing (Martinez-Rucobo *et al.*, 2011). Scp160, Eap1, Asc1, and Bfr1 are part of the SESA network, coordinating spindle pole duplication by regulating the transcription of specific mRNAs, consequently linking translation to nuclear division (Sezen *et al.*, 2009). Bem2 is known to be crucial for bud emergence by regulating Cdc42 (Knaus *et al.*, 2007). The localized enrichment of this kinase to predetermine the future site of bud emergence is also required to allow the deposition of the septin ring. Cdc10 was recovered in the screen and is part of this structure (Cid *et al.*, 1998). Hsl7, Hof1 and Cyk3, functionally interact with the septins during budding (Nishihama *et al.*, 2009; Shulewitz *et al.*, 1999). The septin ring has previously been reported to serve as a signaling scaffold during cytokinesis (Merlini & Piatti, 2011). In this context, it is interesting to note, that the disaggregase Hsp104 (Parsell *et al.*, 1994) was described to cooperate with Hof1 and the actin network to maintain the asymmetric distribution specifically of damaged or aggregated proteins between the mother and daughter cell (Liu *et al.*, 2010; Tessarz *et al.*, 2009).

As the deposition of Cdc10 is severely compromised without direct affection of the spindle geometry or obvious arrest of mitosis at a specific step, it may be rationalized that polyQ proteins interfere with septin assembly or the prior localized enrichment of Cdc42, thereby inhibiting the progression of the cell cycle beyond S-phase (cf. D3.10). However, FACS data do not suggest a strong enrichment of 2N nuclei, which should be expected if septin assembly was not regulating the entry into S-phase by a checkpoint. Morphogenesis checkpoints for the septin ring have been described for later events during mitosis (Howell & Lew, 2012). The data

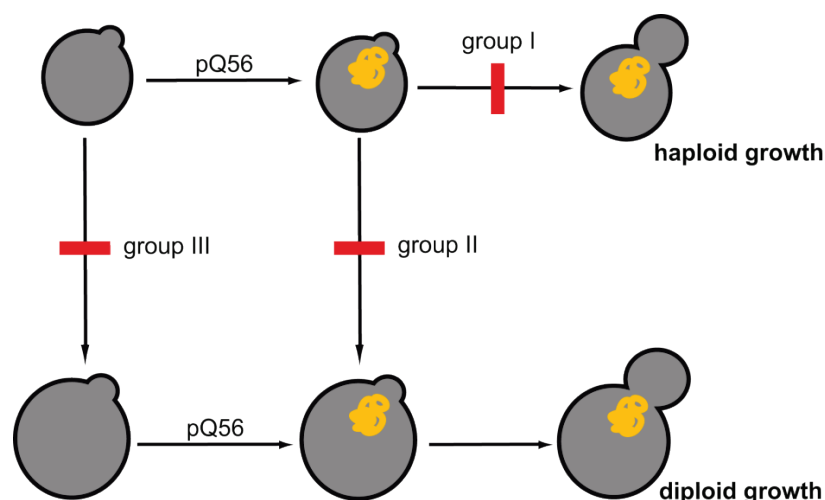


Figure 66: A model for potential interference steps of toxicity enhancing genes. Toxicity is generated by the expression and aggregation of Q₅₆-YFP and the subsequent inability of cells to follow the normal haploid growth cycle. Deletion of group I genes restores this ability and ensures growth as haploid cells. An alternative route is switching to the diploid growth cycle, which under normal conditions is blocked by group II (and group III) genes. This switching event happens for group II genes only in response to the toxic pressure from Q₅₆-YFP. In deletion strains for group III genes, this switching to 2N states happens already under control conditions, leading to constitutive cycling at states of higher ploidy and to resistance against Q₅₆-YFP toxicity.

Discussion

described in the presented study rather suggest a pre-S-phase checkpoint, controlling bud site selection being activated by the interference of polyQ proteins with septin assembly. A fraction of cells may still proceed with DNA synthesis and undergo endoreduplication events as being unable to proceed to cytokinesis without the septin structure assembled. Whether this sequence of events leads to hyperploid survivor colonies and how di- or hyperploid cells become insensitive to polyQ toxicity remains to be elucidated. The genes that are members of group II may be responsible to suppress such endoreduplication events and consequently the corresponding knockout strains may only become di- or hyperploids upon the toxic pressure exerted by polyQ proteins. Group III members, however already exhibit higher ploidy upon transformation with non-toxic constructs. These genes may be involved in other aspects of ploidy maintenance that are not directly related to polyQ toxicity. Apparently, spontaneous conversion to a diploid state in normal haploid strains leads to the appearance of cells of higher ploidy within slowly growing colonies and enables some cells of the initially transformed population to overcome the toxicity of the polyQ stretch, growing to large colonies (cf. D3.2). The low incidence of spontaneously resistant clones with long polyQ stretches implies nevertheless, that these growth-promoting conversions occur rarely, although a certain amount of cells in intoxicated colonies is of higher ploidy. This effect may be due to additional changes in the genome being required to obtain growth at higher ploidy in an originally haploid strain.

To explain the loss of toxicity when members of group I are deleted, different mechanisms have to be considered, however. Most likely in these strains the toxic species may be abolished or its direct targets interfering with septin assembly or deposition may be modified to become insensitive to toxicity. The first seems true for the deletion of *hsp104Δ* and *pho5Δ*. Both strains behave highly similar in all assays described above (cf. D3.8, D3.9) and only *hsp104Δ* has been shown before to prevent aggregate toxicity (Giorgini *et al.*, 2005; Manogaran *et al.*, 2011). How other group I members influence the toxicity phenotype remains nevertheless enigmatic.

Based on the evidence presented, a relation between polyQ resistance and polyploidization in the life cycle of haploid yeast cells becomes obvious (Figure 66). It may be hypothesized that hyperploidization is a pathway to escape toxicity, exerted by aggregation prone proteins.

To understand the native response of cells to protein aggregation, expression microarray analysis was performed on cells growing normally and intoxicated cells (cf. D4.2). Interestingly, no induction of the heat shock response became apparent. The expression changes observed neither related to other previously described responses to a specific challenge like oxidative stress or the diauxic shift. Instead, the overexpression of a protein kinase and several other genes, which are related to mitochondrial biogenesis and maintenance point to a participation of these organelle. Additional evidence for mitochondrial affects also came from the screen of the deletion library. Here, the deletion of the mitochondrial genes *ATP15* and *UGO1* abolished residual growth (cf. D4.1). It may be assumed that secondary to interference with cell division through the septin ring, mitochondria suffer from the presence of the toxic species. The analysis of fluorescently labeled marker proteins for mitochondria suggests that mitochondrial protein levels are reduced when the toxic Q56 species is present (cf. D4.4). It may be speculated that polyQ proteins interfere with protein import and consequently compromise mitochondrial function. Sorbitol needs to be oxidized by oxidation equivalents usually provided by mitochondria prior to catabolic usage. This additional metabolic challenge leads to the full loss of growth capacity when Q₅₆-YFP is present. Both, the deletion of non-essential mitochondrial genes or different

carbon sources cannot be tolerated and lead to lethality. Cells seem to be reacting accordingly with expression changes of genes regulating mitochondrial function and metabolism. It is important to note that these changes are not capable of restoring full normal growth, however.

The comparison of the polyQ system with pathogenic SOD1 mutants reveals that the latter proteins are well tolerated by yeast cells, as no toxicity phenotype can be detected. The colocalization with cellular factors known or considered to be important for aggregate handling supports the notion that different proteins form aggregates with discrete molecular properties (cf. D4.5). However, the nature of these differences might not be understood easily, as even within the group of SOD1 mutants, heterogeneous interaction patterns can be discerned. Yjd1 only interacts with SOD^{G85R}, and Atg16 seems to specifically colocalize with SOD^{G85R} and SOD^{L126X}. Extended studies comparing both models with an extended set of colocalization markers could yield further insight on the molecular interaction patterns, especially when combined with situations when polyQ aggregates become non-toxic (e.g. GdnHCl treatment) or under yet to be defined conditions that render SOD1 mutants toxic. The systems introduced in this work should be specifically powerful to perform such a study, as the only divergent feature of all transgene constructs are the sequences encoding the polyQ stretches and SOD1.

The relevance of the aggregation study in yeast may not be restricted to fungal cells. Although the Hsp104 system is not found in mammals, functionally homologous systems have been described and are currently under intense scrutiny. While septin ring formation and other events during budding is a characteristic of fungal cell division, there notably are similarities to metazoan processes and cellular structures: septins maintain dendritic spine individualization in neurons and have been described to be relevant in the etiology of neuropathological conditions (Saarikangas & Barral, 2011); molecular filters based on actin at the axonal initial segment are responsible for retaining macromolecules in the soma of neurons (Song *et al.*, 2009). Thus, during the maintenance of mammalian neuronal networks such cellular structures might be compromised by polyQ proteins. A compromised mitochondrial function has also been documented for neuropathological disorders (Hashimoto *et al.*, 2003). More specifically, the energy metabolism of patients suffering from HD is severely compromised, which has to be compensated for by an increased uptake of glucose.

In respect to the resistance to toxicity of di- or hyperploid yeast observed in the experiments presented here, it is notable, that for a HD mouse model controversial data were reported on an increased amount of aneuploid cells in mice transgenic for Htt150Q (Petersen *et al.*, 2005; Sathasivam *et al.*, 2001). For AD, however, connections between hyperploid neurons and the pathogenesis of AD have been established (Arendt *et al.*, 2010; Yang *et al.*, 2001). This hyperploidy is potentially caused by the disruption of the mitotic spindle or re-entry into the cell cycle (Borysov *et al.*, 2011, Andorfer *et al.*, 2005). This is contradictory to the rescuing effect of increased ploidy observed in this study, but a more stringent ploidy control system in human neurons may cause the apoptotic reaction finally leading to disease.

Discussion

F Acknowledgements

I would like to thank Prof. Johannes Buchner for giving me the opportunity to perform my doctorate studies in his laboratory. I am grateful for fruitful discussions and his belief in my ability to achieve this doctorate degree.

Additionally, I thank Klaus Richter for providing a challenging project, as well as important ideas for the development of this thesis. He gave me the chance to learn a wide array of methods to answer scientific questions by *in vitro* as well as *in vivo* techniques. I am grateful for the years we spent working as a team, trying to answer exciting questions of chaperone and aggregation cell biology.

My colleagues Veronika Haslbeck, Julia Eckl and Katharina Papsdorf were an amazing company and support at any time, sharing good and sad moments scientifically as well as privately. I hope we will share many more great hours even after I've left the lab.

I am indebted to all the other colleagues of the Buchner Lab, most importantly to Tanja, Natalia and Julia for all the support they provided when the project seemed almost intractable. We walked long ways together and I will always remember the times we shared and hope that our friendship will persist long into the future.

Thank you, Prof. Sevil Weinkauff for being a mentor, whenever I needed your counseling.

Stefan Grötzinger and Stephanie Runde helped me with a plethora of aspects of my thesis. It was awesome to have you here as Master's students! Thank you for sharing half a year – even more – of your life with me and supporting my project.

I would like to thank Bettina Richter and Lisa Schuster for their excellent practical support also with schedules way beyond normal working hours of a technician or a student.

Stefan Jordan provided the opportunity to perform FACS experiments and supported me with encouraging e-mails. Thank you for this and your friendship!

To Susanne Hilber, I am indebted due to her organizational talent making sure there would be money to pay the rent each of the 64 months of my thesis. Thank you for all the conversations and the caring atmosphere you created in this laboratory.

Thank you, Nerea and Julia for correcting the thesis!

Without my friends I would have been lost. Thank you all so much for your patience at every instance I came late due to science stuff. Thank you – most importantly Matthias – for listening to all my complaining and for fighting desperation with a supportive word anytime I needed it.

Athanasios, I am lucky we have met! Without your emotional support, leaving me the freedom to prioritize freely, things would have been even harder to deal with. Ευχαριστώ, αγάπη μου!

Last, but most importantly, I want to thank my parents Josef und Susanna Kaiser and my family, who by anything they could contribute, supported my education. Your love and care carried me through all the years. Without you I would be nothing! I love you!

This work shall specifically honor my caring grandmother Christa Kaiser. I miss you so much.

Acknowledgements

G Figures

Figure 1: Possible states of a generic polypeptide chain.....	12
Figure 2: Models of chaperone functionality.	15
Figure 3: The chaperone cycle of Hsp90.	16
Figure 4: Coding sequences for pQ0, pQ30 and pQ50.	48
Figure 5: Heat shock response and lethality in <i>C. elegans</i>	59
Figure 6: Temperature dependence of the Hsc70 ATPase.....	60
Figure 7: Structural stability of CeHsp70 and HsHsp70.....	60
Figure 8: Hsp70 can be induced by heat stress and Hsc70 depletion.	61
Figure 9: BAG-1 from <i>C. elegans</i> is the sole close relative of human Bag1-L.	62
Figure 10: DNJ-13 is closely related to human DNAJB5 and yeast Sis1.....	62
Figure 11: BAG-1 binding to CeHsc70.....	63
Figure 12: DNJ-13 stimulates CeHsc70.....	64
Figure 13: DNJ-13 binding to CeHsc70 is dependent on ATP.....	65
Figure 14: BAG-1 disrupts *DNJ-13•CeHsc70•ATP.	65
Figure 15: DNj-13 and BAG-1 accelerate hydrolysis synergistically.....	66
Figure 16: Cochaperones are required for substrate refolding.....	67
Figure 17: Maximum refolding is not related to maximum hydrolysis.	67
Figure 18: Lid truncations of CeHsc70.....	68
Figure 19: The stability of truncations of CeHsc70 is largely uncompromised.....	69
Figure 20: CD thermal transitions of CeHsc70.....	69
Figure 21: DSF thermal transitions of CeHsc70 truncations.	70
Figure 22: Substrate refolding requires the substrate binding and lid domains.	70
Figure 23: Impaired Hsp90 function reduces the lifespan.	71
Figure 24: Expression of <i>daf-21</i> in stable and transient lines.	72
Figure 25: Inducibility of selected heat shock proteins.....	73
Figure 26: <i>daf-21</i> RNAi induces heat shock in muscle cells.	74
Figure 27: Reduced <i>daf-21</i> and <i>unc-45</i> levels disrupt the muscular ultrastructure.....	74
Figure 28: Reduction of <i>daf-21</i> or <i>unc-45</i> leads to myosin aggregation.....	75
Figure 29: Focal depositions of MYO-3-GFP are non-diffusible.....	76
Figure 30: The organization of nematodal body wall muscle cells.....	77

Figures

Figure 31: DAF-21 and UNC-45 localize to specific parts of the sarcomeric lattice.....	78
Figure 32: I-band associated Hsp90 is freely diffusible.	79
Figure 33: UNC-45 is diffusible in or stably associated to the sarcomeric lattice.....	80
Figure 34: A population-based toxicity phenotype in yeast.	83
Figure 35: Colony fluorescence of polyQ transformants.....	84
Figure 36: Q ₃₀ -YFP and Q ₅₆ -YFP form aggregates of distinct morphology.	84
Figure 37: Analysis of polyQ proteins in WT yeast.	85
Figure 38: Q ₅₆ -YFP leads to enlarged cells.	86
Figure 39: Yeast transformed with pQ56 exhibit increased DNA content.	86
Figure 40: FACS analysis of large survivor colonies.	87
Figure 41: Increased polidy abolishes polyQ toxicity.	88
Figure 42: Heterozygosity at the <i>MAT</i> locus is not required for rescue.	88
Figure 43: Representative results of the genome-wide screen.....	89
Figure 44: A summary of the screen for genes enhancing the toxicity phenotype of Q ₅₆ -YFP. ..	91
Figure 45: Strains also rescue the toxicity phenotype of HttQ103.	93
Figure 46: The toxicity of HttQ103 is fully abolished in tetraploid yeast strains.....	94
Figure 47: GdnHCl mimicks the deletion of <i>HSP104</i>	95
Figure 48: Q ₅₆ -YFP toxicity is independent of the prion state.	96
Figure 49: Toxic protein levels are largely unaltered in group I strains.	97
Figure 50: Hsp104 levels are unaltered in most group I strains.....	97
Figure 51: Genes enhance toxicity by different mechanisms.	98
Figure 52: Hsp104 and Pho5 are required to obtain WT-like aggregation.....	99
Figure 53: PolyQ toxicity does not severely affect the appearance of spindle markers.	100
Figure 54: Toxic PolyQ proteins interfere with septin ring assembly.	101
Figure 55: Signal range of <i>S. pombe</i> probe sets.....	105
Figure 56: Determination of normalization parameters.....	106
Figure 57: Gene regulation in response to cytotoxicity.	107
Figure 58: Definition of relevance level.	107
Figure 59: Some hits cure an enhanced phenotype on sorbitol.....	109
Figure 60: The effects of toxic polyQ stretches on mitochondria.....	112
Figure 61: Colocalization pattern of Sis1 and polyQ proteins.....	113
Figure 62: Colocalization pattern of Sis1 and pathogenic SOD1 variants.	114
Figure 63: A model for the regulation of CeHsc70's ATPase by DNJ-13 and BAG-1.....	120

Figure 64: A model for the muscular function and localization of DAF-21 and UNC-45. 122

Figure 65: A network of genes enhances polyQ toxicity. 124

Figure 66: A model for potential interference steps of toxicity enhancing genes..... 125

Figures

H Tables

Table 1: Neurodegenerative aggregation diseases.	20
Table 2: Reagents.	32
Table 3: Buffers.	35
Table 4: Enzymes, kits and standards.	35
Table 5: Antibodies.	35
Table 6: Equipment.	37
Table 7: Strains and Organisms.	38
Table 8: Plasmids.	39
Table 9: Oligonucleotides.	39
Table 10: Media.	40
Table 11: Composition of amino acid mixtures.	41
Table 12: Computer programs and databases.	41
Table 13: Transformation mixture.	44
Table 14: Samples for microarray analysis.	49
Table 15: Composition of SDS-PAGE gels.	51
Table 16: Global assessment of RNAi phenotypes of the Hsc70 system.	63
Table 17: Biophysical properties of CeHsc70 variants.	68
Table 18: The dependence of motility on Hsp90 function.	72
Table 19: Genetic analysis of spontaneously occurring large colonies.	87
Table 20: Growth restoring <i>MATa/α</i> strains uncovered in the library.	90
Table 21: Enhancers of Q ₅₆ -YFP toxicity.	92
Table 22: Suppressors of Q ₅₆ -YFP toxicity.	104
Table 23: Overview of samples for gene expression analysis.	105
Table 24: 29 genes are part of the polyQ toxicity response.	109
Table 25: The deletion of toxicity enhancing genes can suppress stronger toxicity on sorbiol.	111
Table 26: A summary of colocalization experiments on polyQ and SOD1 aggregates.	115

I References

- Aguzzi A, Heikenwalder M, Polymenidou M (2007) Insights into prion strains and neurotoxicity. *Nature reviews Molecular cell biology* **8**: 552-561
- Akerfelt M, Morimoto RI, Sistonen L (2010) Heat shock factors: integrators of cell stress, development and lifespan. *Nature reviews Molecular cell biology* **11**: 545-555
- Ali JA, Jackson AP, Howells AJ, Maxwell A (1993) The 43-kilodalton N-terminal fragment of the DNA gyrase B protein hydrolyzes ATP and binds coumarin drugs. *Biochemistry* **32**: 2717-2724
- Amberg DC, Burke DJ, Strathern JN (2006) Isolation of plasmid DNA from yeast cells: a ten-minute preparation. *CSH protocols* **2006**
- Andorfer C, Acker CM, Kress Y, Hof PR, Duff K, Davies P (2005) Cell-cycle reentry and cell death in transgenic mice expressing nonmutant human tau isoforms. *The Journal of neuroscience : the official journal of the Society for Neuroscience* **25**: 5446-5454
- Ao W, Pilgrim D (2000) *Caenorhabditis elegans* UNC-45 is a component of muscle thick filaments and colocalizes with myosin heavy chain B, but not myosin heavy chain A. *The Journal of cell biology* **148**: 375-384
- Aponte RA, Zimmermann S, Reinstein J (2010) Directed evolution of the DnaK chaperone: mutations in the lid domain result in enhanced chaperone activity. *Journal of molecular biology* **399**: 154-167
- Arendt T, Bruckner MK, Mosch B, Losche A (2010) Selective cell death of hyperploid neurons in Alzheimer's disease. *The American journal of pathology* **177**: 15-20
- Arrasate M, Mitra S, Schweitzer ES, Segal MR, Finkbeiner S (2004) Inclusion body formation reduces levels of mutant huntingtin and the risk of neuronal death. *Nature* **431**: 805-810
- Attardi G, Schatz G (1988) Biogenesis of mitochondria. *Annual review of cell biology* **4**: 289-333
- Balch WE, Morimoto RI, Dillin A, Kelly JW (2008) Adapting proteostasis for disease intervention. *Science* **319**: 916-919
- Barral JM, Bauer CC, Ortiz I, Epstein HF (1998) Unc-45 mutations in *Caenorhabditis elegans* implicate a CRO1/She4p-like domain in myosin assembly. *The Journal of cell biology* **143**: 1215-1225
- Barral JM, Hutagalung AH, Brinker A, Hartl FU, Epstein HF (2002) Role of the myosin assembly protein UNC-45 as a molecular chaperone for myosin. *Science* **295**: 669-671
- Basso M, Massignan T, Samengo G, Cheroni C, De Biasi S, Salmona M, Bendotti C, Bonetto V (2006) Insoluble mutant SOD1 is partly oligoubiquitinated in amyotrophic lateral sclerosis mice. *The Journal of biological chemistry* **281**: 33325-33335
- Bates G (2003) Huntingtin aggregation and toxicity in Huntington's disease. *Lancet* **361**: 1642-1644
- Bence NF, Sampat RM, Kopito RR (2001) Impairment of the ubiquitin-proteasome system by protein aggregation. *Science* **292**: 1552-1555
- Bendz H, Ruhland SC, Pandya MJ, Hainzl O, Riegelsberger S, Brauchle C, Mayer MP, Buchner J, Issels RD, Noessner E (2007) Human heat shock protein 70 enhances tumor antigen presentation through complex formation and intracellular antigen delivery without innate immune signaling. *The Journal of biological chemistry* **282**: 31688-31702
- Bernardo P, Blackledge M (2010) Structural biology: Proteins in dynamic equilibrium. *Nature* **468**: 1046-1048

References

- Bernick EP, Zhang PJ, Du S (2010) Knockdown and overexpression of Unc-45b result in defective myofibril organization in skeletal muscles of zebrafish embryos. *BMC cell biology* **11**: 70
- Bertelsen EB, Chang L, Gestwicki JE, Zuiderweg ER (2009) Solution conformation of wild-type *E. coli* Hsp70 (DnaK) chaperone complexed with ADP and substrate. *Proceedings of the National Academy of Sciences of the United States of America* **106**: 8471-8476
- Bimston D, Song J, Winchester D, Takayama S, Reed JC, Morimoto RI (1998) BAG-1, a negative regulator of Hsp70 chaperone activity, uncouples nucleotide hydrolysis from substrate release. *The EMBO journal* **17**: 6871-6878
- Birnby DA, Link EM, Vowels JJ, Tian H, Colacurcio PL, Thomas JH (2000) A transmembrane guanylyl cyclase (DAF-11) and Hsp90 (DAF-21) regulate a common set of chemosensory behaviors in *Caenorhabditis elegans*. *Genetics* **155**: 85-104
- Bocking T, Aguet F, Harrison SC, Kirchhausen T (2011) Single-molecule analysis of a molecular disassemblase reveals the mechanism of Hsc70-driven clathrin uncoating. *Nature structural & molecular biology* **18**: 295-301
- Bodner RA, Outeiro TF, Altmann S, Maxwell MM, Cho SH, Hyman BT, McLean PJ, Young AB, Housman DE, Kazantsev AG (2006) Pharmacological promotion of inclusion formation: a therapeutic approach for Huntington's and Parkinson's diseases. *Proceedings of the National Academy of Sciences of the United States of America* **103**: 4246-4251
- Bolstad BM, Irizarry RA, Astrand M, Speed TP (2003) A comparison of normalization methods for high density oligonucleotide array data based on variance and bias. *Bioinformatics* **19**: 185-193
- Borchelt DR, Lee MK, Slunt HS, Guarnieri M, Xu ZS, Wong PC, Brown RH, Jr., Price DL, Sisodia SS, Cleveland DW (1994) Superoxide dismutase 1 with mutations linked to familial amyotrophic lateral sclerosis possesses significant activity. *Proceedings of the National Academy of Sciences of the United States of America* **91**: 8292-8296
- Borkovich KA, Farrelly FW, Finkelstein DB, Taulien J, Lindquist S (1989) hsp82 is an essential protein that is required in higher concentrations for growth of cells at higher temperatures. *Molecular and cellular biology* **9**: 3919-3930
- Borysov SI, Granic A, Padmanabhan J, Walczak CE, Potter H (2011) Alzheimer Abeta disrupts the mitotic spindle and directly inhibits mitotic microtubule motors. *Cell cycle* **10**: 1397-1410
- Bosco DA, Landers JE (2010) Genetic determinants of amyotrophic lateral sclerosis as therapeutic targets. *CNS & neurological disorders drug targets* **9**: 779-790
- Bosco DA, LaVoie MJ, Petsko GA, Ringe D (2011) Proteostasis and movement disorders: Parkinson's disease and amyotrophic lateral sclerosis. *Cold Spring Harbor perspectives in biology* **3**: a007500
- Brachmann CB, Davies A, Cost GJ, Caputo E, Li J, Hieter P, Boeke JD (1998) Designer deletion strains derived from *Saccharomyces cerevisiae* S288C: a useful set of strains and plasmids for PCR-mediated gene disruption and other applications. *Yeast* **14**: 115-132
- Brehmer D, Rudiger S, Gassler CS, Klostermeier D, Packschies L, Reinstein J, Mayer MP, Bukau B (2001) Tuning of chaperone activity of Hsp70 proteins by modulation of nucleotide exchange. *Nature structural biology* **8**: 427-432
- Brown JR, Lupas AN (1998) What makes a thermophile? *Trends in microbiology* **6**: 349-350
- Brown K, Mastrianni JA (2010) The prion diseases. *Journal of geriatric psychiatry and neurology* **23**: 277-298
- Brujin LI, Houseweart MK, Kato S, Anderson KL, Anderson SD, Ohama E, Reaume AG, Scott RW, Cleveland DW (1998) Aggregation and motor neuron toxicity of an ALS-linked SOD1 mutant independent from wild-type SOD1. *Science* **281**: 1851-1854
- Buchberger A, Theyssen H, Schroder H, McCarty JS, Virgallita G, Milkereit P, Reinstein J, Bukau B (1995) Nucleotide-induced conformational changes in the ATPase and substrate binding domains of the DnaK chaperone provide evidence for interdomain communication. *The Journal of biological chemistry* **270**: 16903-16910

- Buczynski G, Slepnev SV, Sehorn MG, Witt SN (2001) Characterization of a lidless form of the molecular chaperone DnaK: deletion of the lid increases peptide on- and off-rate constants. *The Journal of biological chemistry* **276**: 27231-27236
- Bukau B, Hestekamp T, Lührink J (1996) Growing up in a dangerous environment: a network of multiple targeting and folding pathways for nascent polypeptides in the cytosol. *Trends in cell biology* **6**: 480-486
- Campagnola PJ, Millard AC, Terasaki M, Hoppe PE, Malone CJ, Mohler WA (2002) Three-dimensional high-resolution second-harmonic generation imaging of endogenous structural proteins in biological tissues. *Biophysical journal* **82**: 493-508
- Carra S, Seguin SJ, Lambert H, Landry J (2008) HspB8 chaperone activity toward poly(Q)-containing proteins depends on its association with Bag3, a stimulator of macroautophagy. *The Journal of biological chemistry* **283**: 1437-1444
- Casamassimi A, Napoli C (2007) Mediator complexes and eukaryotic transcription regulation: an overview. *Biochimie* **89**: 1439-1446
- Cashikar AG, Duennwald M, Lindquist SL (2005) A chaperone pathway in protein disaggregation. Hsp26 alters the nature of protein aggregates to facilitate reactivation by Hsp104. *The Journal of biological chemistry* **280**: 23869-23875
- Caughey B, Lansbury PT (2003) Protofibrils, pores, fibrils, and neurodegeneration: separating the responsible protein aggregates from the innocent bystanders. *Annual review of neuroscience* **26**: 267-298
- Ceron J, Rual JF, Chandra A, Dupuy D, Vidal M, van den Heuvel S (2007) Large-scale RNAi screens identify novel genes that interact with the *C. elegans* retinoblastoma pathway as well as splicing-related components with synMuv B activity. *BMC developmental biology* **7**: 30
- Changeux JP, Edelstein SJ (2005) Allosteric mechanisms of signal transduction. *Science* **308**: 1424-1428
- Chattopadhyay M, Valentine JS (2009) Aggregation of copper-zinc superoxide dismutase in familial and sporadic ALS. *Antioxidants & redox signaling* **11**: 1603-1614
- Chen S, Bertheliev V, Yang W, Wetzel R (2001) Polyglutamine aggregation behavior in vitro supports a recruitment mechanism of cytotoxicity. *Journal of molecular biology* **311**: 173-182
- Chernoff YO, Lindquist SL, Ono B, Inge-Vechtsov SG, Liebman SW (1995) Role of the chaperone protein Hsp104 in propagation of the yeast prion-like factor [psi⁺]. *Science* **268**: 880-884
- Chesnokova LS, Slepnev SV, Protasevich II, Sehorn MG, Brouillette CG, Witt SN (2003) Deletion of DnaK's lid strengthens binding to the nucleotide exchange factor, GrpE: a kinetic and thermodynamic analysis. *Biochemistry* **42**: 9028-9040
- Chiti F, Dobson CM (2006) Protein misfolding, functional amyloid, and human disease. *Annual review of biochemistry* **75**: 333-366
- Chiti F, Dobson CM (2009) Amyloid formation by globular proteins under native conditions. *Nature chemical biology* **5**: 15-22
- Cid VJ, Adamikova L, Cenamor R, Molina M, Sanchez M, Nombela C (1998) Cell integrity and morphogenesis in a budding yeast septin mutant. *Microbiology* **144** (Pt 12): 3463-3474
- Ciechanover A, Brundin P (2003) The ubiquitin proteasome system in neurodegenerative diseases: sometimes the chicken, sometimes the egg. *Neuron* **40**: 427-446
- Contamine V, Picard M (2000) Maintenance and integrity of the mitochondrial genome: a plethora of nuclear genes in the budding yeast. *Microbiology and molecular biology reviews* : *MMBR* **64**: 281-315
- Craig EA, Jacobsen K (1984) Mutations of the heat inducible 70 kilodalton genes of yeast confer temperature sensitive growth. *Cell* **38**: 841-849
- Craig EA, Kramer J, Shilling J, Werner-Washburne M, Holmes S, Kosic-Smithers J, Nicolet CM (1989) SSC1, an essential member of the yeast HSP70 multigene family, encodes a mitochondrial protein. *Molecular and cellular biology* **9**: 3000-3008

References

- Cutforth T, Rubin GM (1994) Mutations in Hsp83 and cdc37 impair signaling by the sevenless receptor tyrosine kinase in *Drosophila*. *Cell* **77**: 1027-1036
- D'Amico S, Collins T, Marx JC, Feller G, Gerday C (2006) Psychrophilic microorganisms: challenges for life. *EMBO reports* **7**: 385-389
- David DC, Ollikainen N, Trinidad JC, Cary MP, Burlingame AL, Kenyon C (2010) Widespread protein aggregation as an inherent part of aging in *C. elegans*. *PLoS biology* **8**: e1000450
- Davies SW, Turmaine M, Cozens BA, DiFiglia M, Sharp AH, Ross CA, Scherzinger E, Wanker EE, Mangiarini L, Bates GP (1997) Formation of neuronal intranuclear inclusions underlies the neurological dysfunction in mice transgenic for the HD mutation. *Cell* **90**: 537-548
- Demeler B, Brookes E, Wang R, Schirf V, Kim CA (2010) Characterization of reversible associations by sedimentation velocity with UltraScan. *Macromolecular bioscience* **10**: 775-782
- Deng HX, Shi Y, Furukawa Y, Zhai H, Fu R, Liu E, Gorrie GH, Khan MS, Hung WY, Bigio EH, Lukas T, Dal Canto MC, O'Halloran TV, Siddique T (2006) Conversion to the amyotrophic lateral sclerosis phenotype is associated with intermolecular linked insoluble aggregates of SOD1 in mitochondria. *Proceedings of the National Academy of Sciences of the United States of America* **103**: 7142-7147
- Dill KA, Chan HS (1997) From Levinthal to pathways to funnels. *Nature structural biology* **4**: 10-19
- Dobson CM (2003) Protein folding and misfolding. *Nature* **426**: 884-890
- Dobson CM (2004) Principles of protein folding, misfolding and aggregation. *Seminars in cell & developmental biology* **15**: 3-16
- Doyle SM, Shorter J, Zolkiewski M, Hoskins JR, Lindquist S, Wickner S (2007) Asymmetric deceleration of ClpB or Hsp104 ATPase activity unleashes protein-remodeling activity. *Nature structural & molecular biology* **14**: 114-122
- Du SJ, Li H, Bian Y, Zhong Y (2008) Heat-shock protein 90alpha1 is required for organized myofibril assembly in skeletal muscles of zebrafish embryos. *Proceedings of the National Academy of Sciences of the United States of America* **105**: 554-559
- Duennwald ML, Echeverria A, Shorter J (2012) Small heat shock proteins potentiate amyloid dissolution by protein disaggregases from yeast and humans. *PLoS biology* **10**: e1001346
- Duennwald ML, Jagadish S, Giorgini F, Muchowski PJ, Lindquist S (2006a) A network of protein interactions determines polyglutamine toxicity. *Proceedings of the National Academy of Sciences of the United States of America* **103**: 11051-11056
- Duennwald ML, Jagadish S, Muchowski PJ, Lindquist S (2006b) Flanking sequences profoundly alter polyglutamine toxicity in yeast. *Proceedings of the National Academy of Sciences of the United States of America* **103**: 11045-11050
- Dunn AY, Melville MW, Frydman J (2001) Review: cellular substrates of the eukaryotic chaperonin TRiC/CCT. *Journal of structural biology* **135**: 176-184
- Dupuy D, Bertin N, Hidalgo CA, Venkatesan K, Tu D, Lee D, Rosenberg J, Svrzikapa N, Blanc A, Carnec A, Carvunis AR, Pulak R, Shingles J, Reece-Hoyes J, Hunt-Newbury R, Viveiros R, Mohler WA, Tasan M, Roth FP, Le Peuch C, Hope IA, Johnsen R, Moerman DG, Barabasi AL, Baillie D, Vidal M (2007) Genome-scale analysis of in vivo spatiotemporal promoter activity in *Caenorhabditis elegans*. *Nature biotechnology* **25**: 663-668
- Ehrnhoefer DE, Duennwald M, Markovic P, Wacker JL, Engemann S, Roark M, Legleiter J, Marsh JL, Thompson LM, Lindquist S, Muchowski PJ, Wanker EE (2006) Green tea (-)-epigallocatechin-gallate modulates early events in huntingtin misfolding and reduces toxicity in Huntington's disease models. *Human molecular genetics* **15**: 2743-2751
- Eisen MB, Spellman PT, Brown PO, Botstein D (1998) Cluster analysis and display of genome-wide expression patterns. *Proceedings of the National Academy of Sciences of the United States of America* **95**: 14863-14868
- Elble R (1992) A simple and efficient procedure for transformation of yeasts. *BioTechniques* **13**: 18-20

- Ellis RJ, Minton AP (2003) Cell biology: join the crowd. *Nature* **425**: 27-28
- Ellis RJ, van der Vies SM, Hemmingsen SM (1989) The molecular chaperone concept. *Biochemical Society symposium* **55**: 145-153
- Epstein HF, Thomson JN (1974) Temperature-sensitive mutation affecting myofilament assembly in *Caenorhabditis elegans*. *Nature* **250**: 579-580
- Etard C, Behra M, Fischer N, Hutcheson D, Geisler R, Strahle U (2007) The UCS factor Steif/Unc-45b interacts with the heat shock protein Hsp90a during myofibrillogenesis. *Developmental biology* **308**: 133-143
- Etard C, Roostalu U, Strahle U (2008) Shuttling of the chaperones Unc45b and Hsp90a between the A band and the Z line of the myofibril. *The Journal of cell biology* **180**: 1163-1175
- Faber PW, Alter JR, MacDonald ME, Hart AC (1999) Polyglutamine-mediated dysfunction and apoptotic death of a *Caenorhabditis elegans* sensory neuron. *Proceedings of the National Academy of Sciences of the United States of America* **96**: 179-184
- Fairbanks G, Steck TL, Wallach DF (1971) Electrophoretic analysis of the major polypeptides of the human erythrocyte membrane. *Biochemistry* **10**: 2606-2617
- Feige MJ, Hendershot LM, Buchner J (2010) How antibodies fold. *Trends in biochemical sciences* **35**: 189-198
- Frauenfelder H, Chen G, Berendzen J, Fenimore PW, Jansson H, McMahon BH, Stroe IR, Swenson J, Young RD (2009) A unified model of protein dynamics. *Proceedings of the National Academy of Sciences of the United States of America* **106**: 5129-5134
- Freeman BC, Myers MP, Schumacher R, Morimoto RI (1995) Identification of a regulatory motif in Hsp70 that affects ATPase activity, substrate binding and interaction with HDJ-1. *The EMBO journal* **14**: 2281-2292
- Fukada K, Nagano S, Satoh M, Tohyama C, Nakanishi T, Shimizu A, Yanagihara T, Sakoda S (2001) Stabilization of mutant Cu/Zn superoxide dismutase (SOD1) protein by coexpressed wild SOD1 protein accelerates the disease progression in familial amyotrophic lateral sclerosis mice. *The European journal of neuroscience* **14**: 2032-2036
- Gaiser AM, Brandt F, Richter K (2009) The non-canonical Hop protein from *Caenorhabditis elegans* exerts essential functions and forms binary complexes with either Hsc70 or Hsp90. *Journal of molecular biology* **391**: 621-634
- Gaiser AM, Kaiser CJ, Haslbeck V, Richter K (2011) Downregulation of the Hsp90 system causes defects in muscle cells of *Caenorhabditis elegans*. *PloS one* **6**: e25485
- Gama Sosa MA, De Gasperi R, Elder GA (2012) Modeling human neurodegenerative diseases in transgenic systems. *Human genetics* **131**: 535-563
- Garcia-Mata R, Bebok Z, Sorscher EJ, Sztul ES (1999) Characterization and dynamics of aggresome formation by a cytosolic GFP-chimera. *The Journal of cell biology* **146**: 1239-1254
- Gassler CS, Wiederkehr T, Brehmer D, Bukau B, Mayer MP (2001) Bag-1M accelerates nucleotide release for human Hsc70 and Hsp70 and can act concentration-dependent as positive and negative cofactor. *The Journal of biological chemistry* **276**: 32538-32544
- Gatchel JR, Zoghbi HY (2005) Diseases of unstable repeat expansion: mechanisms and common principles. *Nature reviews Genetics* **6**: 743-755
- Gautschi M, Mun A, Ross S, Rospert S (2002) A functional chaperone triad on the yeast ribosome. *Proceedings of the National Academy of Sciences of the United States of America* **99**: 4209-4214
- Genevaux P, Georgopoulos C, Kelley WL (2007) The Hsp70 chaperone machines of *Escherichia coli*: a paradigm for the repartition of chaperone functions. *Molecular microbiology* **66**: 840-857
- Gershenson A, Gierasch LM (2011) Protein folding in the cell: challenges and progress. *Current opinion in structural biology* **21**: 32-41
- Gidalevitz T, Ben-Zvi A, Ho KH, Brignull HR, Morimoto RI (2006) Progressive disruption of cellular protein folding in models of polyglutamine diseases. *Science* **311**: 1471-1474

References

- Gillan V, Maitland K, McCormack G, Him NA, Devaney E (2009) Functional genomics of hsp-90 in parasitic and free-living nematodes. *International journal for parasitology* **39**: 1071-1081
- Giorgini F, Guidetti P, Nguyen Q, Bennett SC, Muchowski PJ (2005) A genomic screen in yeast implicates kynurenine 3-monooxygenase as a therapeutic target for Huntington disease. *Nature genetics* **37**: 526-531
- Goldberg AL (2003) Protein degradation and protection against misfolded or damaged proteins. *Nature* **426**: 895-899
- Goldschmidt L, Teng PK, Riek R, Eisenberg D (2010) Identifying the amyloome, proteins capable of forming amyloid-like fibrils. *Proceedings of the National Academy of Sciences of the United States of America* **107**: 3487-3492
- Grallert H, Buchner J (2001) Review: a structural view of the GroE chaperone cycle. *Journal of structural biology* **135**: 95-103
- Gray M, Shirasaki DI, Cepeda C, Andre VM, Wilburn B, Lu XH, Tao J, Yamazaki I, Li SH, Sun YE, Li XJ, Levine MS, Yang XW (2008) Full-length human mutant huntingtin with a stable polyglutamine repeat can elicit progressive and selective neuropathogenesis in BACHD mice. *The Journal of neuroscience : the official journal of the Society for Neuroscience* **28**: 6182-6195
- Green RA, Kao HL, Audhya A, Arur S, Mayers JR, Fridolfsson HN, Schulman M, Schloissnig S, Niessen S, Laband K, Wang S, Starr DA, Hyman AA, Schedl T, Desai A, Piano F, Gunsalus KC, Oegema K (2011) A high-resolution *C. elegans* essential gene network based on phenotypic profiling of a complex tissue. *Cell* **145**: 470-482
- Greene MK, Maskos K, Landry SJ (1998) Role of the J-domain in the cooperation of Hsp40 with Hsp70. *Proceedings of the National Academy of Sciences of the United States of America* **95**: 6108-6113
- Grimminger V, Richter K, Imhof A, Buchner J, Walter S (2004) The prion curing agent guanidinium chloride specifically inhibits ATP hydrolysis by Hsp104. *The Journal of biological chemistry* **279**: 7378-7383
- GuhaThakurta D, Palomar L, Stormo GD, Tedesco P, Johnson TE, Walker DW, Lithgow G, Kim S, Link CD (2002) Identification of a novel cis-regulatory element involved in the heat shock response in *Caenorhabditis elegans* using microarray gene expression and computational methods. *Genome research* **12**: 701-712
- Gurney ME, Pu H, Chiu AY, Dal Canto MC, Polchow CY, Alexander DD, Caliendo J, Hentati A, Kwon YW, Deng HX, et al. (1994) Motor neuron degeneration in mice that express a human Cu,Zn superoxide dismutase mutation. *Science* **264**: 1772-1775
- Gutekunst CA, Li SH, Yi H, Mulroy JS, Kuemmerle S, Jones R, Rye D, Ferrante RJ, Hersch SM, Li XJ (1999) Nuclear and neuropil aggregates in Huntington's disease: relationship to neuropathology. *The Journal of neuroscience : the official journal of the Society for Neuroscience* **19**: 2522-2534
- Hageman J, Kampinga HH (2009) Computational analysis of the human HSPH/HSPA/DNAJ family and cloning of a human HSPH/HSPA/DNAJ expression library. *Cell stress & chaperones* **14**: 1-21
- Hageman J, Rujano MA, van Waarde MA, Kakkar V, Dirks RP, Govorukhina N, Oosterveld-Hut HM, Lubsen NH, Kampinga HH (2010) A DNAJB chaperone subfamily with HDAC-dependent activities suppresses toxic protein aggregation. *Molecular cell* **37**: 355-369
- Harrison CJ, Hayer-Hartl M, Di Liberto M, Hartl F, Kuriyan J (1997) Crystal structure of the nucleotide exchange factor GrpE bound to the ATPase domain of the molecular chaperone DnaK. *Science* **276**: 431-435
- Hartl FU, Hayer-Hartl M (2002) Molecular chaperones in the cytosol: from nascent chain to folded protein. *Science* **295**: 1852-1858
- Hashimoto M, Rockenstein E, Crews L, Masliah E (2003) Role of protein aggregation in mitochondrial dysfunction and neurodegeneration in Alzheimer's and Parkinson's diseases. *Neuromolecular medicine* **4**: 21-36

- Haslbeck M, Franzmann T, Weinfurter D, Buchner J (2005a) Some like it hot: the structure and function of small heat-shock proteins. *Nature structural & molecular biology* **12**: 842-846
- Haslbeck M, Miess A, Stromer T, Walter S, Buchner J (2005b) Disassembling protein aggregates in the yeast cytosol. The cooperation of Hsp26 with Ssa1 and Hsp104. *The Journal of biological chemistry* **280**: 23861-23868
- Haslbeck V, Kaiser CJ, Richter K (2012) Hsp90 in non-mammalian metazoan model systems. *Biochimica et biophysica acta* **1823**: 712-721
- Heschl MF, Baillie DL (1990) The HSP70 multigene family of *Caenorhabditis elegans*. *Comparative biochemistry and physiology B, Comparative biochemistry* **96**: 633-637
- Hessling M, Richter K, Buchner J (2009) Dissection of the ATP-induced conformational cycle of the molecular chaperone Hsp90. *Nature structural & molecular biology* **16**: 287-293
- Hietakangas V, Ahlskog JK, Jakobsson AM, Hellesuo M, Sahlberg NM, Holmberg CI, Mikhailov A, Palvimo JJ, Pirkkala L, Sistonen L (2003) Phosphorylation of serine 303 is a prerequisite for the stress-inducible SUMO modification of heat shock factor 1. *Molecular and cellular biology* **23**: 2953-2968
- Hodgson JG, Agopyan N, Gutekunst CA, Leavitt BR, LePiane F, Singaraja R, Smith DJ, Bissada N, McCutcheon K, Nasir J, Jamot L, Li XJ, Stevens ME, Rosemond E, Roder JC, Phillips AG, Rubin EM, Hersch SM, Hayden MR (1999) A YAC mouse model for Huntington's disease with full-length mutant huntingtin, cytoplasmic toxicity, and selective striatal neurodegeneration. *Neuron* **23**: 181-192
- Hohfeld J, Jentsch S (1997) GrpE-like regulation of the hsc70 chaperone by the anti-apoptotic protein BAG-1. *The EMBO journal* **16**: 6209-6216
- Holmberg CI, Hietakangas V, Mikhailov A, Rantanen JO, Kallio M, Meinander A, Hellman J, Morrice N, MacKintosh C, Morimoto RI, Eriksson JE, Sistonen L (2001) Phosphorylation of serine 230 promotes inducible transcriptional activity of heat shock factor 1. *The EMBO journal* **20**: 3800-3810
- Horwich AL, Farr GW, Fenton WA (2006) GroEL-GroES-mediated protein folding. *Chemical reviews* **106**: 1917-1930
- Horwitz J (2003) Alpha-crystallin. *Experimental eye research* **76**: 145-153
- Howell AS, Lew DJ (2012) Morphogenesis and the cell cycle. *Genetics* **190**: 51-77
- Huh WK, Falvo JV, Gerke LC, Carroll AS, Howson RW, Weissman JS, O'Shea EK (2003) Global analysis of protein localization in budding yeast. *Nature* **425**: 686-691
- Inoue T, Hirata K, Kuwana Y, Fujita M, Miwa J, Roy R, Yamaguchi Y (2006) Cell cycle control by daf-21/Hsp90 at the first meiotic prophase/metaphase boundary during oogenesis in *Caenorhabditis elegans*. *Development, growth & differentiation* **48**: 25-32
- Irizarry RA, Bolstad BM, Collin F, Cope LM, Hobbs B, Speed TP (2003) Summaries of Affymetrix GeneChip probe level data. *Nucleic acids research* **31**: e15
- Jaarsma D, Teuling E, Haasdijk ED, De Zeeuw CI, Hoogenraad CC (2008) Neuron-specific expression of mutant superoxide dismutase is sufficient to induce amyotrophic lateral sclerosis in transgenic mice. *The Journal of neuroscience : the official journal of the Society for Neuroscience* **28**: 2075-2088
- Jackson GR, Salecker I, Dong X, Yao X, Arnheim N, Faber PW, MacDonald ME, Zipursky SL (1998) Polyglutamine-expanded human huntingtin transgenes induce degeneration of *Drosophila* photoreceptor neurons. *Neuron* **21**: 633-642
- Jakob U, Meyer I, Bugl H, Andre S, Bardwell JC, Buchner J (1995) Structural organization of procaryotic and eucaryotic Hsp90. Influence of divalent cations on structure and function. *The Journal of biological chemistry* **270**: 14412-14419
- Jana NR, Dikshit P, Goswami A, Kotliarova S, Murata S, Tanaka K, Nukina N (2005) Co-chaperone CHIP associates with expanded polyglutamine protein and promotes their degradation by proteasomes. *The Journal of biological chemistry* **280**: 11635-11640

References

- Jiang H, Nucifora FC, Jr., Ross CA, DeFranco DB (2003) Cell death triggered by polyglutamine-expanded huntingtin in a neuronal cell line is associated with degradation of CREB-binding protein. *Human molecular genetics* **12**: 1-12
- Jiang J, Maes EG, Taylor AB, Wang L, Hinck AP, Lafer EM, Sousa R (2007) Structural basis of J cochaperone binding and regulation of Hsp70. *Molecular cell* **28**: 422-433
- Johnston JA, Illing ME, Kopito RR (2002) Cytoplasmic dynein/dynactin mediates the assembly of aggresomes. *Cell motility and the cytoskeleton* **53**: 26-38
- Johnston JA, Ward CL, Kopito RR (1998) Aggresomes: a cellular response to misfolded proteins. *The Journal of cell biology* **143**: 1883-1898
- Jonsson PA, Ernhill K, Andersen PM, Bergemalm D, Brannstrom T, Gredal O, Nilsson P, Marklund SL (2004) Minute quantities of misfolded mutant superoxide dismutase-1 cause amyotrophic lateral sclerosis. *Brain : a journal of neurology* **127**: 73-88
- Jonsson PA, Graffmo KS, Andersen PM, Brannstrom T, Lindberg M, Oliveberg M, Marklund SL (2006) Disulphide-reduced superoxide dismutase-1 in CNS of transgenic amyotrophic lateral sclerosis models. *Brain : a journal of neurology* **129**: 451-464
- Jordan R, McMacken R (1995) Modulation of the ATPase activity of the molecular chaperone DnaK by peptides and the DnaJ and GrpE heat shock proteins. *The Journal of biological chemistry* **270**: 4563-4569
- Kaganovich D, Kopito R, Frydman J (2008) Misfolded proteins partition between two distinct quality control compartments. *Nature* **454**: 1088-1095
- Kamath RS, Fraser AG, Dong Y, Poulin G, Durbin R, Gotta M, Kanapin A, Le Bot N, Moreno S, Sohrmann M, Welchman DP, Zipperlen P, Ahringer J (2003) Systematic functional analysis of the *Caenorhabditis elegans* genome using RNAi. *Nature* **421**: 231-237
- Kampinga HH, Craig EA (2010) The HSP70 chaperone machinery: J proteins as drivers of functional specificity. *Nature reviews Molecular cell biology* **11**: 579-592
- Kappeli O (1986) Regulation of carbon metabolism in *Saccharomyces cerevisiae* and related yeasts. *Advances in microbial physiology* **28**: 181-209
- Karplus M (1997) The Levinthal paradox: yesterday and today. *Folding & design* **2**: S69-75
- Kim HR, Kang HS, Kim HD (1999) Geldanamycin induces heat shock protein expression through activation of HSF1 in K562 erythroleukemic cells. *IUBMB life* **48**: 429-433
- Kim S, Nollen EA, Kitagawa K, Bindokas VP, Morimoto RI (2002) Polyglutamine protein aggregates are dynamic. *Nature cell biology* **4**: 826-831
- Kitamura A, Kubota H, Pack CG, Matsumoto G, Hirayama S, Takahashi Y, Kimura H, Kinjo M, Morimoto RI, Nagata K (2006) Cytosolic chaperonin prevents polyglutamine toxicity with altering the aggregation state. *Nature cell biology* **8**: 1163-1170
- Knaus M, Pelli-Gulli MP, van Drogen F, Springer S, Jaquenoud M, Peter M (2007) Phosphorylation of Bem2p and Bem3p may contribute to local activation of Cdc42p at bud emergence. *The EMBO journal* **26**: 4501-4513
- Knobloch M, Konietzko U, Krebs DC, Nitsch RM (2007) Intracellular Abeta and cognitive deficits precede beta-amyloid deposition in transgenic arcAbeta mice. *Neurobiology of aging* **28**: 1297-1306
- Kopito RR (2000) Aggresomes, inclusion bodies and protein aggregation. *Trends in cell biology* **10**: 524-530
- Kramer G, Boehringer D, Ban N, Bukau B (2009) The ribosome as a platform for co-translational processing, folding and targeting of newly synthesized proteins. *Nature structural & molecular biology* **16**: 589-597
- Krukenberg KA, Street TO, Lavery LA, Agard DA (2011) Conformational dynamics of the molecular chaperone Hsp90. *Quarterly reviews of biophysics* **44**: 229-255

- Kuemmerle S, Gutekunst CA, Klein AM, Li XJ, Li SH, Beal MF, Hersch SM, Ferrante RJ (1999) Huntington aggregates may not predict neuronal death in Huntington's disease. *Annals of neurology* **46**: 842-849
- Landsverk ML, Li S, Hutagalung AH, Najafov A, Hoppe T, Barral JM, Epstein HF (2007) The UNC-45 chaperone mediates sarcomere assembly through myosin degradation in *Caenorhabditis elegans*. *The Journal of cell biology* **177**: 205-210
- Lashuel HA, Lansbury PT, Jr. (2006) Are amyloid diseases caused by protein aggregates that mimic bacterial pore-forming toxins? *Quarterly reviews of biophysics* **39**: 167-201
- Lee CF, Melkani GC, Yu Q, Suggs JA, Kronert WA, Suzuki Y, Hipolito L, Price MG, Epstein HF, Bernstein SI (2011) *Drosophila* UNC-45 accumulates in embryonic blastoderm and in muscles, and is essential for muscle myosin stability. *Journal of cell science* **124**: 699-705
- Lee EB, Leng LZ, Zhang B, Kwong L, Trojanowski JQ, Abel T, Lee VM (2006) Targeting amyloid-beta peptide (A β) oligomers by passive immunization with a conformation-selective monoclonal antibody improves learning and memory in A β precursor protein (APP) transgenic mice. *The Journal of biological chemistry* **281**: 4292-4299
- Lee GJ, Roseman AM, Saibil HR, Vierling E (1997) A small heat shock protein stably binds heat-denatured model substrates and can maintain a substrate in a folding-competent state. *The EMBO journal* **16**: 659-671
- Li J, Richter K, Buchner J (2011) Mixed Hsp90-cochaperone complexes are important for the progression of the reaction cycle. *Nature structural & molecular biology* **18**: 61-66
- Li J, Soroka J, Buchner J (2012) The Hsp90 chaperone machinery: Conformational dynamics and regulation by co-chaperones. *Biochimica et biophysica acta* **1823**: 624-635
- Liberek K, Lewandowska A, Zietkiewicz S (2008) Chaperones in control of protein disaggregation. *The EMBO journal* **27**: 328-335
- Liberek K, Marszalek J, Ang D, Georgopoulos C, Zylicz M (1991) *Escherichia coli* DnaJ and GrpE heat shock proteins jointly stimulate ATPase activity of DnaK. *Proceedings of the National Academy of Sciences of the United States of America* **88**: 2874-2878
- Liu B, Larsson L, Caballero A, Hao X, Oling D, Grantham J, Nystrom T (2010) The polarisome is required for segregation and retrograde transport of protein aggregates. *Cell* **140**: 257-267
- Lopez-Buesa P, Pfund C, Craig EA (1998) The biochemical properties of the ATPase activity of a 70-kDa heat shock protein (Hsp70) are governed by the C-terminal domains. *Proceedings of the National Academy of Sciences of the United States of America* **95**: 15253-15258
- Louvion JF, Warth R, Picard D (1996) Two eukaryote-specific regions of Hsp82 are dispensable for its viability and signal transduction functions in yeast. *Proceedings of the National Academy of Sciences of the United States of America* **93**: 13937-13942
- Mangiarini L, Sathasivam K, Seller M, Cozens B, Harper A, Hetherington C, Lawton M, Trotter Y, Lehrach H, Davies SW, Bates GP (1996) Exon 1 of the HD gene with an expanded CAG repeat is sufficient to cause a progressive neurological phenotype in transgenic mice. *Cell* **87**: 493-506
- Manogaran AL, Hong JY, Hufana J, Tyedmers J, Lindquist S, Liebman SW (2011) Prion formation and polyglutamine aggregation are controlled by two classes of genes. *PLoS genetics* **7**: e1001386
- Marcinowski M, Holler M, Feige MJ, Baerend D, Lamb DC, Buchner J (2011) Substrate discrimination of the chaperone BiP by autonomous and cochaperone-regulated conformational transitions. *Nature structural & molecular biology* **18**: 150-158
- Martin A, Baker TA, Sauer RT (2005) Rebuilt AAA + motors reveal operating principles for ATP-fuelled machines. *Nature* **437**: 1115-1120
- Martinez-Rucobo FW, Sainsbury S, Cheung AC, Cramer P (2011) Architecture of the RNA polymerase-Spt4/5 complex and basis of universal transcription processivity. *The EMBO journal* **30**: 1302-1310

References

- Matsumoto G, Kim S, Morimoto RI (2006) Huntingtin and mutant SOD1 form aggregate structures with distinct molecular properties in human cells. *The Journal of biological chemistry* **281**: 4477-4485
- Mattson MP, Magnus T (2006) Ageing and neuronal vulnerability. *Nature reviews Neuroscience* **7**: 278-294
- Mayer MP, Bukau B (2005) Hsp70 chaperones: cellular functions and molecular mechanism. *Cellular and molecular life sciences : CMLS* **62**: 670-684
- Mayer RJ, Lowe J, Lennox G, Landon M, MacLennan K, Doherty FJ (1989) Intermediate filament-ubiquitin diseases: implications for cell sanitization. *Biochemical Society symposium* **55**: 193-201
- McCarty JS, Buchberger A, Reinstein J, Bukau B (1995) The role of ATP in the functional cycle of the DnaK chaperone system. *Journal of molecular biology* **249**: 126-137
- McHaourab HS, Godar JA, Stewart PL (2009) Structure and mechanism of protein stability sensors: chaperone activity of small heat shock proteins. *Biochemistry* **48**: 3828-3837
- McKay SJ, Johnsen R, Khattra J, Asano J, Baillie DL, Chan S, Dube N, Fang L, Goszczynski B, Ha E, Halfnight E, Hollebakk R, Huang P, Hung K, Jensen V, Jones SJ, Kai H, Li D, Mah A, Marra M, McGhee J, Newbury R, Pouzyrev A, Riddle DL, Sonnhammer E, Tian H, Tu D, Tyson JR, Vatcher G, Warner A, Wong K, Zhao Z, Moerman DG (2003) Gene expression profiling of cells, tissues, and developmental stages of the nematode *C. elegans*. *Cold Spring Harbor symposia on quantitative biology* **68**: 159-169
- Merlini L, Piatti S (2011) The mother-bud neck as a signaling platform for the coordination between spindle position and cytokinesis in budding yeast. *Biological chemistry* **392**: 805-812
- Mizushima N, Noda T, Ohsumi Y (1999) Apg16p is required for the function of the Apg12p-Apg5p conjugate in the yeast autophagy pathway. *The EMBO journal* **18**: 3888-3896
- Mogk A, Schlieker C, Friedrich KL, Schonfeld HJ, Vierling E, Bukau B (2003) Refolding of substrates bound to small Hsps relies on a disaggregation reaction mediated most efficiently by ClpB/DnaK. *The Journal of biological chemistry* **278**: 31033-31042
- Morley JF, Morimoto RI (2004) Regulation of longevity in *Caenorhabditis elegans* by heat shock factor and molecular chaperones. *Molecular biology of the cell* **15**: 657-664
- Morozova-Roche LA, Jones JA, Noppe W, Dobson CM (1999) Independent nucleation and heterogeneous assembly of structure during folding of equine lysozyme. *Journal of molecular biology* **289**: 1055-1073
- Morshauer RC, Wang H, Flynn GC, Zuiderweg ER (1995) The peptide-binding domain of the chaperone protein Hsc70 has an unusual secondary structure topology. *Biochemistry* **34**: 6261-6266
- Muchowski PJ, Schaffar G, Sittler A, Wanker EE, Hayer-Hartl MK, Hartl FU (2000) Hsp70 and hsp40 chaperones can inhibit self-assembly of polyglutamine proteins into amyloid-like fibrils. *Proceedings of the National Academy of Sciences of the United States of America* **97**: 7841-7846
- Mumberg D, Muller R, Funk M (1995) Yeast vectors for the controlled expression of heterologous proteins in different genetic backgrounds. *Gene* **156**: 119-122
- Nagai Y, Inui T, Popiel HA, Fujikake N, Hasegawa K, Urade Y, Goto Y, Naiki H, Toda T (2007) A toxic monomeric conformer of the polyglutamine protein. *Nature structural & molecular biology* **14**: 332-340
- Narayanaswamy R, Levy M, Tsechansky M, Stovall GM, O'Connell JD, Mirrieles J, Ellington AD, Marcotte EM (2009) Widespread reorganization of metabolic enzymes into reversible assemblies upon nutrient starvation. *Proceedings of the National Academy of Sciences of the United States of America* **106**: 10147-10152
- Niesen FH, Berglund H, Vedadi M (2007) The use of differential scanning fluorimetry to detect ligand interactions that promote protein stability. *Nature protocols* **2**: 2212-2221
- Nishihama R, Schreiter JH, Onishi M, Vallen EA, Hanna J, Moravcevic K, Lippincott MF, Han H, Lemmon MA, Pringle JR, Bi E (2009) Role of Inn1 and its interactions with Hof1 and Cyk3

- in promoting cleavage furrow and septum formation in *S. cerevisiae*. *The Journal of cell biology* **185**: 995-1012
- Nollen EA, Garcia SM, van Haften G, Kim S, Chavez A, Morimoto RI, Plasterk RH (2004) Genome-wide RNA interference screen identifies previously undescribed regulators of polyglutamine aggregation. *Proceedings of the National Academy of Sciences of the United States of America* **101**: 6403-6408
- Okamoto K, Hirai S, Iizuka T, Yanagisawa T, Watanabe M (1991) Reexamination of granulovacuolar degeneration. *Acta neuropathologica* **82**: 340-345
- Olzscha H, Schermann SM, Woerner AC, Pinkert S, Hecht MH, Tartaglia GG, Vendruscolo M, Hayer-Hartl M, Hartl FU, Vabulas RM (2011) Amyloid-like aggregates sequester numerous metastable proteins with essential cellular functions. *Cell* **144**: 67-78
- Packschies L, Theyssen H, Buchberger A, Bukau B, Goody RS, Reinstein J (1997) GrpE accelerates nucleotide exchange of the molecular chaperone DnaK with an associative displacement mechanism. *Biochemistry* **36**: 3417-3422
- Palleros DR, Welch WJ, Fink AL (1991) Interaction of hsp70 with unfolded proteins: effects of temperature and nucleotides on the kinetics of binding. *Proceedings of the National Academy of Sciences of the United States of America* **88**: 5719-5723
- Panov AV, Gutekunst CA, Leavitt BR, Hayden MR, Burke JR, Strittmatter WJ, Greenamyre JT (2002) Early mitochondrial calcium defects in Huntington's disease are a direct effect of polyglutamines. *Nature neuroscience* **5**: 731-736
- Parker JA, Connolly JB, Wellington C, Hayden M, Dausset J, Neri C (2001) Expanded polyglutamines in *Caenorhabditis elegans* cause axonal abnormalities and severe dysfunction of PLM mechanosensory neurons without cell death. *Proceedings of the National Academy of Sciences of the United States of America* **98**: 13318-13323
- Parkes TL, Elia AJ, Dickinson D, Hilliker AJ, Phillips JP, Boulianne GL (1998) Extension of *Drosophila* lifespan by overexpression of human SOD1 in motorneurons. *Nature genetics* **19**: 171-174
- Parsell DA, Kowal AS, Singer MA, Lindquist S (1994) Protein disaggregation mediated by heat-shock protein Hsp104. *Nature* **372**: 475-478
- Pearl LH, Prodromou C (2006) Structure and mechanism of the Hsp90 molecular chaperone machinery. *Annual review of biochemistry* **75**: 271-294
- Petersen A, Stewenius Y, Bjorkqvist M, Gisselsson D (2005) Euploidy in somatic cells from R6/2 transgenic Huntington's disease mice. *BMC cell biology* **6**: 34
- Pfund C, Lopez-Hoyo N, Ziegelhoffer T, Schilke BA, Lopez-Buesa P, Walter WA, Wiedmann M, Craig EA (1998) The molecular chaperone Ssb from *Saccharomyces cerevisiae* is a component of the ribosome-nascent chain complex. *The EMBO journal* **17**: 3981-3989
- Picard D (2002) Heat-shock protein 90, a chaperone for folding and regulation. *Cellular and molecular life sciences : CMLS* **59**: 1640-1648
- Piccioni F, Pinton P, Simeoni S, Pozzi P, Fascio U, Vismara G, Martini L, Rizzuto R, Poletti A (2002) Androgen receptor with elongated polyglutamine tract forms aggregates that alter axonal trafficking and mitochondrial distribution in motor neuronal processes. *FASEB journal : official publication of the Federation of American Societies for Experimental Biology* **16**: 1418-1420
- Pierpaoli EV, Sandmeier E, Baici A, Schonfeld HJ, Gisler S, Christen P (1997) The power stroke of the DnaK/DnaJ/GrpE molecular chaperone system. *Journal of molecular biology* **269**: 757-768
- Poirier MA, Li H, Macosko J, Cai S, Amzel M, Ross CA (2002) Huntingtin spheroids and protofibrils as precursors in polyglutamine fibrilization. *The Journal of biological chemistry* **277**: 41032-41037
- Popp S, Packschies L, Radzwill N, Vogel KP, Steinhoff HJ, Reinstein J (2005) Structural dynamics of the DnaK-peptide complex. *Journal of molecular biology* **347**: 1039-1052

References

- Powers ET, Morimoto RI, Dillin A, Kelly JW, Balch WE (2009) Biological and chemical approaches to diseases of proteostasis deficiency. *Annual review of biochemistry* **78**: 959-991
- Pratt WB, Toft DO (2003) Regulation of signaling protein function and trafficking by the hsp90/hsp70-based chaperone machinery. *Experimental biology and medicine* **228**: 111-133
- Prudencio M, Hart PJ, Borchelt DR, Andersen PM (2009) Variation in aggregation propensities among ALS-associated variants of SOD1: correlation to human disease. *Human molecular genetics* **18**: 3217-3226
- Prusiner SB (1982) Novel proteinaceous infectious particles cause scrapie. *Science* **216**: 136-144
- Richter K, Haslbeck M, Buchner J (2010) The heat shock response: life on the verge of death. *Molecular cell* **40**: 253-266
- Richter K, Soroka J, Skalniak L, Leskovaar A, Hessling M, Reinstein J, Buchner J (2008) Conserved conformational changes in the ATPase cycle of human Hsp90. *The Journal of biological chemistry* **283**: 17757-17765
- Rist W, Graf C, Bukau B, Mayer MP (2006) Amide hydrogen exchange reveals conformational changes in hsp70 chaperones important for allosteric regulation. *The Journal of biological chemistry* **281**: 16493-16501
- Rodriguez F, Arsene-Ploetze F, Rist W, Rudiger S, Schneider-Mergener J, Mayer MP, Bukau B (2008) Molecular basis for regulation of the heat shock transcription factor sigma32 by the DnaK and DnaJ chaperones. *Molecular cell* **32**: 347-358
- Rosen DR, Siddique T, Patterson D, Figlewicz DA, Sapp P, Hentati A, Donaldson D, Goto J, O'Regan JP, Deng HX, et al. (1993) Mutations in Cu/Zn superoxide dismutase gene are associated with familial amyotrophic lateral sclerosis. *Nature* **362**: 59-62
- Ross CA, Poirier MA (2004) Protein aggregation and neurodegenerative disease. *Nature medicine* **10 Suppl**: S10-17
- Russell R, Wali Karzai A, Mehl AF, McMacken R (1999) DnaJ dramatically stimulates ATP hydrolysis by DnaK: insight into targeting of Hsp70 proteins to polypeptide substrates. *Biochemistry* **38**: 4165-4176
- Rutherford SL, Lindquist S (1998) Hsp90 as a capacitor for morphological evolution. *Nature* **396**: 336-342
- Saarikangas J, Barral Y (2011) The emerging functions of septins in metazoans. *EMBO reports* **12**: 1118-1126
- Sanchez I, Mahlke C, Yuan J (2003) Pivotal role of oligomerization in expanded polyglutamine neurodegenerative disorders. *Nature* **421**: 373-379
- Sarthy AV, Schopp C, Idler KB (1994) Cloning and sequence determination of the gene encoding sorbitol dehydrogenase from *Saccharomyces cerevisiae*. *Gene* **140**: 121-126
- Sasaki S, Warita H, Murakami T, Shibata N, Komori T, Abe K, Kobayashi M, Iwata M (2005) Ultrastructural study of aggregates in the spinal cord of transgenic mice with a G93A mutant SOD1 gene. *Acta neuropathologica* **109**: 247-255
- Sathasivam K, Woodman B, Mahal A, Bertaux F, Wanker EE, Shima DT, Bates GP (2001) Centrosome disorganization in fibroblast cultures derived from R6/2 Huntington's disease (HD) transgenic mice and HD patients. *Human molecular genetics* **10**: 2425-2435
- Saudou F, Finkbeiner S, Devys D, Greenberg ME (1998) Huntingtin acts in the nucleus to induce apoptosis but death does not correlate with the formation of intranuclear inclusions. *Cell* **95**: 55-66
- Schaupp A, Marcinowski M, Grimminger V, Bosl B, Walter S (2007) Processing of proteins by the molecular chaperone Hsp104. *Journal of molecular biology* **370**: 674-686
- Scheufler C, Brinker A, Bourenkov G, Pegoraro S, Moroder L, Bartunik H, Hartl FU, Moarefi I (2000) Structure of TPR domain-peptide complexes: critical elements in the assembly of the Hsp70-Hsp90 multichaperone machine. *Cell* **101**: 199-210

- Schirmer EC, Glover JR, Singer MA, Lindquist S (1996) HSP100/Clp proteins: a common mechanism explains diverse functions. *Trends in biochemical sciences* **21**: 289-296
- Schlecht R, Erbse AH, Bukau B, Mayer MP (2011) Mechanics of Hsp70 chaperones enables differential interaction with client proteins. *Nature structural & molecular biology* **18**: 345-351
- Schnell JR, Dyson HJ, Wright PE (2004) Structure, dynamics, and catalytic function of dihydrofolate reductase. *Annual review of biophysics and biomolecular structure* **33**: 119-140
- Schrader EK, Harstad KG, Matouschek A (2009) Targeting proteins for degradation. *Nature chemical biology* **5**: 815-822
- Schroder H, Langer T, Hartl FU, Bukau B (1993) DnaK, DnaJ and GrpE form a cellular chaperone machinery capable of repairing heat-induced protein damage. *The EMBO journal* **12**: 4137-4144
- Sezen B, Seedorf M, Schiebel E (2009) The SESA network links duplication of the yeast centrosome with the protein translation machinery. *Genes & development* **23**: 1559-1570
- Sha B, Lee S, Cyr DM (2000) The crystal structure of the peptide-binding fragment from the yeast Hsp40 protein Sis1. *Structure* **8**: 799-807
- Shankar GM, Li S, Mehta TH, Garcia-Munoz A, Shepardson NE, Smith I, Brett FM, Farrell MA, Rowan MJ, Lemere CA, Regan CM, Walsh DM, Sabatini BL, Selkoe DJ (2008) Amyloid-beta protein dimers isolated directly from Alzheimer's brains impair synaptic plasticity and memory. *Nature medicine* **14**: 837-842
- Sharma S, Chakraborty K, Muller BK, Astola N, Tang YC, Lamb DC, Hayer-Hartl M, Hartl FU (2008) Monitoring protein conformation along the pathway of chaperonin-assisted folding. *Cell* **133**: 142-153
- Shi YY, Hong XG, Wang CC (2005) The C-terminal (331-376) sequence of Escherichia coli DnaJ is essential for dimerization and chaperone activity: a small angle X-ray scattering study in solution. *The Journal of biological chemistry* **280**: 22761-22768
- Shibata N, Asayama K, Hirano A, Kobayashi M (1996) Immunohistochemical study on superoxide dismutases in spinal cords from autopsied patients with amyotrophic lateral sclerosis. *Developmental neuroscience* **18**: 492-498
- Shorter J (2011) The mammalian disaggregase machinery: Hsp110 synergizes with Hsp70 and Hsp40 to catalyze protein disaggregation and reactivation in a cell-free system. *PLoS one* **6**: e26319
- Shulewitz MJ, Inouye CJ, Thorner J (1999) Hsl7 localizes to a septin ring and serves as an adapter in a regulatory pathway that relieves tyrosine phosphorylation of Cdc28 protein kinase in *Saccharomyces cerevisiae*. *Molecular and cellular biology* **19**: 7123-7137
- Slepenkov SV, Patchen B, Peterson KM, Witt SN (2003) Importance of the D and E helices of the molecular chaperone DnaK for ATP binding and substrate release. *Biochemistry* **42**: 5867-5876
- Smith DF (1998) Sequence motifs shared between chaperone components participating in the assembly of progesterone receptor complexes. *Biological chemistry* **379**: 283-288
- Smith GR, Sternberg MJ, Bates PA (2005) The relationship between the flexibility of proteins and their conformational states on forming protein-protein complexes with an application to protein-protein docking. *Journal of molecular biology* **347**: 1077-1101
- Sondermann H, Scheufler C, Schneider C, Hohfeld J, Hartl FU, Moarefi I (2001) Structure of a Bag/Hsc70 complex: convergent functional evolution of Hsp70 nucleotide exchange factors. *Science* **291**: 1553-1557
- Song AH, Wang D, Chen G, Li Y, Luo J, Duan S, Poo MM (2009) A selective filter for cytoplasmic transport at the axon initial segment. *Cell* **136**: 1148-1160
- Srikakulam R, Liu L, Winkelmann DA (2008) Unc45b forms a cytosolic complex with Hsp90 and targets the unfolded myosin motor domain. *PLoS one* **3**: e2137

References

- Stafford WF, 3rd (1992) Boundary analysis in sedimentation transport experiments: a procedure for obtaining sedimentation coefficient distributions using the time derivative of the concentration profile. *Analytical biochemistry* **203**: 295-301
- Storchova Z, Breneman A, Cande J, Dunn J, Burbank K, O'Toole E, Pellman D (2006) Genome-wide genetic analysis of polyploidy in yeast. *Nature* **443**: 541-547
- Strub BR, Parkes TL, Mukai ST, Bahadorani S, Coulthard AB, Hall N, Phillips JP, Hilliker AJ (2008) Mutations of the withered (whd) gene in *Drosophila melanogaster* confer hypersensitivity to oxidative stress and are lesions of the carnitine palmitoyltransferase I (CPT I) gene. *Genome / National Research Council Canada = Genome / Conseil national de recherches Canada* **51**: 409-420
- Stuart JK, Myszkowski DG, Joss L, Mitchell RS, McDonald SM, Xie Z, Takayama S, Reed JC, Ely KR (1998) Characterization of interactions between the anti-apoptotic protein BAG-1 and Hsc70 molecular chaperones. *The Journal of biological chemistry* **273**: 22506-22514
- Su PH, Li HM (2010) Stromal Hsp70 is important for protein translocation into pea and *Arabidopsis* chloroplasts. *The Plant cell* **22**: 1516-1531
- Sun L, Edelmann FT, Kaiser CJ, Papsdorf K, Gaiser AM, Richter K (2012) The lid domain of *Caenorhabditis elegans* Hsc70 influences ATP turnover, cofactor binding and protein folding activity. *PLoS one* **7**: e33980
- Swain JF, Dinler G, Sivendran R, Montgomery DL, Stotz M, Gierasch LM (2007) Hsp70 chaperone ligands control domain association via an allosteric mechanism mediated by the interdomain linker. *Molecular cell* **26**: 27-39
- Symersky J, Zhang Y, Schormann N, Li S, Bunzel R, Pruett P, Luan CH, Luo M (2004) Structural genomics of *Caenorhabditis elegans*: structure of the BAG domain. *Acta crystallographica Section D, Biological crystallography* **60**: 1606-1610
- Szabo A, Langer T, Schroder H, Flanagan J, Bukau B, Hartl FU (1994) The ATP hydrolysis-dependent reaction cycle of the *Escherichia coli* Hsp70 system DnaK, DnaJ, and GrpE. *Proceedings of the National Academy of Sciences of the United States of America* **91**: 10345-10349
- Takai K, Nunoura T, Sako Y, Uchida A (1998) Acquired thermotolerance and temperature-induced protein accumulation in the extremely thermophilic bacterium *Rhodothermus obamensis*. *Journal of bacteriology* **180**: 2770-2774
- Takayama S, Bimston DN, Matsuzawa S, Freeman BC, Aime-Sempe C, Xie Z, Morimoto RI, Reed JC (1997) BAG-1 modulates the chaperone activity of Hsp70/Hsc70. *The EMBO journal* **16**: 4887-4896
- Tam S, Geller R, Spiess C, Frydman J (2006) The chaperonin TRiC controls polyglutamine aggregation and toxicity through subunit-specific interactions. *Nature cell biology* **8**: 1155-1162
- Taylor JP, Hardy J, Fischbeck KH (2002) Toxic proteins in neurodegenerative disease. *Science* **296**: 1991-1995
- Taylor JP, Tanaka F, Robitschek J, Sandoval CM, Taye A, Markovic-Plese S, Fischbeck KH (2003) Aggresomes protect cells by enhancing the degradation of toxic polyglutamine-containing protein. *Human molecular genetics* **12**: 749-757
- Terada K, Mori M (2000) Human DnaJ homologs dj2 and dj3, and bag-1 are positive cochaperones of hsc70. *The Journal of biological chemistry* **275**: 24728-24734
- Tessarz P, Schwarz M, Mogk A, Bukau B (2009) The yeast AAA+ chaperone Hsp104 is part of a network that links the actin cytoskeleton with the inheritance of damaged proteins. *Molecular and cellular biology* **29**: 3738-3745
- Thinakaran G, Koo EH (2008) Amyloid precursor protein trafficking, processing, and function. *The Journal of biological chemistry* **283**: 29615-29619
- Thomas JH, Birnby DA, Vowels JJ (1993) Evidence for parallel processing of sensory information controlling dauer formation in *Caenorhabditis elegans*. *Genetics* **134**: 1105-1117

- Todd MJ, Viitanen PV, Lorimer GH (1994) Dynamics of the chaperonin ATPase cycle: implications for facilitated protein folding. *Science* **265**: 659-666
- Treusch S, Cyr DM, Lindquist S (2009) Amyloid deposits: protection against toxic protein species? *Cell cycle* **8**: 1668-1674
- Tzankov S, Wong MJ, Shi K, Nassif C, Young JC (2008) Functional divergence between co-chaperones of Hsc70. *The Journal of biological chemistry* **283**: 27100-27109
- van Ham TJ, Holmberg MA, van der Goot AT, Teuling E, Garcia-Arencibia M, Kim HE, Du D, Thijssen KL, Wiersma M, Burggraaff R, van Bergeijk P, van Rheenen J, Jerre van Veluw G, Hofstra RM, Rubinsztein DC, Nollen EA (2010) Identification of MOAG-4/SERF as a regulator of age-related proteotoxicity. *Cell* **142**: 601-612
- Vassall KA, Stubbs HR, Primmer HA, Tong MS, Sullivan SM, Sobering R, Srinivasan S, Briere LA, Dunn SD, Colon W, Meiering EM (2011) Decreased stability and increased formation of soluble aggregates by immature superoxide dismutase do not account for disease severity in ALS. *Proceedings of the National Academy of Sciences of the United States of America* **108**: 2210-2215
- Venkatraman P, Wetzel R, Tanaka M, Nukina N, Goldberg AL (2004) Eukaryotic proteasomes cannot digest polyglutamine sequences and release them during degradation of polyglutamine-containing proteins. *Molecular cell* **14**: 95-104
- Venolia L, Waterston RH (1990) The unc-45 gene of *Caenorhabditis elegans* is an essential muscle-affecting gene with maternal expression. *Genetics* **126**: 345-353
- Viitanen PV, Gatenby AA, Lorimer GH (1992) Purified chaperonin 60 (groEL) interacts with the nonnative states of a multitude of *Escherichia coli* proteins. *Protein science : a publication of the Protein Society* **1**: 363-369
- Voellmy R (2004) Transcriptional regulation of the metazoan stress protein response. *Progress in nucleic acid research and molecular biology* **78**: 143-185
- Voss AK, Thomas T, Gruss P (2000) Mice lacking HSP90beta fail to develop a placental labyrinth. *Development* **127**: 1-11
- Vowels JJ, Thomas JH (1992) Genetic analysis of chemosensory control of dauer formation in *Caenorhabditis elegans*. *Genetics* **130**: 105-123
- Walker FO (2007) Huntington's disease. *Lancet* **369**: 218-228
- Walsh DM, Tseng BP, Rydel RE, Podlisny MB, Selkoe DJ (2000) The oligomerization of amyloid beta-protein begins intracellularly in cells derived from human brain. *Biochemistry* **39**: 10831-10839
- Walsh P, Bursac D, Law YC, Cyr D, Lithgow T (2004) The J-protein family: modulating protein assembly, disassembly and translocation. *EMBO reports* **5**: 567-571
- Wang J, Xu G, Li H, Gonzales V, Fromholt D, Karch C, Copeland NG, Jenkins NA, Borchelt DR (2005) Somatodendritic accumulation of misfolded SOD1-L126Z in motor neurons mediates degeneration: alphaB-crystallin modulates aggregation. *Human molecular genetics* **14**: 2335-2347
- Wang X, Arai S, Song X, Reichart D, Du K, Pascual G, Tempst P, Rosenfeld MG, Glass CK, Kurokawa R (2008) Induced ncRNAs allosterically modify RNA-binding proteins in cis to inhibit transcription. *Nature* **454**: 126-130
- Waterston RH (1988) Muscle. In *The nematode C. elegans*, Wood WB (ed), pp 281-335. New York: Cold Spring Harbor Laboratory Press
- Wawrzynow A, Banecki B, Wall D, Liberek K, Georgopoulos C, Zylicz M (1995) ATP hydrolysis is required for the DnaJ-dependent activation of DnaK chaperone for binding to both native and denatured protein substrates. *The Journal of biological chemistry* **270**: 19307-19311
- Weber-Ban EU, Reid BG, Miranker AD, Horwich AL (1999) Global unfolding of a substrate protein by the Hsp100 chaperone ClpA. *Nature* **401**: 90-93
- Welch WJ, Feramisco JR (1982) Purification of the major mammalian heat shock proteins. *The Journal of biological chemistry* **257**: 14949-14959

References

- Werner-Washburne M, Braun E, Johnston GC, Singer RA (1993) Stationary phase in the yeast *Saccharomyces cerevisiae*. *Microbiological reviews* **57**: 383-401
- Werner-Washburne M, Stone DE, Craig EA (1987) Complex interactions among members of an essential subfamily of hsp70 genes in *Saccharomyces cerevisiae*. *Molecular and cellular biology* **7**: 2568-2577
- White JK, Auerbach W, Duyao MP, Vonsattel JP, Gusella JF, Joyner AL, MacDonald ME (1997) Huntingtin is required for neurogenesis and is not impaired by the Huntington's disease CAG expansion. *Nature genetics* **17**: 404-410
- Wiech H, Buchner J, Zimmermann M, Zimmermann R, Jakob U (1993) Hsc70, immunoglobulin heavy chain binding protein, and Hsp90 differ in their ability to stimulate transport of precursor proteins into mammalian microsomes. *The Journal of biological chemistry* **268**: 7414-7421
- Wigley WC, Fabunmi RP, Lee MG, Marino CR, Muallem S, DeMartino GN, Thomas PJ (1999) Dynamic association of proteasomal machinery with the centrosome. *The Journal of cell biology* **145**: 481-490
- Williams AJ, Paulson HL (2008) Polyglutamine neurodegeneration: protein misfolding revisited. *Trends in neurosciences* **31**: 521-528
- Willingham S, Outeiro TF, DeVit MJ, Lindquist SL, Muchowski PJ (2003) Yeast genes that enhance the toxicity of a mutant huntingtin fragment or alpha-synuclein. *Science* **302**: 1769-1772
- Winzler EA, Shoemaker DD, Astromoff A, Liang H, Anderson K, Andre B, Bangham R, Benito R, Boeke JD, Bussey H, Chu AM, Connelly C, Davis K, Dietrich F, Dow SW, El Bakkoury M, Foury F, Friend SH, Gentalen E, Giaever G, Hegemann JH, Jones T, Laub M, Liao H, Liebundguth N, Lockhart DJ, Lucau-Danila A, Lussier M, M'Rabet N, Menard P, Mittmann M, Pai C, Rebischung C, Revuelta JL, Riles L, Roberts CJ, Ross-MacDonald P, Scherens B, Snyder M, Sookhai-Mahadeo S, Storms RK, Veronneau S, Voet M, Volckaert G, Ward TR, Wysocki R, Yen GS, Yu K, Zimmermann K, Philippsen P, Johnston M, Davis RW (1999) Functional characterization of the *S. cerevisiae* genome by gene deletion and parallel analysis. *Science* **285**: 901-906
- Wittung-Stafshede P, Guidry J, Horne BE, Landry SJ (2003) The J-domain of Hsp40 couples ATP hydrolysis to substrate capture in Hsp70. *Biochemistry* **42**: 4937-4944
- Wojcik C, Schroeter D, Wilk S, Lamprecht J, Paweletz N (1996) Ubiquitin-mediated proteolysis centers in HeLa cells: indication from studies of an inhibitor of the chymotrypsin-like activity of the proteasome. *European journal of cell biology* **71**: 311-318
- Wormbase web site, <http://www.wormbase.org>, release WS231, date 02/24/2012
- Worrall LJ, Walkinshaw MD (2007) Crystal structure of the C-terminal three-helix bundle subdomain of *C. elegans* Hsp70. *Biochemical and biophysical research communications* **357**: 105-110
- Wytenbach A, Sauvageot O, Carmichael J, Diaz-Latoud C, Arrigo AP, Rubinsztein DC (2002) Heat shock protein 27 prevents cellular polyglutamine toxicity and suppresses the increase of reactive oxygen species caused by huntingtin. *Human molecular genetics* **11**: 1137-1151
- Xu J, Reumers J, Couceiro JR, De Smet F, Gallardo R, Rudyak S, Cornelis A, Rozenski J, Zwolinska A, Marine JC, Lambrechts D, Suh YA, Rousseau F, Schymkowitz J (2011) Gain of function of mutant p53 by coaggregation with multiple tumor suppressors. *Nature chemical biology* **7**: 285-295
- Yam AY, Xia Y, Lin HT, Burlingame A, Gerstein M, Frydman J (2008) Defining the TRiC/CCT interactome links chaperonin function to stabilization of newly made proteins with complex topologies. *Nature structural & molecular biology* **15**: 1255-1262
- Yang Y, Geldmacher DS, Herrup K (2001) DNA replication precedes neuronal cell death in Alzheimer's disease. *The Journal of neuroscience : the official journal of the Society for Neuroscience* **21**: 2661-2668
- Yeyati PL, Bancewicz RM, Maule J, van Heyningen V (2007) Hsp90 selectively modulates phenotype in vertebrate development. *PLoS genetics* **3**: e43

- Young JC (2010) Mechanisms of the Hsp70 chaperone system. *Biochemistry and cell biology = Biochimie et biologie cellulaire* **88**: 291-300
- Young JC, Agashe VR, Siegers K, Hartl FU (2004) Pathways of chaperone-mediated protein folding in the cytosol. *Nature reviews Molecular cell biology* **5**: 781-791
- Young JC, Obermann WM, Hartl FU (1998) Specific binding of tetratricopeptide repeat proteins to the C-terminal 12-kDa domain of hsp90. *The Journal of biological chemistry* **273**: 18007-18010
- Zhang S, Feany MB, Saraswati S, Littleton JT, Perrimon N (2009) Inactivation of Drosophila Huntingtin affects long-term adult functioning and the pathogenesis of a Huntington's disease model. *Disease models & mechanisms* **2**: 247-266
- Zhu X, Zhao X, Burkholder WF, Gragerov A, Ogata CM, Gottesman ME, Hendrickson WA (1996) Structural analysis of substrate binding by the molecular chaperone DnaK. *Science* **272**: 1606-1614
- Zoghbi HY, Orr HT (2000) Glutamine repeats and neurodegeneration. *Annual review of neuroscience* **23**: 217-247

